NUREG/CR-1353
LA-8273-MS

Informal Report

Preliminary Calculations Related to the Accident at Three Mile Island

University of California

LOS ALAMOS SCIENTIFIC LABORATORY
Post Office Box 1663 Los Alamos, New Mexico 87545

Available from

GPO Sales Program
Division of Technical Information and Document Control
U. S. Nuclear Regulatory Commission
Washington, D. C. 20555

and

National Technical Information Service
Springfield, Virginia 22161

NUREG/CR-1353
LA-8273-MS
Informal Report
R4

Preliminary Calculations Related to the Accident at Three Mile Island

J. R. Ireland
P. K. Mast
T. R. Wehner
P. B. Bleiweis
W. L. Kirchner
M. G. Stevenson

Manuscript submitted: February 1980
Date published: March 1980

Prepared for
Office of Nuclear Regulatory Research
US Nuclear Regulatory Commission
Washington, DC 20555

NRC FIN No. A7049

UNITED STATES
DEPARTMENT OF ENERGY
CONTRACT W-7405-ENG. 36

CONTENTS

FIGURES

FIGURES (cont)

TABLES

TABLES (cont)

PRELIMINARY CALCULATIONS RELATED TO THE ACCIDENT AT THREE MILE ISLAND

by

J. R. Ireland, P. K. Mast, T. R. Wehner,
P. B. Bleiweis, W. L. Kirchner, and M. G. Stevenson

ABSTRACT

The Three Mile Island nuclear plant (TMI-2) was modeled using the Transient Reactor Analysis Code (TRAC-P1A)[1] and a preliminary calculation, which simulated the initial part of the accident that occurred on March 28, 1979, was performed. The purpose of this calculation was to provide a better understanding of the system thermal-hydraulic and core thermal-mechanical response during the first 3 h and to evaluate how well TRAC compared to the overall accident scenario and measured system parameters. As a result of this base-case calculation, several parametric calculations were performed to investigate hypothetical variations to the TMI-2 accident sequence to determine the significance of system/operator actions on the course of the accident. Finally, based upon the results of the base-case calculation, estimates were made regarding the extent of core damage and the amount of hydrogen produced as a result of the zirconium-steam reaction.

I. INTRODUCTION AND SUMMARY

The Los Alamos Scientific Laboratory (LASL) has an extensive program, funded by the US Nuclear Regulatory Commission (NRC), in the development, verification, and application of computer methods, specifically the Transient Reactor Analysis Code (TRAC), for the analysis of Light-Water Reactor (LWR) accidents.[1] Additional efforts for NRC involve investigations of phenomena relevant to High-Temperature Gas-Cooled Reactor (HTGR) and Liquid-Metal Cooled Fast Breeder Reactor (LMFBR) accidents. This report discusses preliminary studies of the Three Mile Island Unit 2 (TMI-2) accident based on available methods and data. The report reproduces, with the exception of minor editing, a draft report submitted September 1, 1979 to The President's Commission on the Accident at Three Mile Island and to the NRC Special Inquiry Group. The work reported includes:

- A TRAC base-case calculation out to 3 h into the accident sequence.

- TRAC parametric calculations. These are the same as the base case except for a single hypothetical change in the system conditions, such as assuming the high-pressure injection (HPI) system operated as designed rather than as in the accident.

- Fuel rod cladding failure, cladding oxidation due to zirconium metal-steam reactions, hydrogen release due to cladding oxidation, cladding ballooning, cladding embrittlement, and subsequent cladding breakup estimates based on TRAC-calculated cladding temperatures and system pressures. Estimates beyond initial gross fuel rod deformation must be regarded as speculative since the TRAC calculations currently assume intact core geometry.

Some conclusions of this work are:

- The TRAC base-case accident calculation agrees very well with known system conditions to nearly 3 h into the accident.

- The parametric calculations indicate that, loss-of-core cooling was most influenced by the throttling of HPI flows, given the

accident initiating events and the pressurizer electromagnetic-operated relief valve (PORV) failing to close as designed.

- Failure of nearly all the rods and gaseous fission product gas release from the failed rods is predicted to have occurred at about 2 h and 30 min. This is consistent with radiation montiors at TMI-2.

- Cladding oxidation (zirconium-steam reaction) up to 3 h resulted in the production of approximately 40 kg of hydrogen. It is highly probable that hydrogen generation continued beyond that time.

A. TRAC Base-Case Calculation

A description of the first released version of the TRAC code, TRAC-P1A, and the current status of its verification is contained in Ref. 2. TRAC-P1A is a steam-water (two-phase) systems analysis code designed specifically to produce physically accurate (best estimate) predictions of large-break loss-of-coolant accidents (LOCAs). TRAC calculations of a large number of LOCA-related experiments, such as in the Semiscale and LOFT facilities at the Idaho National Engineering Laboratory (INEL), have agreed very well with the experimental data, and considerable confidence can be placed in its modeling of the rapid blowdown, refill, and reflood phases typical of large-break LOCAs. Its calculational capabilities were not developed for and have not been tested against long time duration experiments typical of the TMI-2 accident. In particular, TRAC-P1A does not presently account for noncondensible gases (such as hydrogen generated by zirconium-steam reactions or nitrogen which may be injected from core flooding accumulators), nor does it account for changing core geometry due to cladding ballooning, rupture, oxidation, breakup, or fuel motion. Nevertheless, the TRAC-P1A base-case results are in very good agreement with known system conditions during the first 3 h of the TMI-2 accident. Further, much can be learned concerning the system hydraulics and the core thermal-

mechanical behavior by examining the TRAC results, as summarized below and discussed in detail in Sec. II.

The TRAC model of the TMI-2 system for these calculations used 24 cells in the reactor vessel and 42 cells for the two system loops. The core fuel rods were modeled initially using three axial levels and two azimuthal regions per level, with average, high-power, and low-power fuel rods per region. This vessel noding was used to calculate the steady-state system conditions and the first 81 min of the transient. The pressurizer relief valve (PORV) was modeled using a pipe module, allowing a direct calculation of the flow out the PORV. The once-through steam generators (OTSG) were modeled on both primary and secondary sides, but with boundary conditions used to model the balance of the secondary system. Based on the TMI-2 recorded power level, a TRAC steady-state calculation was performed to generate the initial conditions prior to the accident. These conditions are in very good agreement with available TMI-2 data.

Using these self-consistent initial conditions, the TRAC transient calculation was begun. Operator and system actions were simulated in TRAC using plant data, event chronologies, and in certain cases, assumptions necessary to give results which matched known system conditions (these are outlined in detail in Sec. II). The first 30 min of the accident sequence are well simulated by TRAC, particularly system pressure, loop temperatures, and pressurizer level. During the period from 30 min to 81 min coolant is continuously lost through the PORV and the letdown system. Calculated core temperatures remain low, however, due to the good cooling provided by boiling in the core, which offsets the coolant losses and maintains the system pressure stable.*

At 81 min, a more finely noded vessel model was used to provide more axial levels. This enhances the accuracy of predictions of the core thermal conditions and two-phase natural circulation through the system. Due to continual coolant loss, calculated core void fractions

---

*Throughout this discussion we will use present tense when describing calculated events and conditions which may or may not be known to have occurred in the accident.

increase and primary coolant pump flow rates slowly decrease due to void formation in the coolant. Primary system pressure falls steadily after 91 min as increased auxiliary feedwater flow is introduced into the A loop OTSG. After the A loop pumps are tripped at 100 min, phase separation occurs throughout the system. This results in partial core uncovering and loss-of-coolant circulation through the loops. At 120 min, upper core temperatures begin to rise rapidly (0.25 K/s). At 138 min, the PORV block valve is closed resulting in a gradual increase in core liquid inventory. At about 160 min, the water inventory in the core has boiled down again such that water is in the lower plenum and partially in the lower core, resulting in a steep axial temperature gradient in the core. Since upward-moving steam velocities are very low (less than 0.1 m/s) the steam becomes very superheated in the upper part of the core and, as a result, the cladding and fuel heat up sharply. When the cladding temperatures reach 1 300 K, zirconium-steam reactions (exothermic) begin and the upper core temperatures begin rising at about 0.7 K/s. This temperature excursion was probably terminated in the accident when the HPI was returned to nonthrottled flow rates at 3 h and 20 min, enhancing the core cooling rate (TRAC calculations were terminated at 3 h since the core modeling was no longer realistic).

The results of this TRAC base-case calculation show good agreement with measured system parameters out to nearly 3 h and provide a foundation for: making detailed comparisons against alternative system/operator responses during the accident sequence, investigating longer term TMI-2 accident events, and making estimates of the reactor core thermal-mechanical behavior.

B. TRAC Parametric Calculations

This section of the study was performed to investigate hypothetical variations to the TMI-2 accident sequence to determine the significance of system/operator actions on the course of the accident. It is not intended to judge system design or operator response as related to the TMI-2 accident; rather, its purpose is to serve as a basis for future discussion on reactor system design, instrumentation, and operation.

Within the time constraints of this preliminary study, five parametric cases were run with TRAC. These specific cases were requested by the NRC TMI Special Inquiry Group. The INEL is supplying additional parametric cases. The primary variations of interest were: (1) start of auxiliary feedwater supply after initiation of the accident, (2) the effect of degraded HPI, (3) the effect of early tripping of the main coolant pumps, and (4) the effect of a cold-leg break of area equivalent to the PORV throat area. The delay (up to 1 h) of auxiliary feedwater supply as compared to immediate initiation results, in the TRAC calculations, in very little difference in the long-term behavior of the system from that of the base case. This conclusion is of importance to the TRAC base calculation since it demonstrates that the primary system behavior was a relatively weak function of the details of the secondary system performance.

The parametric case with HPI operating as designed resulted in significant deviations from the base case. After the pressure dropped below the HPI setpoint and full flow was initiated, the HPI flow was sufficient to maintain the system pressure at a higher level than the base case. This resulted in a higher break flow than the base case, but more importantly, maintained the coolant in a subcooled state, preventing a core temperature excursion. This calculation indicates that no core damage would have occurred as long as HPI flow was supplied.

The influence of the main coolant pumps was examined by a parametric case in which the pumps were tripped immediately upon initiation of the accident. This calculation was not run as far out in time as the base case, but the available results indicate that after a flow coastdown transition period of 40 min, phase separation begins in the system. Based on comparison with the base-case calculation in which phase separation occurred after the A loop pumps were tripped, we expect that this case would result in a similar core temperature transient beginning approximately 45 min earlier than the base case.

The final parametric case performed was a cold-leg break simulation. A break area equivalent to the PORV throat area was assumed and located in the A loop pump discharge line. The initial transient is characterized by a higher system pressure than in the base case. This occurs

because the equivalent area cold-leg small-break flows are lower than out the PORV in the base case. This case was not run to completion, but, given the same character of letdown and makeup flows as occurred in the base case, this case could depressurize with core flood tank activation and subsequent core flooding.

C. Core Thermal-Mechanical Response

The concern in a reactor accident is the potential for release of radioactive materials. The amount of radioactive material available for release is determined by the state of the reactor core before the accident, but the amount actually released is determined by temperatures and other system conditions during the accident. Of particular interest are when significant cladding failures first occur and allow release of fission product gases to the primary coolant system. Continued fuel heatup can result in release of volatile fission products from the surface and matrix of the fuel pellets and, if not terminated, fuel pellet melting. Phenomena which influence the core behavior include cladding ballooning before failure, cladding oxidation, embrittlement, and hydogen generation from zirconium-steam reactions.

Calculations indicate that considerable local cladding ballooning was likely prior to failure and should have resulted in some degree of local flow blockages. However, the best estimate cladding failure time of about 2-1/2 h using TRAC-calculated temperatures, while not including local flow starvations, agrees well with indications of substantial radioactive material release. Since there was very little steam flow through the core during the temperature excursion leading to these initial cladding failures, then ballooning should not have influenced failure times substantially. However, local flow reductions due to ballooning could have been a contributor to anamolous fuel bundle outlet temperatures measured later in the accident.

The calculated cladding failure times of about 2-1/2 h are shown (Sec. D) to be not very sensitive to initial rod pressures or the accepted criteria used for failure predictions. The major controlling factor is the high cladding temperatures occurring in the upper part of

the core after about 2 h. The calculations indicate that essentially all of the rods should have failed, thus releasing most of the core inventory of gaseous fission products.

Further calculations based on TRAC results indicate about 37 kg of hydrogen were produced by 3 h into the transient (the TRAC calculations were terminated at that time). This reaction causes swelling and embrittlement of the Zircaloy cladding. Calculations of possible thermal-shock induced failures assuming the hot cladding was quenched shortly after 3 h show that ductile cladding would not have suffered further failures from thermal shock. However, the swollen and embrittled oxidized cladding probably would have. Thus, the axial length of cladding which was oxidized (roughly the upper third of the core) might have failed extensively during reflood, if reflood occurred quickly. We have not performed detailed calculations beyond 3 h, and since the TRAC calculations beyond about 2-1/2 h do not model many of the complicated core phenomena, these estimated cladding conditions are somewhat speculative. However, the TRAC-calculated system pressure does agree quite well with the measured pressure out to almost 3 h (to the time at which substantial hydrogen generation begins). Thus, the core thermal conditions used for the cladding behavior calculations to this time should not be too unrealistic.

D. Hypothetical Sequence Questions

Some specific questions were addressed to us by the President's Commission on the Accident at Three Mile Island. Several of these are covered by the parametric cases summarized in the preceding section. Responses to the complete set are provided below. Those which go beyond the analyses discussed above must be regarded as speculative.

1. What would have been the effect if the auxiliary feedwater system had been available as designed?

In this case (as discussed above and in Sec. III.C of this report), the system would have started depressurizing somewhat earlier than

occurred, but after about 30 min there would have been little difference in the two cases.

2. What would have been the effect if the PORV had closed as designed (assuming auxiliary feedwater was made available at 8 min as occurred)?

Although we did not analyze this case, it is likely there would have been no severe problem. In the accident, water was lost through the PORV and not restored through the HPI system. If the water had not been lost, then a relatively mild pressure transient would have occurred until auxiliary feedwater restored cooling.

3. What would have been the effect if the HPI had not been throttled?

The TRAC parametric case that examined this situation is reported in Sec. III.A. There is more water put in by the HPI than lost through the PORV. The core remains covered and no primary system voids occur. This situation could continue as long as sufficient water was available to the HPI. Evenutally, some final heat sink other than this makeup water, such as the low-pressure safety system, would have to be used to continue cooldown.

4. What would have been the effect if auxiliary feedwater had not been available at any time?

A TRAC parametric case (reported in Sec. III.B) assumed a 60-min delay in auxiliary feedwater. The system equilibrates between energy produced in the core and removed through the PORV. The system pressure remains about 1.5-2.0 MPa (225-300 psia) higher than in the base case due to the lack of heat transfer in the steam generators. The flow out the PORV is higher and the system would empty sooner than in the base case. Core uncovering and heatup would probably begin about 1 h earlier than in the base case.

5. What would have been the effect if the pressurizer relief block valve had not been closed at 2 h and 20 min?

Although we have not analyzed this case, we expect the system would have depressurized until the core flood tanks were activated, which would probably have reflooded and cooled the core.

6. What would have been the effect if the HPI had remained throttled indefinitely?

The TRAC base-case calculation indicates a core peak temperature rise rate of about 0.7 K/s over the last 1 000 s calculated (out to 11 000 s). If extrapolated linearly, this indicates initiation of fuel melting at about 3 h and 45 min. However, the TRAC modeling does not include several effects (such as cladding ballooning, cladding swelling, noncondensible gas in the steam flow, radiation heat transfer) which might have influenced the core heatup rate beyond 2-1/2 h. This extrapolation to incidence of fuel melting is thus speculative.

II. TMI-2 BASE-CASE CALCULATION

The TRAC-P1A computer code[1] was used to model and simulate the initial part of the accident that occurred at the Three Mile Island, Unit-2, nuclear power plant on March 28, 1979. The purposes of this calculation were to:

- Provide insight into the system thermal-hydraulic phenomena which occurred during the initial accident stages.
- Provide a basis to evaluate hypothetical alternative system/operator responses during the accident.
- Provide an estimate of core thermal response as a basis for calculations of cladding deformation, oxidization, and failure.
- Evaluate and assess the applicability of TRAC to non-LOCA accident scenarios.

TRAC is a best estimate, nonequilibrium, multidimensional, thermal-hydraulic, steam-water (two-phase) systems analysis computer code written specifically to analyze LOCAs in LWRs. References 1 and 2 to this report contain a complete description of the code and a demonstration of its successful assessment against a wide range of experiments. One important point concerning TRAC is made here. The maximum time-step size for stable computations is limited to a value which when multiplied by the fluid velocity in each computational cell, yields a length smaller than the length of that computational cell. Typically, this results in time-step sizes less than a tenth of a second. For application of TRAC to large-break LOCAs, this is not a limiting concern; however, for transients of considerable duration (several thousand seconds) computer running times are quite large (many hours on a CDC-7600 class machine). Finally, even when relatively large time steps (fractions of a second) are permissible based on the above condition, smaller time steps are necessary to control numerical error. This problem has a direct bearing

on the model described in the next section. Typically, TRAC calculations of reactor systems use on the order of 750 cells; for the TMI-2 accident prediction, practical computing limitations constrained the total number to less than 100.

A. TRAC TMI-2 Model

A schematic of the TRAC noding used for the TMI-2 model is shown in Fig. 1. The model consists of a vessel and two primary coolant loops. Each loop contains a primary coolant pump and OTSG. The HPI to each cold leg is modeled, and the letdown system and pressurizer are attached to the A loop. In the actual system there are two cold legs per loop, each with a primary coolant pump, but these were combined in the TRAC model to reduce the number of cells.

The three-dimensional vessel noding is shown in Fig. 2. The vessel consists of 177 fuel assemblies with 208 fuel rods per assembly (the 15 x 15 array also includes guide tubes). These fuel assemblies are modeled in TRAC using three axial levels, one radial ring, and two azimuthal sectors, for a total of six TRAC core cells. (Levels 2, 3, and 4 in Fig. 2.) With this noding, only two average fuel rods (24.3 kW/m) are used for coupling the fuel rod heat transfer to the fluid dynamics. Two additional rods are also used to model the high- and low-power rods in the core (35.8 and 12.0 kW/m, respectively). The lower plenum, upper plenum, and upper head region are each modeled using one axial level. The entire TRAC vessel model consists of 2 radial rings, 6 axial levels, and 2 azimuthal segments for a total of 24 vessel cells. The vessel noding described above was used for the steady-state calculation and during the first 81 min of the transient. After 81 min, the vessel noding was changed to yield more axial detail for natural convection and core thermal calculations. This revised noding is shown in Fig. 3.

The hot-leg noding consists of three cells in each hot leg to model the inlet nozzle, vertical riser, and "candy-cane" regions. (Components 1 and 11, Fig. 1.) The pressurizer is modeled as a constant pressure break for the steady-state calculation (component 121 in Fig. 1). For

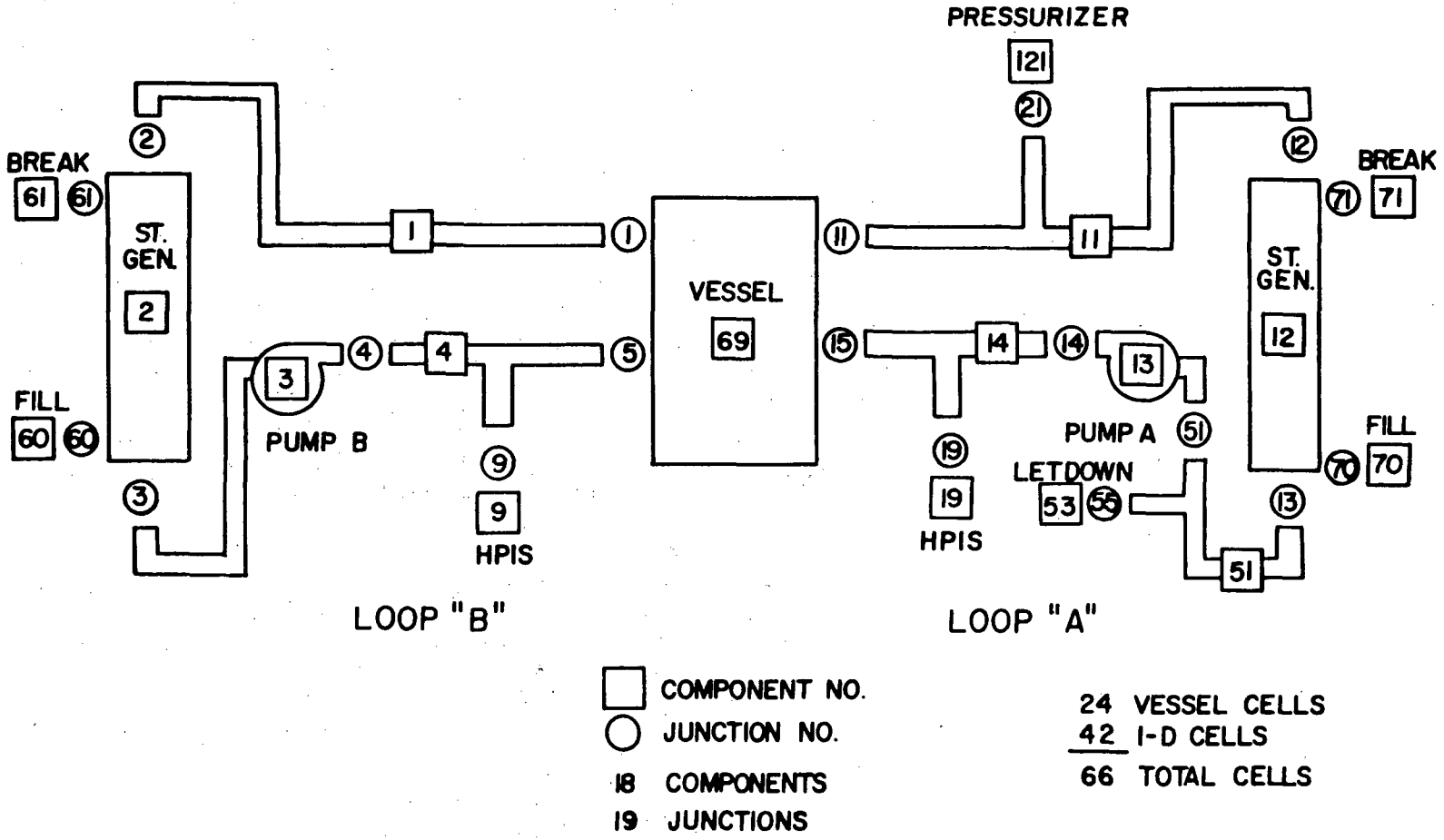

Fig. 1. TRAC noding schematic for TMI-2.

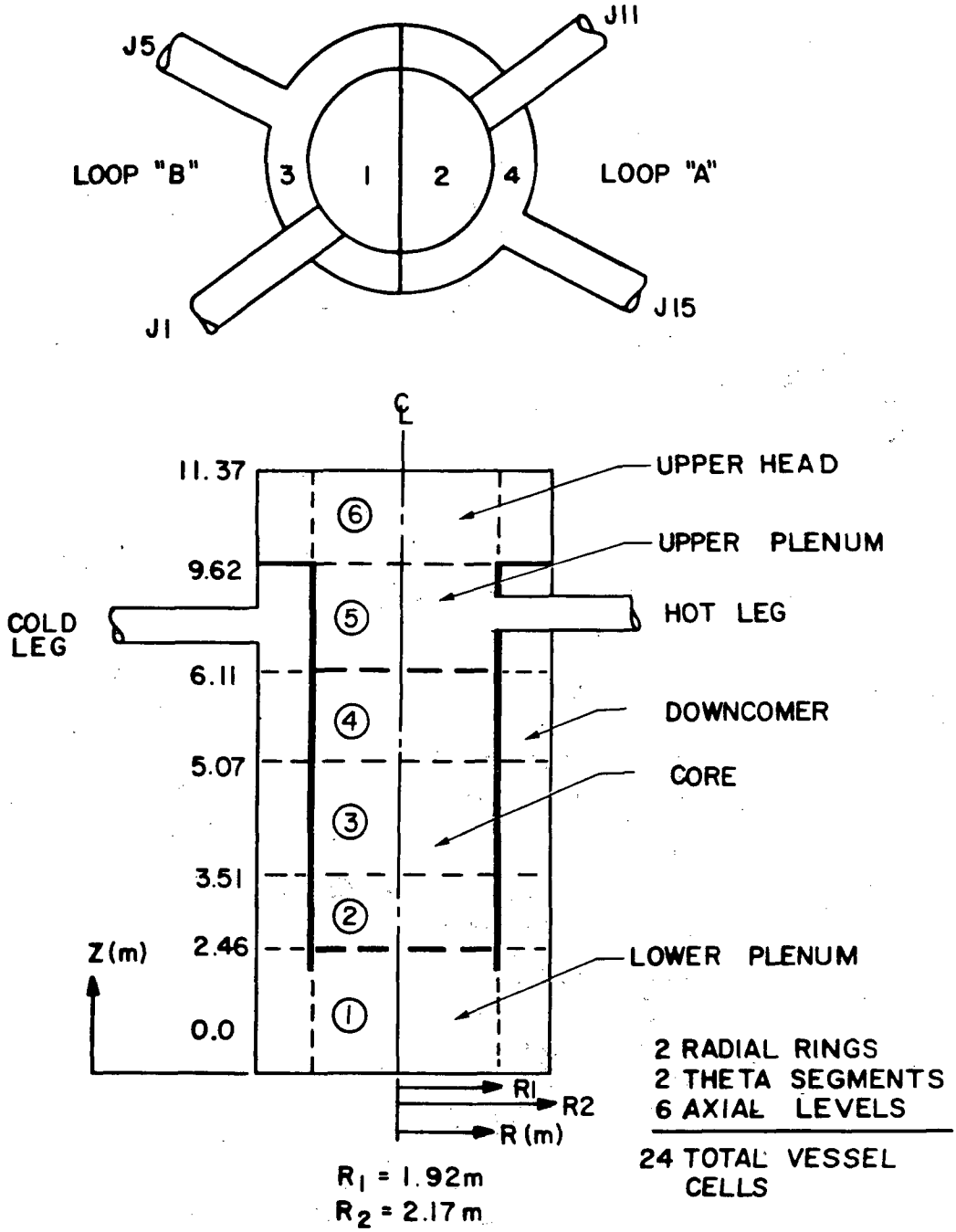

Fig. 2. Vessel noding used for first 81 min.

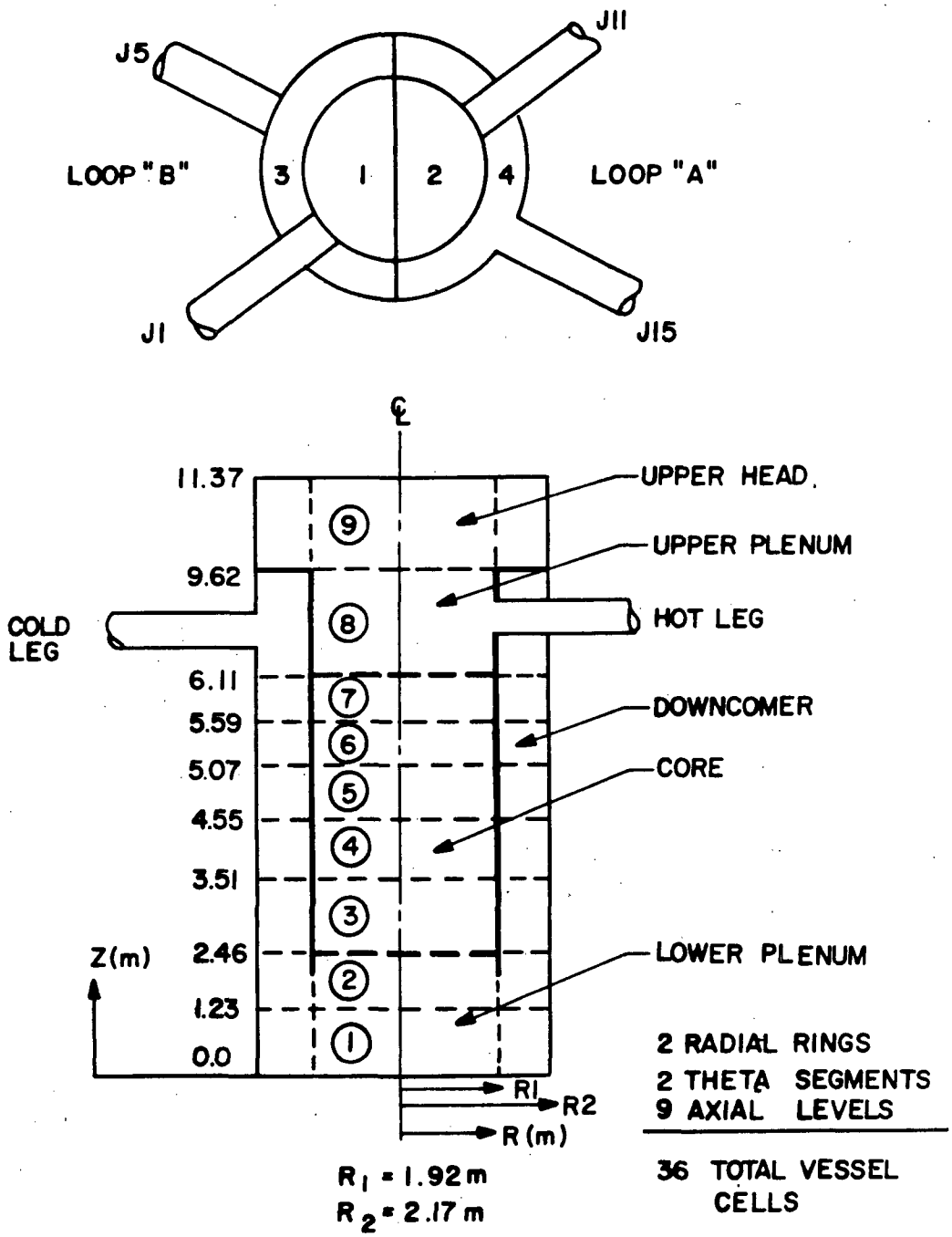

Fig. 3. Vessel noding used after 81 min.

the transient calculation, however, the pressurizer is modeled using two pipe components as shown in Fig. 4. The lower pipe models part of the pressurizer surge line and the bottom section of the pressurizer and the upper pipe models the top of the pressurizer and the pressurizer relief valve. The choking in the relief valve is modeled by using the fully implicit hydrodynamics option (one-dimensional components) in TRAC. Using very fine noding, the choking is calculated naturally from an implicit solution of the equations of mass, momentum, and energy. The OTSGs are modeled using seven cells on the primary side and five cells on the secondary side (Fig. 5). The complete secondary system is not modeled; the boundary conditions to the OTSGs describing the feedwater flow and steam line back-pressure are given by known system conditions during the accident.

B. Steady-State Calculation

Based on the geometry and noding described above, a steady-state calculation was performed to obtain initial conditions prior to the accident. The input parameters for the steady-state calculation are shown in Table I.[3] TRAC-calculated initial conditions are shown in Table II along with a comparison with the results from the Babcock and Wilcox (B&W) code CRAFT-2.[4] The agreement appears to be quite good for all parameters. The differences in flow rates and temperatures can be attributed to the fact that CRAFT-2 used 100% power, whereas, for TMI-2 on March 28, 1979, the power was actually 97%, which was the value used in TRAC. The difference between the calculated primary system water masses is due to the fact that TRAC includes the mass of the steam generator secondary side but CRAFT-2 does not.

C. Transient Calculation

Using the steady-state results, the transient calculation was initiated. For the transient, boundary conditions were required for the steam generator secondary side, pressurizer relief valve back-pressure, etc. These boundary conditions are summarized in Table III and shown

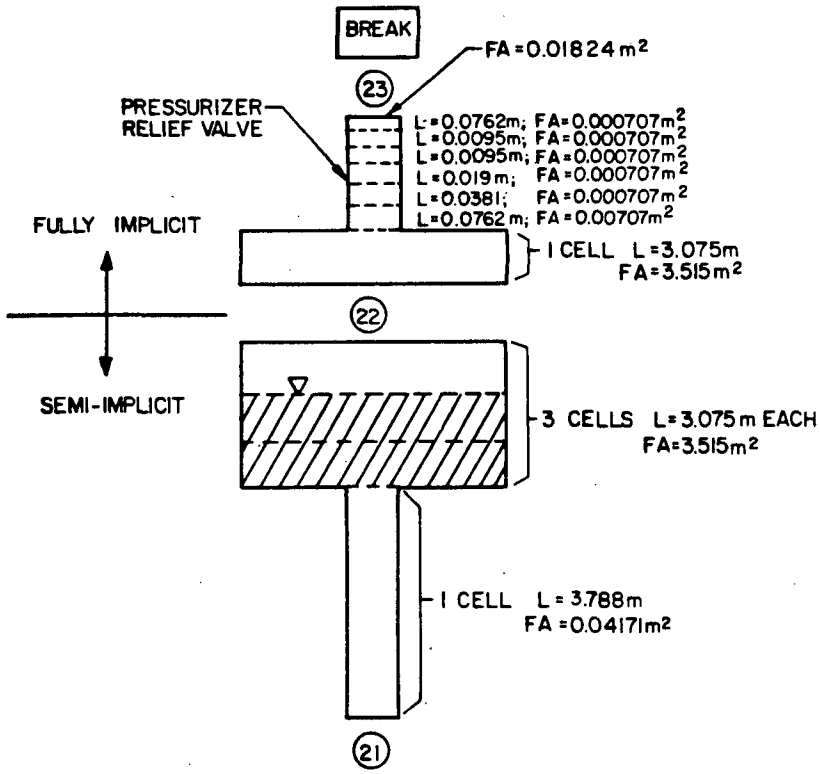

Fig. 4. TRAC pressurizer model.

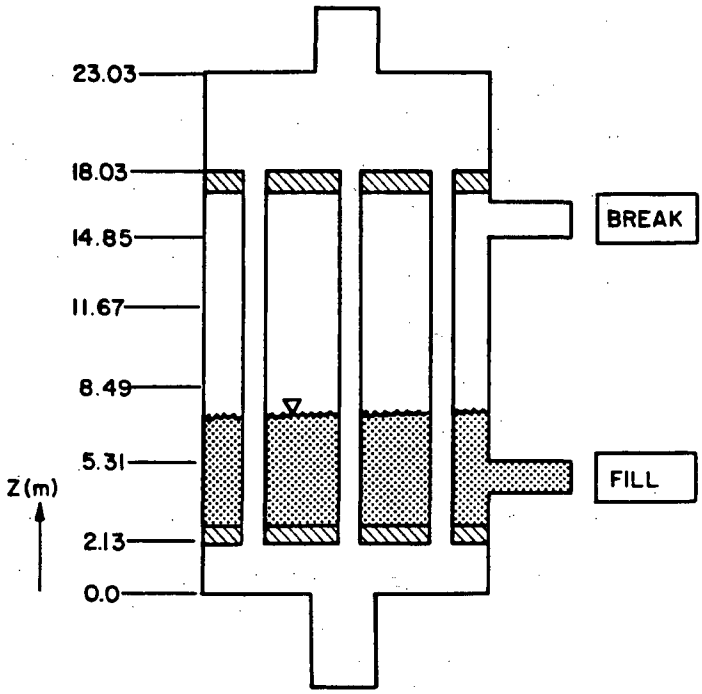

Fig. 5. TRAC steam generator model.

TABLE I

THREE MILE ISLAND - UNIT 2

TRAC Input Parameters

	Parameter	Value
1.	Initial Power (97% of rated)	$2.711\ 78 \times 10^9$ W
2.	Relative Axial Power Shape (3 levels - bottom to top)	0.64, 1.0, 0.76
3.	Relative Radial Power Shape	1.0
4.	Core Average Linear Power	$2.014\ 4 \times 10^4$ W/m
5.	Peak Rod Linear Power	$2.444\ 2 \times 10^4$ W/m
6.	High Power Rod Linear Power	$3.589\ 2 \times 10^4$ W/m
7.	Low Power Rod Linear Power	$1.197\ 5 \times 10^4$ W/m
8.	Pressurizer Pressure	$1.477\ 21 \times 10^7$ Pa

in Figs. 6-11. A sequence of events was also needed to simulate operator interaction with the system and actual plant signals or trips that occurred. Using available information,[5-8] a sequence of events was developed and is shown in Table IV. The values used for HPI, makeup, and letdown flows were obtained from plant data and event chronology, where available. For certain portions of the transient some of the conditions had to be assumed. These assumptions and others used for the transient are shown in Table V.

The transient calculation was initiated by turning off the feedwater flow to the steam generators. As the system pressurizes above normal operating range the PORV at the top of the pressurizer opens. The system pressure continues to rise until the reactor is scrammed at about 10 s. A depressurization period then begins and the system pressure drops until the steam generator secondary side dries out at about 2 min. The system again begins to pressurize due to loss of heat sink in the steam generators and continues until auxiliary feedwater flow is established at about 8 min. Then, the system depressurizes due to enhanced heat transfer in the steam generators until an equilibrium state is achieved between the decay heat produced in the core, energy removal

TABLE II

THREE MILE ISLAND - UNIT 2

Calculated Initial Conditions at Steady State

	Parameter	TRAC	CRAFT-2
1.	Average Hot-leg Temperature at Vessel Outlet (K)	592.3	593.0
2.	Average Cold-leg Temperature at Vessel Inlet (K)	564.1	564.5
3.	Total Primary System Flow Rate (2 loops) (kg/s)	17 027.0	17 375.5
4.	Average Hot-leg Pressure at Vessel Outlet (Pa)	1.475×10^7	1.472×10^7
5.	Average Cold-leg Pressure at Vessel Inlet (Pa)	1.504×10^7	1.534×10^7
6.	Pump ΔP (Pa)	7.87×10^5	7.87×10^5
7.	Steam Generator Secondary Side Flow Rate (each) (kg/s)	700.0	
8.	Average Steam Generator Secondary Side Pressure (Pa)	65.5×10^6	
9.	Cladding Surface Temperatures at Core Level 2: (K)		
	a. Average Rod	605.0	
	b. High Power Rod	614.1	
	c. Low Power Rod	595.0	
10.	Total Primary System Water Mass (kg)	2.774×10^5	2.765×10^5

in the steam generators, and energy removal through the break. Figure 12 shows the actual TMI-2 pressure history for the first 30 min of the accident and the comparison with the TRAC calculation.[9] Figure 13 shows the loop fluid temperature response for the first 30 min and the comparison with TRAC. The pressure and temperature comparisons are in good agreement with the data for this period.

During the first 30 min, the pressurizer water level initially drops, then rises, as shown in Fig. 12. When the PORV opens, saturated steam

TABLE III

THREE MILE ISLAND - UNIT 2

Boundary Conditions

1. Reactor Power vs Time
2. Pump Speed vs Time:

A.	Pump Loop B:	$0 \leq t \leq 4\,380.0$	125.7 rad/s
		$t > 4\,380.0$	0.0 rad/s
B.	Pump Loop A:	$0 \leq t \leq 6\,000.0$	125.7 rad/s
		$t > 6\,000.0$	0.0 rad/s

3. HPI Flow vs Time
4. Pressurizer Relief Valve Back-pressure vs Time
5. Steam Generator Steam Line Back-pressure vs Time
6. Steam Generator Feedwater Flow vs Time

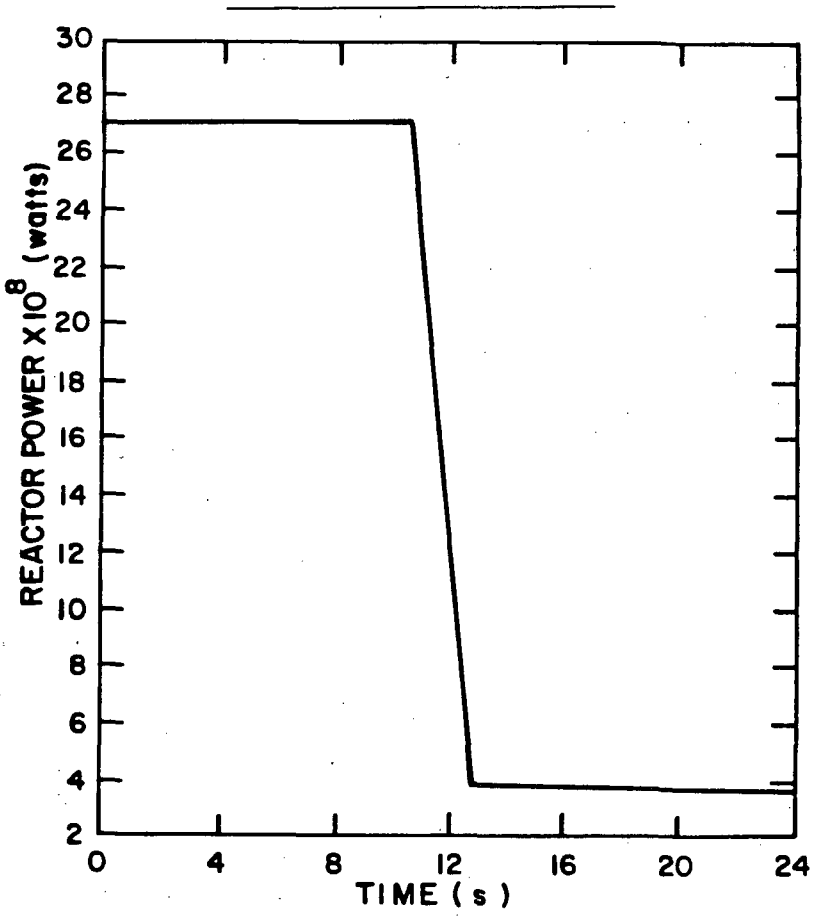

Fig. 6. Reactor power.

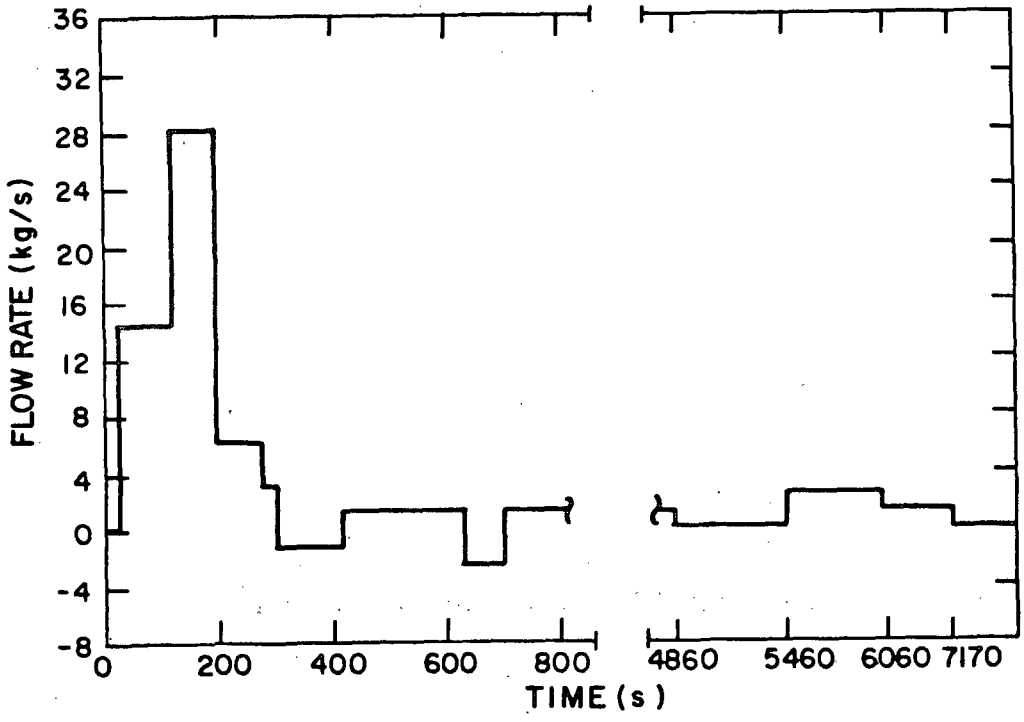

Fig. 7. HPI flow rate for each loop.

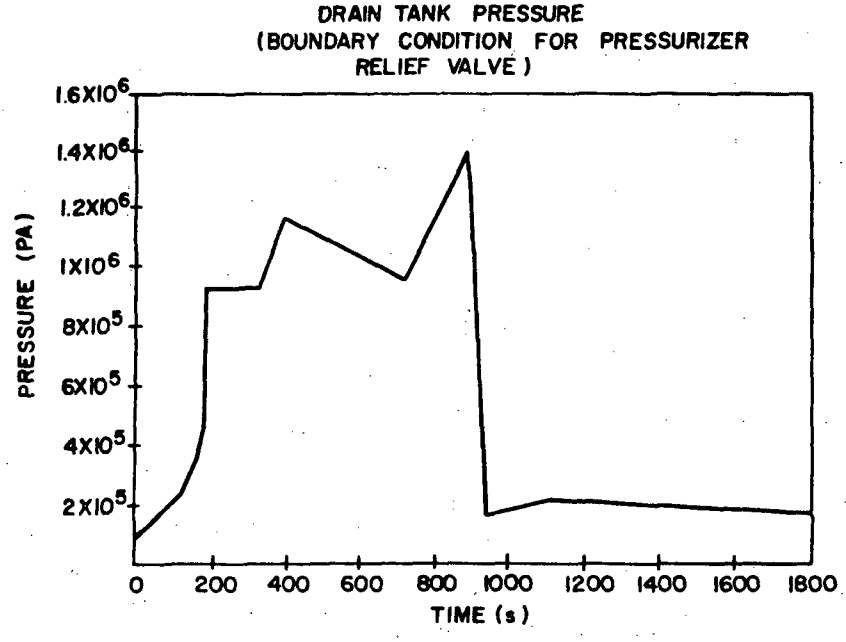

Fig. 8. Relief valve back-pressure.

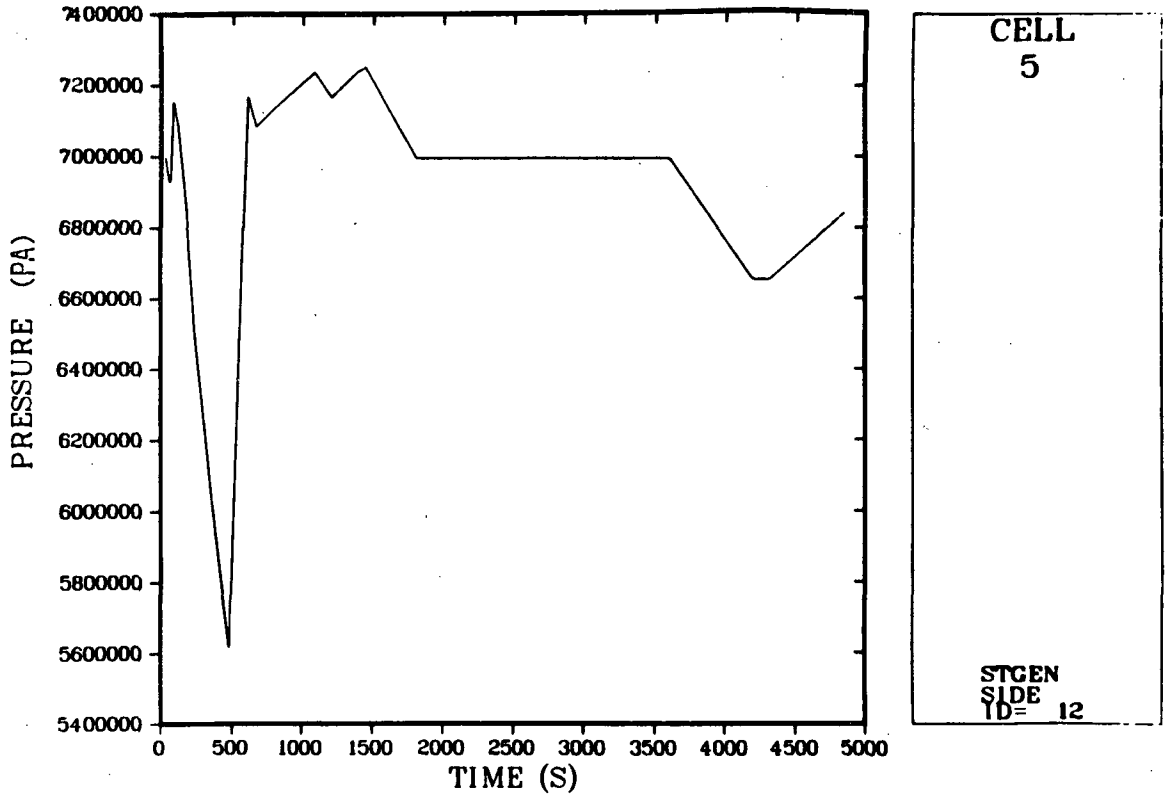

Fig. 9. A Loop steam generator back-pressure.

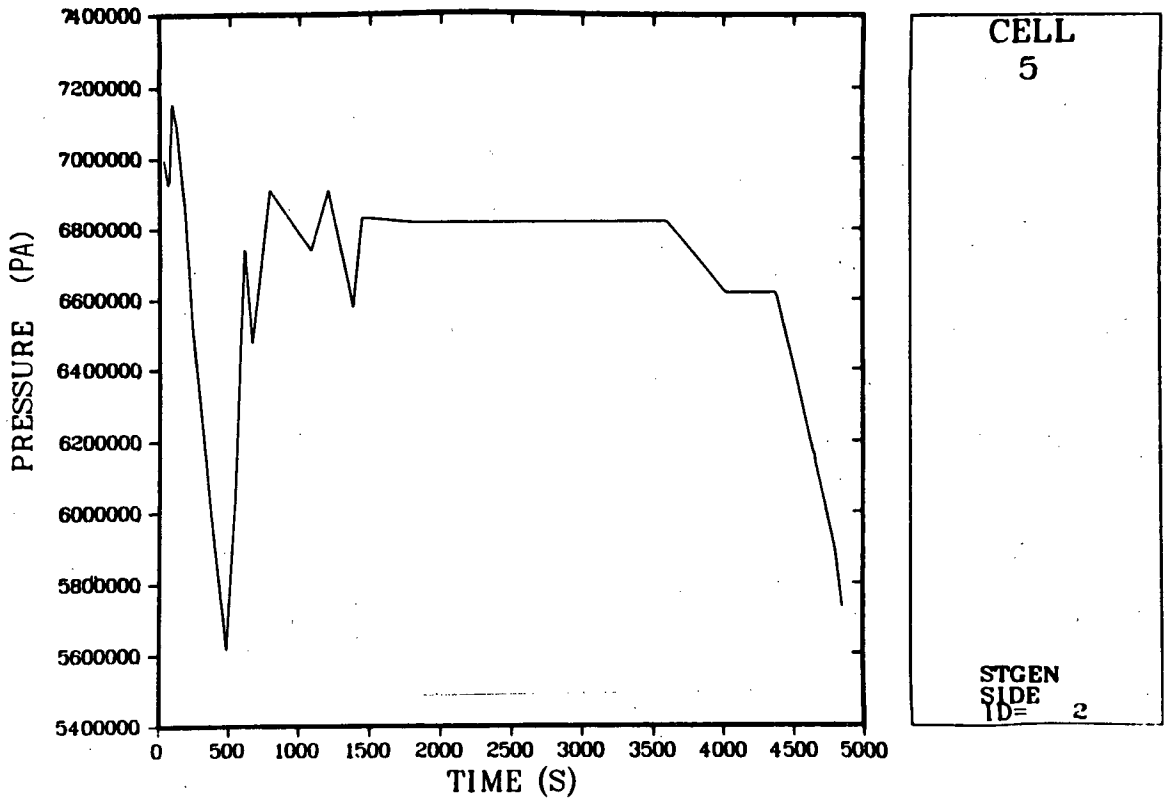

Fig. 10. B Loop steam generator back-pressure.

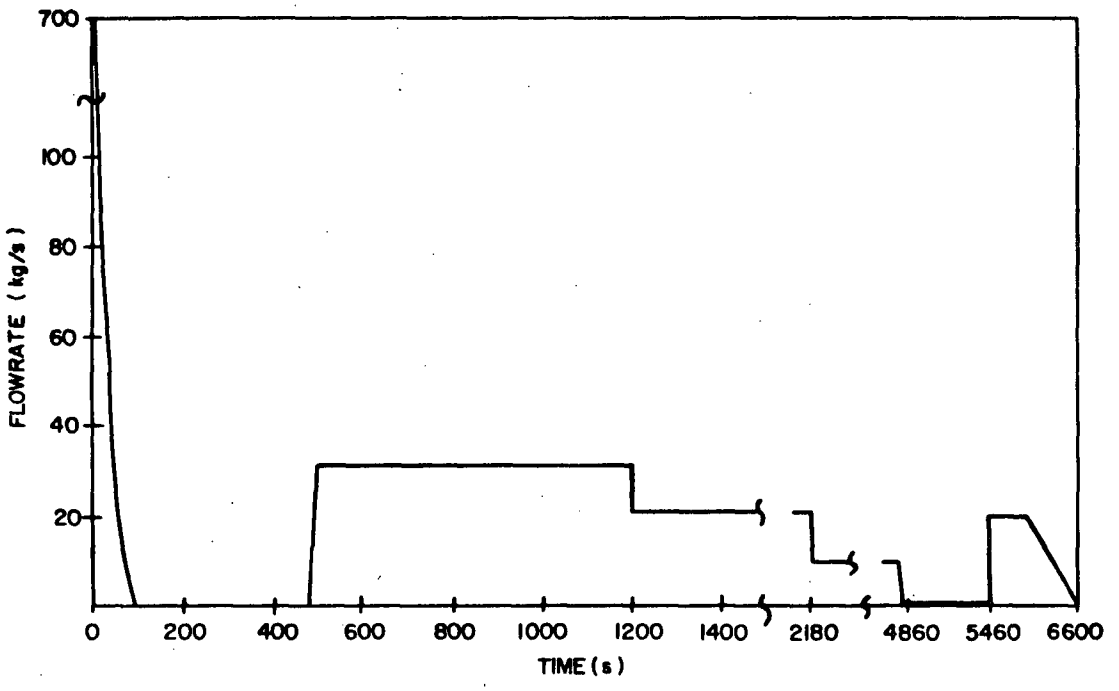

Fig. 11. Auxiliary feedwater flow for each steam generator.

at the top of the pressurizer rapidly escapes and the pressurizer water level rises as the steam volume at the top of the pressurizer is replaced with a two-phase mixture. When the two-phase mixture begins to leave the PORV, the mass flow rate increases and the water level begins to drop rapidly as the pressurizer empties. The pressurizer continues to empty until the makeup and HPI systems are started, at which time the water level begins to rise. The makeup, letdown, and HPI flows used during the first 8 min were mainly to control the water level in the pressurizer. The pressurizer then remains full until the water becomes saturated at about 10 min. At this time, flashing of the water begins as the system depressurizes and the water level drops until the system pressure stabilizes. The pressurizer then fills and remains essentially full until approximately 85 min.

For the period from 30 min until 80 min, the system is in a quasi-steady-state mode in which the energy produced in the reactor core is removed primarily in the steam generators. Due to good heat transfer in the steam generators, the primary system pressure closely follows the back-pressure on the secondary side (Figs. 9, 10, and 14). The fluid temperatures in the system are at saturation during this time and are

TABLE IV

THREE MILE ISLAND - UNIT 2

Sequence of Events Used for Base-Case Calculation

Time (s)	Event
0.0	Loss of Feedwater Flow
10.5	Trip Reactor Power
13.0	Start Make-up Pump 1A Full Flow 27.5 kg/s
120.0	Start Make-up Pump 1C Full Flow 27.5 kg/s
194.0	Throttle Pumps 1A and 1C to 6.1 kg/s each
278.0	Trip Pump 1C - Continue Pump 1A at 6.1 kg/s
300.0	Initiate Letdown Flow of 8.6 kg/s
418.0	Reduce Letdown Flow to 4.5 kg/s
480.0	Start Auxiliary Feedwater Flow of 31.3 kg/s (each OTSG)
624.0	Trip Pump 1A - Continue Letdown Flow
700.0	Start Pump 1A (Makeup + HPI = 1.85 kg/s)
3 824.0	Turn Off Letdown
4 380.0	Trip Primary Pumps - Loop B
4 860.0	Turn Off HPI and Auxiliary Feedwater Flow
5 460.0	Initiate HPI - 4.4 kg/s
	Initiate Letdown - 4.4 kg/s
	Initiate Auxiliary Feedwater Flow to OTSG "A" - 31.3 kg/s
6 000.0	Trip Primary Pumps - Loop A
6 060.0	Reduce HPI - 2.2 kg/s
	Increase Letdown - 15.0 kg/s
7 170.0	Turn Off HPI and Decrease Letdown - 4.5 kg/s
8 280.0	Shut Pressurizer Block Valve and Turn Off Letdown

TABLE V

ASSUMPTIONS FOR TMI BASE CASE

1. Decay Power Obtained from "Nuclear Legislative Advisory Service," Issue 17, April 13, 1979.
2. Feedwater Flow vs Time Ramped to Zero Over a 90-s Time Interval at Beginning of Transient. (90 s was used in order to account for the stored water mass in the OTSG downcomer.)
3. Make-up Pump Full Flow Capacity of 27.5 kg/s (each).
4. Throttled Flow Rate for Make-up Pumps of 6.1 kg/s.
5. Letdown Flow is Assumed to be Equal to Make-up Flow for $T < 13$ s for $T > 8\ 280.0$.
6. Letdown Flow Greater Than Make-up + HPI for $600 \leq t \leq 8\ 280$ s.
7. Auxiliary Feedwater Flow is 31.3 kg/s for each OTSG (later reduced to match secondary side water level).
8. Pressurizer Relief Valve Noding Determined by Using Rated Saturated Steam Flow Conditions of 15.0 kg/s.
9. From t = 101 min until 120 min, 15 kg/s Letdown Flow was Used to Match Primary System Pressure.
10. Pressurizer heaters and sprayers were not modeled.

---

following the system pressure. Figures 14-16 show the actual pressure and temperature histories, along with the TRAC calculation. Since the pressure is relatively constant during this period, the break flow out the PORV is also constant at about 20 kg/s. (Fig. 17.) Coolant is continually being lost from the system through the PORV. Also, coolant is being lost through the letdown system since it was assumed that letdown flow was in excess of HPI and makeup flows by about 2.7 kg/s. The system is at saturation during this period and coolant is being continually lost, producing voids throughout the primary side. Figure 18 shows a void fraction profile in the vessel for the first 80 min. The curves represent the void fraction in each axial level from the bottom to the top of the vessel (refer to Fig. 2 for the vessel noding diagram). The upper head completely voids at about 27 min and remains voided for the entire calculation.

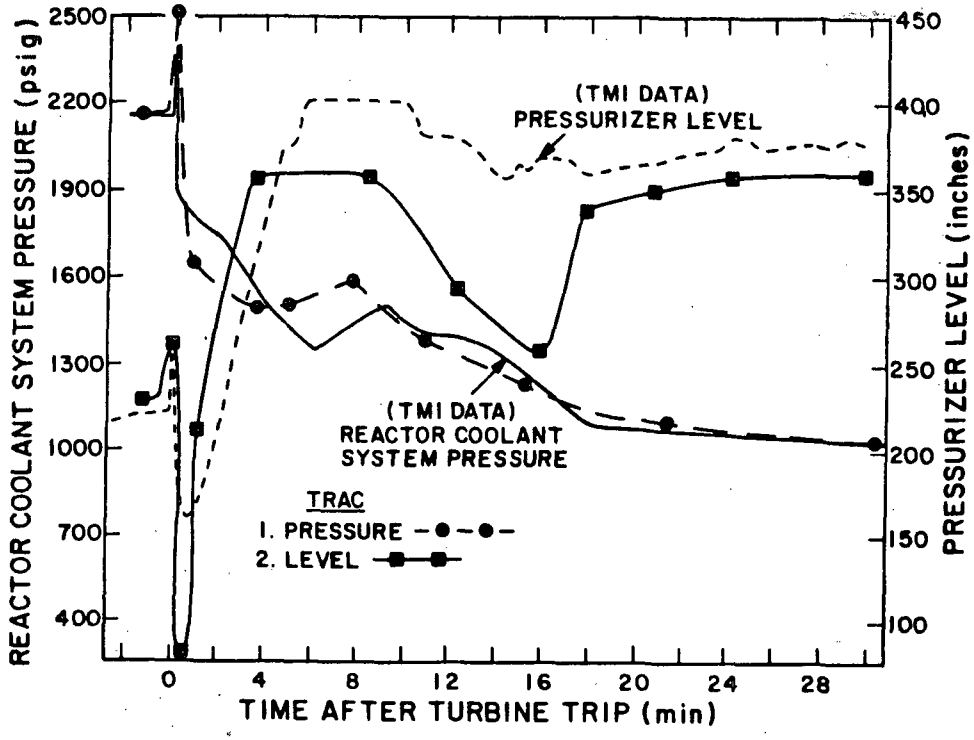

Fig. 12. TRAC comparisons with TMI data for first 30 min.

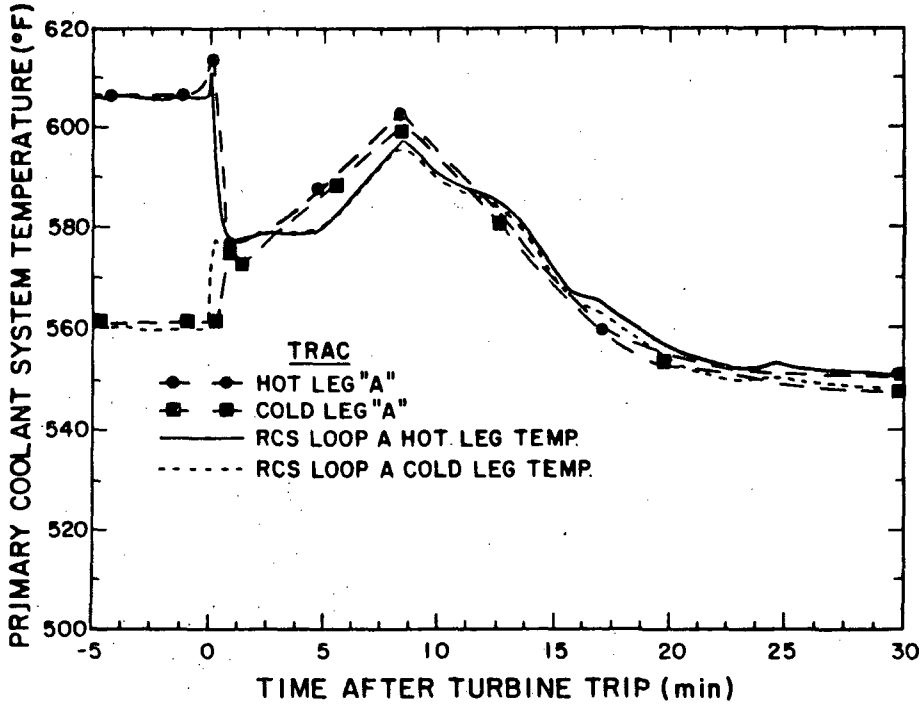

Fig. 13. A Loop fluid temperature comparisons.

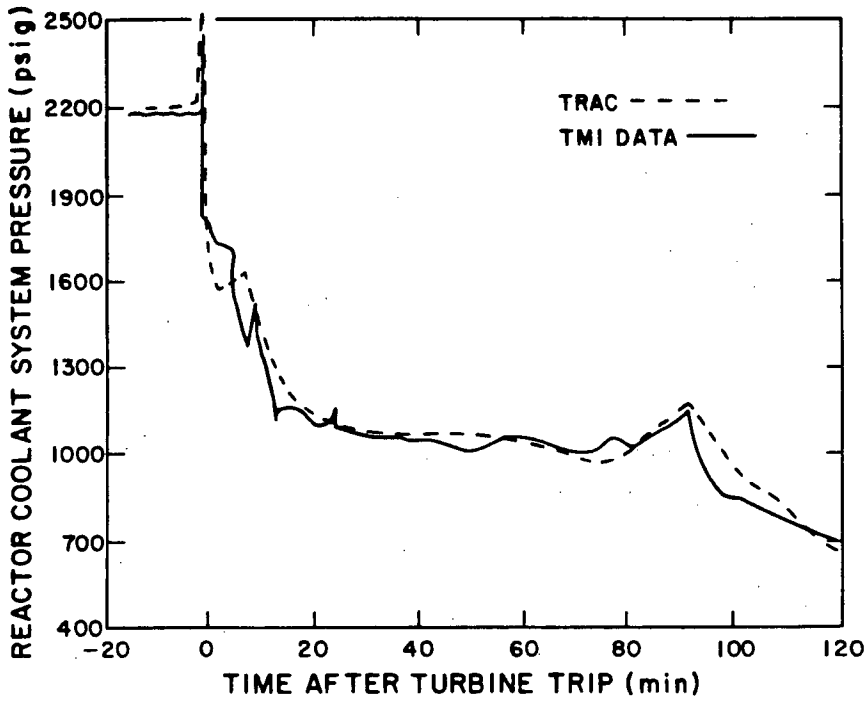

Fig. 14. System pressure comparisons out to 120 min.

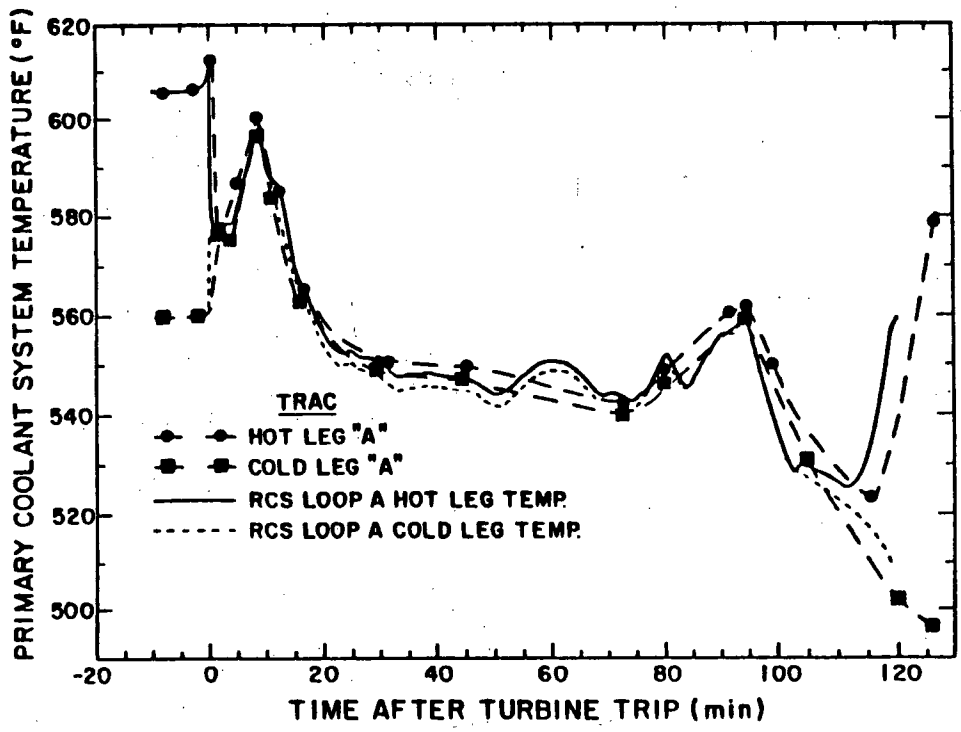

Fig. 15. A Loop fluid temperature comparisons out to 120 min.

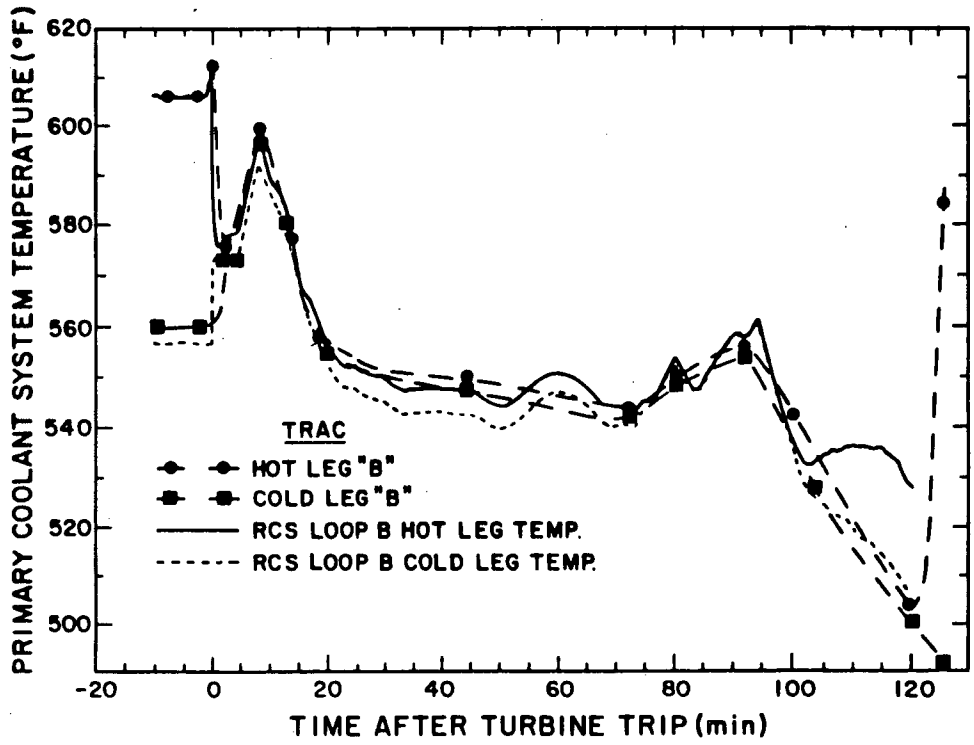

Fig. 16. B Loop fluid temperature comparisons out to 120 min.

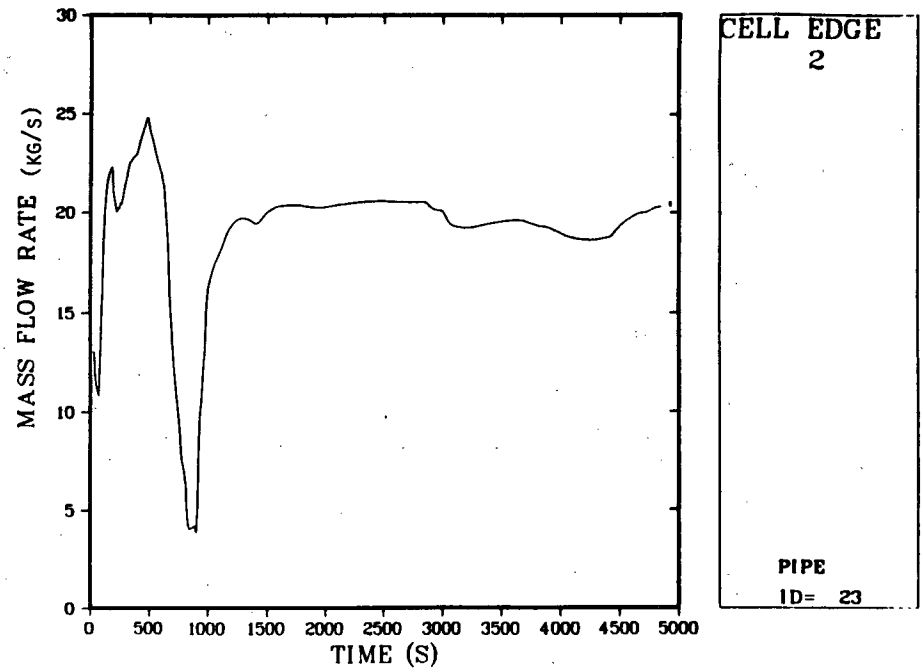

Fig. 17. Pressurizer relief valve flow rate for first 81 min.

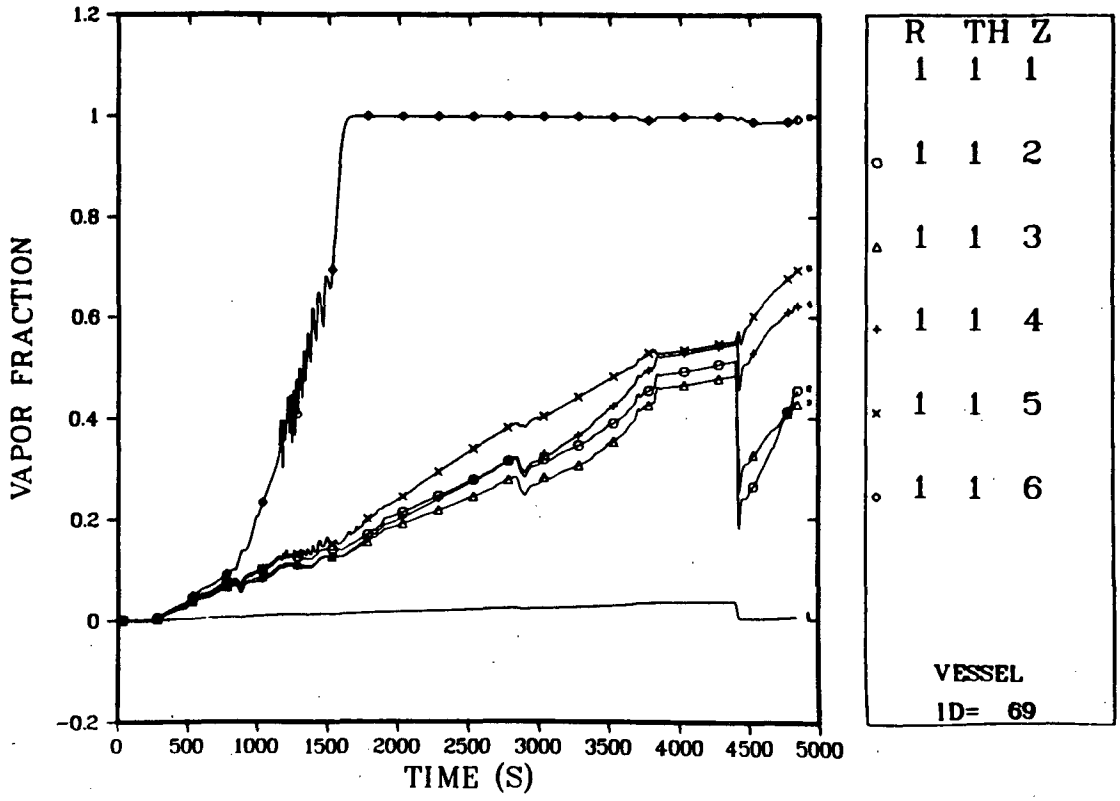

Fig. 18. Vessel void fraction profile out to 81 min.

The core regions are producing voids at roughly a constant rate until the B Loop pumps are tripped at 73 min. At this time, phase separation occurs in the B Loop and the resulting elevation head in the loop is high enough to force some water into the vessel. This results in a void fraction drop in the core region, but this additional water is rapidly boiled off. Although the void fraction in the core is increasing during this period, the fuel rods remain cool due to nucleate boiling heat transfer in the core region. The fuel rods remain cool until the core partially uncovers at 101 min. Since there are significant voids throughout the system, the pump heads and mass flow rates are degrading due to two-phase flow losses. (See Appendix for pump mass flow rates and other system variables during this period.) Although the B Loop pumps are tripped at 73 min, the fuel rods remain cool due to adequate forced convection from the A Loop pumps and the PORV flow.

For the period from 80 min to 138 min, the system is in more of a transient mode as opposed to the previous quasi-steady mode. The transient mode first starts when the B Loop pumps are tripped and the secondary side pressure of the B Loop OTSG begins to drop (Fig. 10). This drop in back-pressure causes the primary side to also drop slightly in pressure until adequate heat transfer (forced convection) is lost. When this happens, the system pressure begins to rise (Fig. 14) due to loss of heat transfer in the B Loop steam generator and the increasing A Loop steam generator back-pressure (Fig. 9). Since the A Loop pumps are still running, good heat transfer is still available through the A Loop steam generator, causing the primary system pressure to follow the secondary side pressure. At 91 min, the primary system pressure begins to decrease due to increased auxiliary feedwater flow to the A Loop steam generator and increased letdown flow. This also causes the pressurizer water level to decrease (Fig. 19). The system pressure continues to decrease at a constant rate until the A Loop pumps are tripped. The slope of the pressure curve then changes due to loss of forced convection through the A Loop steam generator. The TRAC calculation does not show this change in slope as dramatically as the data (Fig. 14); however, the agreement is still reasonable. The loop temperatures are shown in Figs. 15 and 16. During this time, the temperatures are essentially following the system pressure.

When the A Loop pumps are tripped at 100 min, phase separation occurs throughout the system and the core becomes partially uncovered (top two core levels in the vessel, Fig. 3). This is graphically illustrated in Fig. 20 which shows the void fraction profile in the vessel (note that the vessel noding was refined at 80 min to more accurately track the water level in the core, Fig. 3). When the core uncovers, the fuel rod temperatures (hot rod) increase to about 700 K (Fig. 21). This temperature rise was terminated due to core rewetting caused by some of the water in the loops emptying out into the vessel. As in the case when the B Loop pumps were tripped, phase separation in the loops results in an elevation head in the steam generator which is large enough to force some water into the vessel. This additional water in the core begins to boil off as the system depressurizes and the core again begins to uncover

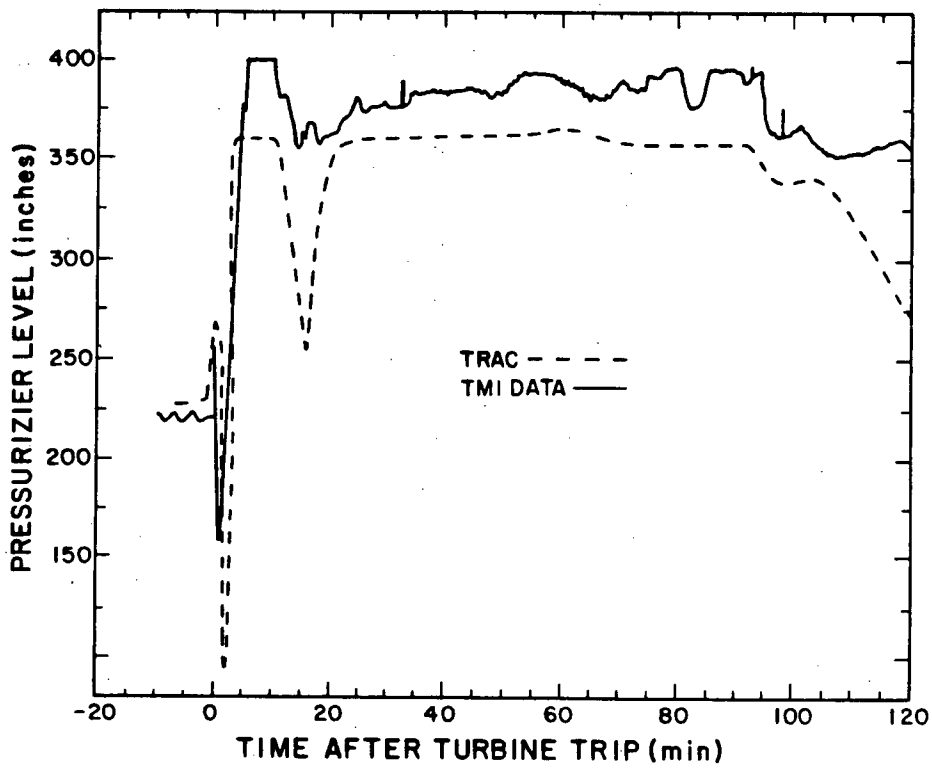

Fig. 19. Pressurizer water level comparisons out to 120 min.

at about 120 min. From this point on, the fuel rods continue to increase in temperature.

The beginning of core uncovering at 100 min, as calculated by TRAC, is in agreement with the data analyzed by EPRI.[5] For example, in comparing the mass inventory in the primary system from the TRAC calculation to that reported by EPRI, it is seen that after 100 min TRAC calculates the total system mass loss to be 1.275×10^5 kg, while EPRI gives a range of 1.05×10^5 kg (minimum) to 1.235×10^5 (maximum). TRAC is calculating about 3% higher mass loss than the EPRI maximum estimate.

It is important to note that in order for TRAC to calculate the depressurization from 100-138 min, a large letdown flow had to be used (15.0 kg/s). This is because the PORV flow severely degrades (Fig. 22) after the A Loop pumps trip and the water level drops in the pressurizer (Fig. 19). The PORV flow drops from 20 kg/s to an average of about 6 kg/s over this period. Another variable that is important during this period is the HPI flow rate. Several sequence of events reports

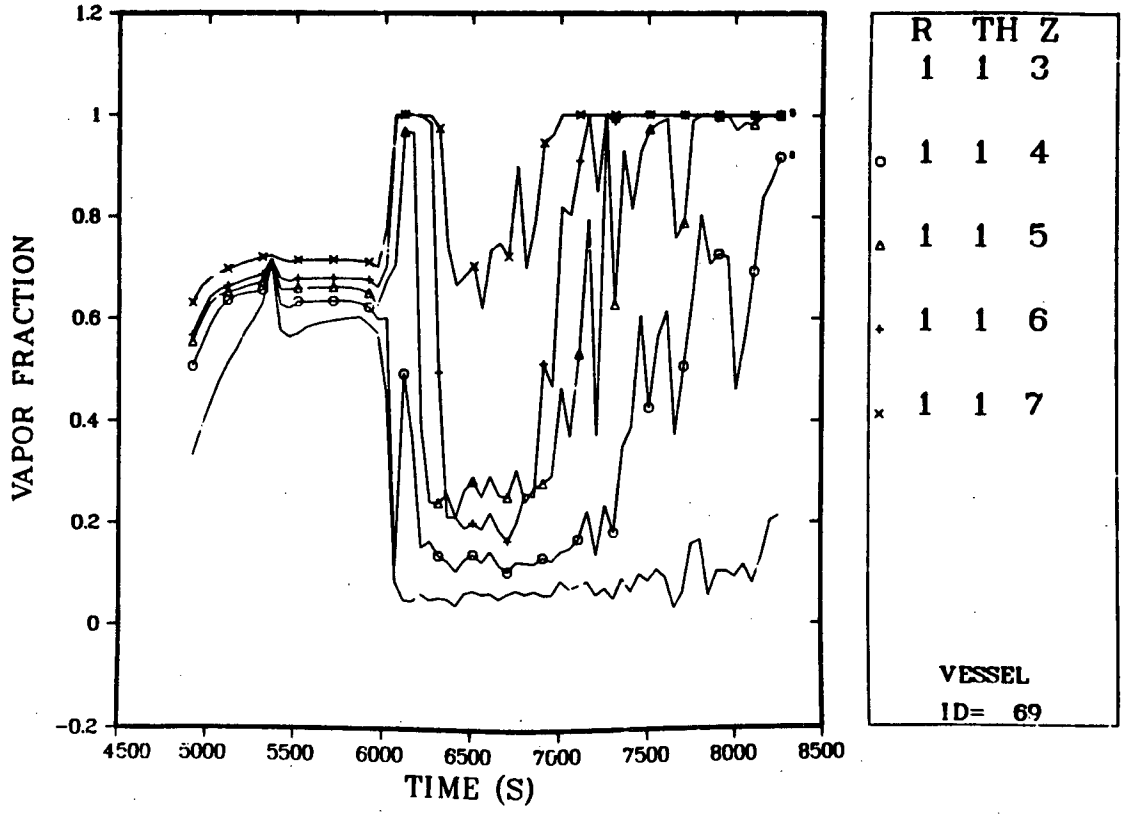

Fig. 20. Core void fraction axial profile after 81 min.

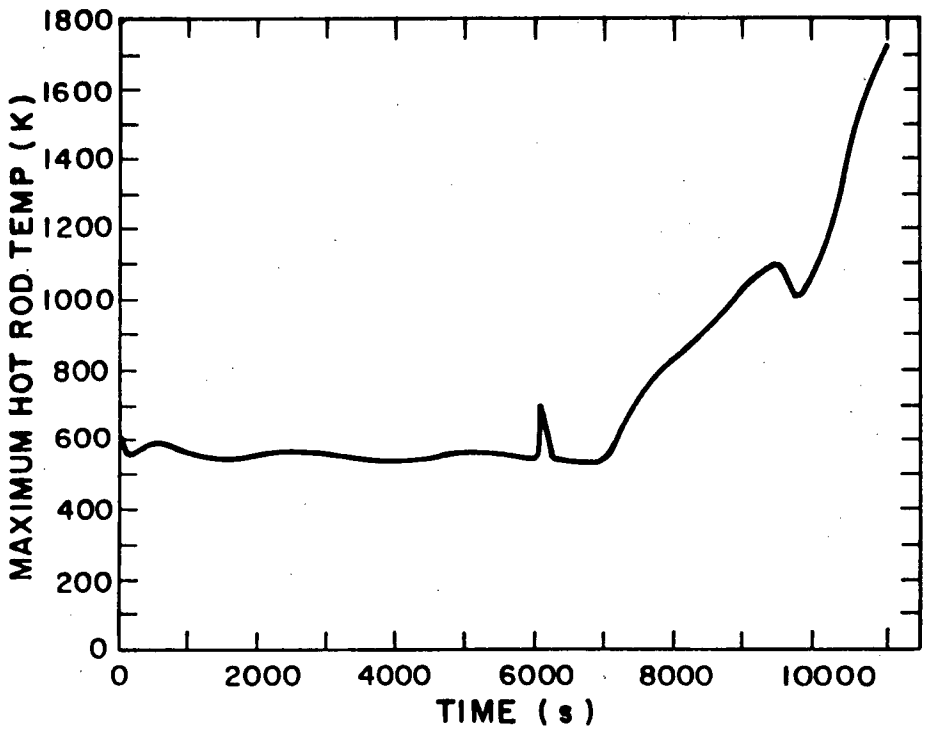

Fig. 21. Maximum hot-rod cladding temperature.

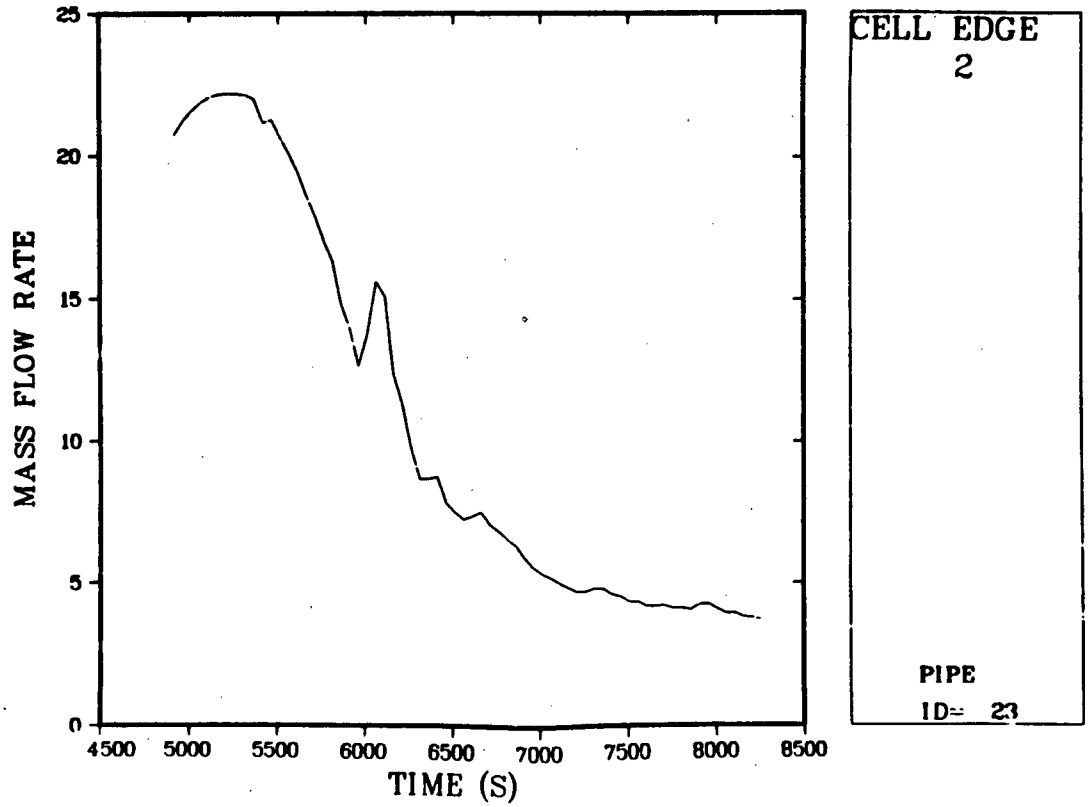

Fig. 22. Pressurizer relief valve flow rate after 81 min.

state that HPI flow was increased after 100 min, but no values are given. If it was increased, condensation would also cause the system to depressurize. However, since no value was given, the best estimate value of 2.2 kg/s was used. The letdown flow used during this period accounts for the flow rate drop in the PORV and the increased HPI flow.

From about 120-138 min the water level in the core is dropping and the rods are heating up at roughly 1 K every 4 s. The vapor velocities are on the order of 0.5 m/s and the PORV and letdown flow rates enhance the flow rate through the core. This causes the heat transfer coefficients to be higher than those calculated by natural convection. The loops are essentially void after 138 min, water remaining only in the pump suction legs. (Refer to the Appendix for additional plots during this period.) The pressurizer level drops, due mainly to liquid flashing caused by depressurization and increased letdown.

At 138 min, the block valve was shut on the pressurizer. In the TRAC calculation, it was also assumed that after 138 min the makeup and

letdown flows are equal. When the block valve is shut, the steam flow in the core stagnates, since there is no path for the vapor to escape. Also, the water in the pump suction legs (loop seals) prevents any flow through the loops, hence, there is no natural circulation through the system. The system begins to pressurize and continues to pressurize for the remainder of the calculation. Figure 23 shows the TRAC calculated pressure history compared to the TMI data. Also shown is the pressurizer water level history. During this period the vapor velocities through the core are generally less than 0.1 m/s and the heat transfer coefficients are very low (on the order of 50 W/m^2s K, representative of natural convection to superheated steam). The vapor begins to superheat since the flow is stagnant and the rod temperatures continue to increase (Fig. 21). Figure 24 shows the vapor temperature in the core during this period for each axial level in the vessel. The corresponding core void fraction profile is shown in Fig. 25.

As soon as the PORV is shut, a pressure oscillation moves through the system which causes some of the water in the lower plenum to be forced up into the core. This is the reason core level 4 has a decrease in void fraction for several hundred seconds. Eventually, this core level dries out at about 160 min. Before this core region dries out it begins to boil the water rapidly and the boiling causes the vapor velocities through the core to increase for a short period of time. The increased vapor velocities cause the heat transfer coefficients to increase and the vapor temperatures to drop, with a resulting drop in rod temperatures (see Figs. 21 and 24 at 9 600 s). But, as soon as this core level dries out the vapor velocities decrease, the vapor begins to superheat, and the rods again heat up. The rods continue to heat up at roughly the same rate as before (1 K every 4 s) until the zirconium-steam reaction begins to provide a significant additional heat source (at 1 273 K). After this time the temperature rise rate increases to about 1 K per s. The calculation was stopped once the temperatures exceeded 1 650 K.

During this period, the lower plenum in the vessel remains full of water and the bottom core level has roughly 70% water remaining in it. Only the top 75% of the core is uncovered. The fuel rod temperatures

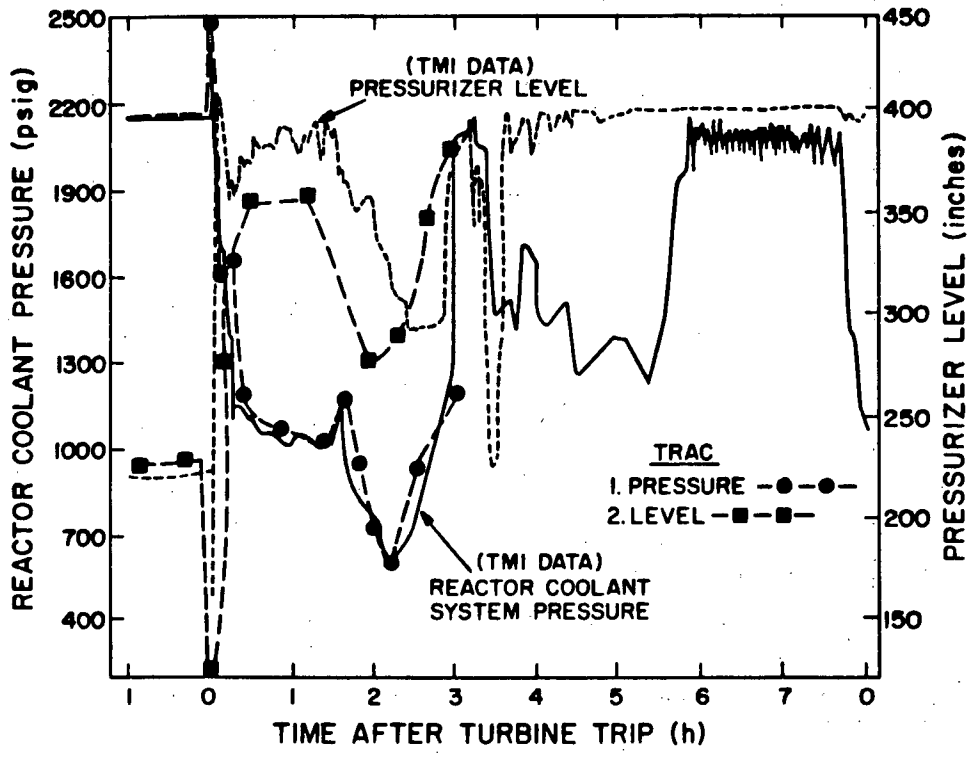

Fig. 23. TRAC comparisons with TMI data out to 3 h.

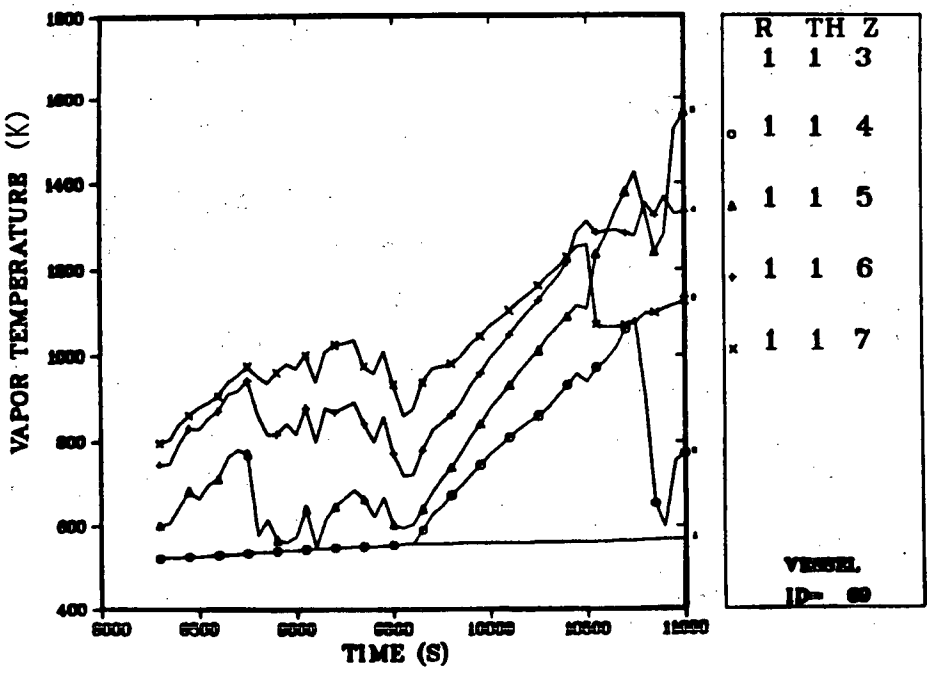

Fig. 24. Core vapor temperature axial profile.

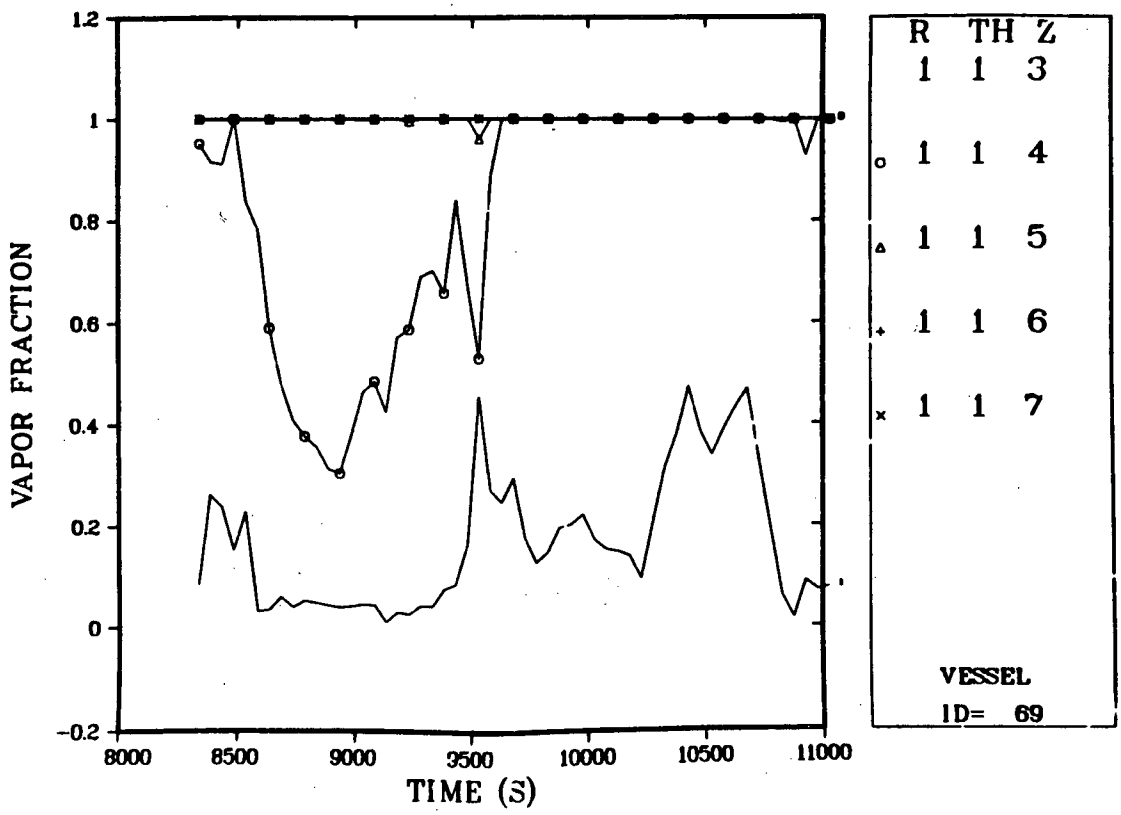

Fig. 25. Core void fraction axial profile after 81 min.

Fig. 25. Core void fraction axial profile after 81 min.

remain relatively cool in the lower core region (see Appendix for additional plots during this period). Also, referring back to Fig. 23, the pressurizer level is increasing both in the TRAC calculation and the TMI data during this time. The pressurizer never empties because steam produced in the core "holds up" the water in the pressurizer.

Overall, for the sequence of events and assumptions used, the TRAC results are in good agreement with the TMI-2 data and they satisfy the objectives listed at the beginning of this section.

III. TRAC PARAMETRIC CALCULATIONS

This section summarizes the results of five TMI-2 parametric calculations performed with TRAC. The first three parametric cases (see Table VI) involve variations in the time of initiation of the auxiliary feedwater and also variations in the HPI flows. The auxiliary feedwater is delayed 60 min following accident initiation in cases A-3 and A-6.* Case A-3 uses full HPI when the pressure is less than 110×10^5 Pa (1 600 psia) and case A-6 assumes "degraded" HPI flows (degraded means as it happened during the TMI-2 accident). Case A-4 assumes that the auxiliary feedwater is turned on at the time of accident initiation and also assumes degraded HPI flows. The fourth parametric calculation assumes that all main coolant pumps trip simultaneously with the reactor trip at 10 s. The last case investigates the effect of a small break in a primary coolant cold leg. All other boundary and initial conditions for these calculations are the same as in the base case described in the previous section. The pressure on the secondary side of the OTSG used for these cases was assumed to be the same as that used for the base case. Since the steam generator secondary side tends to dry out in the calculations to be described, there is only a weak dependence on OTSG secondary side pressure. The TRAC system noding was also the same as used in the base case (Figs. 1-4).

A. Delayed Auxiliary Feedwater/Full HPI (Case A-3)

Figure 26 shows the calculated pressure in a TRAC cell located in the upper plenum for the first 5 000 s of the transient in case A-3. Also shown is the base case pressure for the same cell (other pressures in the vessel are similar). As mentioned previously, case A-3 assumes full HPI flows at a setpoint of approximately 110×10^5 Pa (1 600 psia)

---

*These specific cases were requested by the NRC/TMI Special Inquiry Group and the case number designations are that groups. (The base case was designated A-5.) Other cases are being provided by the Idaho National Engineering Laboratory.

TABLE VI

TRAC PARAMETRIC CALCULATIONS

	Run Conditions	Comments	Case Designation[a]
1.	Auxiliary feedwater delayed until 60 min following accident initiation. Full HPI on when P < 1 600 psia.		A-3
2.	Auxiliary feedwater delayed until 60 min following accident initiation. Degraded HPI.	"Degraded" HPI means as occurred during TMI-2 accident.	A-6
3.	Auxiliary feedwater turned on at accident initiation. Degraded HPI.		A-4
4.	All main coolant pumps tripped at accident initiation. Degraded HPI.		D-2
5.	Cold-leg break with area equivalent to EMOV. Degraded HPI.		---

[a]Case nomenclature adopted by NRC/TMI Special Inquiry Group.[6] Base case was designated A-5.

and a delay in auxiliary feedwater of 60 min. As can be seen from Fig. 26, the initial pressure for case A-3 matches that of the base case until the HPI setpoint is reached. Beyond this point, the HPI is sufficient to keep the pressure in case A-3 at a quasi-steady-state level much higher than the pressure of the base case. Figures 27 and 28 show the HPI mass flow rate (there are two HPI systems with equal flow rates) and the mass flow rate out of the break for case A-3, respectively. Due to a lack of detailed information, the HPI flows are modeled as constant velocity fills after the setpoint is reached. Thus, both HPI flows remain constant at approximately 32 kg/s. The total HPI flows exceed the

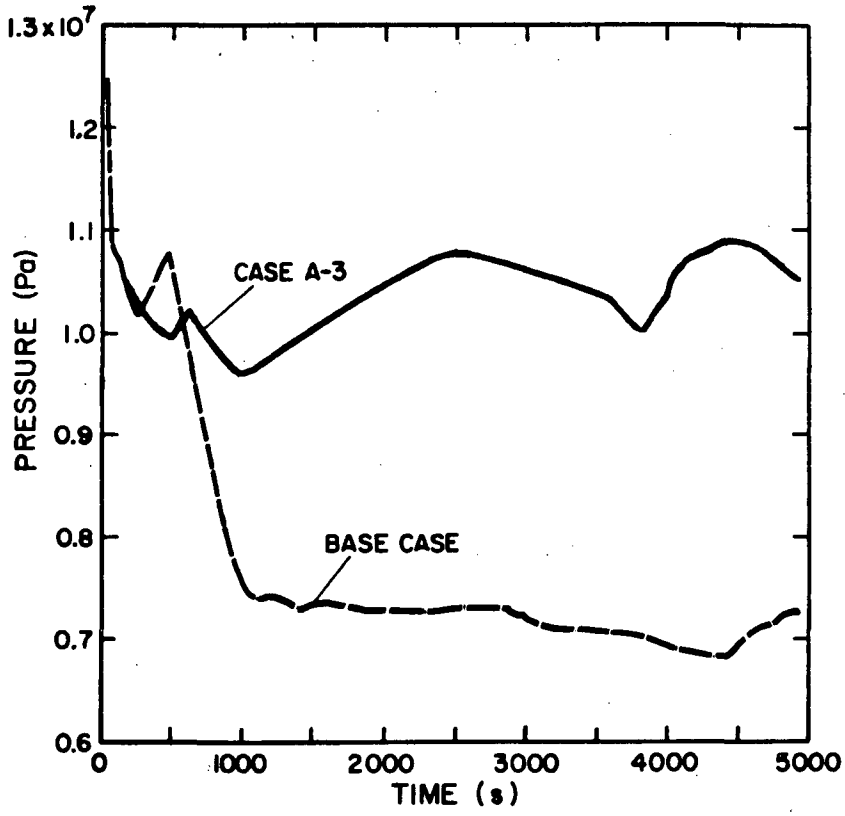

Fig. 26. Parametric case A-3 pressure comparison with base case.

flow out of the break for the first 3 000-4 000 s of the transient. From this point on the total HPI flow rate is approximately equal to the break mass flow rate. Thus, the system is essentially running in a steady-state forced convection mode throughout the transient (assuming the main coolant pumps remain on) and there are no voids formed in the vessel at all for case A-3. Figure 29 shows midplane hot-rod temperatures for case A-3 and the base case. Since no voids form in the core for case A-3 the rod temperatures are well below those of the base case. This calculation was run further out in time than shown in the graphs and the rod temperatures for case A-3 remained low. The delay in auxiliary feedwater injection of 60 min had no effect on the long-term results of this transient. Thus, for this particular case the importance of full HPI flows far outshadows any delay in the auxiliary feedwater and makes the consequences of this transient mild compared to the base case.

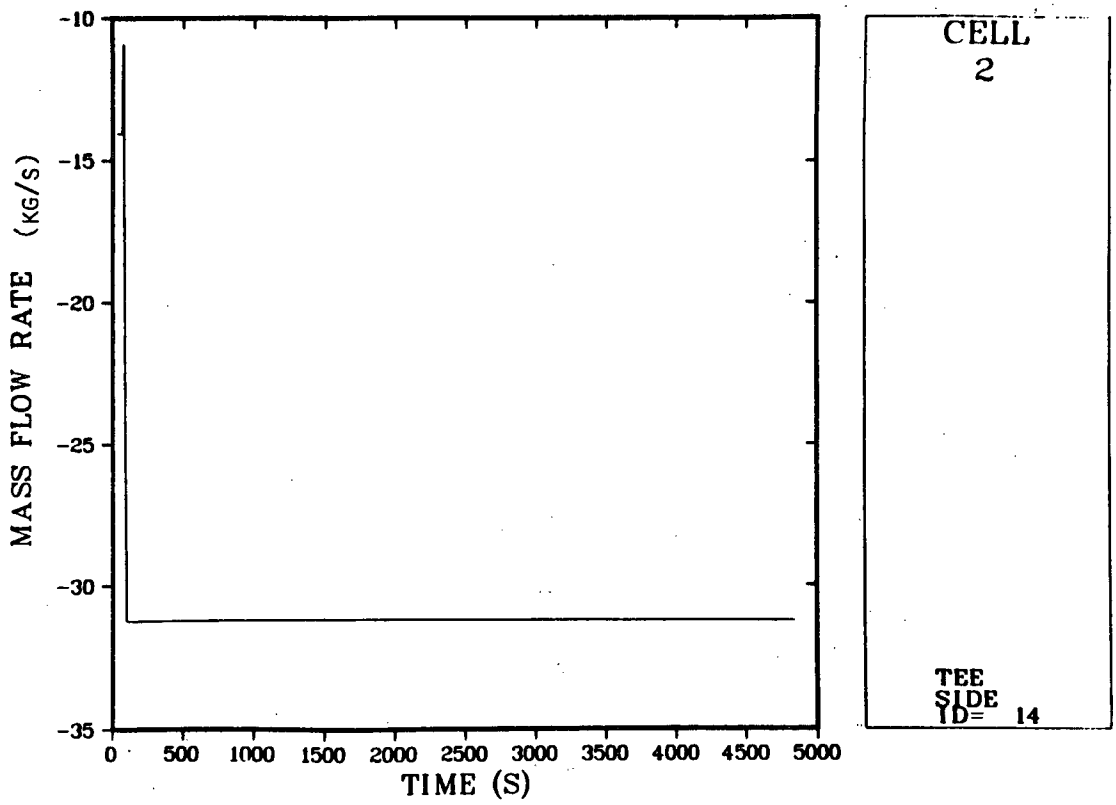

Fig. 27. Case A-3 HPI flow rate (minus indicates flow into system).

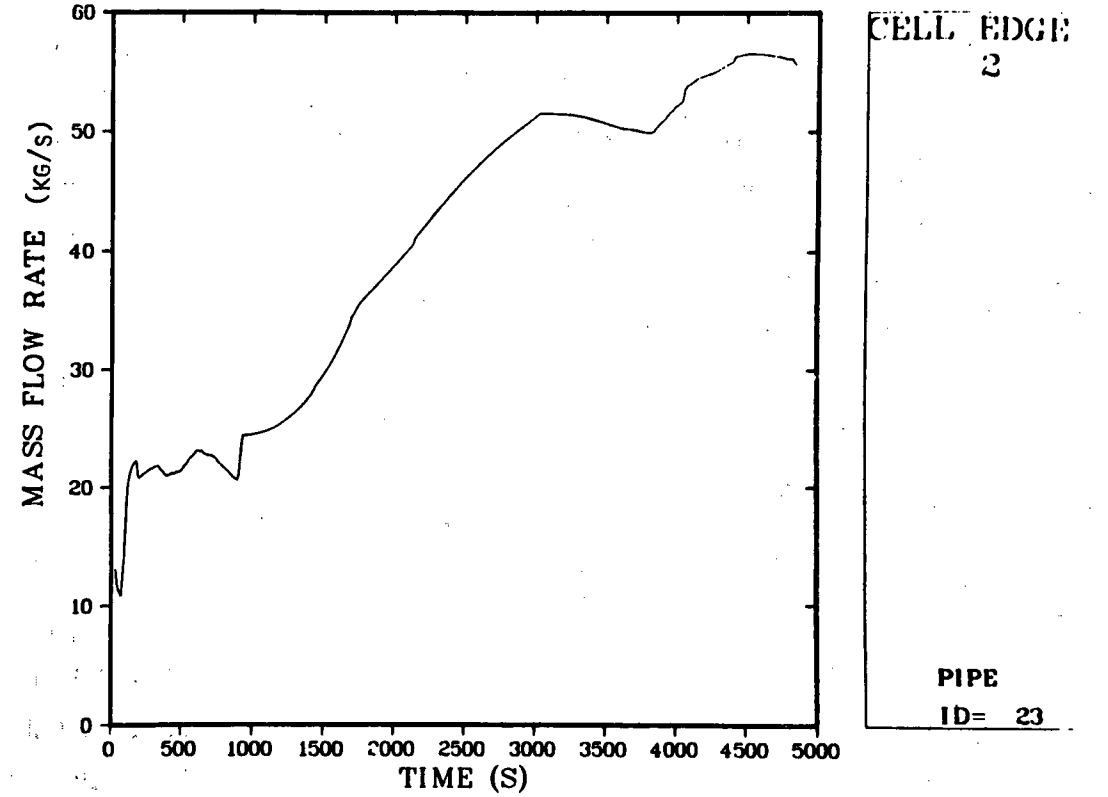

Fig. 28. Case A-3 mass flow out PORV.

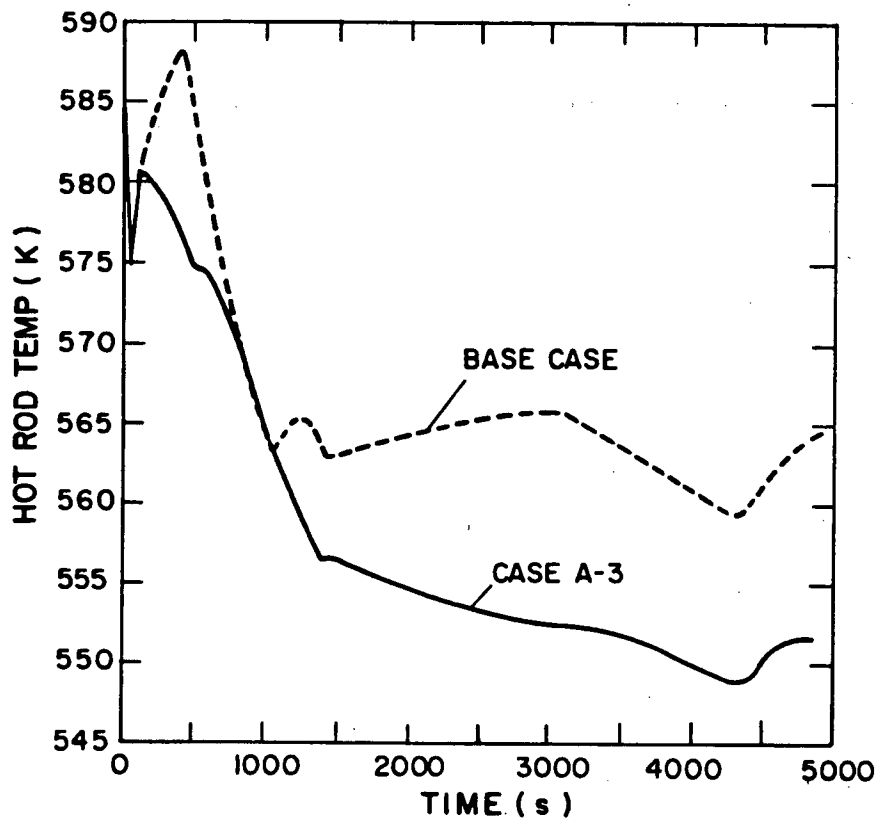

Fig. 29. Case A-3 hot-rod temperature vs base case.

B. Delayed Auxiliary Feedwater/Degraded HPI (Case A-6)

Case A-6 is similar to case A-3 except that degraded HPI flows are used rather than full HPI flows. Figure 30 shows the time history of the pressure for case A-6 and the base case for the first 5 000 s of the transient. Since the auxiliary feedwater is delayed 60 min in case A-6, the pressure in this case remains high compared to the base case until the heat sink is restored at 3 600 s (the base-case auxiliary feedwater comes on at about 500 s). Unlike case A-3, the pressure remains high due to vapor production and a lack of adequate energy removal, since there is very little HPI flow entering the vessel. The upper head in the base case voids more rapidly than case A-6 while the core and upper plenum in case A-6 void more rapidly than the base case, which explains the higher pressures in case A-6. Hot-rod temperature comparisons are shown in Fig. 31 for case A-6 and the base case. The behavior is very similar to that of the pressure. Case A-6 temperatures are 30-40 K higher than the base case until the auxiliary feedwater is initiated at 3 600 s, then these temperatures drop because of more efficient energy removal and

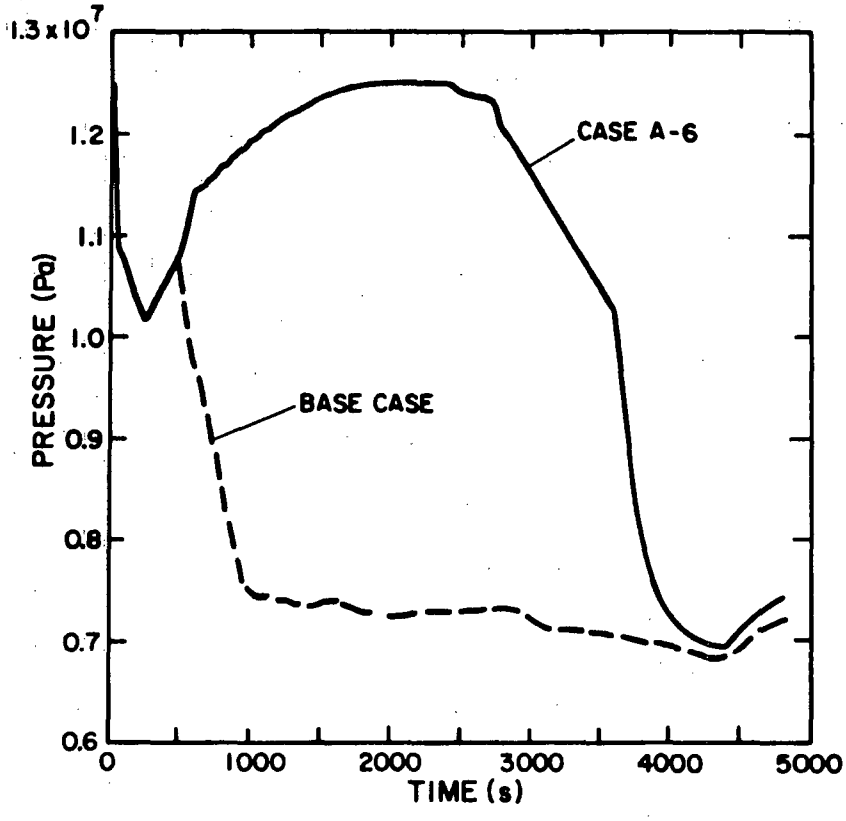

Fig. 30. Case A-6 pressure history vs base case.

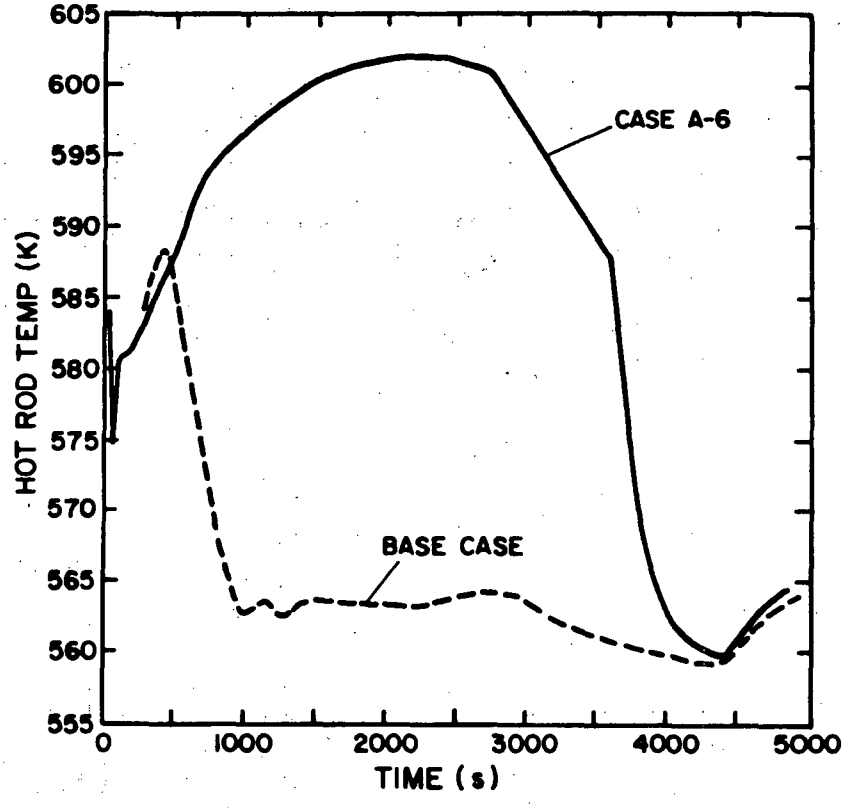

Fig. 31. Case A-6 hot-rod temperature vs base case.

follow the base case. It appears that a delay in auxiliary feedwater, at least during the initial 5 000 s of the accident, does not make an appreciable difference in the long-term response of the system since the behavior of case A-6 matches, very closely, that of the base case after initiation of auxiliary feedwater flows.

C. Full Auxiliary Feedwater/Degraded HPI (Case A-4)

Case A-4 differs from the base case and case A-6 since there is no time delay assumed for the initiation of auxiliary feedwater. Case A-4 assumes degraded HPI flows. Figure 32 shows a pressure comparison of case A-4 and the base case for the first 3 500 s of the transient. Since the base case assumes a delay of about 500 s for auxiliary feedwater, the pressure decay for the base case is not as rapid as that of case A-4. However, after about 1 000 s, the pressures for the two cases are almost identical. The hot-rod temperatures follow this same trend as shown in Fig. 33, where the base case temperatures remain higher than those for case A-4 until 500 s, at which time the base-case temperatures drop to about the same level as those for case A-4. It is obvious from the results of case A-4 that, again, auxiliary feedwater delay makes little difference on the long-term behavior of the transient.

D. Main Coolant Pumps Tripped (Case D-2)

This parametric calculation is designated case D-2 and assumes that all main coolant pumps trip at the time of reactor trip ($t \cong 10$ s). The calculation was not run far enough to be compared in detail with the base case. The discussion to follow will be based on comparisons of calculations of the first 4 000 s of the transient and somewhat speculative extrapolations beyond that time. Figure 34 shows a plot of the upper plenum pressures for the base case and case D-2 for the first 4 000 s of the transient. Initially, the pressure decays monotonically for the first 600 s to a level slightly higher than the base case. At about 2 500 s the pressure rises back up to a level much higher than the base case. This is mainly due to increased vapor production in the core

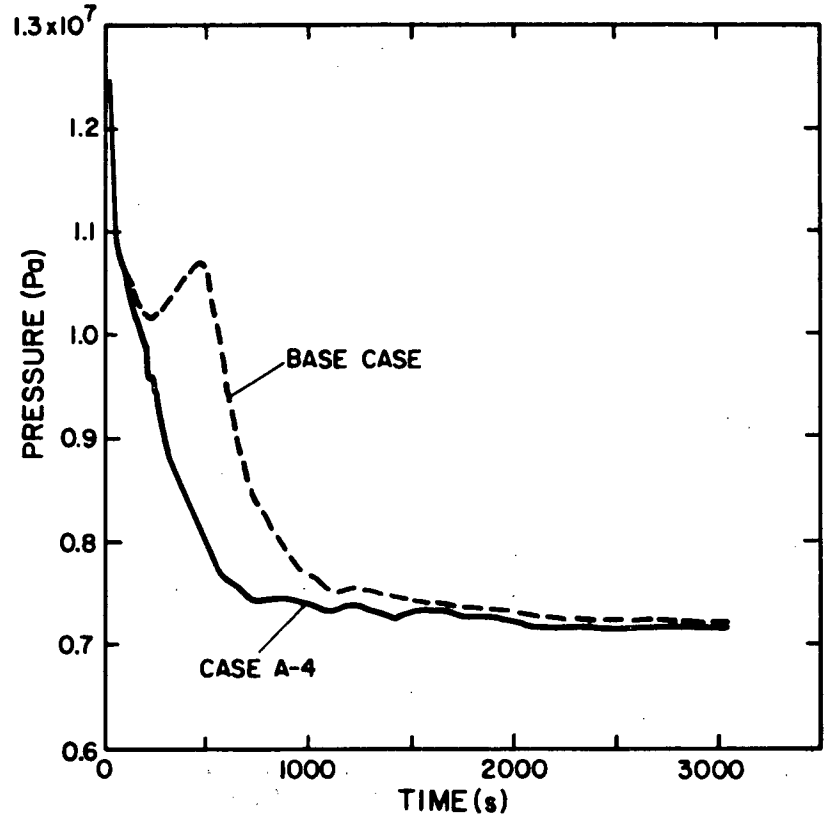

Fig. 32. Case A-4 pressure history vs base case.

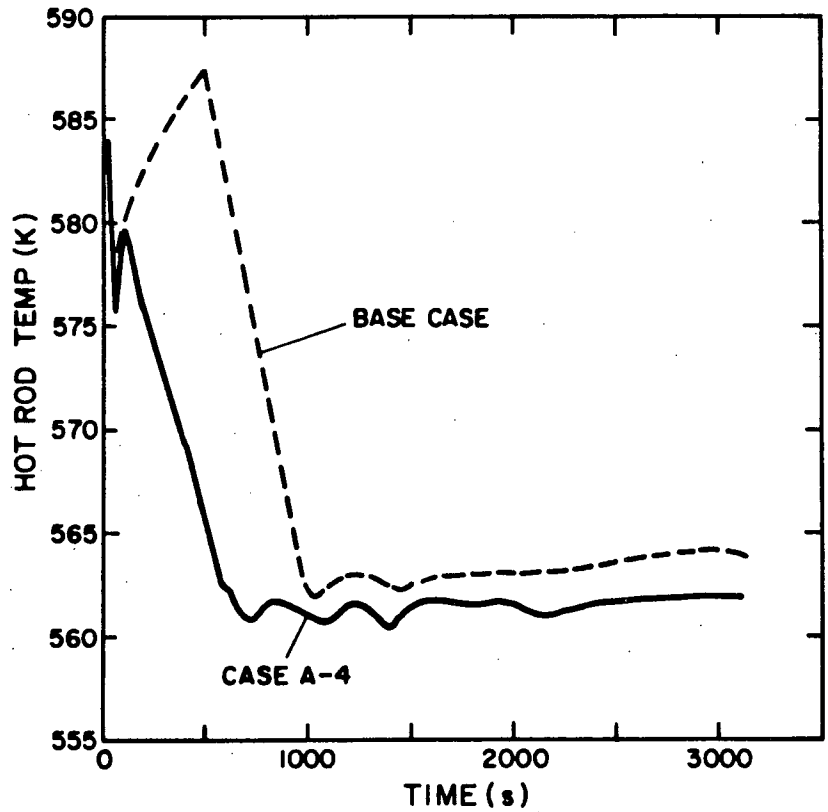

Fig. 33. Case A-4 hot-rod temperature vs base case.

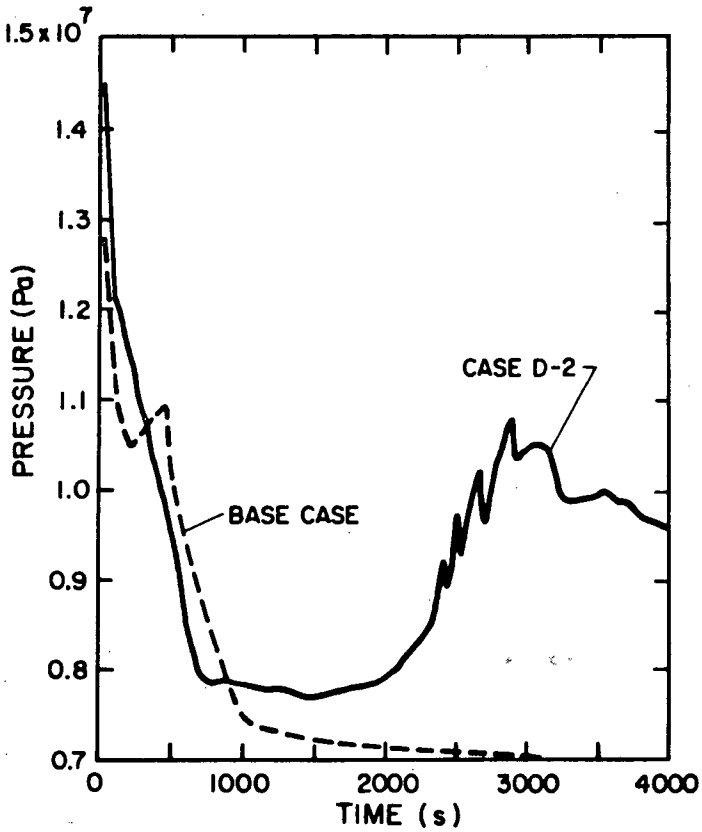

Fig. 34. Case D-2 pressure history vs base case.

and upper plenum resulting from phase separation in the vessel. Figure 35 shows void fraction plots for each level in the vessel at the same radial and axial position. It can be seen from this figure that phase separation occurs in case D-2 around 2 500 s (the lower levels fill with water and the upper levels void). A similar plot for the base case can be found in Fig. 18. Partial phase separation in the base case occurs at about 4 400 s (when the B Loop pumps are tripped). A more complete phase separation occurs in the base case at about 6 000 s when the A Loop pumps are tripped. Therefore, it might be expected that the cladding temperatures in case D-2 would increase rapidly on the order of 1 h before they do in the base case. One might also expect cladding failure to occur at 1-1/2 to 2 h into the transient for this case.

E. Cold-Leg Break Parametric Case

As a comparison to the base case, a cold-leg break was calculated using TRAC with the same break flow area as the PORV in the base case.

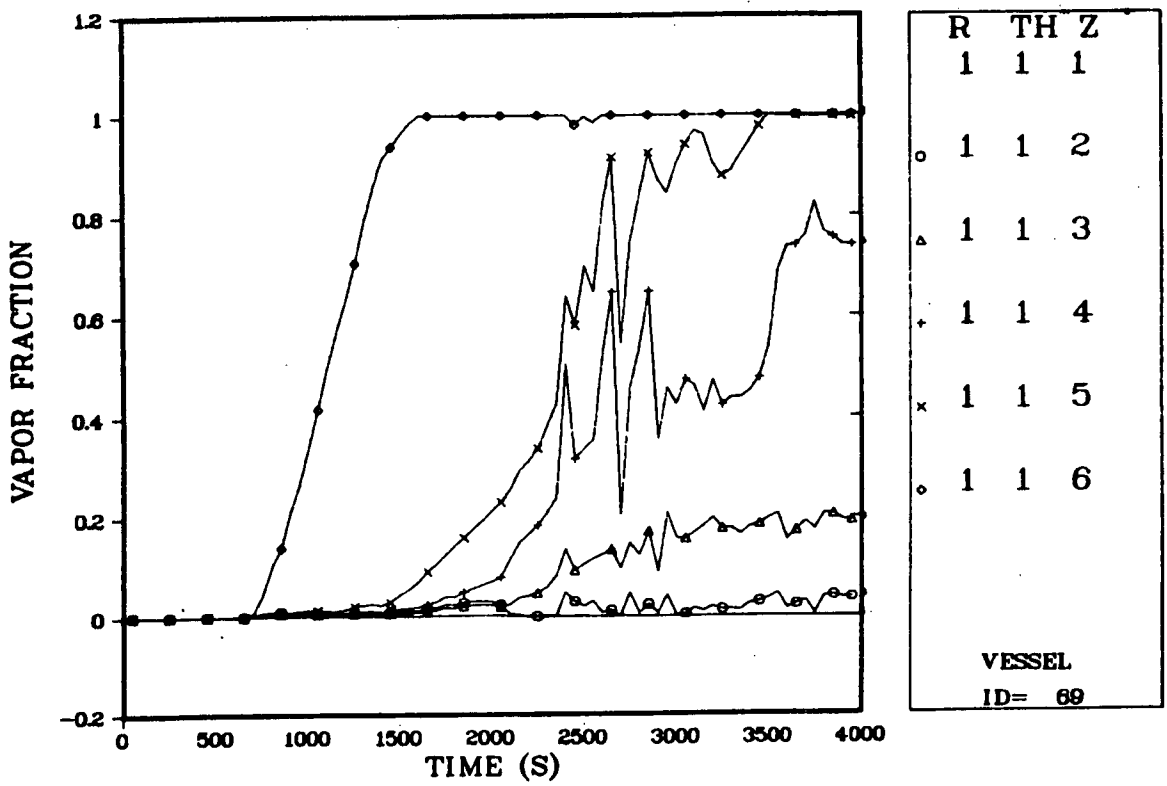

Fig. 35. Case D-2 core void fractions indicating onset of flow separation.

The break was located on the A Loop in the pump discharge line (Fig. 1). All other conditions were the same as in the base case with the exception of the HPI on the A Loop, which was not modeled.

The calculation was carried out to about 20 min when the system pressure had stabilized. The pressure after 20 min was about 15 bars higher than the base case. Since the break is located on the cold leg, a lower quality two-phase mixture escapes from the system than in the base case; thus, the volumetric flow rate is lower and the pressure remains higher. During this time, the pressurizer remains almost full of water as in the base case.

Thus, it appears from the calculation that if the break occurred in the cold leg with the same flow area as the PORV, the system would have depressurized at a slower rate as compared to the base case. Based on these results, after the pumps trip on A Loop and phase separation occurs as in the base case, the water in A Loop would probably drain out the break rather than empty into the vessel as in the base case. This would result in the core uncovering and remaining uncovered. Some flow

would still come into the vessel from B Loop as in the base case, but this probably would not be sufficient enough to completely quench the core. The fuel rods would then heat up similar to the base case after 100 min. It is possible, however, that in this case the system would depressurize sufficiently (block valve closure prevents this in the base case) such that the core flood tanks would be activated and terminate the heat up.

IV. CORE THERMAL-MECHANICAL RESPONSE

The severe off-normal conditions that the Zircaloy-clad fuel rods were subjected to during the TMI accident were likely to have caused several potentially important phenomena, including cladding ballooning prior to failure, cladding failure (rupture), cladding swelling and hydrogen evolution caused by zirconium oxidation, and, finally, possible thermal stress-induced cladding fracture and fragmentation during reflood. Each of these five phenomena will be considered in detail based on the TRAC calculations out to 3 h in the accident. Included below is a section detailing the calculations related to each particular phenomenon. Where possible, the predicted behavior will be compared to the actual behavior as inferred from the data accumulated during the accident. Thus, for example, the predicted fuel rod failure (rupture) time can be compared to the time at which high radiation levels were first observed.

The calculations reported below used the results of the base-case TRAC calculation. The information used from TRAC included the system pressure and cladding temperatures as a function of time. For the system pressure, we used the upper plenum pressure shown in Fig. 36. This single pressure can be used to represent the pressure everywhere in the core since the pressure drop across the core is small compared to the average system pressure. The TRAC representation of the core includes one radial node, two azimuthal sectors, and five axial nodes in the core. Thus, we have cladding temperature data for two average rods (the two azimuthal nodes) at five axial levels (Figs. 37 and 38). In addition to the average rods, TRAC also calculates temperatures for a hot rod. The hot-rod cladding temperatures (for the two azimuthal nodes) are shown in Figs. 39 and 40. In addition, the vapor fractions at each of the five axial levels (representing the water inventory in the core as a function of time) are shown in Fig. 41. This plot is useful in understanding some of the axial variations in the cladding temperature.

A. Cladding Ballooning

Cladding ballooning is the relatively large permanent increase in diameter (also called azimuthal or diametral strain) that the Zircaloy

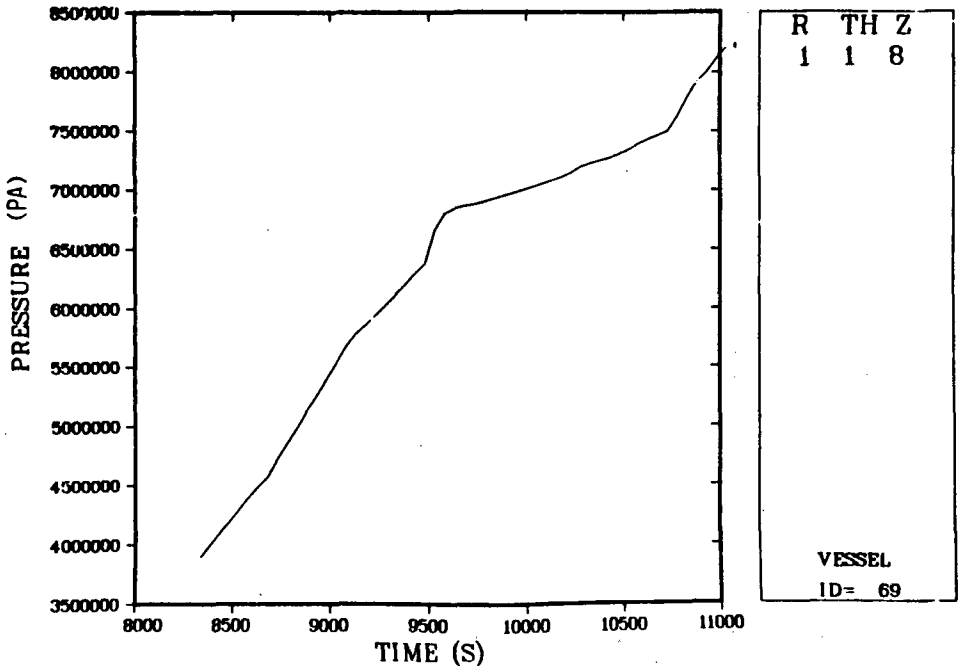

Fig. 36. Upper plenum pressure history.

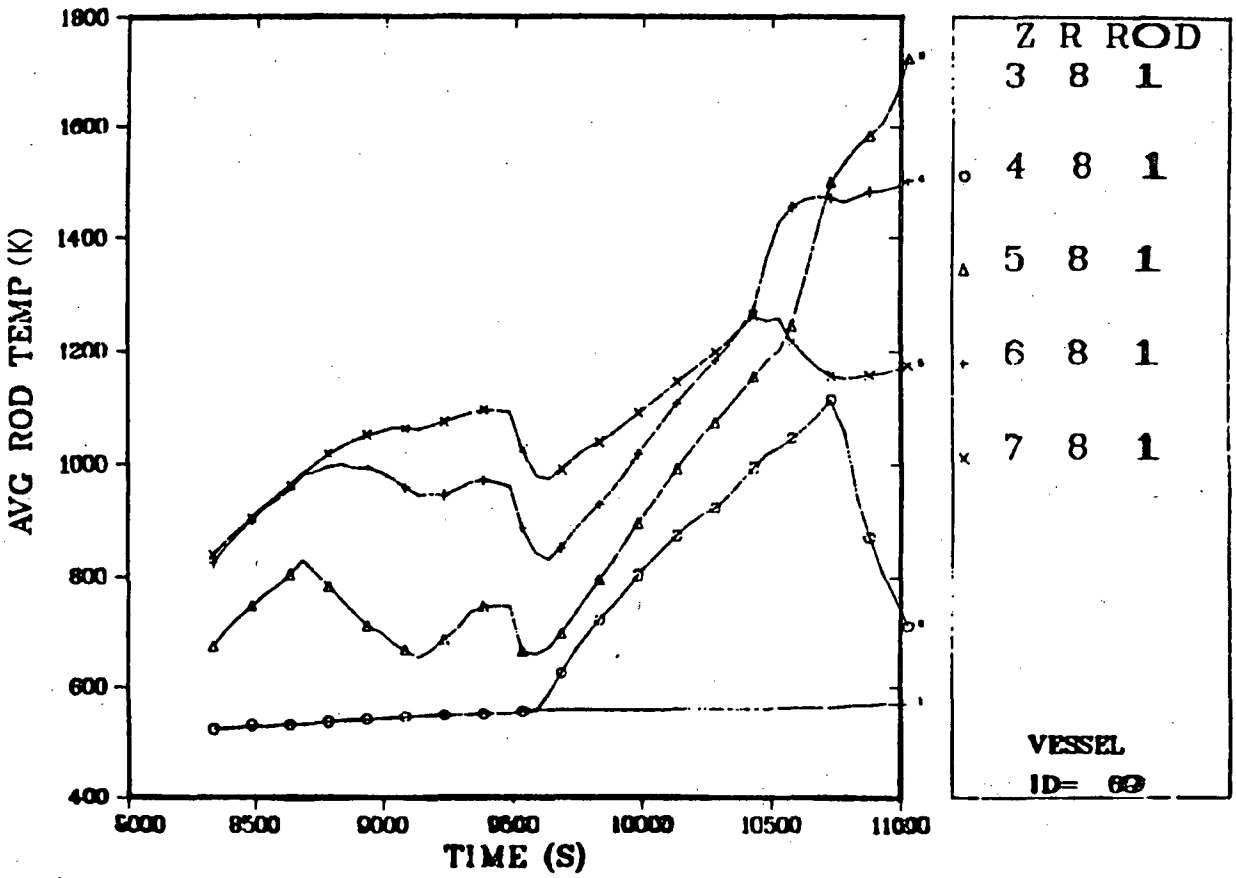

Fig. 37. Axial distribution of average cladding temperatures (azimuthal zone one).

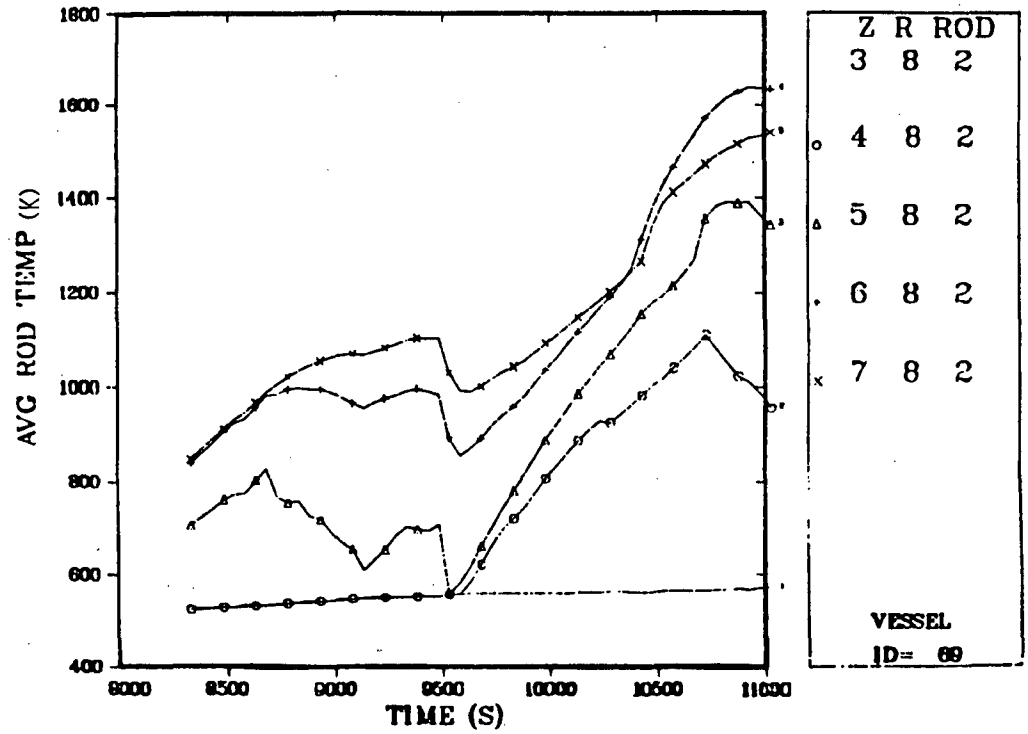

Fig. 38. Axial distribution of average cladding temperatures (azimuthal zone two).

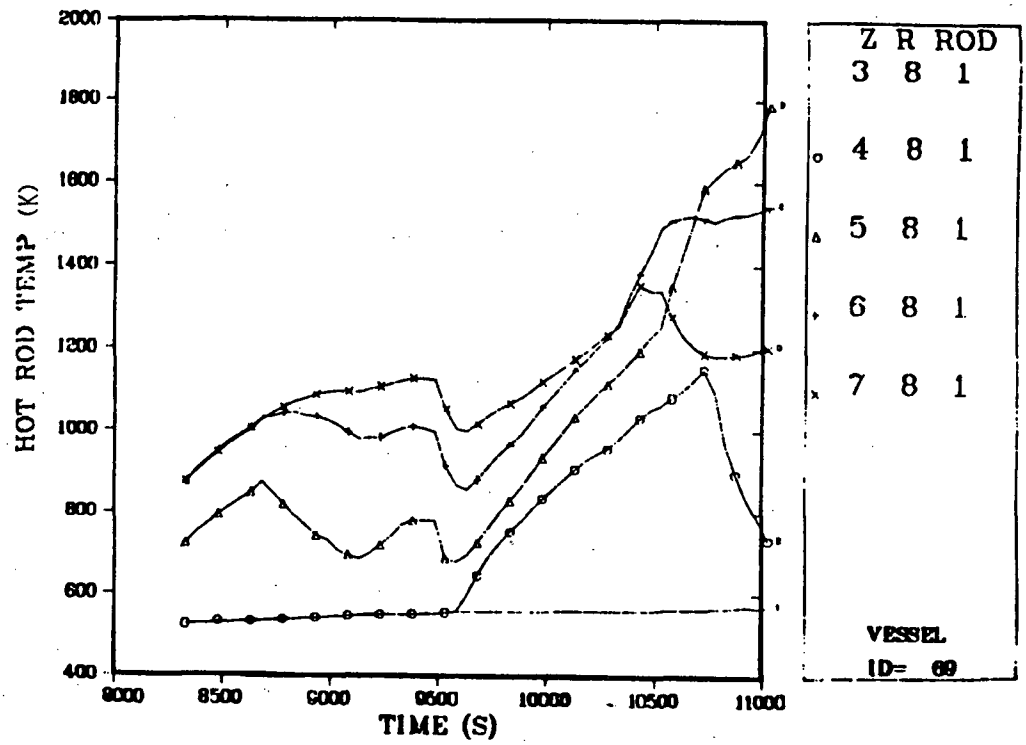

Fig. 39. Axial distribution of hot-rod cladding temperatures (azimuthal zone one).

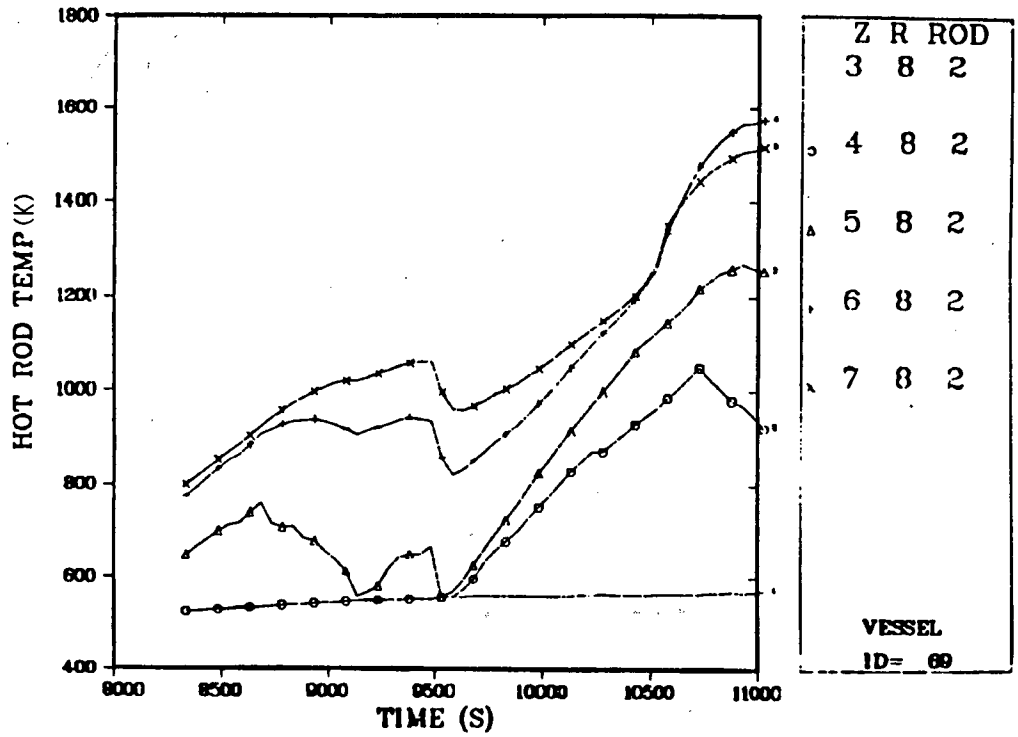

Fig. 40. Axial distribution of hot-rod cladding temperatures (azimuthal zone two).

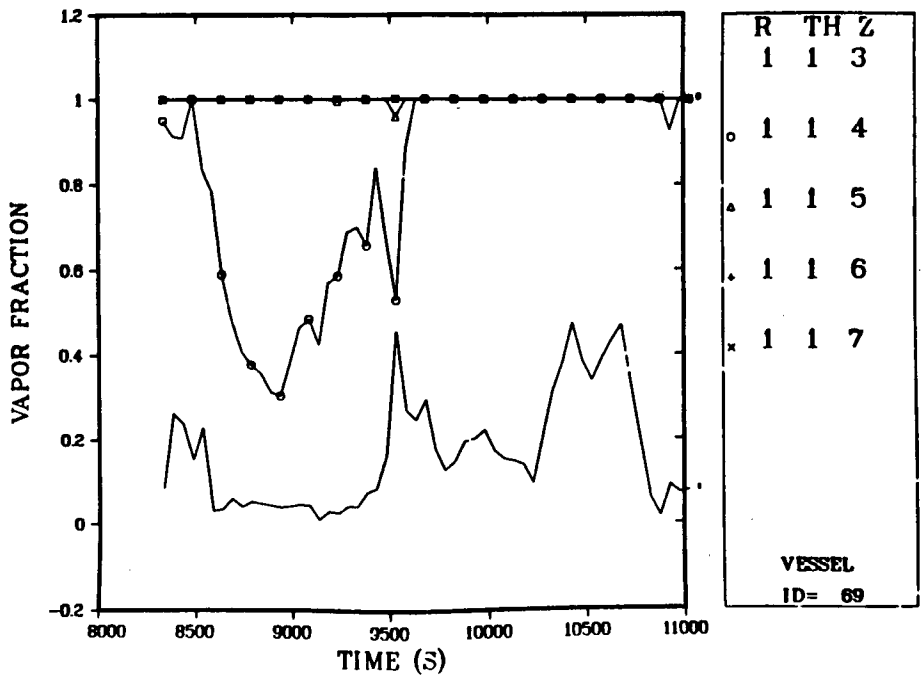

Fig. 41. Axial distribution of void fraction in reactor vessel.

cladding experiences during a transient prior to eventual failure. There are four features of the fuel rods and/or the transient that tend to promote ballooning. These are:

1. Zircaloy cladding is very ductile (that is, it experiences large deformations prior to failure),

2. The rods are initially prepressurized to about 30 atmospheres (at room temperature) to prevent cladding creepdown during normal steady-state operation,

3. The system pressure during the transient is considerably below the normal operating pressure of about 2 200 psia, and

4. The cladding temperature is considerably above the normal steady-state operating temperature.

Ballooning is directly related (to first order) to the pressure drop across the cladding (rod internal pressure minus system pressure) and the local cladding temperature. The large pressure drop across the cladding and the high cladding temperature are expected to lead to large cladding ballooning and likely cladding failure. As will be shown in the next section, cladding failure is indeed calculated to occur.

A large diametral cladding strain is potentially important because of the effect on the coolability of the fuel rods. The increased size of the fuel rods leads to a decrease in the volume available for the coolant (steam and/or water). Hence, to maintain the same level of cooling, it would be necessary to increase the coolant velocity by an amount that is (neglecting changes in the heat transfer coefficient) inversely proportional to the change (decrease) in the coolant channel area. This change in coolant channel area with increase in cladding diameter is illustrated in Fig. 42.

For the TMI plant design, the pitch-to-diameter ratio (S/D) is about 1.3 and the flow area A can be expressed as

$$A = S^2[1 - (\pi/4)\, D^2/S^2] \qquad (1)$$

$$\sim 0.536\, S^2.$$

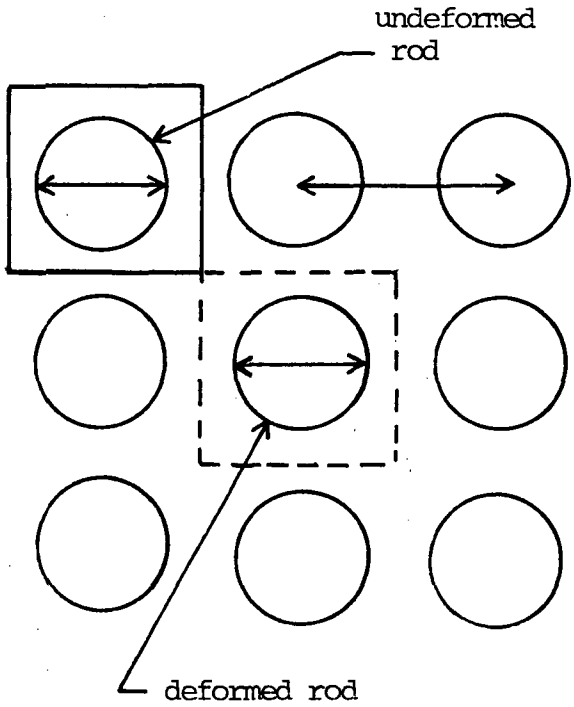

S = rod-to-rod spacing (rod pitch)

D = undeformed cladding diameter

A = initial coolant channel area per rod

$$A = S^2 - \pi \frac{D^2}{4}$$

D' = deformed cladding diameter

A' = restricted coolant channel area per rod

$$A' = S^2 - \pi \frac{(D')^2}{4}$$

Fig. 42. Reduction in channel area with cladding ballooning.

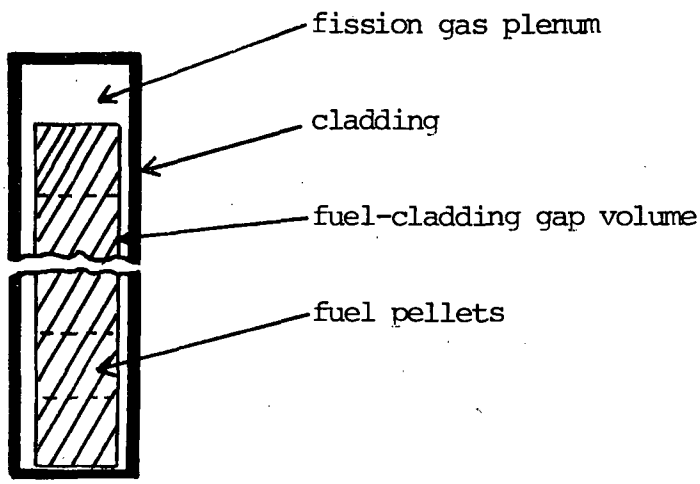

Fig. 43. Fuel rod model.

In other words, the volume occupied by the coolant is 53.6% of the core volume.

The maximum increase in cladding diameter that can occur prior to contact between adjacent fuel rods, occurs when the deformed cladding diameter D; just equals the rod pitch, S. The diametral strain for this case is given by

$$\frac{\Delta D}{D} \equiv \frac{D' - D}{D} \tag{2}$$

$$= \frac{S - D}{D}$$

$$\sim 0.3 \ .$$

Thus, a diametral strain of 30% just barely results in rod-to-rod contact. The restricted coolant channel area, A', for this case is given by

$$A' = S^2 - \pi \frac{D'^2}{4} \tag{3}$$

$$= 0.215 \ S^2 \ .$$

In other words, the coolant volume fraction has been reduced from about 53.6% down to 21.5%.

In the next section of this report, it will be shown that the fuel rods are calculated to fail (rupture) during the first 3 h of the accident. Using this fact, it is relatively simple to calculate a maximum cladding diametral strain that occurs just at the time of failure. The accepted handbook of materials properties for use in the analysis of LWR fuel rod behavior, MATPRO-Version 11,[10] provides a correlation that relates the circumferential cladding elongation (or diametral strain) to the local temperature.[10] (Note that this correlation is quite approximate because the effects of cladding stress, strain, and strain rate are ignored.) This correlation is given by

for $T < 1090$

$$\frac{\Delta D}{D} = (0.198 + 4.16 \times 10^{-4} T + 2.06 \times 10^{-7} T^2)R F \quad (4)$$

for $1090 < T < 1170$

$$\frac{\Delta D}{D} = (9.0623 - 7.492 \times 10^{-3} T)F \quad (5)$$

for $1170 < T < 1600$

$$\frac{\Delta D}{D} = (- 1.436 + 2.045 \times 10^{-3} T - 4.82 \times 10^{-7} T^2)F \quad (6)$$

for $T > 1600$

$$\frac{\Delta D}{D} = 0.6021 F \quad (7)$$

where

T = cladding temperature (K),

R = factor to account for the effect of cold work and irradiation, and

F = factor to account for the effect of cladding temperature gradient.

The calculated failure temperatures from Sec. IV.B are high (about 1 000 K). It can be seen from Eq. (5) that this temperature is very close to the temperature of 1 090 above which the effects of cold work and irradiation no longer need to be considered (they are completely annealed out). Furthermore, the cladding is shown to be hot for an extended period of time prior to failure (Figs. 37-40). Thus, it is reasonable to assume that the effects of cold work and irradiation are very nearly annealed out and R is about 1.0. In addition, the temperature gradient across the cladding is very small (a few degrees) because the transient is much longer than the thermal time constant of the fuel rod. The expression for the factor F[10] is given as

$$F = \exp(- 0.0111 \Delta T) \quad (8)$$

where ΔT = temperature variation across the cladding (K). For a ΔT of only a few degrees, F is also very close to 1.0.

Making these approximations and using a typical calculated failure temperature of about 1 000 K, Eq. (4) predicts a diametral failure strain of 0.82. This is clearly larger than the strain of 0.3 that is required to cause rod-to-rod contact. Thus, it appears that even if we are over-predicting the cladding strain using Eq. (4), it is most likely that enough strain does occur to cause rod-to-rod contact and the associated restriction in flow area. Any possible feedback on the subsequent cool-ability of the core (see for example, Ref. 11) is not included in the TRAC calculations.

The large strains calculated above do not occur over the entire axial extent of the fuel pins. From Figs. 37-40 it can be seen that only axial nodes 6 and 7 (the upper third of the core) reach a high temperature prior to cladding failure at about 1 000 K. The axial level just below these two nodes is almost 200 K cooler at the time of rod failure. Thus, the cladding ballooning in all but the upper third of the core is expected to be much smaller. Also, the largest deformations are likely to be localized so that the flow area reductions may not be as large as noted above.

B. Initial Cladding Rupture

Fuel rod cladding rupture is an important phenomenon because of the associated release into the system of the free (not in the fuel matrix) gaseous fission product inventory contained in the rod. This section of the report details the assumptions used and the calculations done in determining the time of initial fuel rod rupture during the TMI accident. The points discussed will be the time of initial fuel rod failures (predictions for the hot rods), the temporal coherence of these failures (failure of the hot rod vs the average rod, for example), and the sensitivity of the calculated rod failure time to the assumed pressure in the rod.

The conditions that lead to fuel rod failure are the same conditions listed as causing cladding ballooning (high internal rod pressure, low

system pressure, and high cladding temperature). The consequences of fuel rod failure are release of the free gaseous fission product inventory in the rod. For this particular calculation, it is possible to check on the accuracy of the prediction since the time at which high radioactivity levels were first measured should correspond to the time of multiple fuel rod failures.

Two separate predictions of rod failure were made; both of which require a knowledge of the Zircaloy cladding hoop stress and temperature. To calculate the cladding hoop stress, we model the fuel rod as a closed cylinder as shown in Fig. 43. The void volume inside this fuel rod (fission gas plenum, fuel-cladding gap volume, fuel crack volume, pellet dish volume, etc.) is pressurized by the initial fill gas (the rods are prepressurized to about 30 atmospheres to prevent creepdown of the cladding during steady-state irradiation) as well as any fission gas released from the fuel matrix during power operation. Because of the long time scale of the TMI-2 accident, it is reasonable to assume that this internal rod pressure is axially uniform within the rod.

Given the internal rod pressure as well as the pressure outside the fuel rod in the coolant channel, we can approximate the three principal stresses (radial, circumferential, and axial) in the cladding as

$$\sigma_r = (P_i + P_o)/2 \tag{9}$$

$$\sigma_\theta = (P_i - P_o)\frac{d}{2t} \tag{10}$$

$$\sigma_z = (P_i - P_o)\frac{d}{4t} \tag{11}$$

where

P_i = internal rod pressure,

P_o = coolant channel pressure,

d = average diameter of Zircaloy cladding, and

t = thickness of the cladding.

The circumferential stress [Eq. (10)], together with the local cladding temperature can be used to make a prediction of cladding failure.

In our analysis, we have used two separate, independent failure criteria. The first of these is a failure hoop stress criterion as given in MATPRO-11.[10] This criterion predicts cladding failure to occur when the circumferential stress [as calculated in Eq. (10)] exceeds a rupture stress given by

$$\sigma_{rupture} = 10^{(8.42 + 2.78 \times 10^{-3} T - 4.87 \times 10^{-6} T^2 + 1.49 T^3)} \quad (12)$$

where T = the cladding temperature (K).

To check the validity of this criterion, we also used a failure criterion based on the results of some Zircaloy creep-rupture tests performed at the Chalk River Facility in Canada.[12] In these tests, sections of unirradiated cladding were pressurized to some known internal pressure and heated to temperatures typical of those that might be experienced during an accident. The measured cladding failure times from these tests are shown in Fig. 44 as a function of cladding temperature and internal pressure.

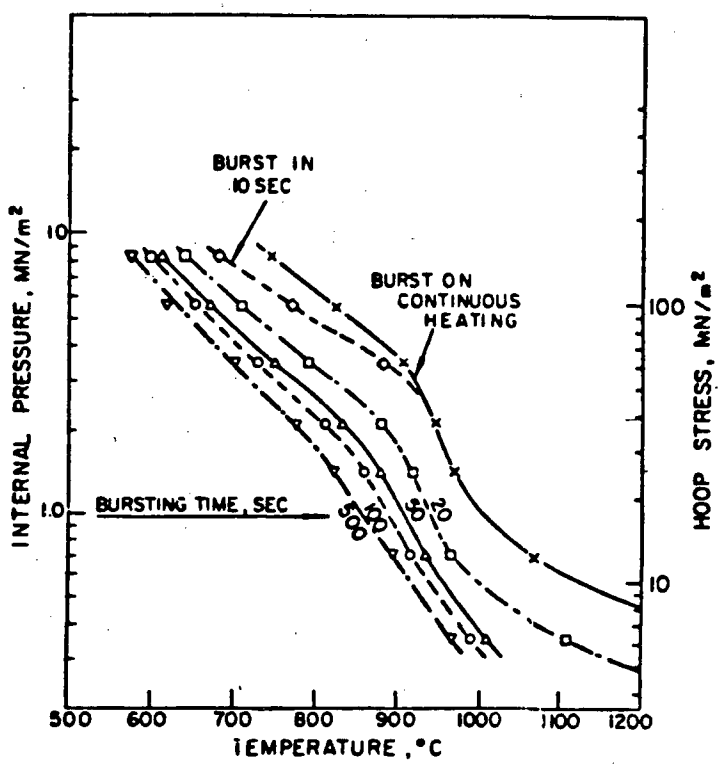

Fig. 44. Cladding burst failure conditions.

To use this cladding rupture data, it is necessary to extrapolate from the temperature/pressure data points in the experiments to the conditions encountered during the TMI-2 accident. The Larson-Miller parameter[13] is a useful tool to aid in this extrapolation. It has been found that, to a good approximation, one can define a temperature independent constant that relates the stress-rupture lifetime of a material to the material temperature. For any given stress state, this constant (the Larson-Miller parameter) is given by

$$LMP = T \cdot [\log t_r + c] \tag{13}$$

where

T = material temperature,

t_r = stress-rupture lifetime, and

c = constant dependent only on what the material is (usually taken as about 20).

A least squares fit of the stress-rupture data (from Fig. 44) to Eq. (13) was made in order to determine the Larson-Miller parameter as a function of cladding circumferential stress. (Actually, the Larson-Miller parameter was calculated at seven stress levels and a linear interpolation was used elsehwere). Thus, knowing the cladding hoop stress, one can calculate an appropriate Larson-Miller parameter. This value, along with the cladding temperature, can then be used [Eq. (13)] to calculate the cladding stress-rupture lifetime.

Knowing the stress-rupture lifetime as a function of time, one can use a linear life fraction rule failure criterion[14] to calculate cladding failure. Such a criterion states that over an increment of time Δt during which the cladding stress-rupture lifetime is $t_r(\sigma_\theta,T)$(thus σ_θ and T are constant during the time increment), a fraction of the cladding "life" is consumed equal to

$$LF = \frac{\Delta t}{t_r(\sigma_\theta,T)} . \tag{14}$$

This can easily be extended to the case where σ_θ and T vary with time (as during the accident) by defining a life fraction as a function of

time given by

$$LF(t) = \int_0^t \frac{dt'}{t_r(\sigma_\theta(t'),T(t'))} \cdot \qquad (15)$$

Failure is assumed to occur when LF = 1.0.

For each prediction of cladding failure, the state of the fuel rod was obtained from the results of the base-case TRAC calculation. The TRAC calculation provided the hot- and average-rod temperatures (Figs. 37-40) and the system pressure (Fig. 36). To calculate the cladding hoop stress, it was also necessary to estimate the rod internal pressure. As was mentioned previously, the rods were prepressurized to about 30 atm (room temperature) to prevent cladding creepdown. In addition, the fission gas produced during steady-state operation (that gas not trapped within the fuel grains) also contributes to the rod pressurization. B&W estimates[15] of this contribution raise the effective initial rod pressure (at room temperature) to about 42 atm.

Knowing the initial internal pressure, the pressure during the transient can be estimated from

$$P_i = P_{io} \cdot \frac{\langle T_{gas} \rangle}{298} \qquad (16)$$

where

P_{io} = room temperature pressure of gas in rod and

$\langle T_{gas} \rangle$ = average temperature of gas in rod (K).

For simplicity, the axially averaged cladding temperature $\langle T_{clad} \rangle$ is used as the average gas temperature (since this is readily available from the TRAC results).

It should be noted that Eq. (16) does not account for potential changes in the amount of volume available to accommodate fission gas (due to the locally large cladding strains discussed in the previous section, for example). Because of the possible error associated with

ignoring this effect, as well as the uncertainty in the initial (room temperature) pressure in the rod, we analyzed rod failure for a range of initial rod pressures (25-42 atm).

A first item of concern is the relative agreement between the two methods of predicting failure. In most cases, the calculated agreement is excellent (within 2 min). Only for low initial rod pressure is it possible to see a discrepancy of as much as 10 min. This occurred when failure was calculated to occur near the dip in the cladding temperature (at about 9 700 s). In this case, the life fraction failure prediction gave the earlier prediction in all cases. This is reasonable because a life fraction criterion is capable of calculating incremental "damage" during the period of time from about 9 600 s to about 10 000 s, whereas the ultimate hoop stress criterion would not predict failure to occur within that range. Based on these results, we will use the life fraction rule failure prediction as the best estimate.

Cladding failure was calculated for average rod No. 1 for initial rod pressures ranging from 25-42 atm. These results are shown in Table VII. For a wide range of initial pressures (30-42 atm), cladding failure is calculated to have occurred over a narrow 8-min period of time lasting from 2 h and 25 min to 2 h and 33 min. Only at the lowest initial pressure of 25 atm does the cladding survive through the entire dip in cladding temperature (at about 9 700 s) and fail at the later time of 2 h and 50 min. In all cases, failure is calculated to occur in the top axial fuel rod node (in the top 0.5 m of the core).

The general insensitivity in cladding failure time with changes in initial rod pressure is an indication of how rapidly the cladding temperature is increasing at that time (about 0.5 K/s or more). Thus, since the failure temperature at 25 atm (initial pressure) vs 42 atm (initial pressure) varies by a few hundred degrees, it is only a matter of minutes before the cladding temperature increases from the lower failure temperature (high pressure) to the higher failure temperature (low pressure).

A similar analysis was performed for the hot rod. A comparison of Figs. 37 and 39 shows the general similarity between the temperature traces for the hot and average rods. Thus, we expect similar behavior

TABLE VII

VARIATION IN AVERAGE ROD FAILURE TIME WITH INITIAL ROD PRESSURE

Initial Rod Pressure (atm)	Failure Time (s)
25	10 230 (2 h and 50 min)
30	9 195 (2 h and 33 min)
32.5	8 985 (2 h and 30 min)
35	8 872 (2 h and 28 min)
40	8 743 (2 h and 26 min)
42	8 711 (2 h and 25 min)

---

to that calculated for the average rod with somewhat earlier failure times. The results of the analysis for the hot rod are shown in Table VIII. As can be seen from this table, the failure times for the hot rod are about 2-6 min earlier than the failure times for the average rod. Thus, there is little variation in failure time across the core. However, these results have not accounted for the possibility of random early and late failure.

Using the TRAC base case for temperature histories, it is concluded that multiple fuel rod failures occurred at between 2 h and 25 min and 2 h and 35 min into the accident somewhere in the upper 0.5 m of the core.

TABLE VIII

VARIATION IN HOT-ROD FAILURE TIME WITH INITIAL ROD PRESSURE

Initial Rod Pressure (atm)	Failure Time (s)
25	9 237 (2 h and 34 min)
30	8 840 (2 h and 27 min)
35	8 679 (2 h and 25 min)
40	8 614 (2 h and 24 min)
42	8 582 (2 h and 23 min)

For very low internal rod pressures, the failures could have been delayed as late as until 2 h and 55 min. In addition, it is concluded that most of the rods in the core failed (based on the comparison between the average and hot rod). The calculated failure time of 2 h and 30 min is consistent with the observed response of the containment dome radiation detector. A large increase in the radiation level was observed at about 2 h and 35 min into the accident,[7] very close to the time of our failure prediction.

C. Oxidation of Cladding

This section summarizes results of calculations to determine the cladding zirconium dioxide layer thickness, the flow area reduction due to the volumetric expansion associated with oxidation, cladding weight gain due to oxidation, and hydrogen generation during the early stages of the TMI accident. Cladding temperatures, from the axial segment of the fuel rod with the highest temperatures, and plenum pressures used in the calculations come from TRAC code results. Cladding properties used are taken from MATPRO-11.[10]

Temperature data can be used to determine the extent of oxidation of the other cladding surface exposed to water or steam. Cladding temperatures vs time are obtained from TRAC code results as shown in Figs. 37-40.

Cladding oxidation during the approximately three-months steady-state reactor operation prior to the start of the transient is negligible. Because oxidation is so much faster at higher temperatures[10] only high-temperature oxidation is considered. For temperatures above 1 083 K the oxide thickness[10] in meters can be calculated from

$$X_2 = \left[(X_1)^2 + 2.252 \times 10^{-6} \int_{t_1}^{t_2} \exp(-\ 1.806 \times 10^4 T(t))dt\right]^{1/2} , \quad (17)$$

where

t = time (s),

t_1 = time at beginning of time interval (s),

t_2 = time at end of time interval (s),

T = temperature (K),

X_1 = oxide thickness at beginning of time interval (m), and

X_2 = oxide thickness at end of time interval (m).

The integral in Eq. (17) is evaluated with the trapezoidal rule. Temperatures vs time, extracted from Fig. 37 for evaluating the integral, are shown in Table IX. Linear interpolation is used between tabulated values. The oxide thickness, plotted vs time in Fig. 45, reaches a maximum of about 113 μm at about 11 050 s (3:04:10).

Although cladding oxidation results in a 50% volume expansion, the reduction of the effective cross-sectional coolant flow area is negligible because of the insignificant increase in cladding diameter. Of the original 675 μm thickness of Zircaloy cladding, 600 μm of Zircaloy remains

TABLE IX
TEMPERATURES VS TIME USED IN CALCULATION OF
OXIDE THICKNESS AND WEIGHT GAIN

Time (s)	Temperature (K)
9 379	1 033
9 930	1 103
10 020	1 133
10 170	1 173
10 260	1 216
10 330	1 305
10 470	1 433
10 570	1 503
10 660	1 523
10 760	1 620
10 330	1 643
11 000	1 710
11 050	1 732

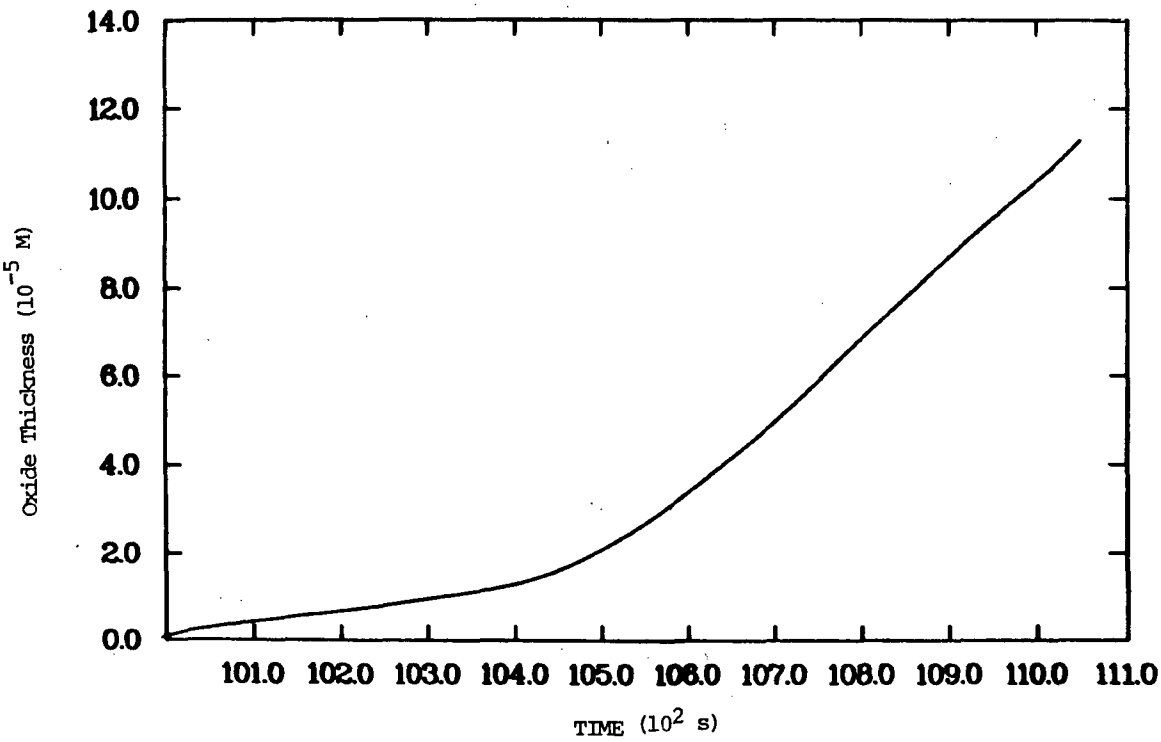

Fig. 45. Plot of zirconium-oxide thickness vs time.

at 11 050 s (3:04:10). The oxidation is significant also since it embrittles the cladding, making it more susceptible to brittle fracture.

In the same manner, the cladding weight gain from oxidation is calculated. For temperatures above 1 083 K, the total weight gain[10] in kg/m^2 can be calculated from

$$W_2 = \left[(W_1)^2 + 3.360 \times 10^1 \int_{t_1}^{t_2} \exp(-\,2.007 \times 10^4/T)\,dt\right]^{1/2}, \quad (18)$$

where

W_1 = total weight gain at beginning of time interval (kg/m^2),

W_2 = total weight gain at end of time interval (kg/m^2),

and other quantities are as previously defined. The total weight gain, plotted vs time in Fig. 46, reaches a maximum of about 0.23 kg/m^2 at about 11 050 s (3:04:10).

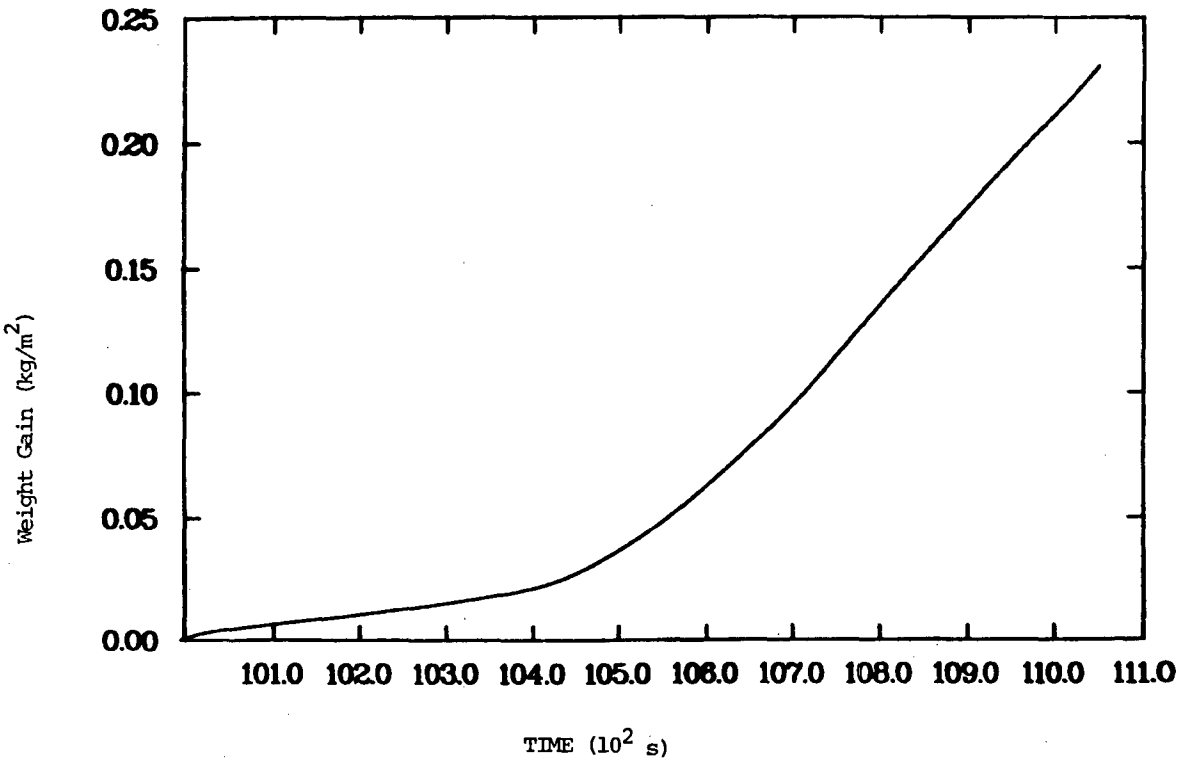

Fig. 46. Zirconium-oxide weight gain per unit cladding area.

Since the outside diameter of the cladding is 10.92 mm, the weight gain per unit length of fuel rod is calculated to be 7.9 g/m. This is the mass of oxygen per unit length of fuel rod that has reacted with the cladding. Assuming that all of this oxygen was produced by dissociation of water and based on the molecular weights of hydrogen and oxygen, the mass of hydrogen released is one-eighth the mass of oxygen reacted, about 1.0 g/m.

The perfect gas law is used to determine the volume of hydrogen released per unit length of fuel rod.

$$V = \frac{mRT}{MP} \quad , \tag{19}$$

where

V = volume of hydrogen per unit length of fuel rod (m^3/m),
m = mass of hydrogen per unit length of fuel rod (kg/m),
R = universal gas constant, 8.31 (J/mole·K),
T = plenum temperature (K),

M = molecular weight of hydrogen (kg/mole), and

P = plenum pressure (Pa).

Values for plenum temperature and pressure of 1 500 K and 8.5 MPa, respectively, are estimated from TRAC code results.

$$V = \frac{(1.0 \times 10^{-3})(8.31)(1500)}{(2 \times 10^{-3})(8.5 \times 10^{6})}$$

$$= 7.3 \times 10^{-4}\ m^3/m$$

$$= 0.73\ \ell/m\ .$$

Thus, approximately 0.73 liters of hydrogen are generated per meter of oxidized fuel rod. From TRAC results, the total amount of hydrogen generated can be determined by assuming a 1-m length of cladding surface has oxidized on each of the 36, 816 fuel rods. The resultant volume of hydrogen produced is 27 m^3 (37 kg), a substantial quantity of hydrogen.

This calculation may be incorrect compared to the actual condition of the reactor. Not all of the fuel rods were at the temperatures indicated from TRAC code calculations. In fact, in-core thermocouple readings 4-5 h after the start of the accident[7] indicate some large variations in temperature from subassembly to subassembly. In addition, the length and thickness of cladding oxidized on each fuel rod can be expected to vary considerably across the core. In light of these considerations, the calculated oxidation and hydrogen generation are thought to be an overestimate of the actual oxidation and hydrogen generation in the early stages (before 3 h) of the TMI accident. However, hydrogen generation probably continued after 3 h.

For cladding temperatures above 1 273 K, the TRAC code calculates the oxide penetration depth and the heat generation from the exothermic metal-water reaction. Oxidation penetration depth is calculated from an empirical rate law developed from isothermal experiments.[16] The TRAC code does not include the effect of the change in cladding properties due to oxidation, nor does it include the effect of the reduced cross-sectional coolant flow area due to the 50% volume expansion of Zircaloy upon oxidation.

The TRAC calculations include five axial levels in the core. This greater detail shows that almost all cladding oxidation occurs near, or above, the core midplane. The lower portion of the core is cooled by water which remains in the lower portion of the core during much of the first 3 h. Figure 41 shows the axial void fraction distribution for various core levels after the PORV block valve was closed. The lower level has a consistently low void fraction indicating the presence of water in the lower region of the core. The upper portion of the core is probably not as oxidized as the midplane region because temperatures are lower due to a smaller heat rate near the top of the core.

By determining the volume of oxygen reacted from the oxygen penetration depths calculated by the TRAC code, it is possible to quantify the amount of hydrogen produced by the metal-water reaction. The resultant mass of hydrogen calculated with this method is 39 kg. The two methods of determining hydrogen generation are close enough to give confidence in the results. Agreement is very good because the axially varying amount of oxidation calculated by the TRAC code can be approximated by considering oxidation of a 1-m section of the core's cladding.

D. Cladding Mechanical Response During Subsequent Cooldown

During the first 3 h of the TMI accident, the cladding of the fuel rods experienced increasingly higher temperatures. Shortly after 3 h, relatively cold water was added to the reactor core due to resumed HPI. The mechanical reaction of the cladding can be severe in these circumstances. In particular, it is important to determine whether the cladding could have failed and perhaps fragmented due to thermal shock.

The life fraction calculations discussed above showed that the cladding failed at approximately 9 000 s (2:30:00). This failure was due to a pressure difference between the inner and outer walls of the cladding at the elevated temperatures. This ductile type of failure, not caused by the temperature gradient in the cladding, can be expected to produce a perforation in the cladding. This perforation permits venting of fission gas to the coolant channel, thus eliminating any pressure difference between the inside and outside of the cladding.

Therefore, pressure effects cannot enhance further failure due to thermal shock.

To determine the possibility of cladding failure due to thermal shock, some estimation of the spatial temperature variation in the cladding with time during reflood is essential. Without a thermal gradient in the cladding, thermal stresses would not be induced. To simplify the analysis of temperature in the cladding, any zirconium dioxide layer is ignored and the initial temperature of the cladding is assumed uniform.

At the time of reflood, the outer surface is assumed to be suddenly cooled by the cold water being pumped into the core. Because the cladding thickness-to-diameter ratio is small, less than 7%, the curvature effects can be neglected and the cladding can be modeled as a slab. We assume that immediately before reflood, the cladding and coolant temperatures are approximately equal, and given by T_o. At the time of reflood we assume that the coolant temperature instantaneously changes to some lower temperature, T_∞.

An approximate technique using Kantorovich profiles[17] can be used to determine the temperature distribution with time. Initially, the outer surface temperature will decrease while the inner surface temperature remains constant. The temperature change at the outer surface of the cladding when the inner surface just begins to change, approximates the largest expected differential temperature change, ΔT, to be used in the determination of thermal stress. With the approximate technique outlined above, ΔT can be shown to be given by the expression

$$\Delta T = \frac{(T_o - T_\infty)}{(1 + 2/Bi)} , \qquad (20)$$

where Bi, the Biot number, is given by

$$Bi = \frac{ht}{K} . \qquad (21)$$

h is the heat transfer coefficient, t is the cladding thickness, and k is the thermal conductivity of the cladding. The dimensionless Biot number is a ratio of convective heat transfer to conductive heat transfer. The larger Biot number becomes, the larger ΔT becomes.

To estimate the largest reasonable ΔT, the large values of $(T_o - T_\infty)$ and Bi should be used. From TRAC code results, an acceptable large value of h is 10^4 w/m^2·K. The thickness of TMI cladding is 0.675 mm. The thermal conductivity of Zircaloy[10] is about 25 w/m·K. From Eq. (21), Bi = 0.27.

At approximately 3 h into the accident, the cladding temperature is about 1 650 K. The largest possible change in coolant temperature, $(T_o - T_\infty)$, at reflood is approximately 1 000 K. With these values the largest ΔT to expect, from Eq. (20), is about 120 K. The value of ΔT = 120 K is used in the subsequent stress calculations. This value represents the largest possible differential temperature change in the cladding.

The maximum stress in the cladding will be the tensile hoop stress at the outer surface given by the expression[18]

$$\sigma = f \frac{E\alpha\Delta T}{(1-\nu)} \tag{22}$$

where σ is stress, E is Young's modulus, α is the linear coefficient of thermal expansion, ν is Poisson's ratio, and f is a factor to take into account inelastic, or plastic, deformation. Young's modulus is approximately 3×10^{10} Pa,[10] the linear coefficient of thermal expansion is about 4×10^{-3} K^{-1},[10] and Poisson's ratio is approximately 0.5, the correct value for a material which behaves plastically.

The factor f can be shown to be given by the expression[19]

$$f = \left[1 + \frac{3}{2} \frac{E}{(1-\nu^2)} \left(\frac{\partial\sigma}{\partial\varepsilon}\right)^{-1}\right]^{-1} , \tag{23}$$

where ε is strain. From the MATPRO expression for the yield surface,[10] for strains between 1 and 50% with a strain rate of 10^{-4} s^{-1}, $\partial\sigma/\partial\varepsilon$ is between 1 and 50 MPa. An average value of 10 MPa is used to evaluate f. Results of the calculation yield $f = 3 \times 10^{-4}$.

The maximum stress is calculated to be 7.2 MPa. This value of stress is far below the stress at which failure due to thermal shock can occur according to MATPRO-11 data for unoxidized Zircaloy. However, oxidation embrittled cladding may fail due to thermal shock. Experiments

by Kassner, et al.,[20] showed that for isothermal oxidation at 1 300 K, 1 400 K, 1 500 K, and 1 600 K for 10 000 s, 2 000 s, 700 s, and 300 s, respectively, followed by a quench from 840-410 K, cladding failed. Temperature results from the TRAC code calculation indicated that this oxidation criterion is met. If reflooding of the oxidized upper section of the core occurred rapidly, then thermal shock failure may have occurred. If thermal shock failure did occur, then the oxidized upper portion of the cladding is expected to have fragmented. This assumes that the Zircaloy had not melted before reflood.

E. Summary of Core Thermal-Mechanical Response

We have presented calculations detailing the likely fuel rod damage that occurred during the first 3 h of the accident. The first form of damage that was calculated to occur was ballooning of the very ductile Zircaloy cladding prior to rupture. The amount of ballooning that was calculated is substantial, up to 80% including the large strains at the localized rupture site. The TMI fuel bundle design allows 30% ballooning before rod-to-rod contact occurs. Thus, at least some substantial reductions in flow area in about the upper 1 m of the core seems likely.

This reduction in flow area should have resulted in some degree of local flow starvation. However, the agreement between the best estimate massive cladding failure times and the time of the first substantial radioactive material release indicate that the TRAC-calculated cladding temperatures (at that time in the accident) are reasonably accurate. Since there was very little steam flow through the core during the temperature excursion leading to these initial rod failures, ballooning should not have influenced failure times substantially. However, local flow reductions due to ballooning (and oxidation-induced swelling) could have been a contributor to some of the anomalous fuel bundle outlet temperatures measured later in the accident.

The large pressure drops across the cladding and the high cladding temperatures led to cladding failures (rupture). The best estimate prediction indicates that failure in most rods occurred at between 2 h and

25 min and 2 h and 35 min into the accident in the upper 1 m of the core. The local cladding temperature at this time was about 1 000 K. As previously mentioned, these times correspond well with the time at which high radiation levels were first measured.

The range of failure times indicated represents both the estimated variation in failure time with radial location in the core as well as the uncertainty in failure time due to uncertainty in internal rod pressure. Calculations indicated that failure times were relatively insensitive to the rod pressure. Rather, the dominant controlling factor was the high cladding temperature. In addition, the difference in calculated failure times between the TRAC average and hot rods is small, on the order of 10 min. Thus, it appears likely that most of the rods in the core failed around 2 h and 30 min into the accident.

Subsequent to the initial cladding failures and radioactivity release, the major phenomenon the fuel rod undergoes is cladding oxidation. This oxidation of the Zircaloy leads to three important consequences: swelling of the oxidized cladding layer, release of hydrogen gas during the oxidation process, and embrittlement of the cladding due to oxidation.

The calculations performed to predict oxide layer formation indicate that up to about 3 h into the accident, the maximum oxide layer thickness for the average rod is about 113 μm cladding thickness. Thus, the effective increase in cladding diameter due to oxidation to this point is only about 76 μm. This represents a negligible increase (initial cladding diameter is about 11 mm) and should not affect the coolability of the fuel pin.

Oxidation of about 75 μm of the cladding thickness does, however, lead to significant hydrogen generation. Because of the small difference between the cool-, average-, and hot-rod temperatures, cladding oxidation is predicted to occur radially throughout the core. Axially, about the upper one-third to one-half of the core is affected. Using these assumptions, the calculated amount of hydrogen generated at 3 h is about 40 kg. At the temperature/pressure conditions calculated (by TRAC) to exist in the core at between 2-3 h into the accident, this amount of gas would occupy a volume of about 27 m^3. Further hydrogen release should have occurred after 3 h.

One other consequence of cladding oxidation is cladding embrittlement. This phenomenon is important relative to the possible fracture and fragmentation of the cladding during the first reflood. While the TRAC calculation terminates well short of the (at least partial) reflood that occurs at about 3 h and 20 min, estimates have been made of the thermal stress induced in the cladding during reflood and the likelihood of fracture at that time. These calculations indicate that the ductile unoxidized Zircaloy as well as the lightly oxidized cladding will survive the quenching process. Only the cladding that has seen prolonged periods of high temperatures (greater than about 1 600 K) is likely to fail under these conditions. Thus, if reflood occurred rapidly, it is possible that up to about one-third of the axial extent of the core may have undergone cladding fragmentation. It should be remembered, however, that since detailed TRAC calculations were not done for this stage of the accident, these estimates of cladding fragmentation are speculative.

AUTHORSHIP AND ACKNOWLEDGMENTS

A large number of people from the Reactor Safety Program at LASL have contributed directly and indirectly to the preparation of this report. The main contributors are listed below according to prime responsibility and contribution to each section of this report.

TRAC Base-Case Calculation:	J. R. Ireland
TRAC Parametric Calculations:	J. R. Ireland P. B. Bleiweis
Core Thermal-Mechanical Response:	P. K. Mast T. R. Wehner
Report Compilation:	W. L. Kirchner M. G. Stevenson

REFERENCES

1. "TRAC-P1A, An Advanced Best Estimate Computer Program for PWR LOCA Analysis," Los Alamos Scientific Laboratory report LA-7777-MS (May 1979).

2. J. C. Vigil and R. J. Pryor, "Transient Reactor Analysis Code (TRAC) Development and Assessment," Los Alamos Scientific Laboratory report submitted for publication in Nuclear Safety.

3. "Three Mile Island Nuclear Station, Unit 2," License Application, FSAR, Vol. 1-10 (Metropolitan Edison Co., 1974).

4. Babcock and Wilcox communication.

5. EPRI communication.

6. L. S. Tong, US Nuclear Regulatory Commission, private communication (July 26, 1979).

7. "Investigation Into the March 28, 1979 Three Mile Island Accident By Office of Inspection and Enforcement," US Nuclear Regulatory Commission Investigative Report No. 50-320/79-10, NUREG-0600 (August 1979).

8. "Nuclear Legislative Advisory Service," Issue 17 (April 13, 1979).

9. General Public Utilities communication to US Nuclear Regulatory Commission (May 15, 1979).

10. "MATPRO-Version 11: A Handbook of Materials Properties for Use in the Analysis of Light-Water Reactor Fuel Rod Behavior," compiled and edited by D. L. Hagrman and Gregory A. Reymann, EG&G Idaho, Inc., report NUREG/CR-0497, TREE-1280, Idaho Falls, Idaho (February 1979).

11. P. C. Holland and R. B. Duffey, "A Method of Calculating the Effect of Clad Ballooning on Loss-of-Coolant Accident Temperature Transients," Nuclear Science and Engineering 58, 1-20 (1975).

12. D. G. Hardy, "High-Temperature Expansion and Rupture Behavior of Zircaloy Tubing," Topical Meeting on Water-Reactor Safety, Salt Lake City, Utah (March 1973).

13. J. B. Conway, "Stress-Rupture Parameters: Origin, Calculation, and Use," Gordon and Breach, Science Publishers, New York (1969).

14. J. L. Straalsund, "Correlation of Transient-Test Data with Conventional Mechanical Properties Data," Nuclear Technology 25 (March 1975).

15. M. L. Picklesimer, "Bounding Estimates of Damage to Zircaloy Fuel Cladding in the TMI Core at Three Hours After the Start of the Accident, March 28, 1979," Memorandum for File, US Nuclear Regulatory Commission (June 20, 1979).

16. J. V. Cathcart, "Zirconium Metal-Water Oxidation Kinetics IV: Reaction Rate Studies," Oak Ridge National Laboratory report ORNL/NUREG-17.

17. V. S. Arpaci, Conduction Heat Transfer (Addison-Wesley Publishing Co., Reading, Massachusetts, 1966) pp. 76-83.

18. J. H. Faupel, Engineering Design (John Wiley and Sons, Inc., New York, 1964) p. 867.

19. P. K. Mast, "The Los Alamos Failure Model (LAFM): A Code for the Prediction of LMFBR Fuel Pin Failure," Los Alamos Scientific Laboratory report LA-7161-MS (March 1978).

20. T. F. Kassner, "LWR Safety Research Program Quarterly Progress Reports, Part III," Argonne National Laboratory report ANL-78-25, NUREG/CR-0089 (October-December 1977) pp. 31-44.

APPENDIX

ADDITIONAL PLOTS FOR BASE-CASE CALCULATION

$0 \leq T \leq 81$ min

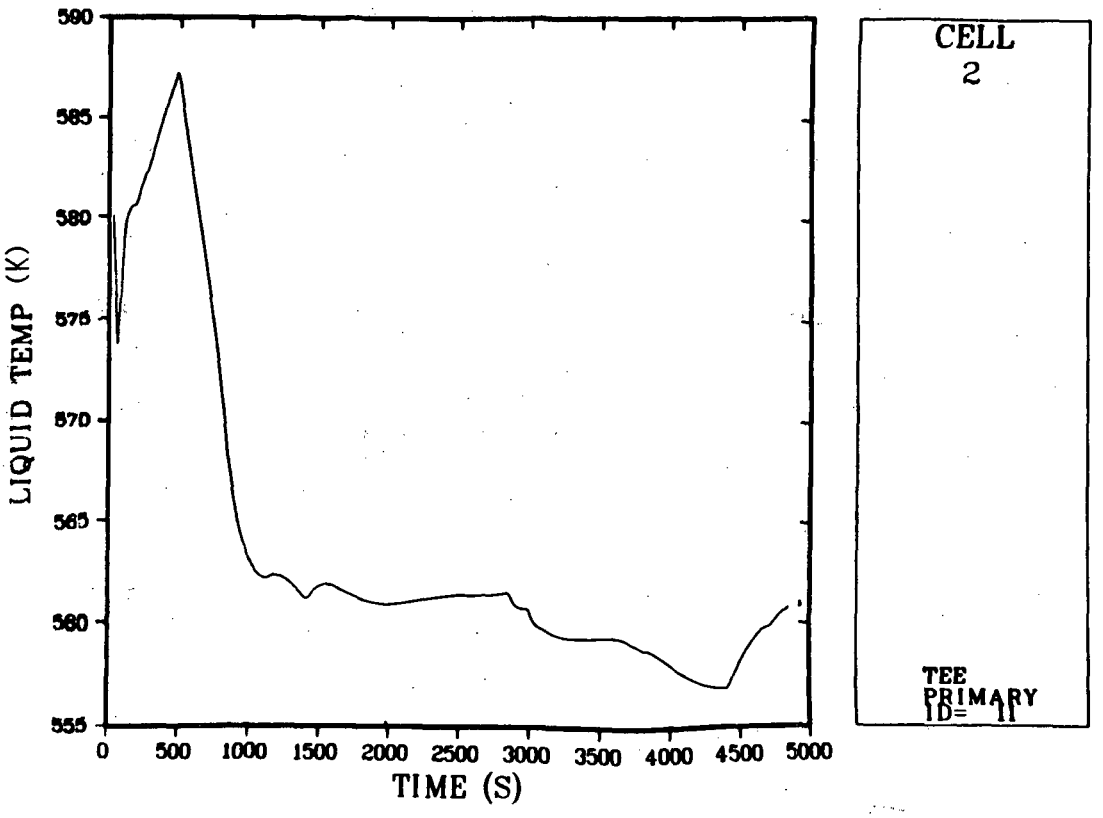

A Loop hot-leg liquid temperature.

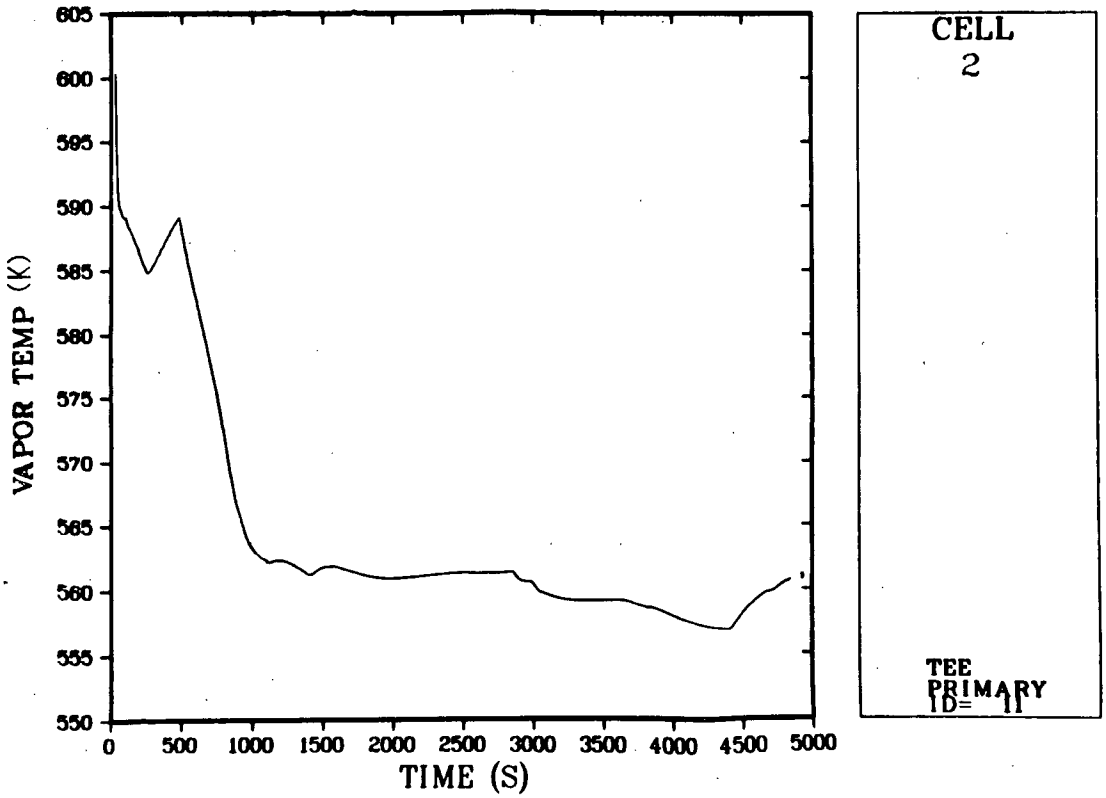

A Loop hot-leg vapor temperature.

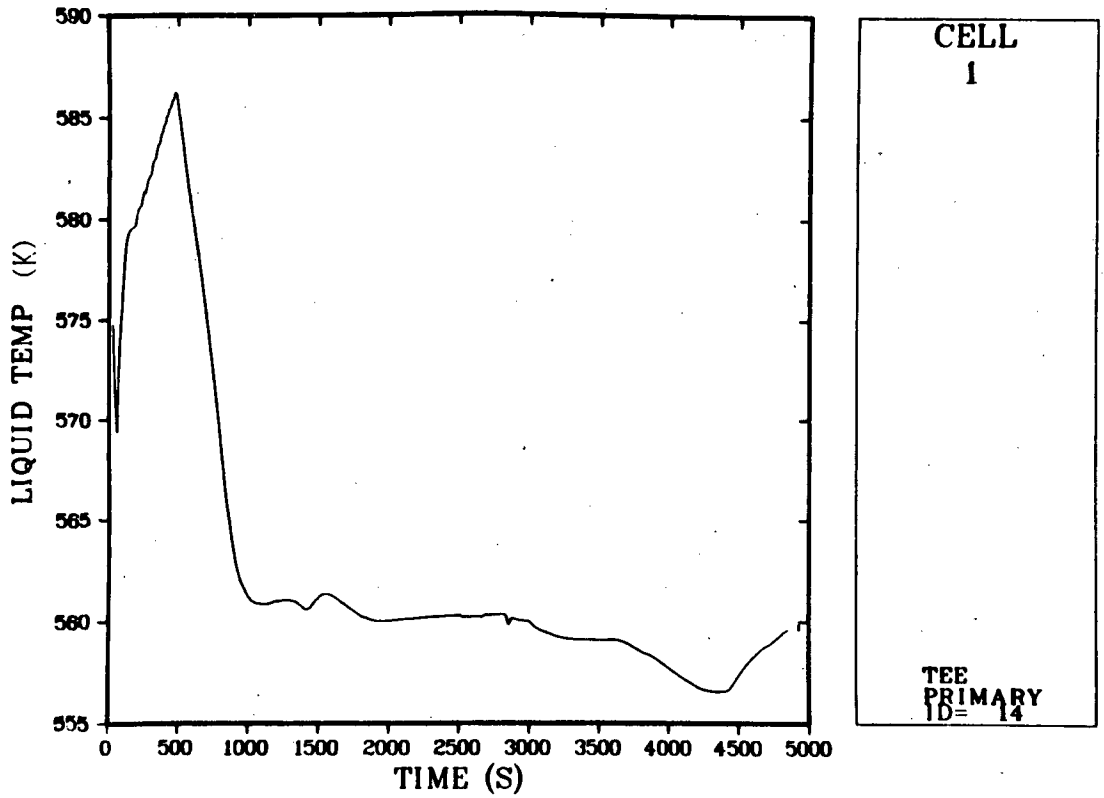

A Loop cold-leg liquid temperature.

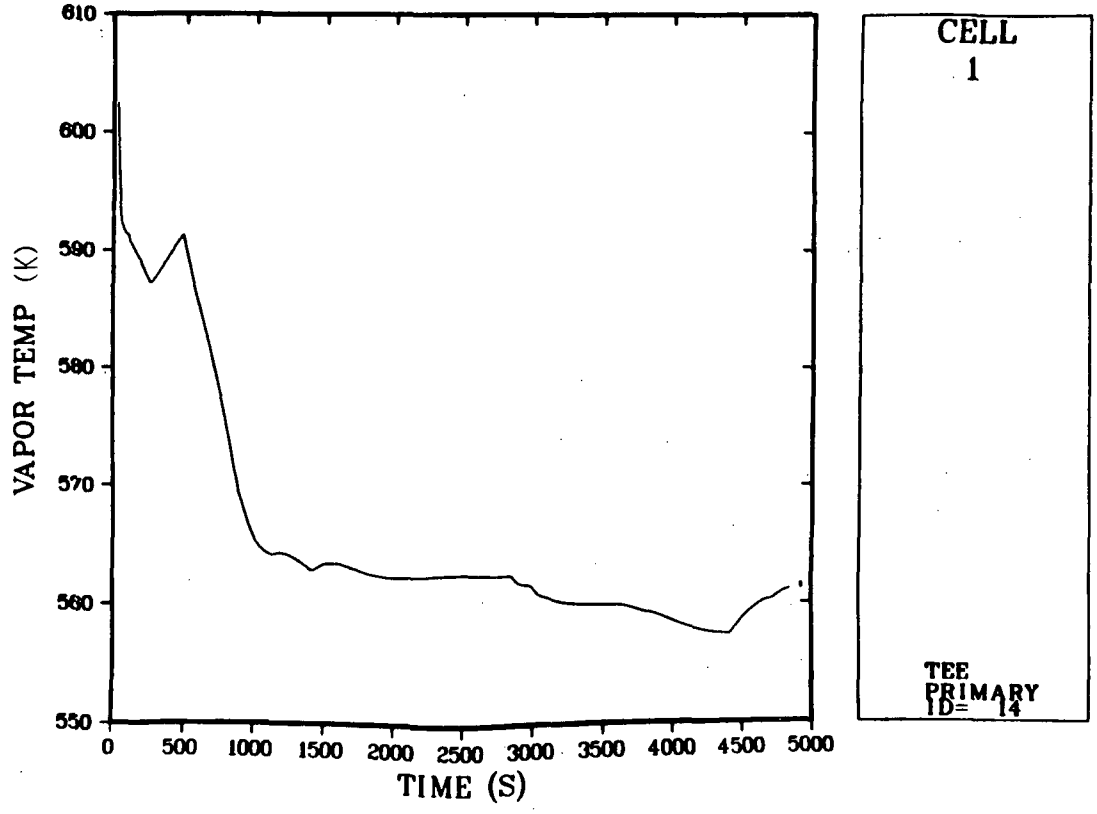

A Loop cold-leg vapor temperature.

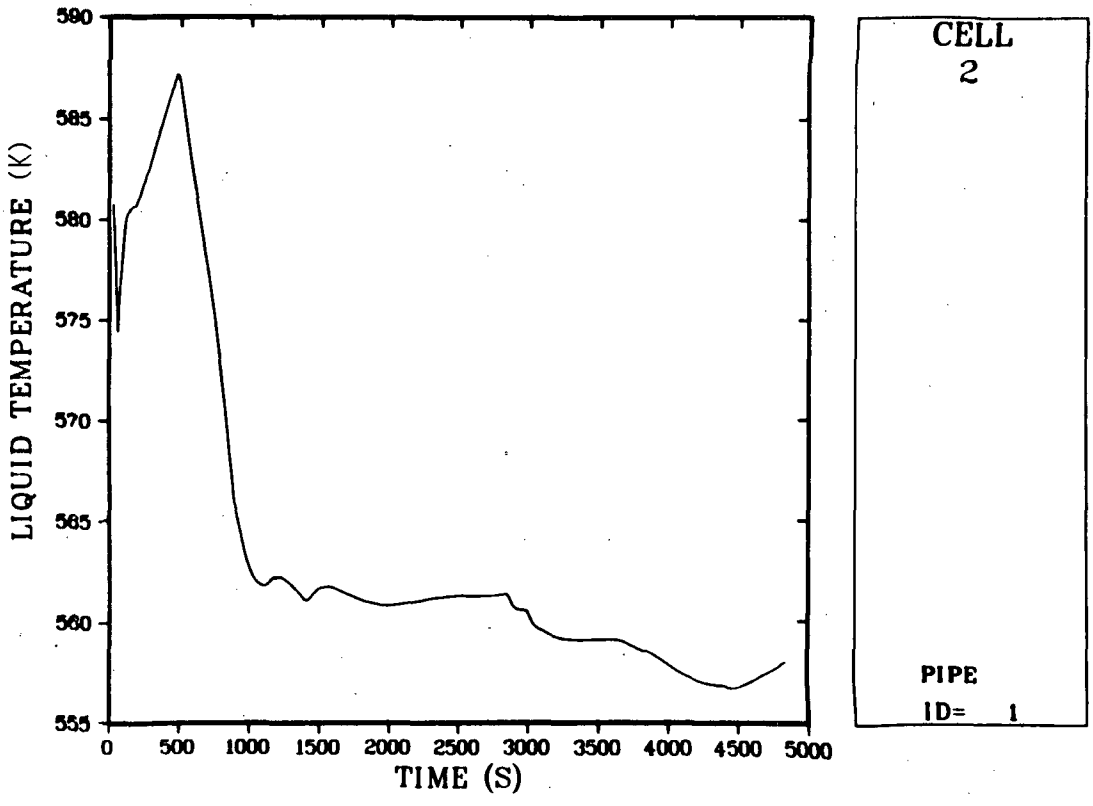

B Loop hot-leg liquid temperature.

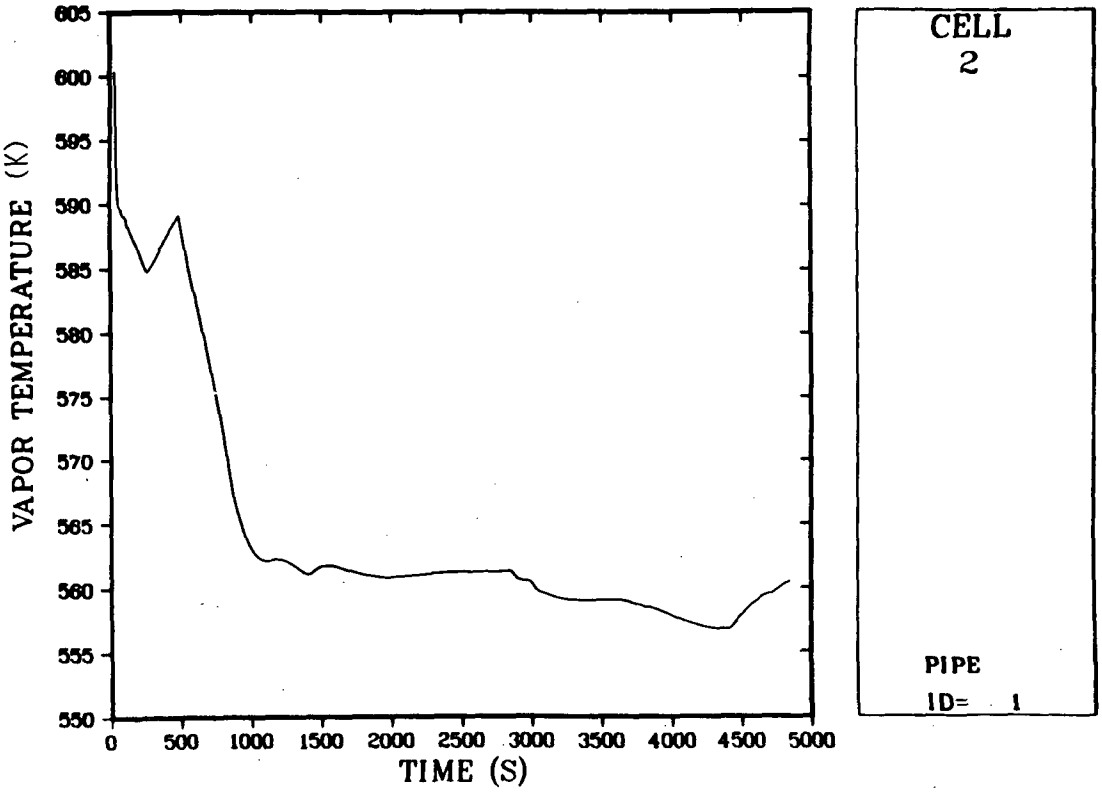

B Loop hot-leg vapor temperature.

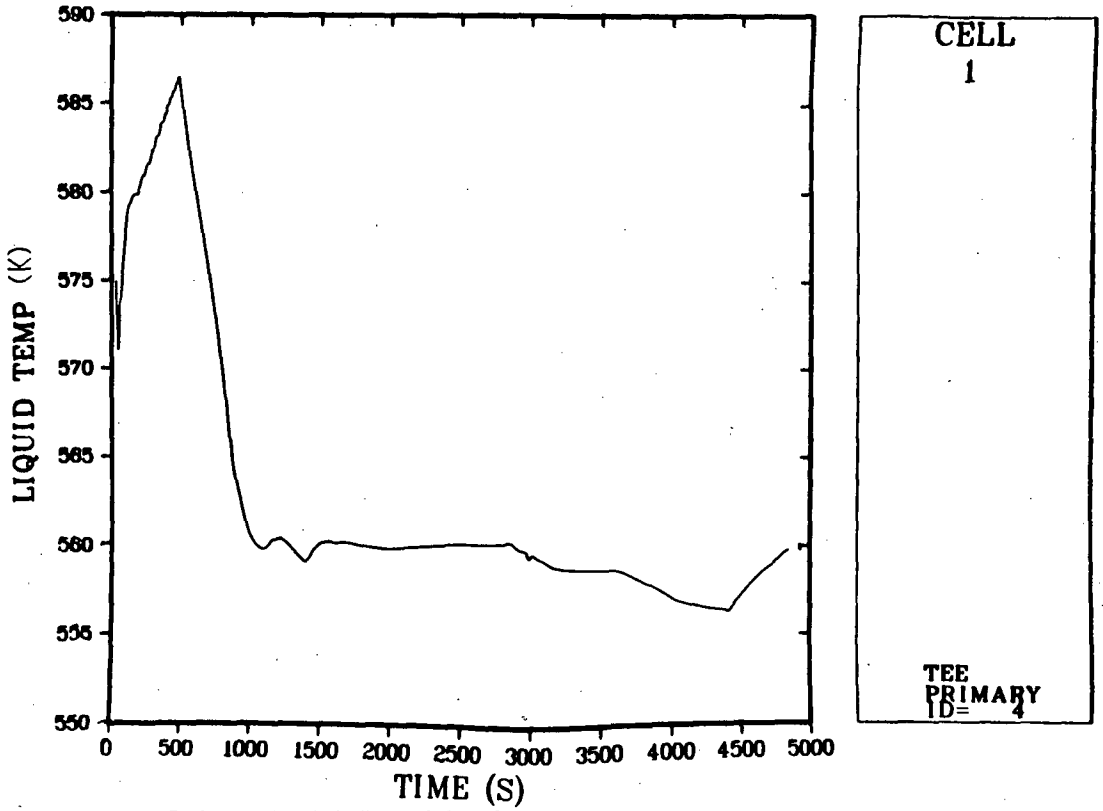

B Loop cold-leg liquid temperature.

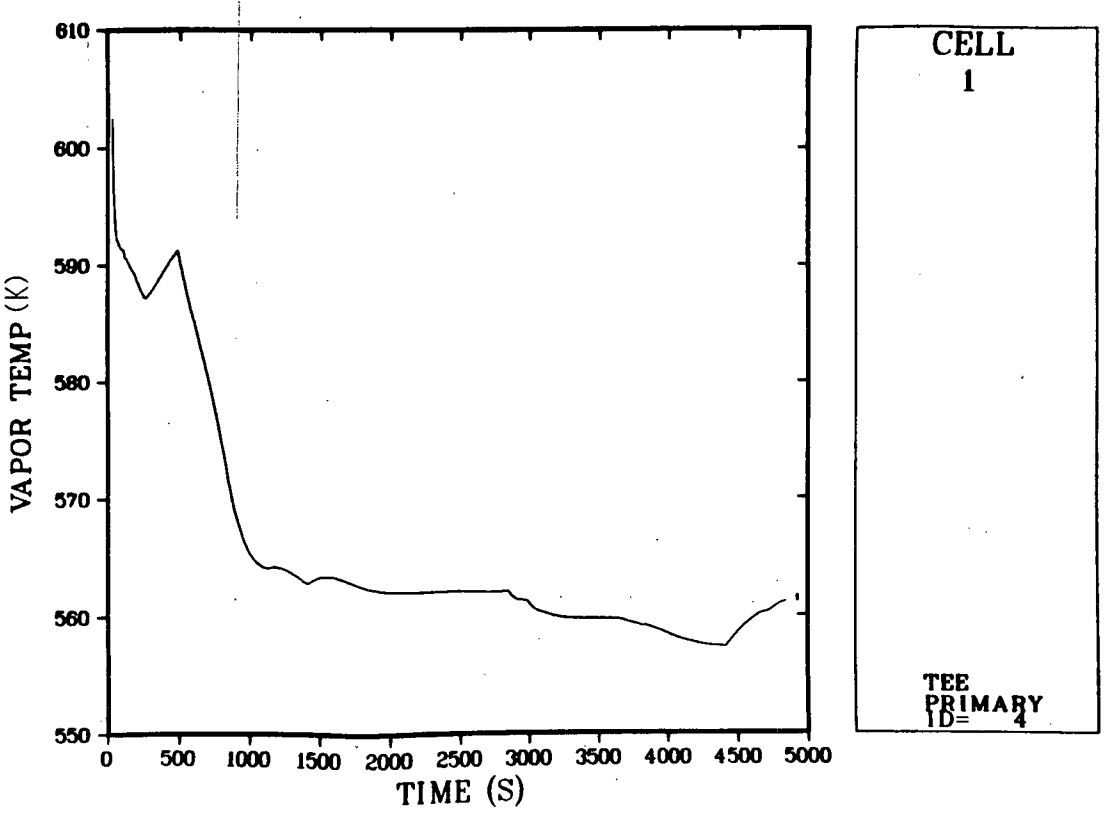

B Loop cold-leg vapor temperature.

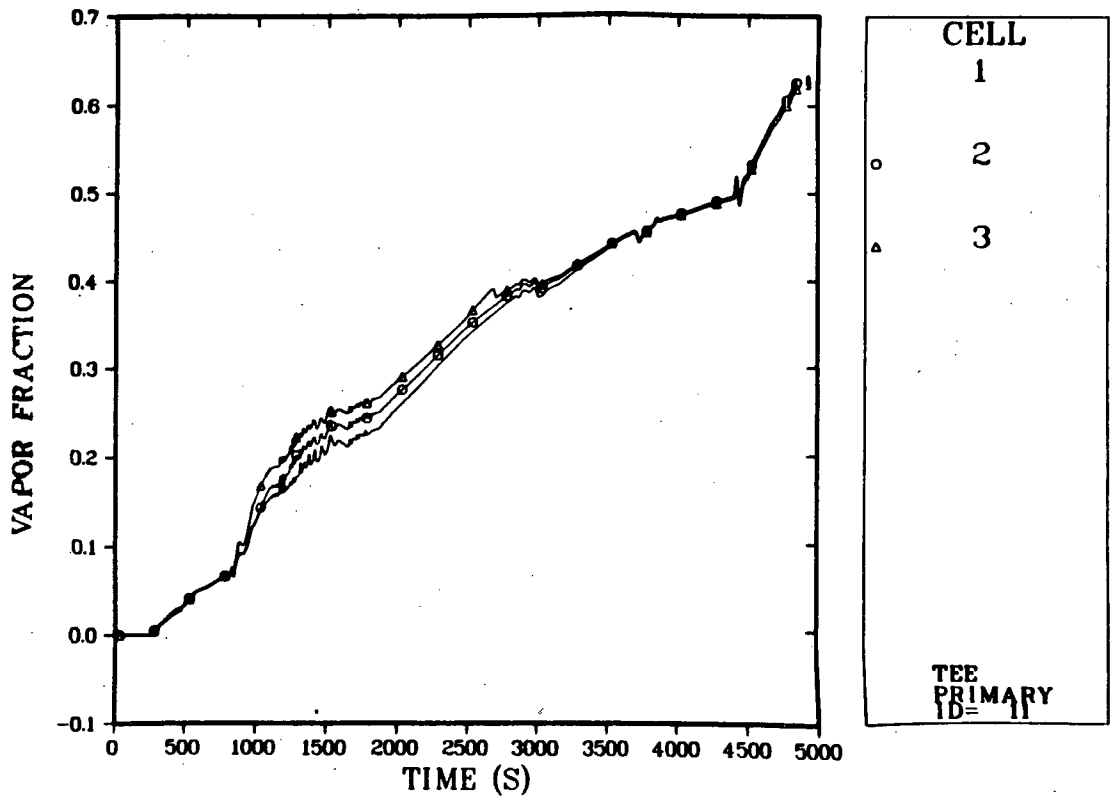

A Loop hot-leg void fraction distribution (Cells 1, 2, 3).

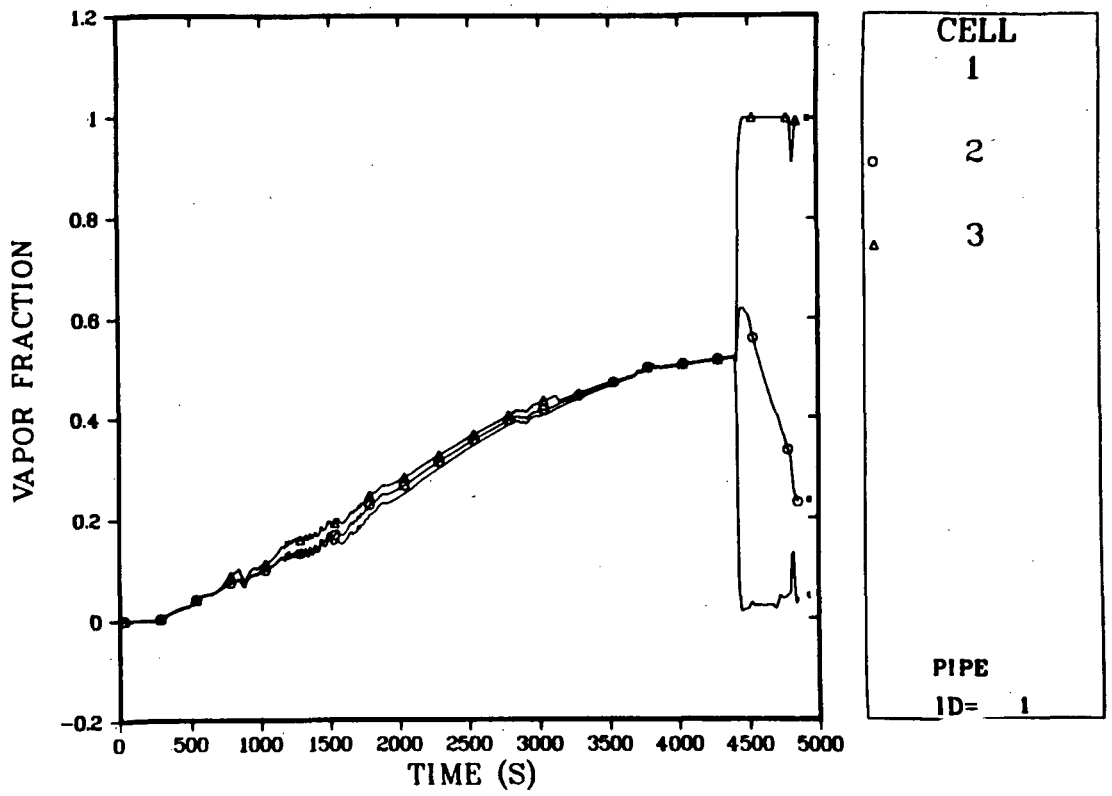

B Loop hot-leg void fraction distribution (Cells 1, 2, 3).

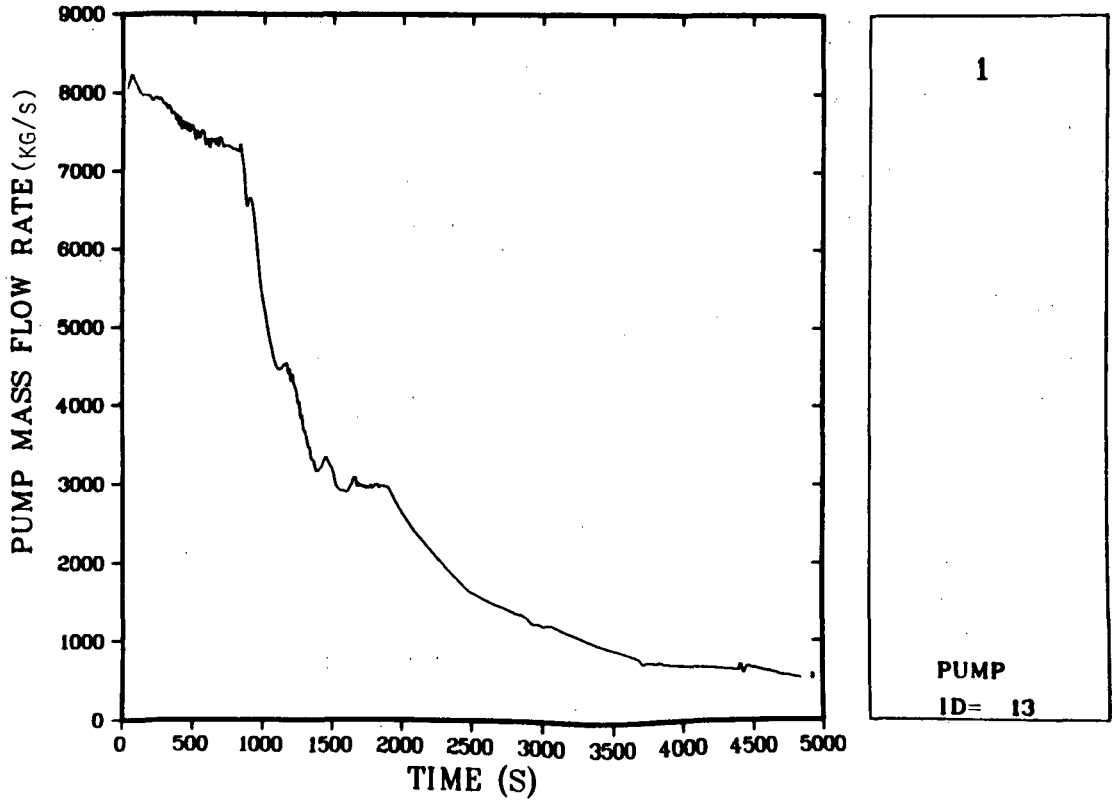

A Loop pump mass flow rate.

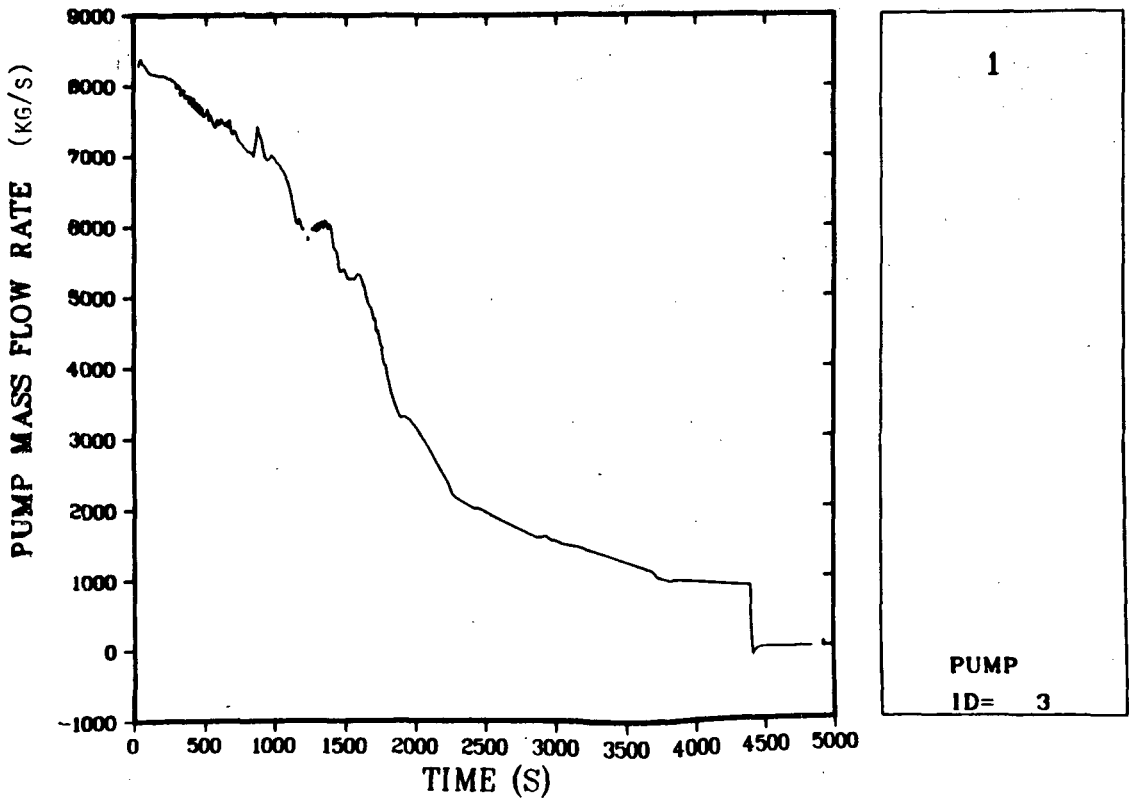

B Loop pump mass flow rate.

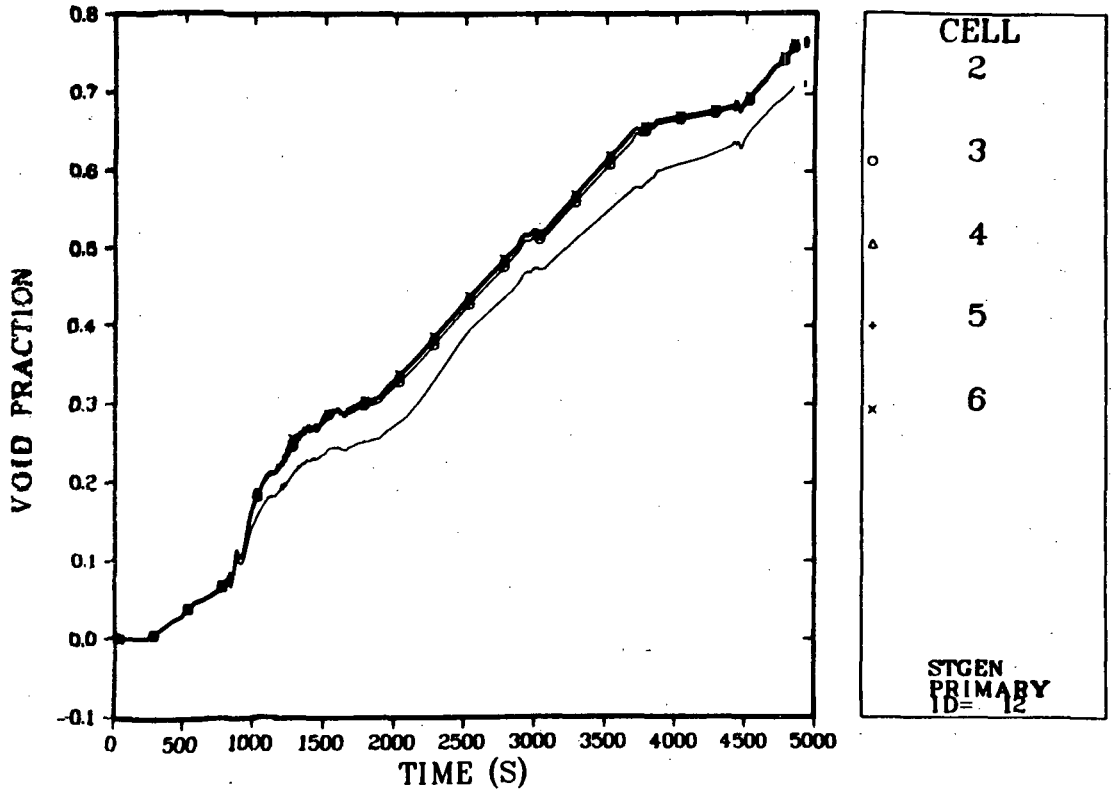

A Loop steam generator void fraction distribution.

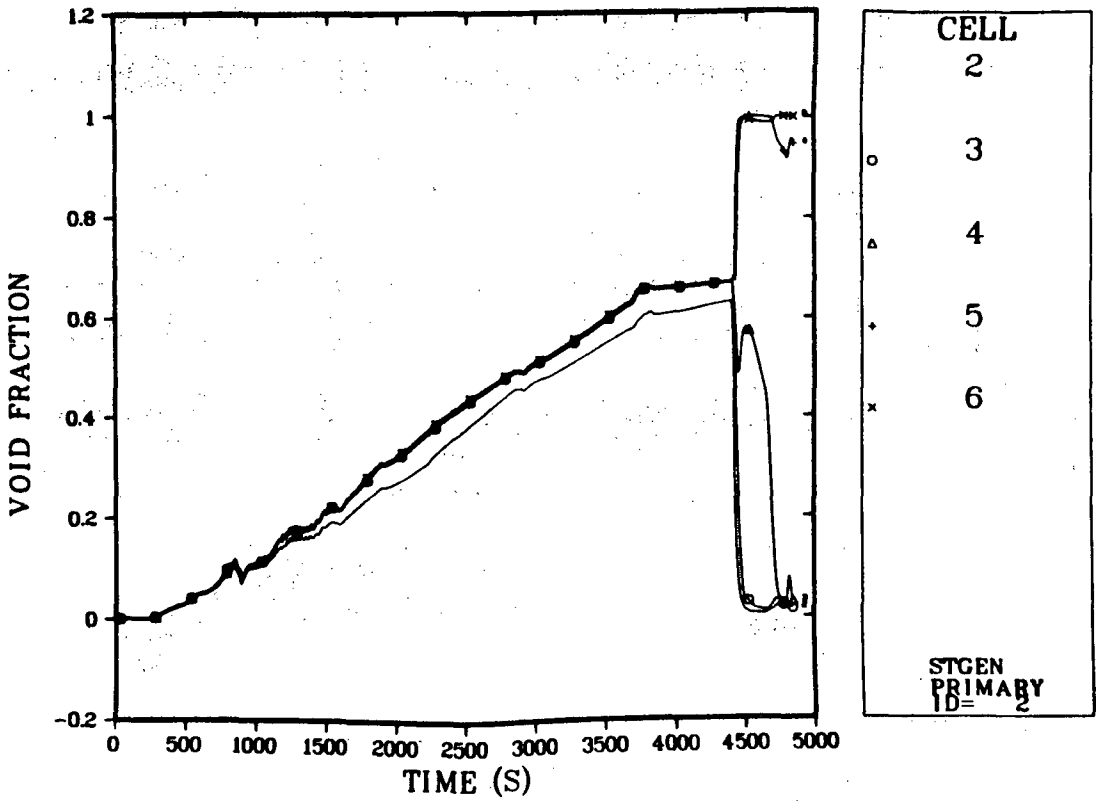

B Loop steam generator void fraction distribution.

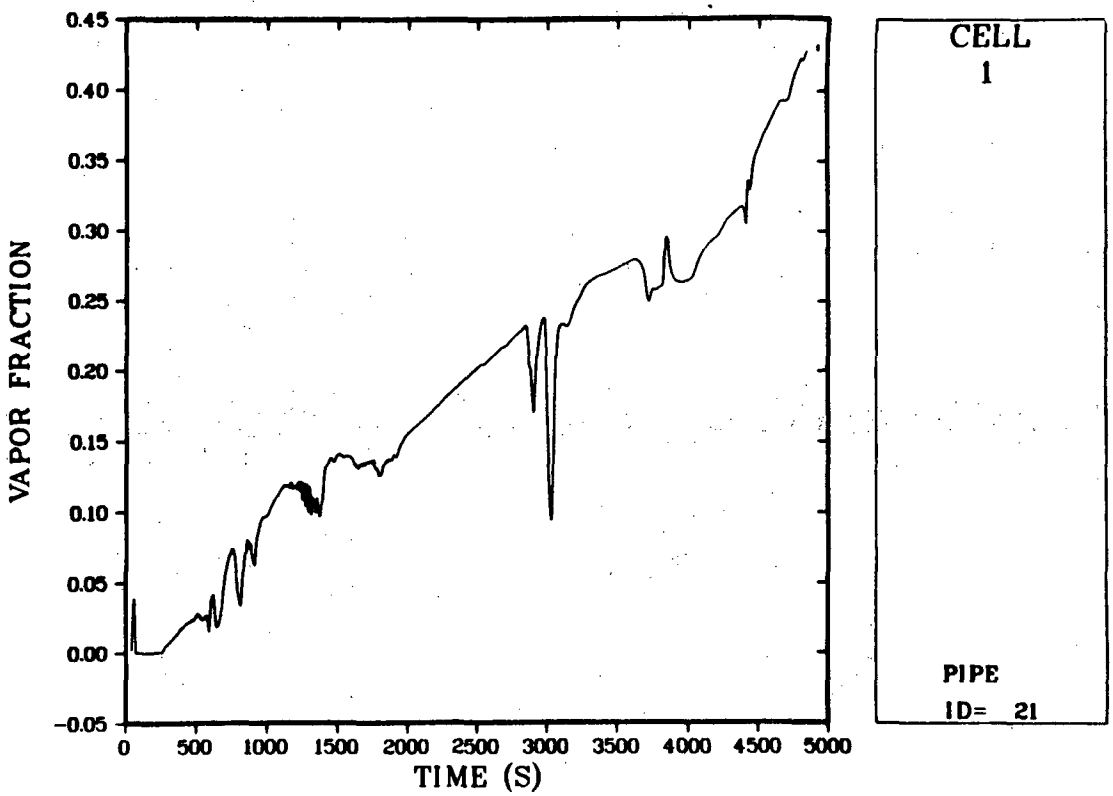

Pressurizer surge line void fraction.

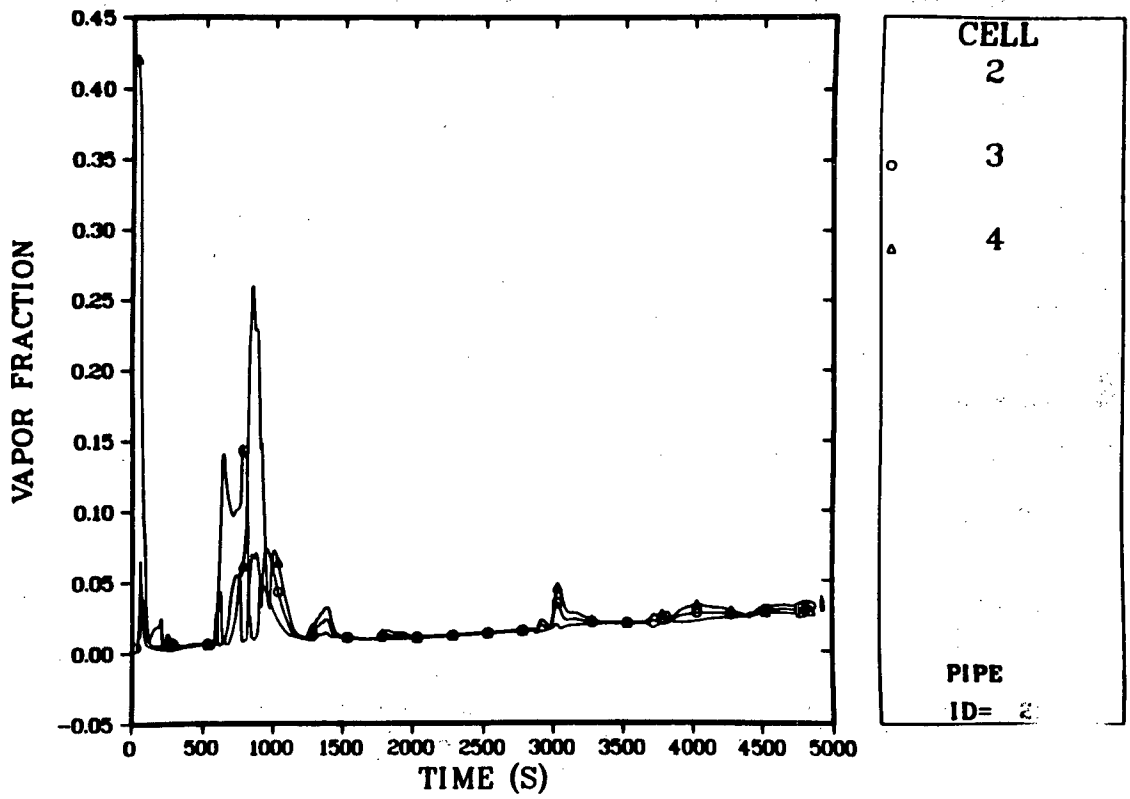

Pressurizer void fraction distribution (first 3 cells).

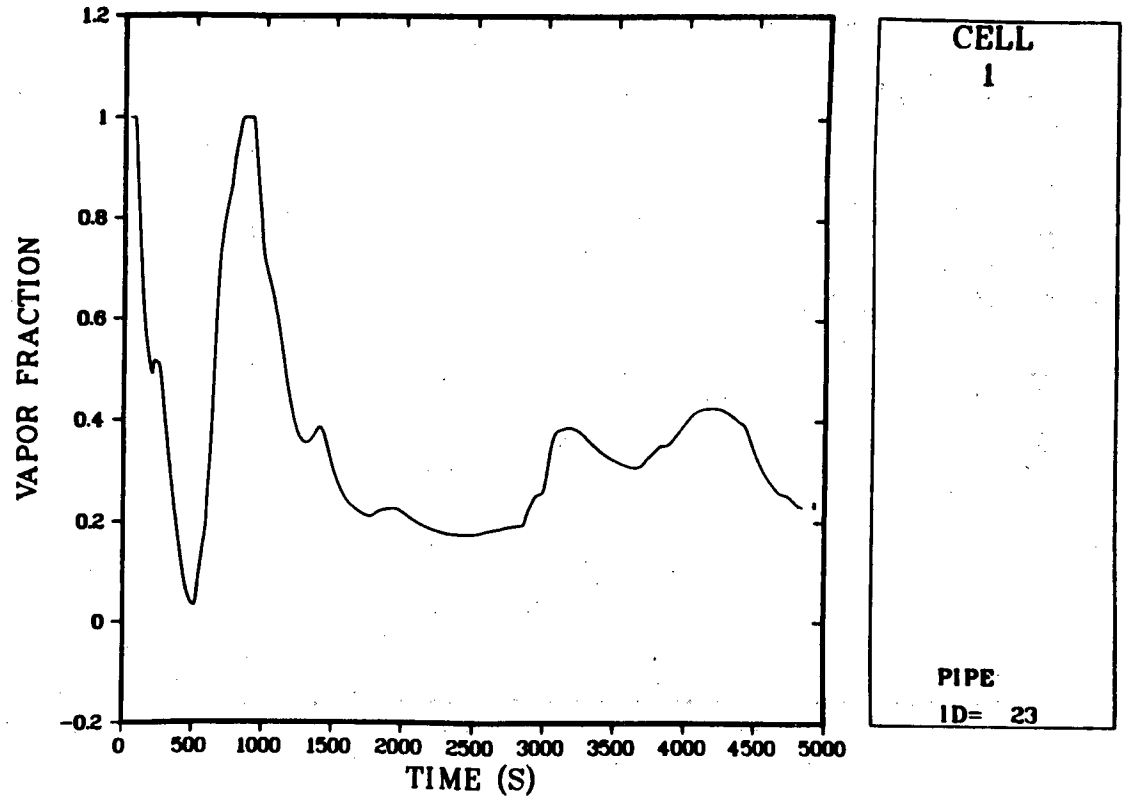

Pressurizer void fraction (top cell).

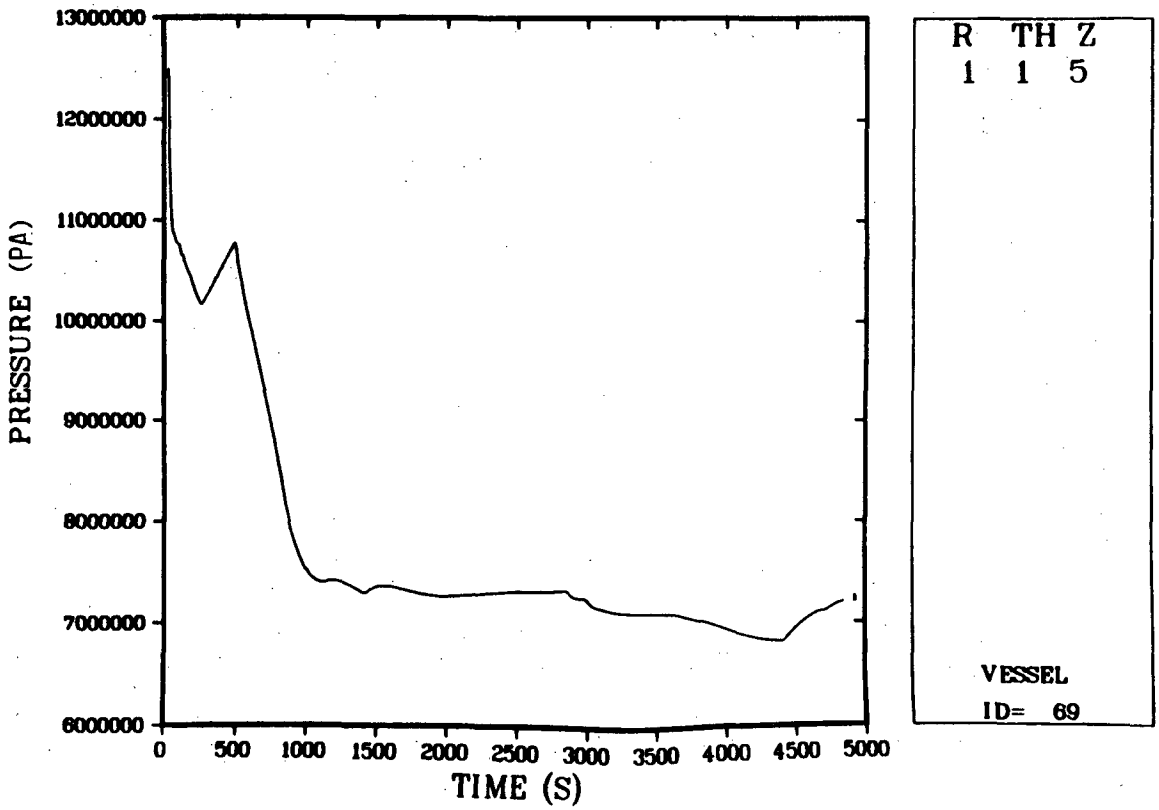

Upper plenum pressure.

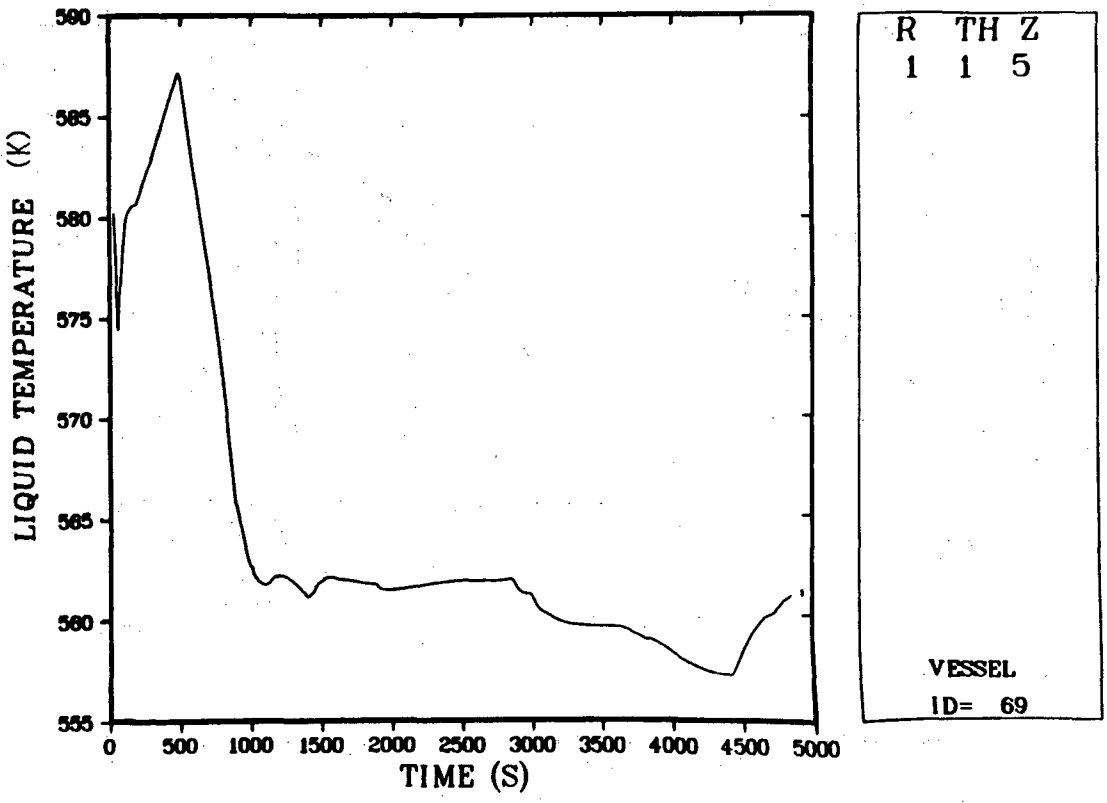

Upper plenum liquid temperature.

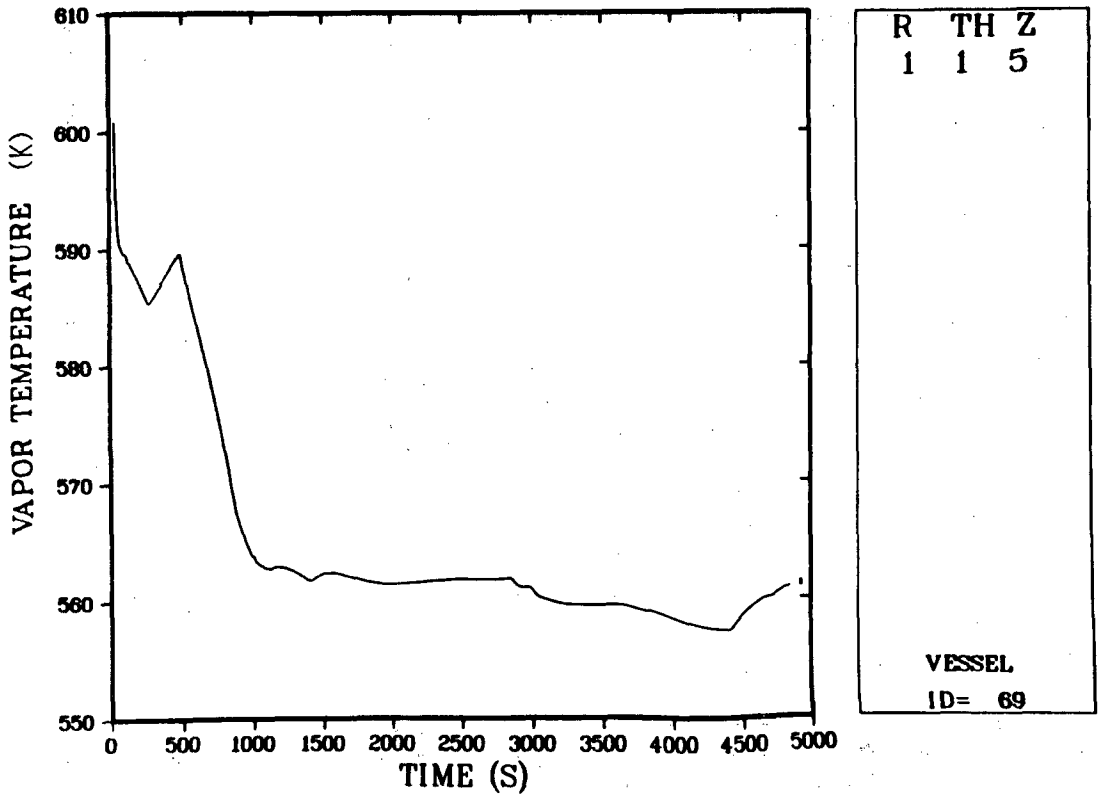

Upper plenum vapor temperature.

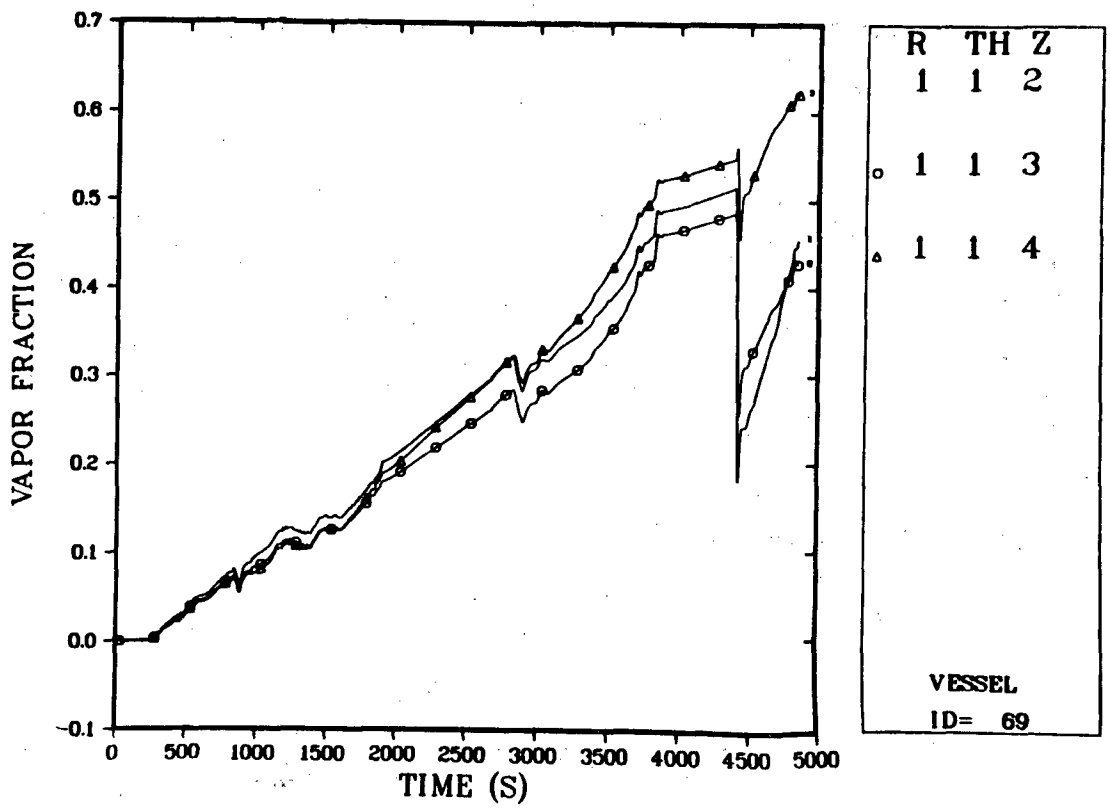

Core void fraction profile (axial direction - Cell 1).

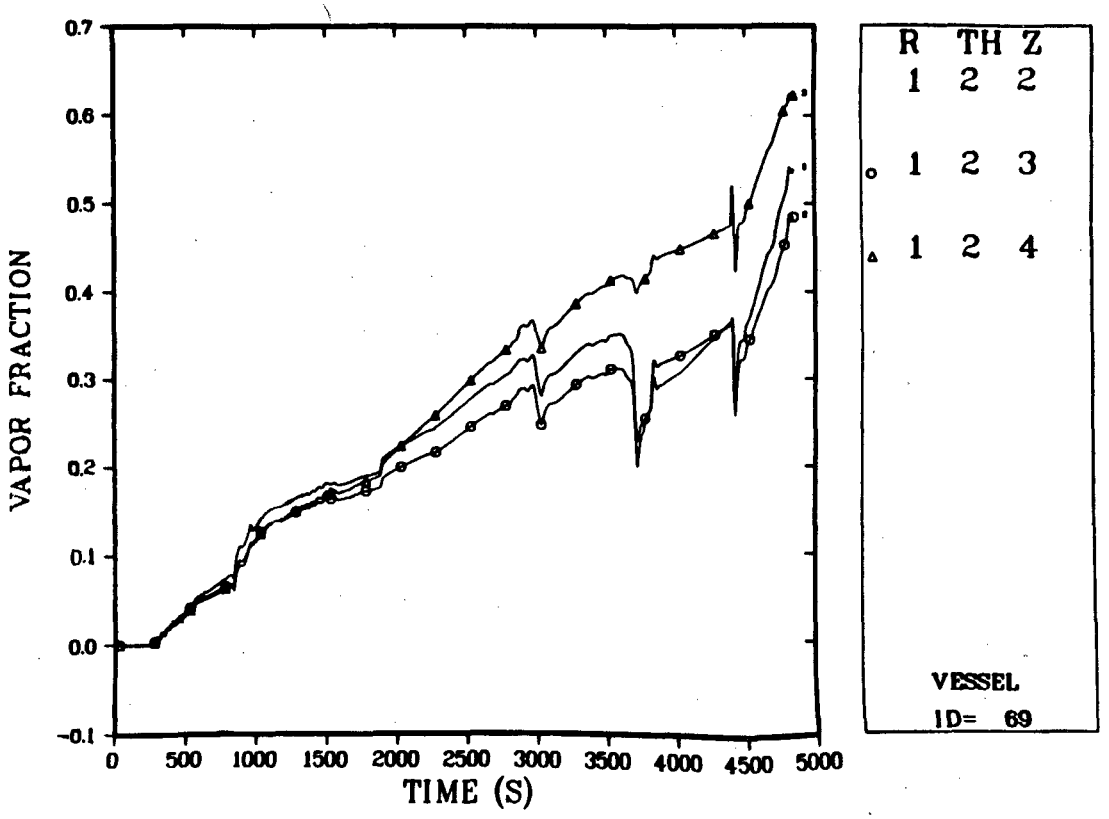

Core void fraction profile (axial direction - Cell 2).

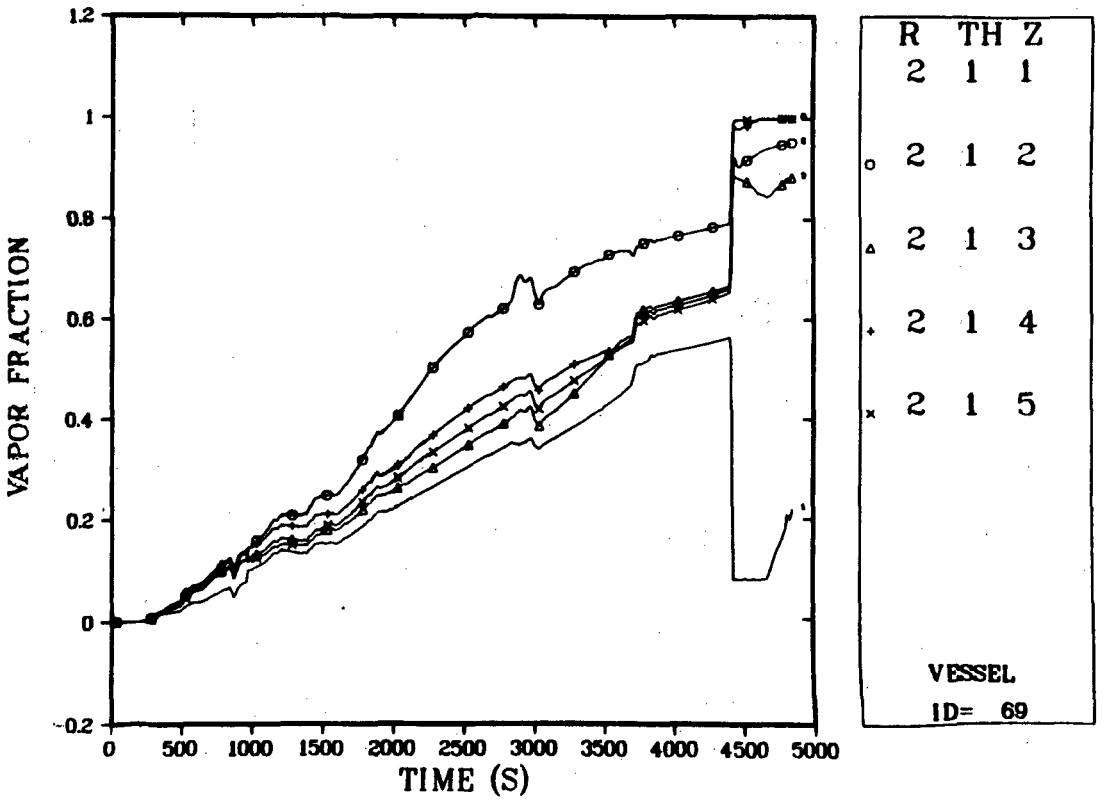

Downcomer void fraction profile.

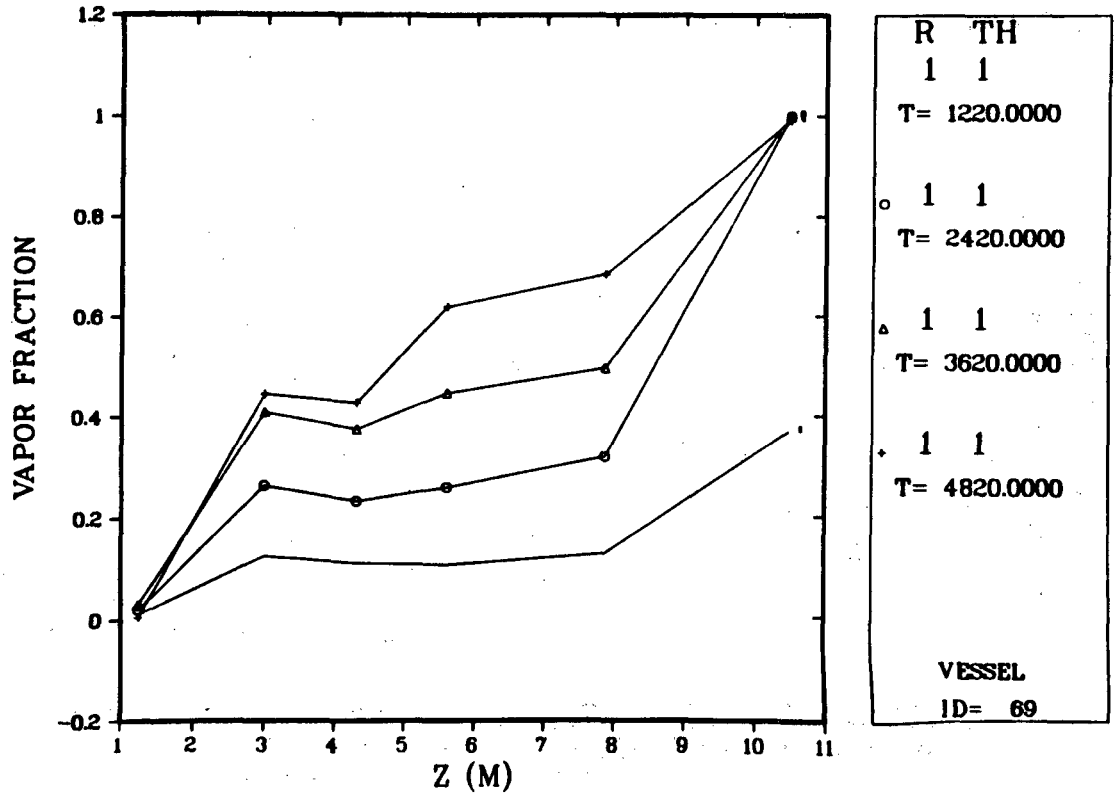

Vessel void fraction profile vs time.

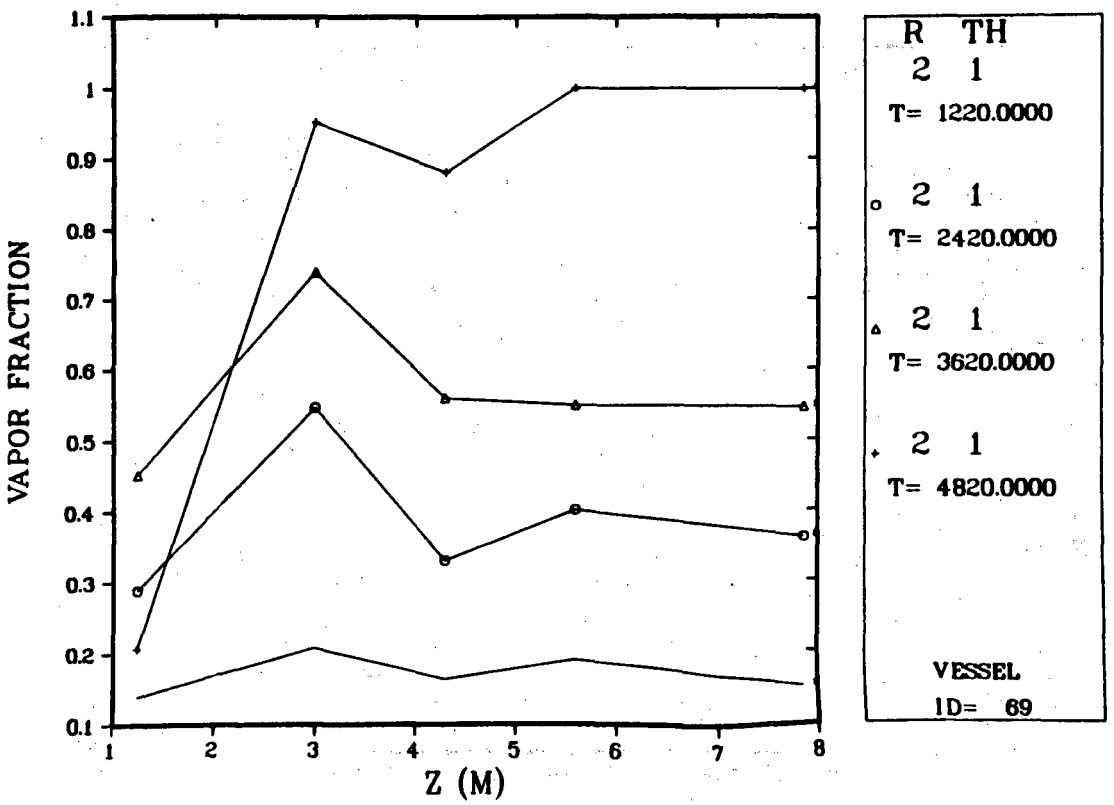

Downcomer void fraction profile vs time.

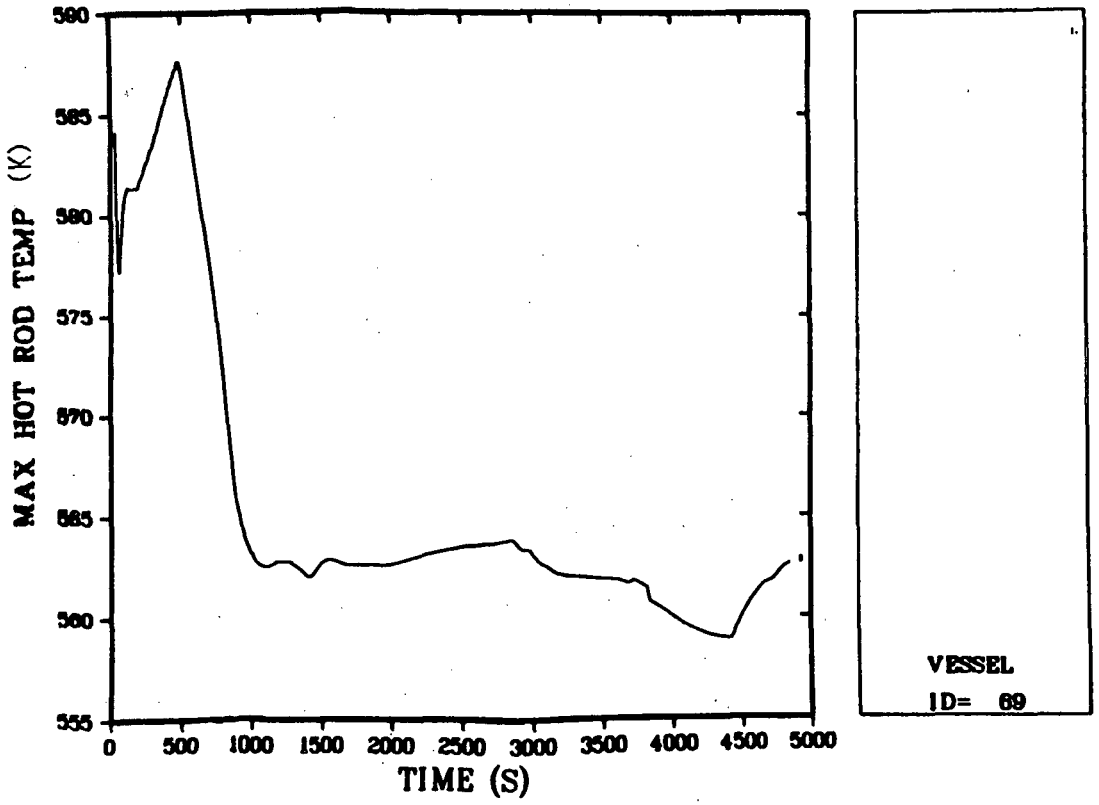

Maximum hot-rod temperature.

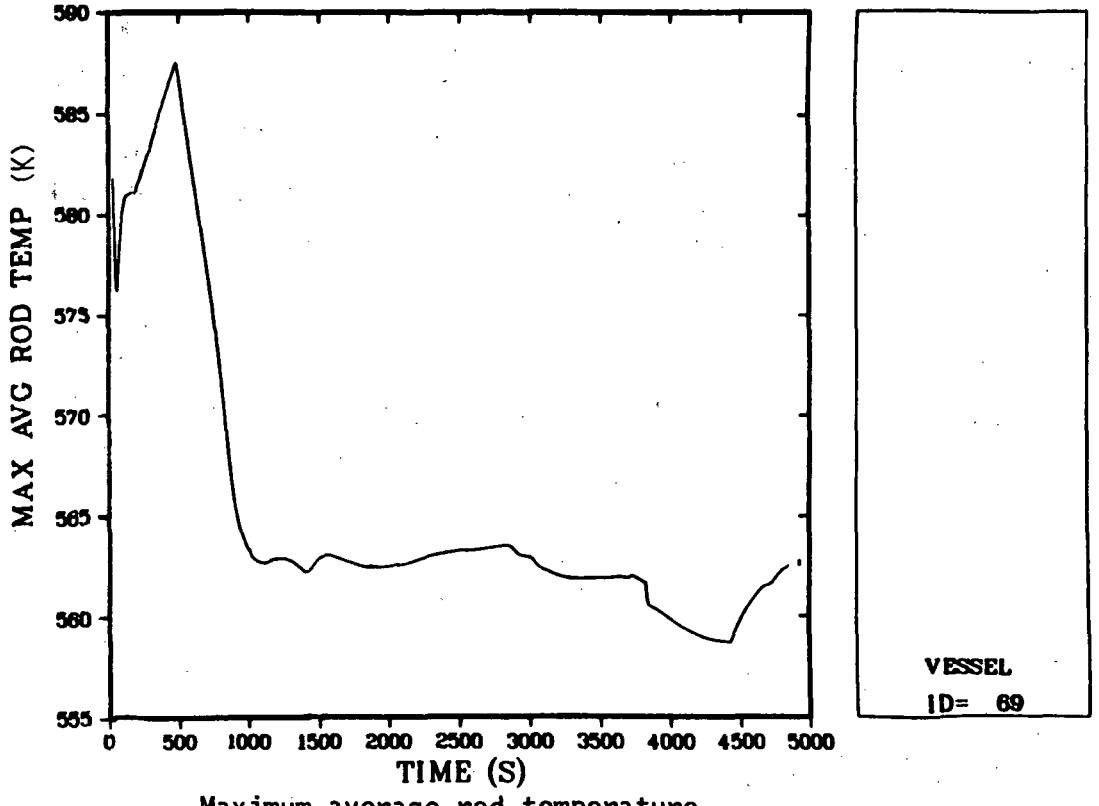

Maximum average rod temperature.

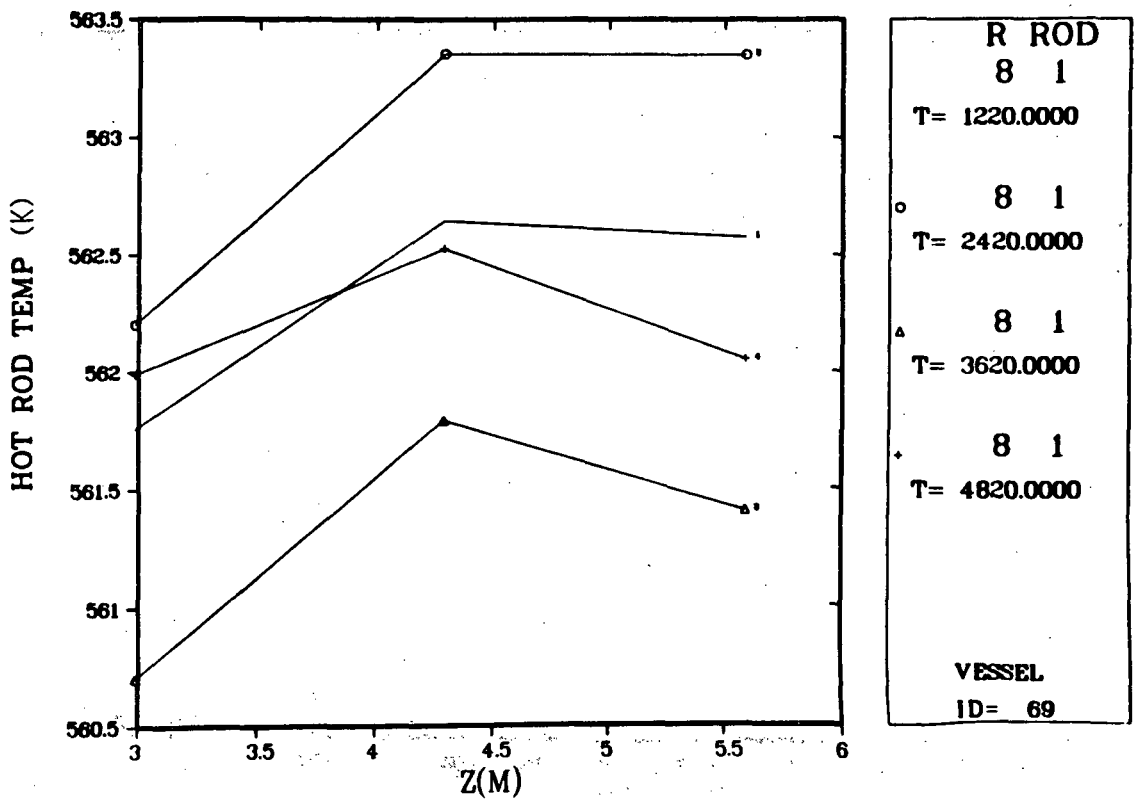

Hot-rod temperature profile vs time (Rod 1).

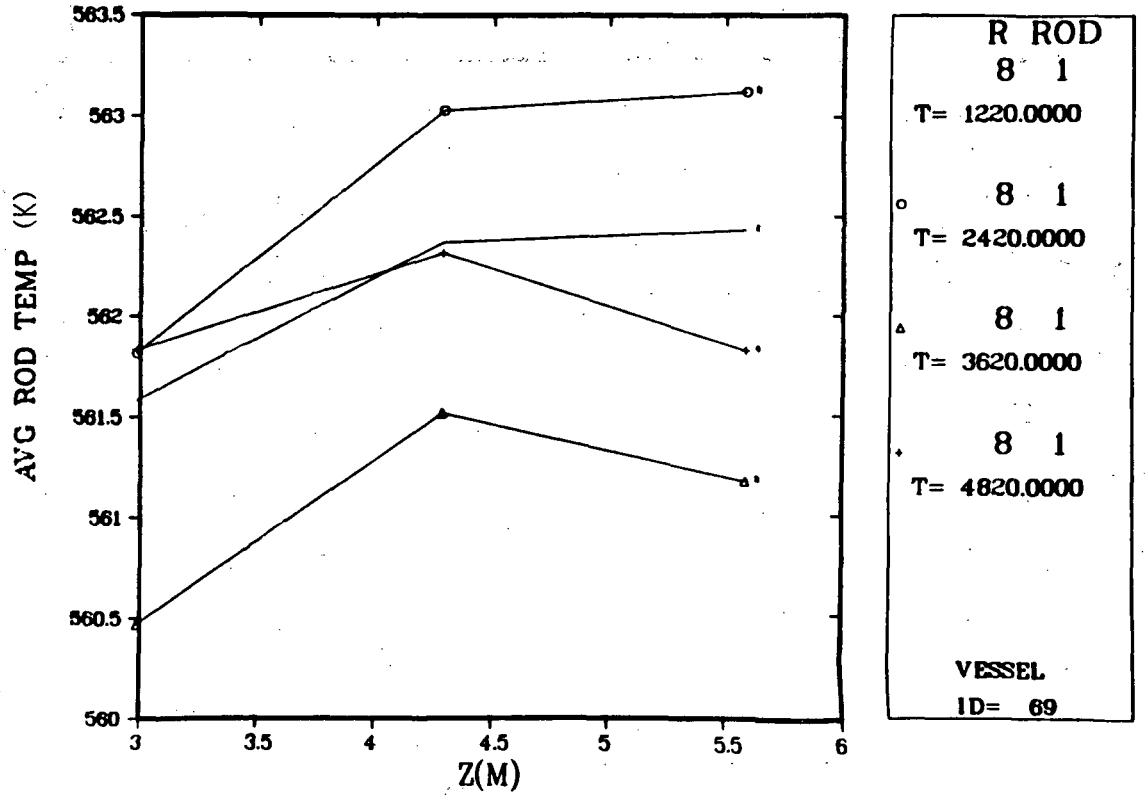

Average rod temperature profile vs time (Rod 1).

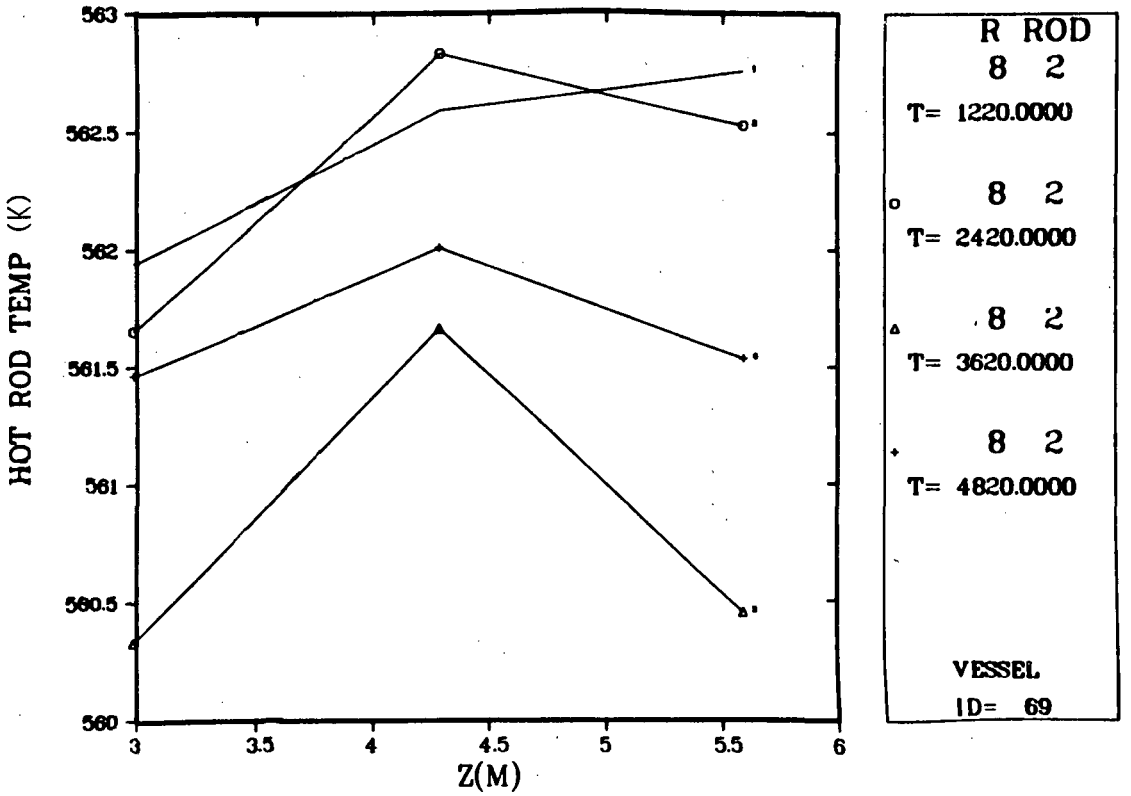

Hot-rod temperature profile vs time (Rod 2).

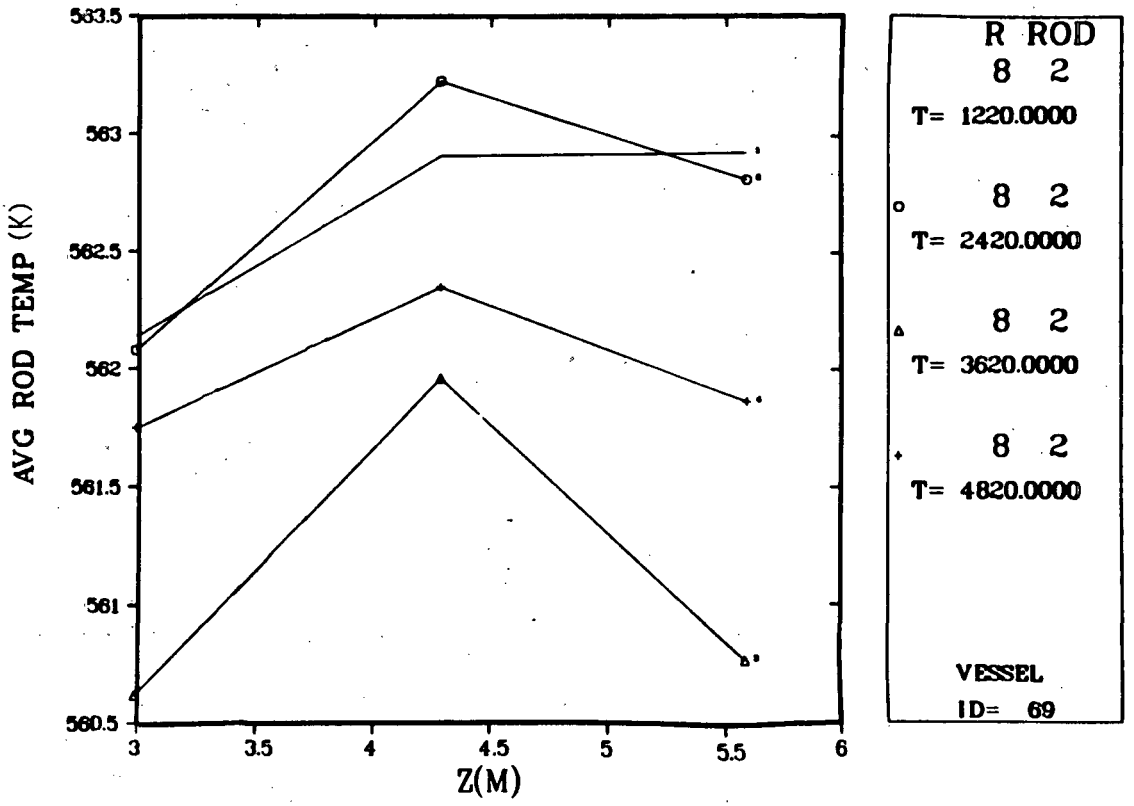

Average rod temperature profile vs time (Rod 2).

81 min $\leq$ T $\leq$ 138 min

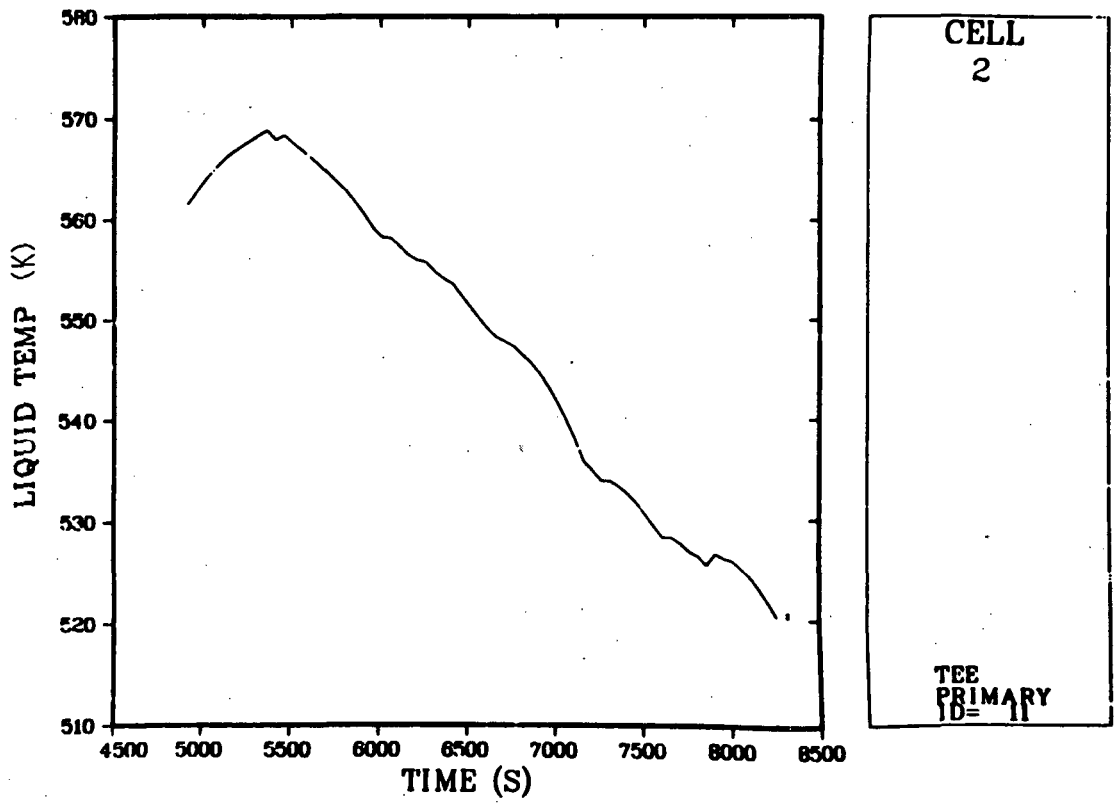

A Loop hot-leg liquid temperature.

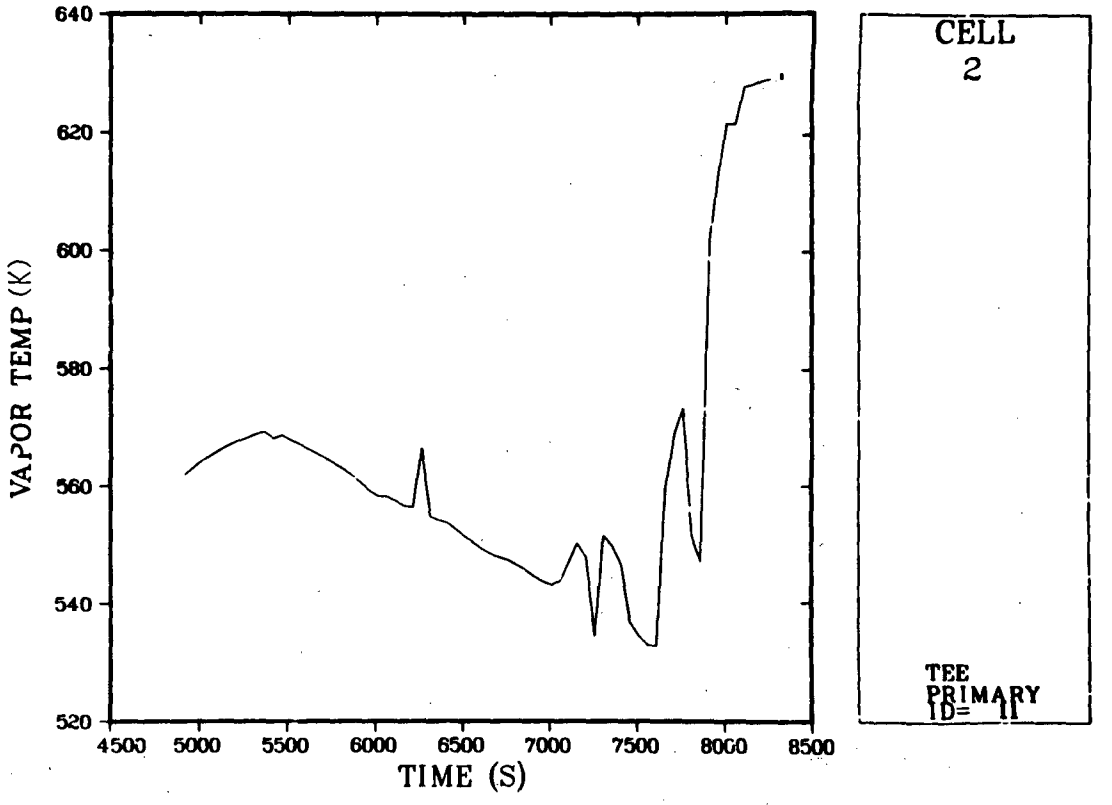

A Loop hot-leg vapor temperature.

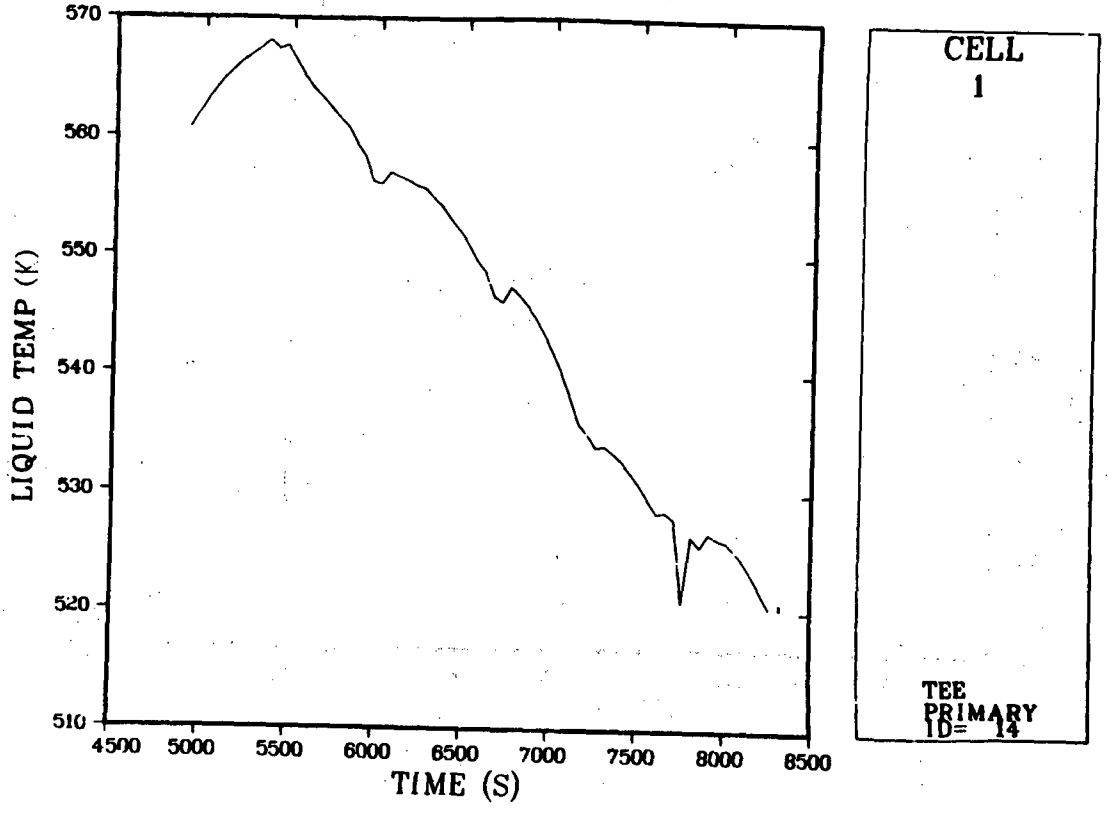

A Loop cold-leg liquid temperature.

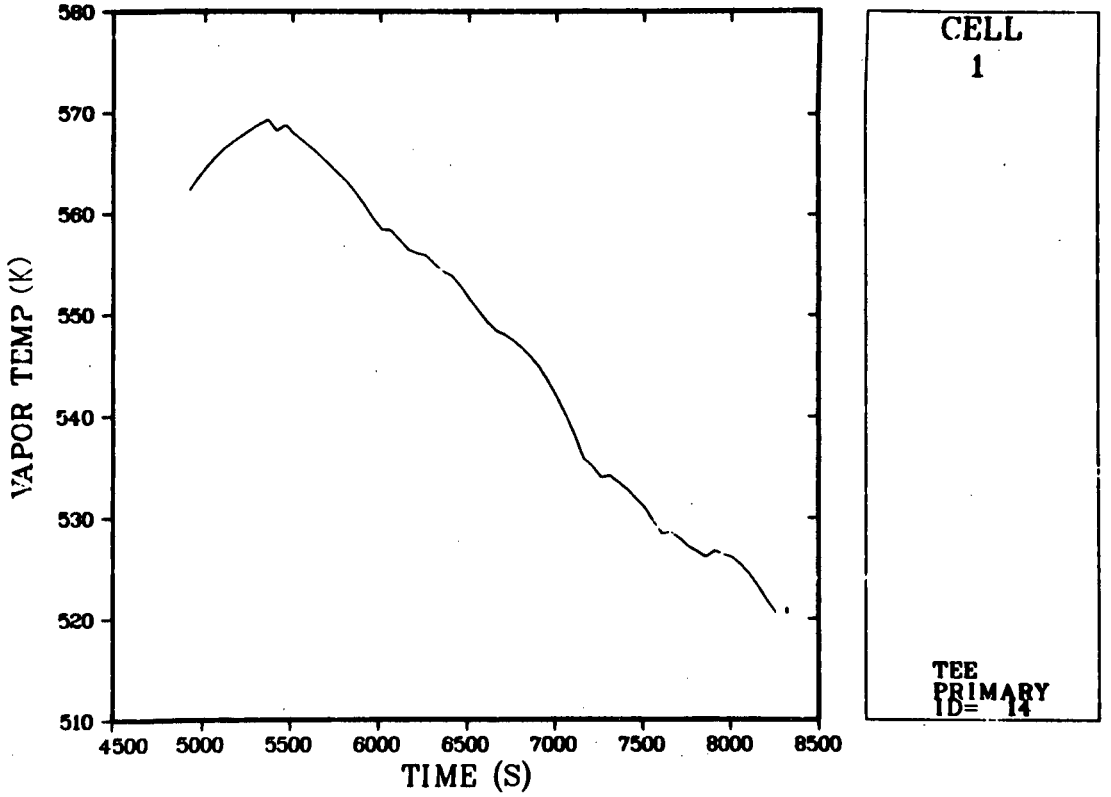

A Loop cold-leg vapor temperature.

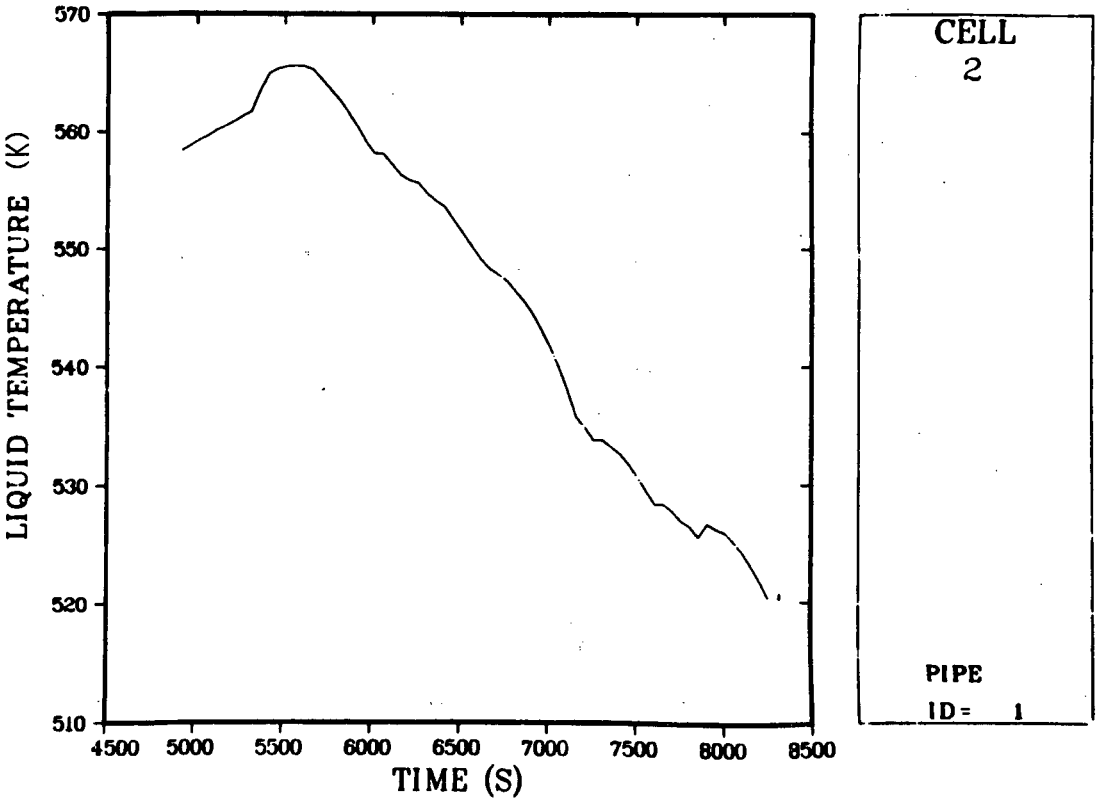

B Loop hot-leg liquid temperature.

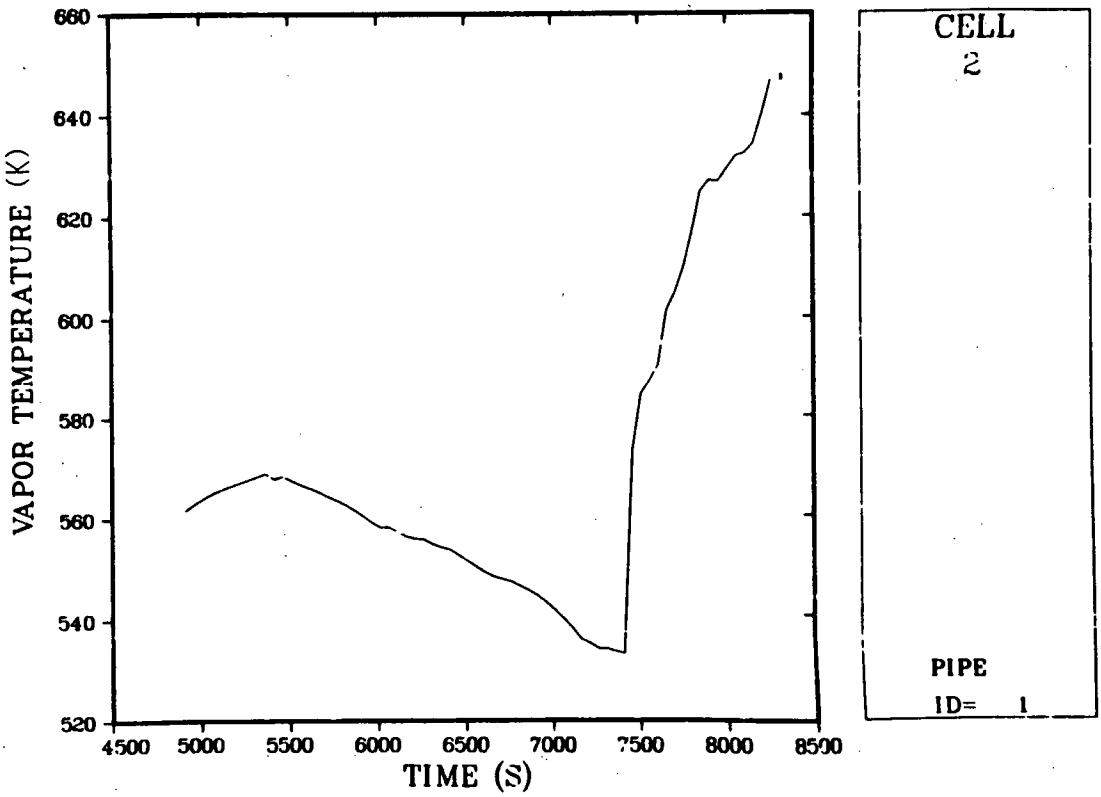

B Loop hot-leg vapor temperature.

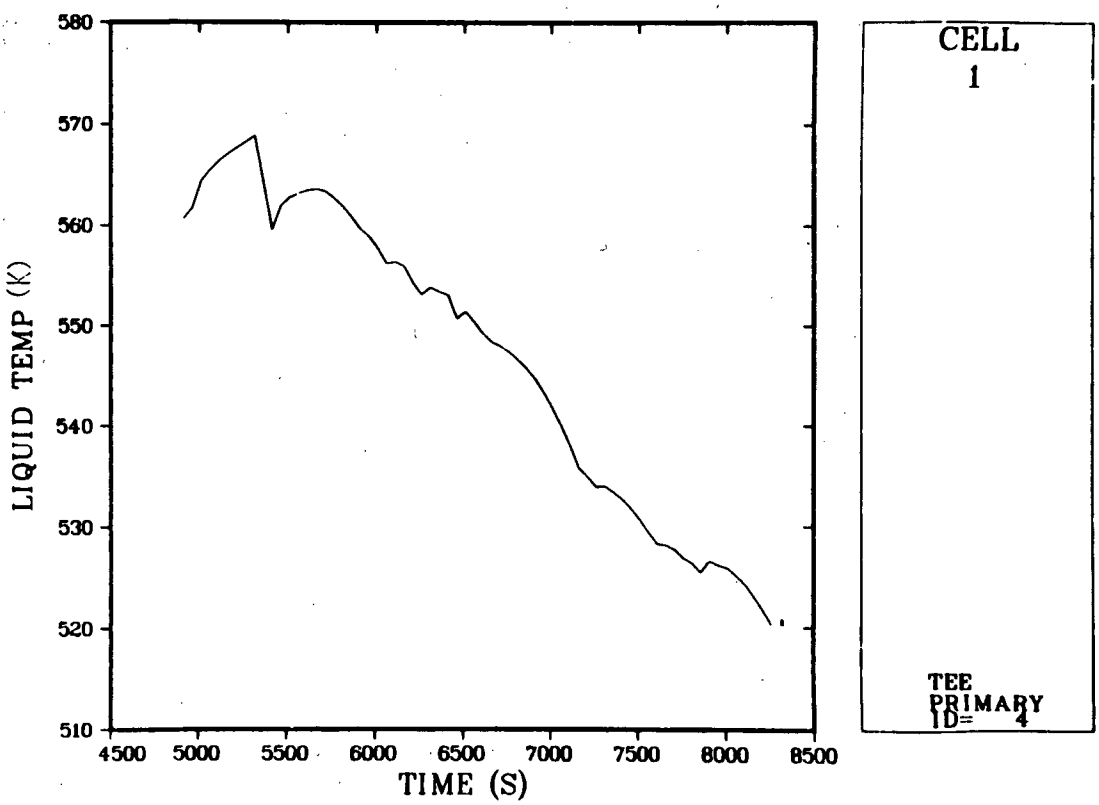

B Loop cold-leg liquid temperature.

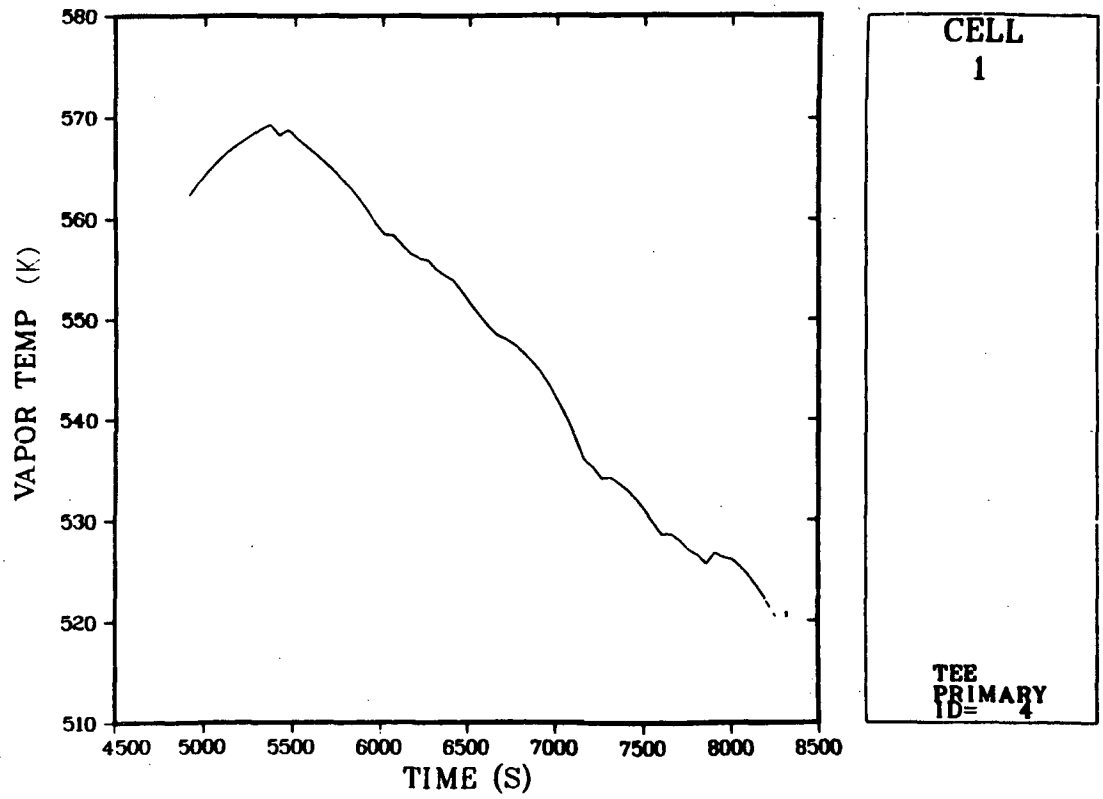

B Loop cold-leg vapor temperature.

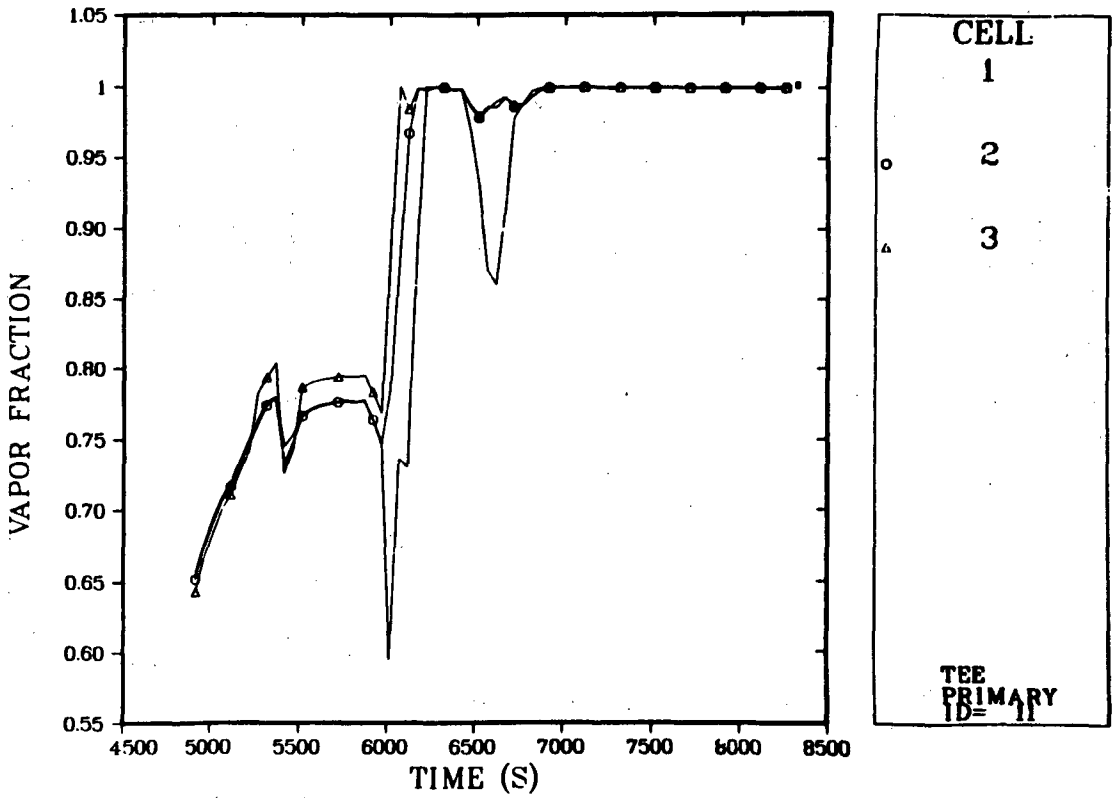

A Loop hot-leg void fraction distribution (Cells 1, 2, 3).

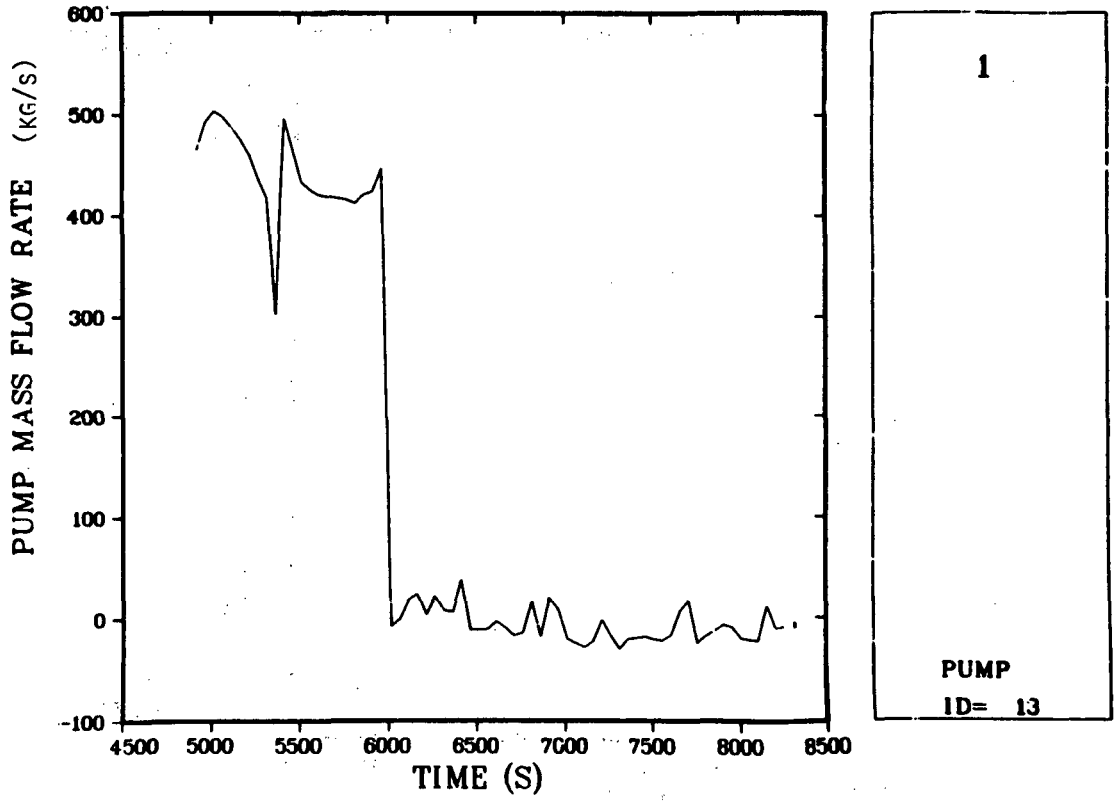

A Loop pump mass flow rate.

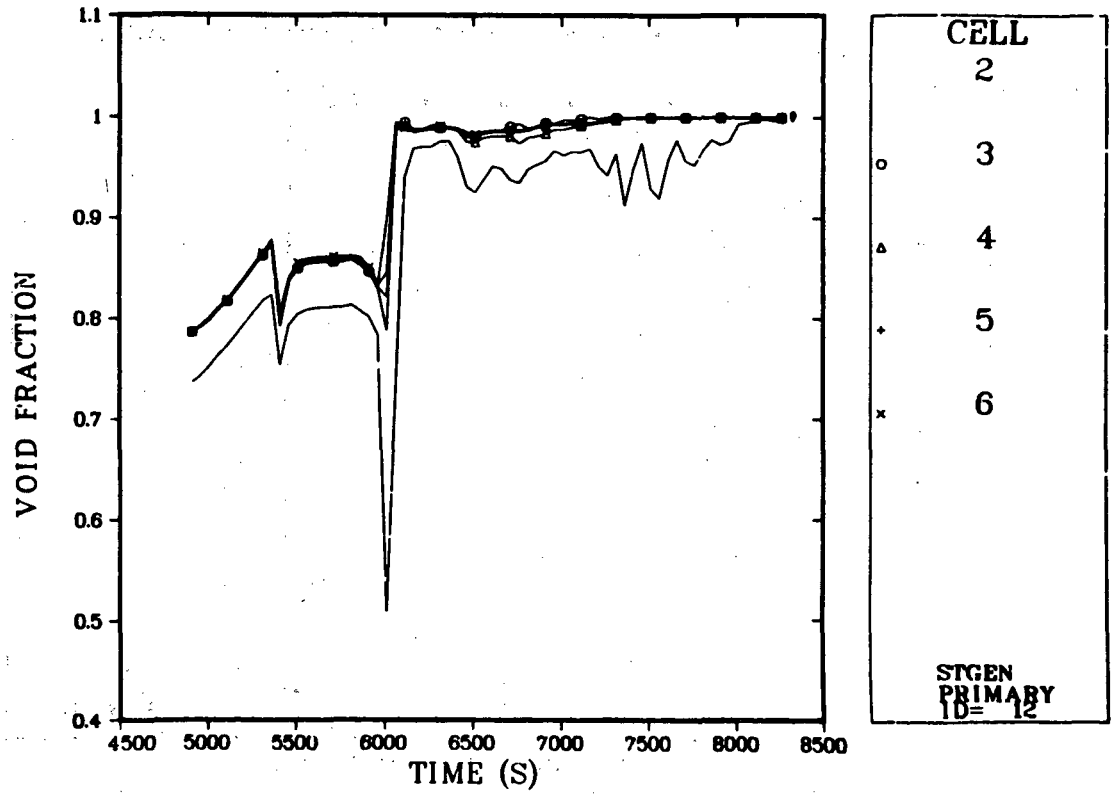

A Loop steam generator void fraction distribution.

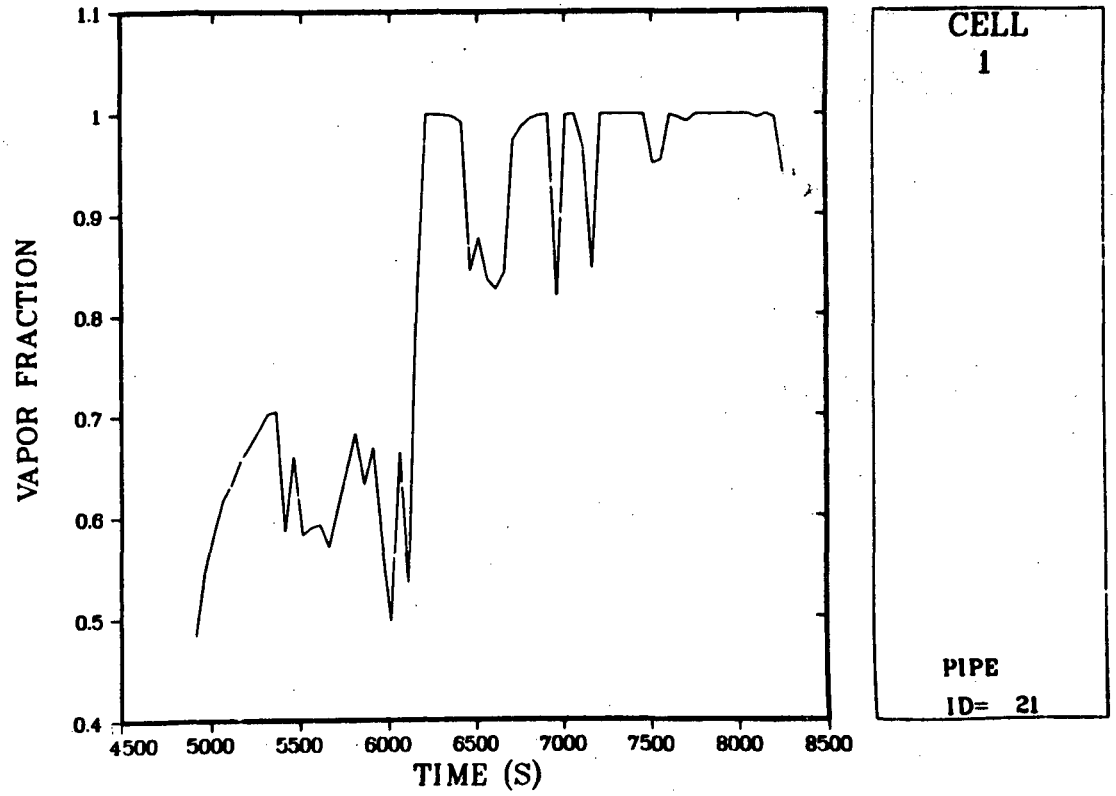

Pressurizer surge line void fraction.

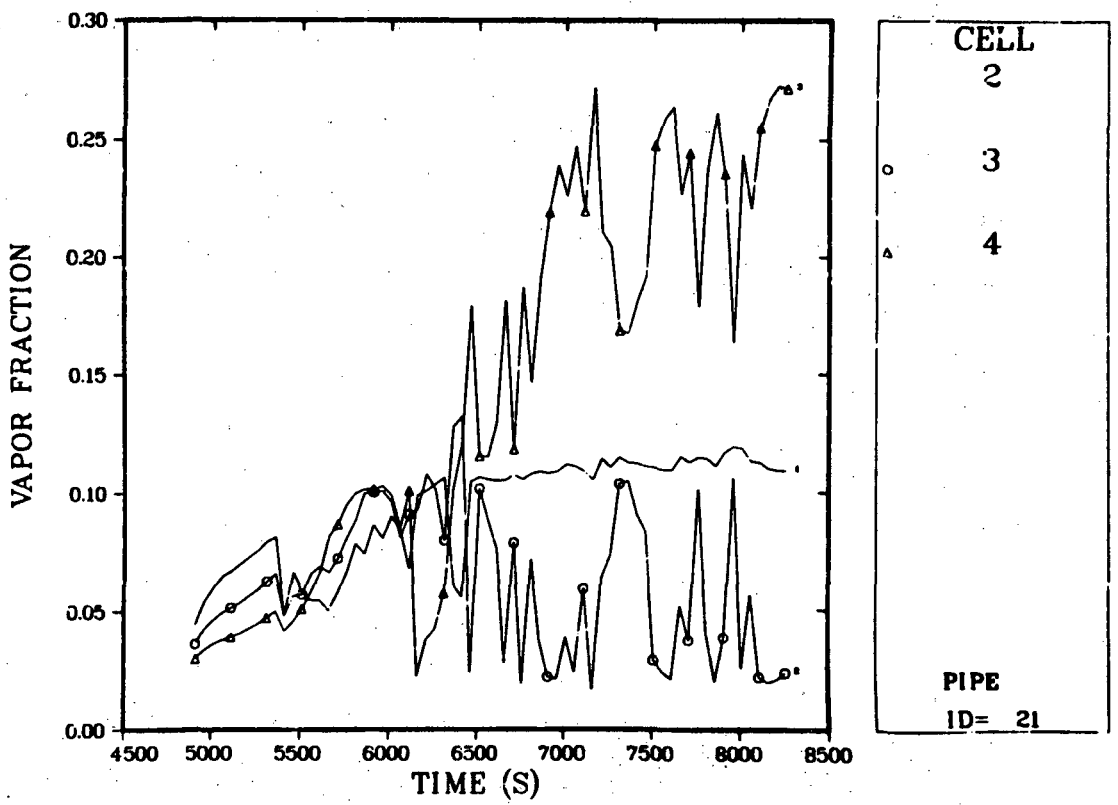

Pressurizer void fraction distribution (first 3 cells).

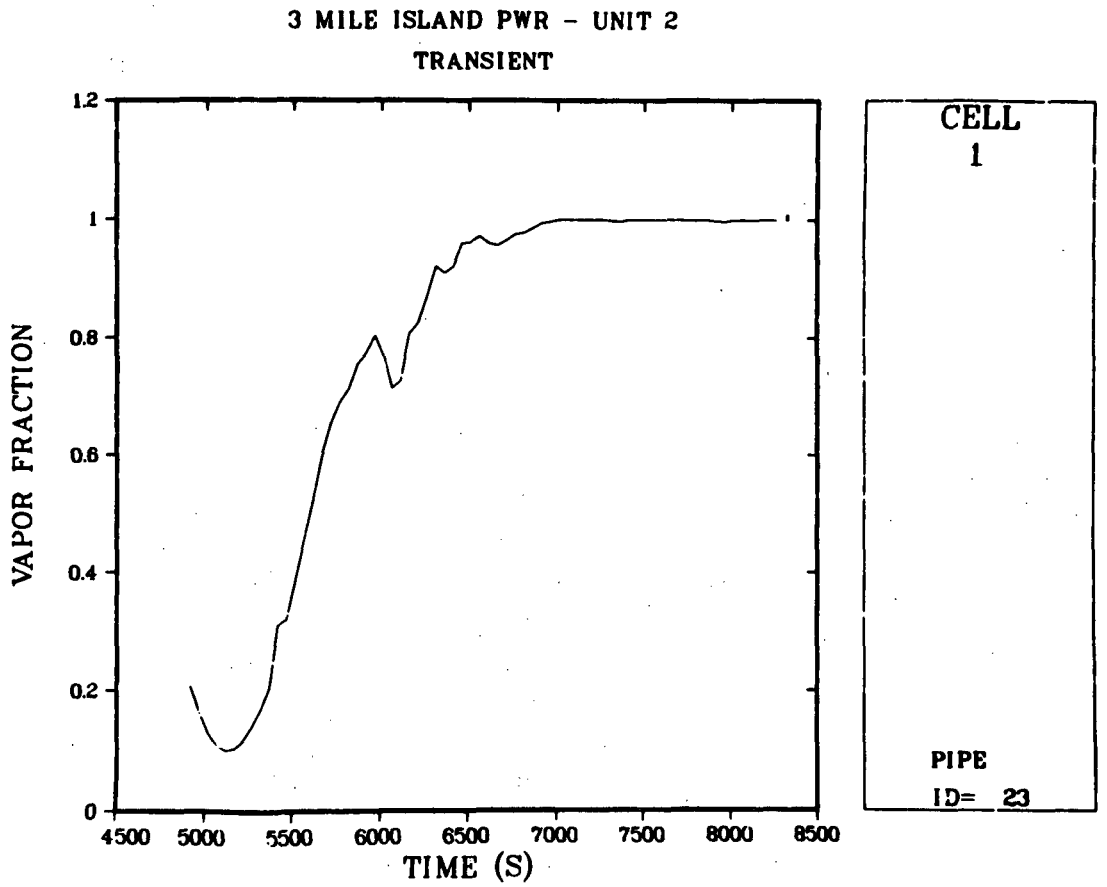

Pressurizer void fraction (top cell).

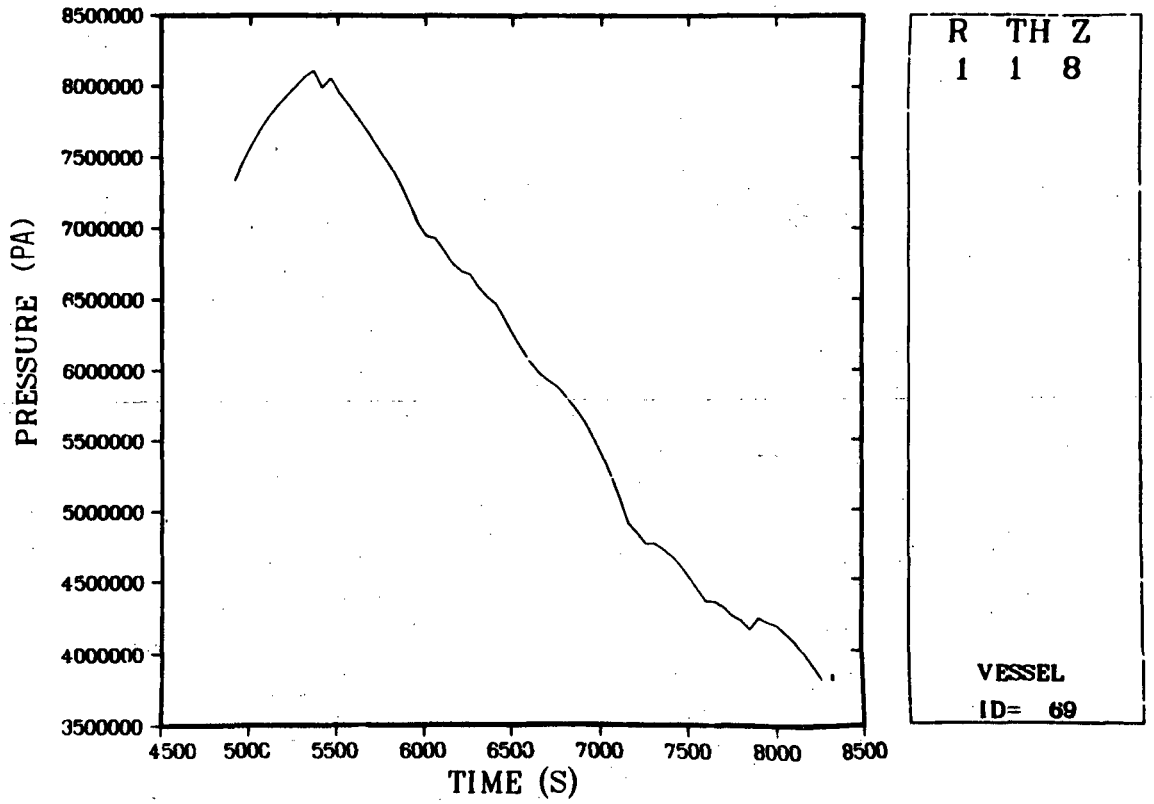

Upper plenum pressure.

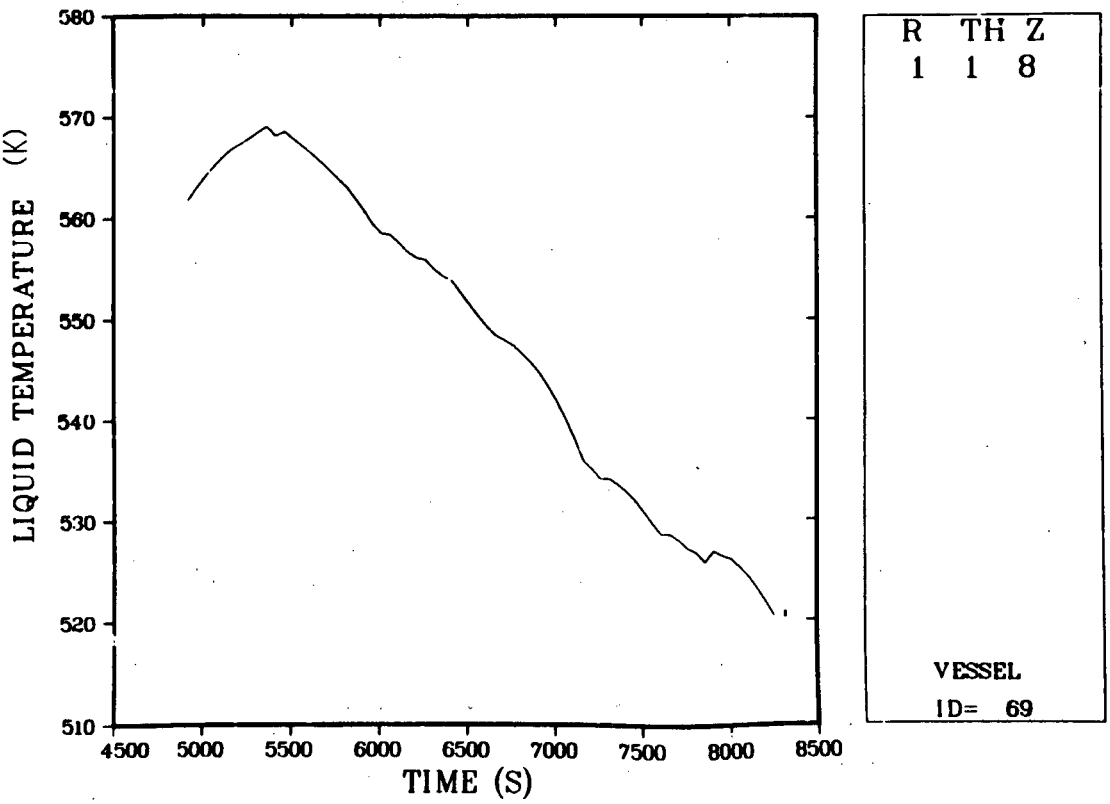

Upper plenum liquid temperature.

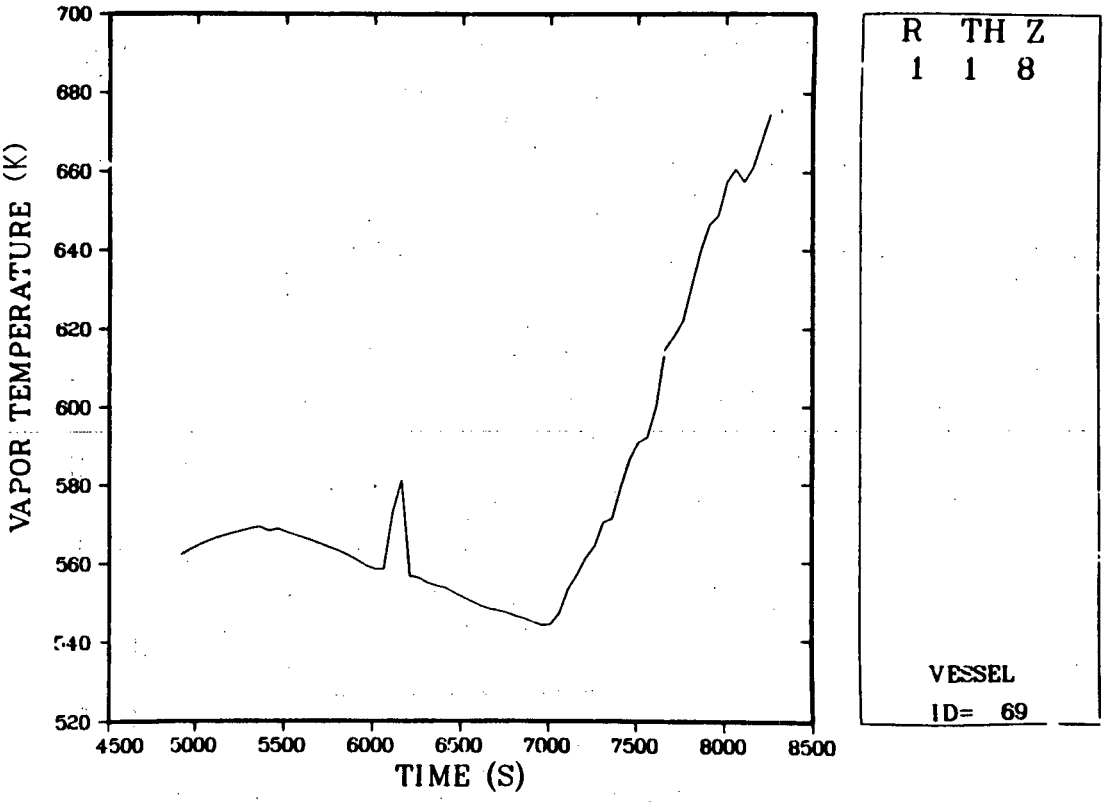

Upper plenum vapor temperature.

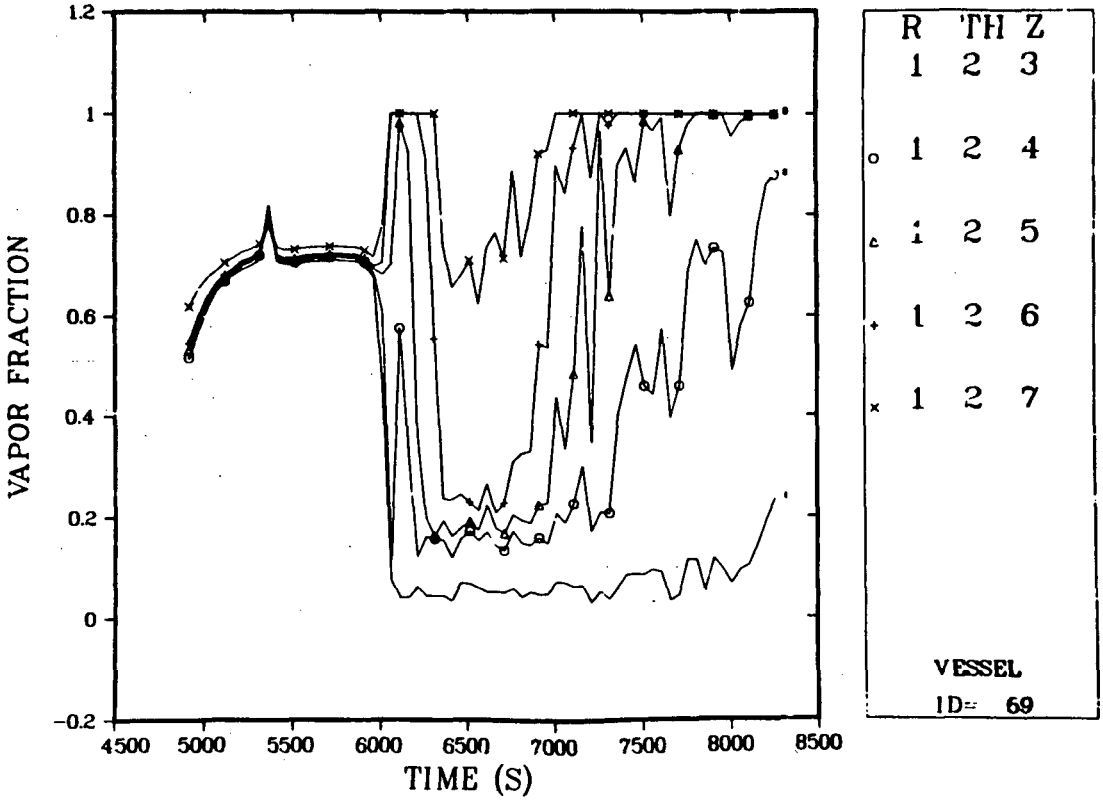

Core void fraction profile (axial direction).

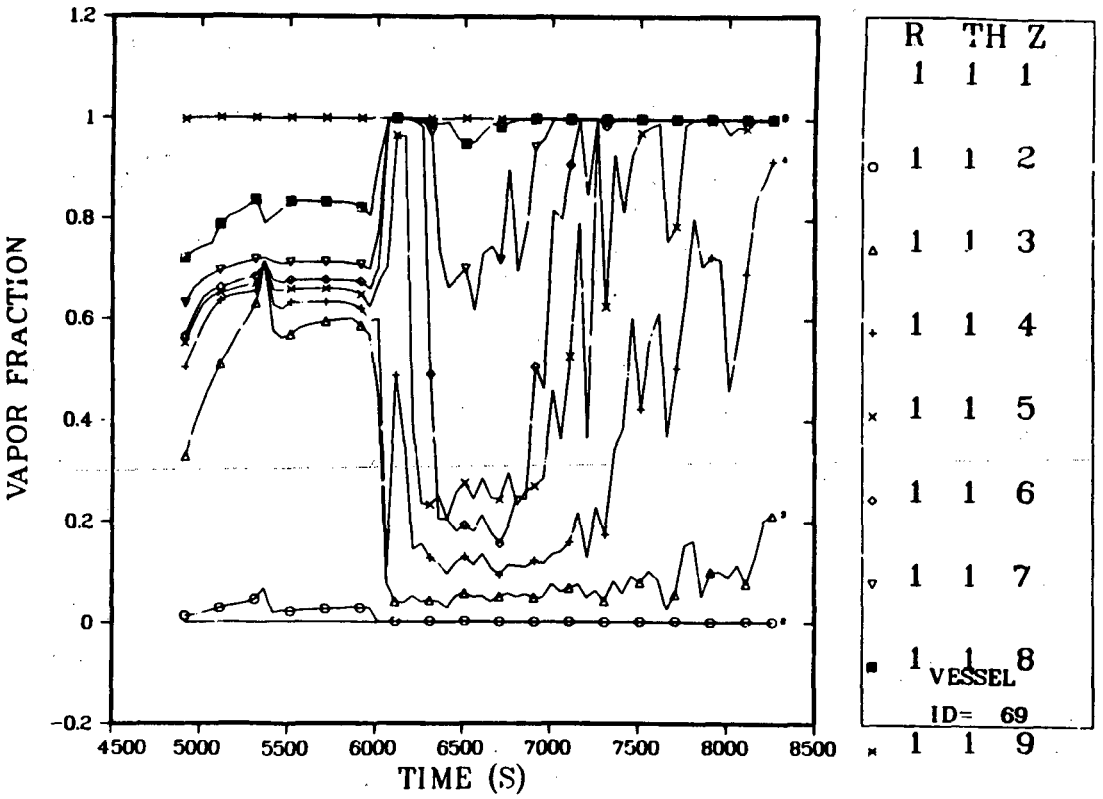

Vessel void fraction profile (axial direction - first azimuthal cell).

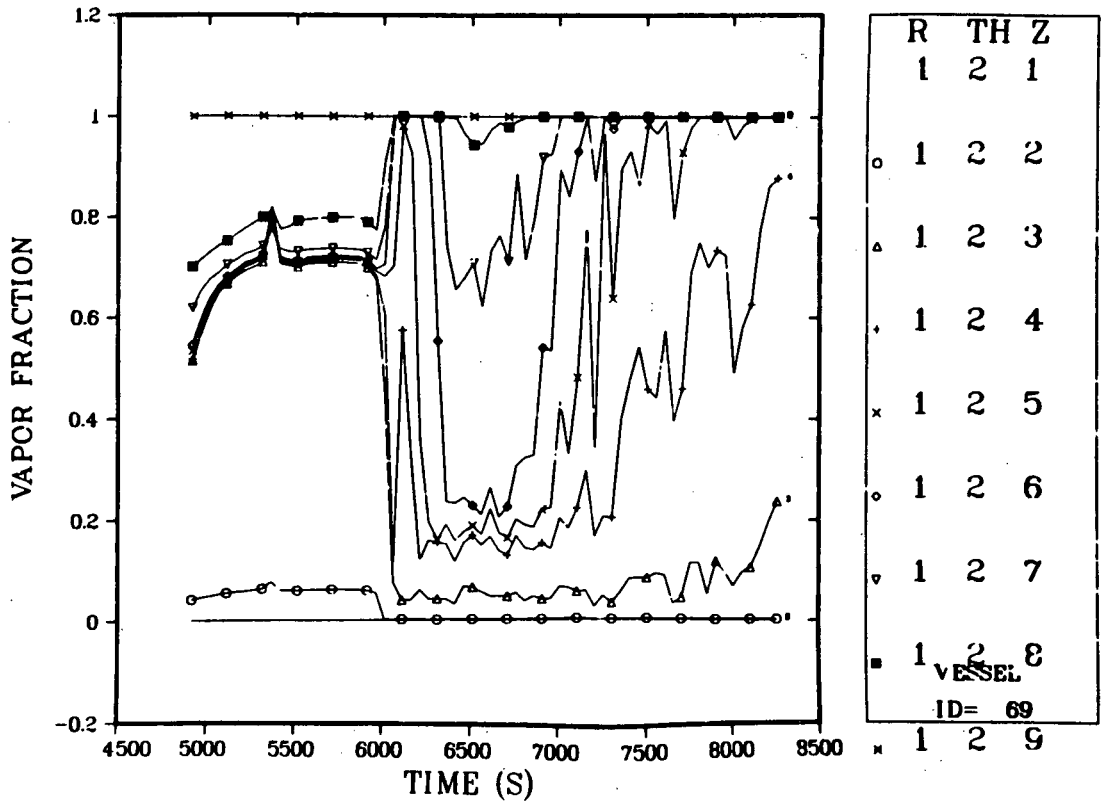

Vessel void fraction profile (axial direction - second azimuthal cell).

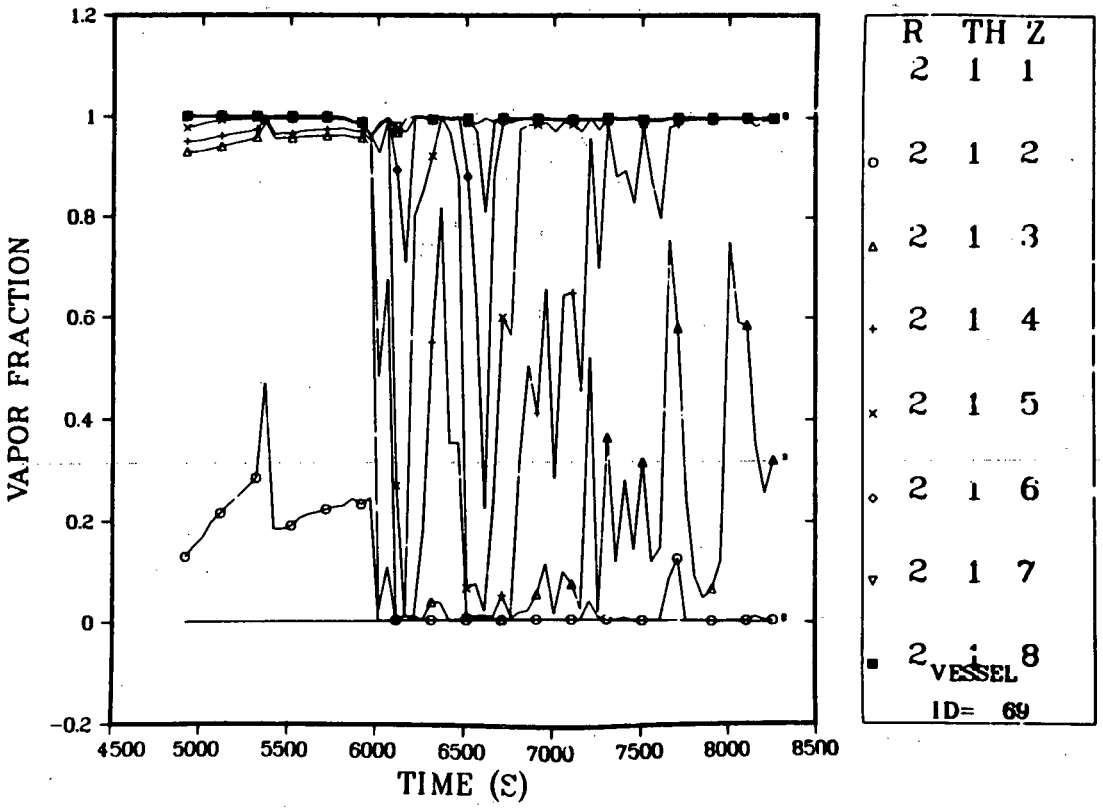

Downcomer void fraction profile (Cell 1).

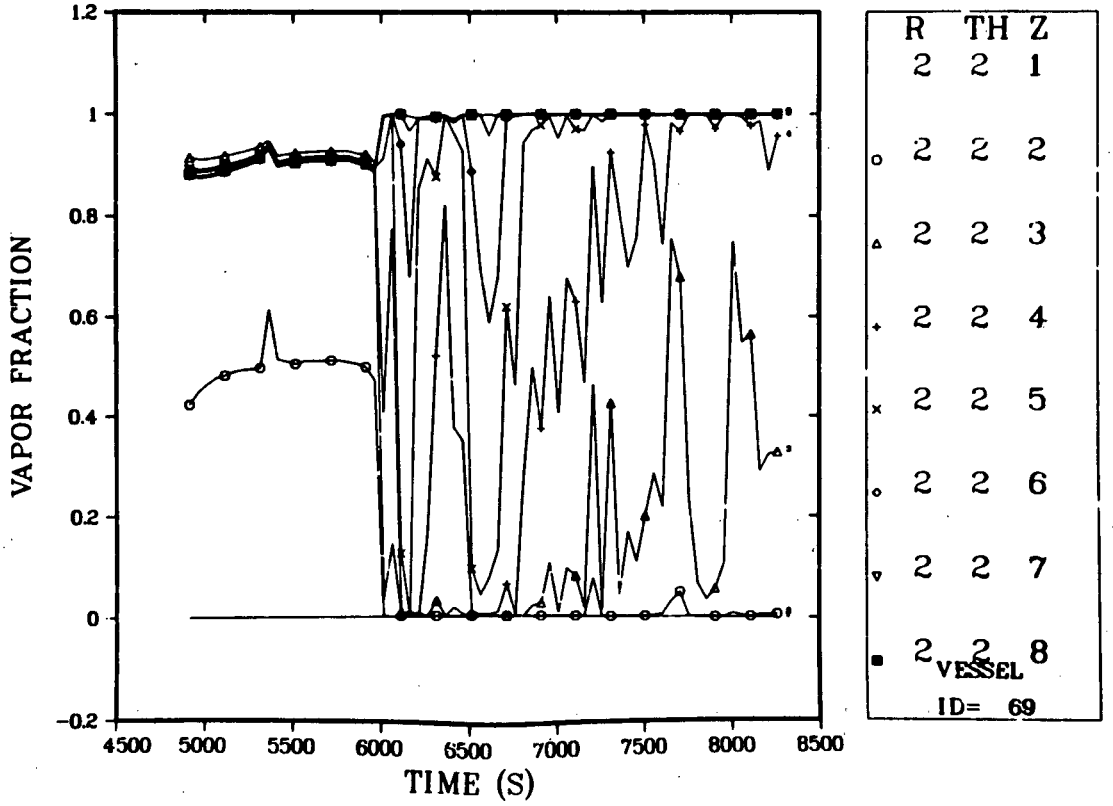

Downcomer void fraction profile (Cell 2).

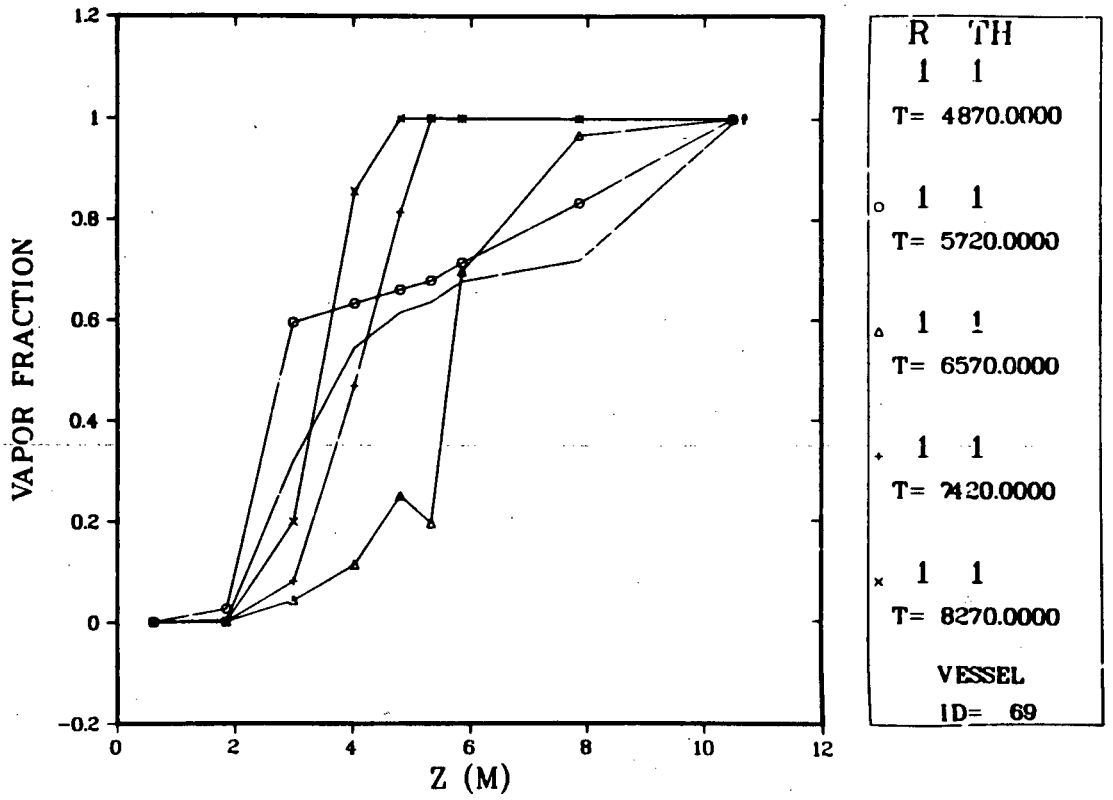

Vessel void fraction profile vs time (Cell 1).

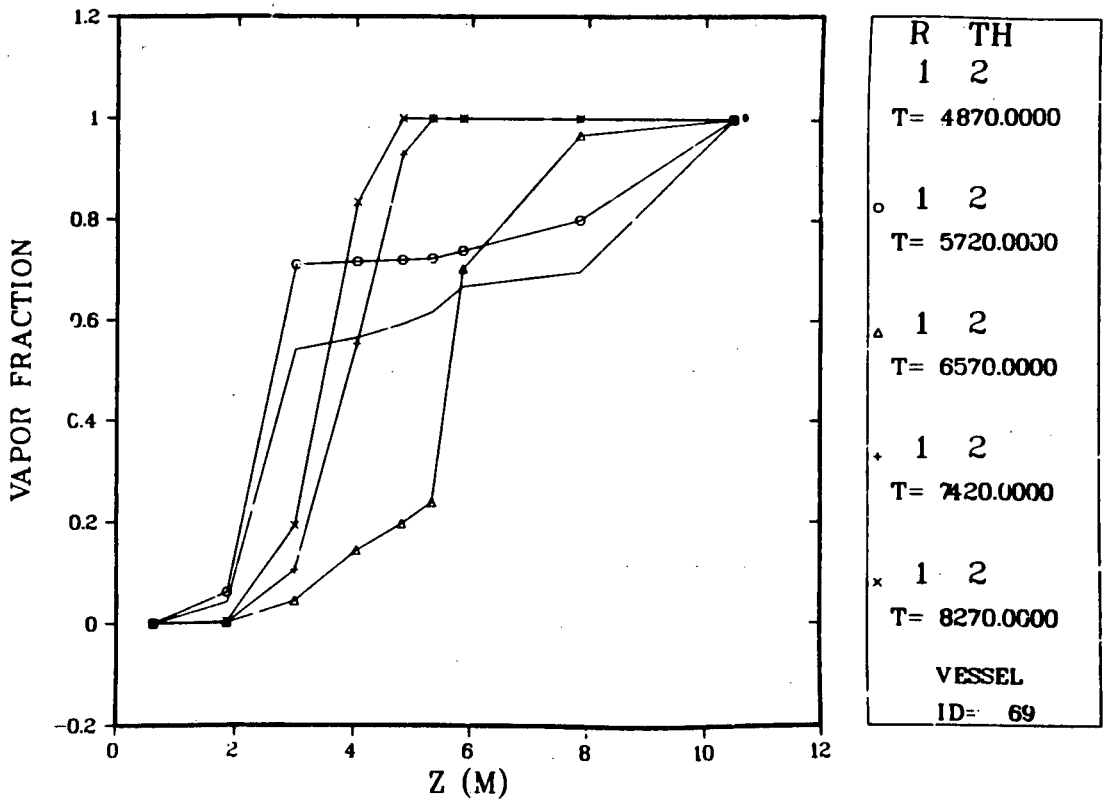

Vessel void fraction profile vs time (Cell 2).

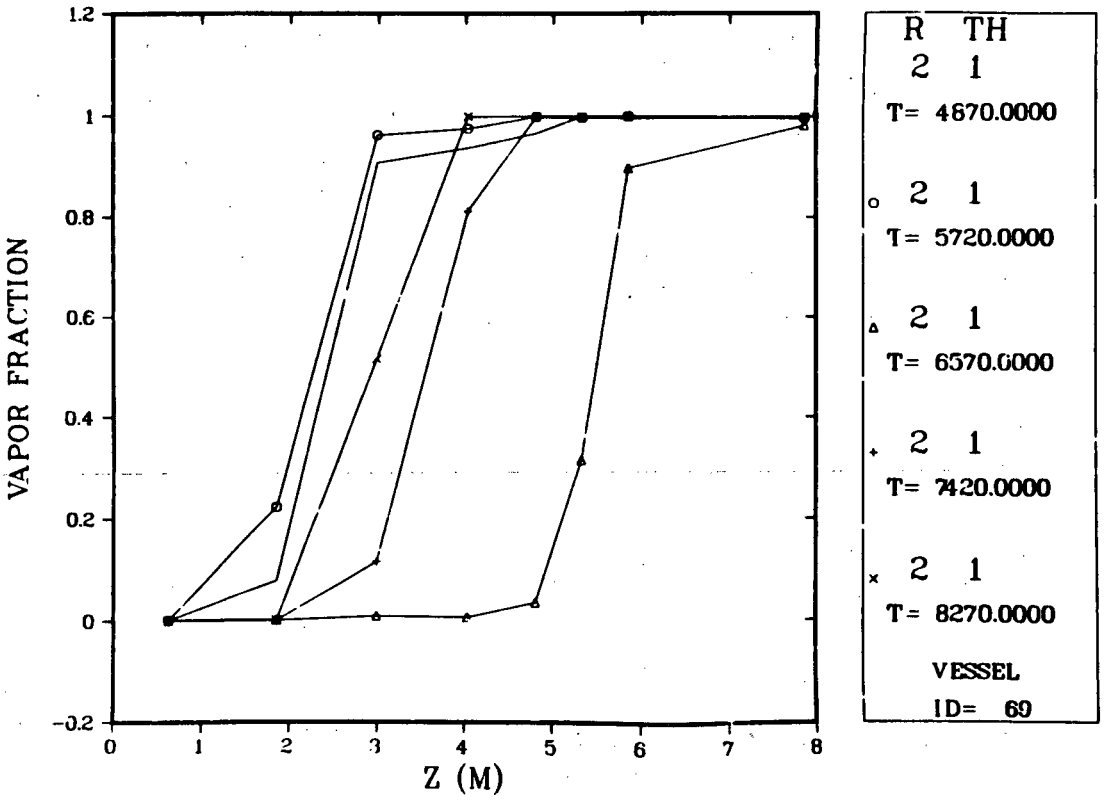

Downcomer void fraction profile vs time.

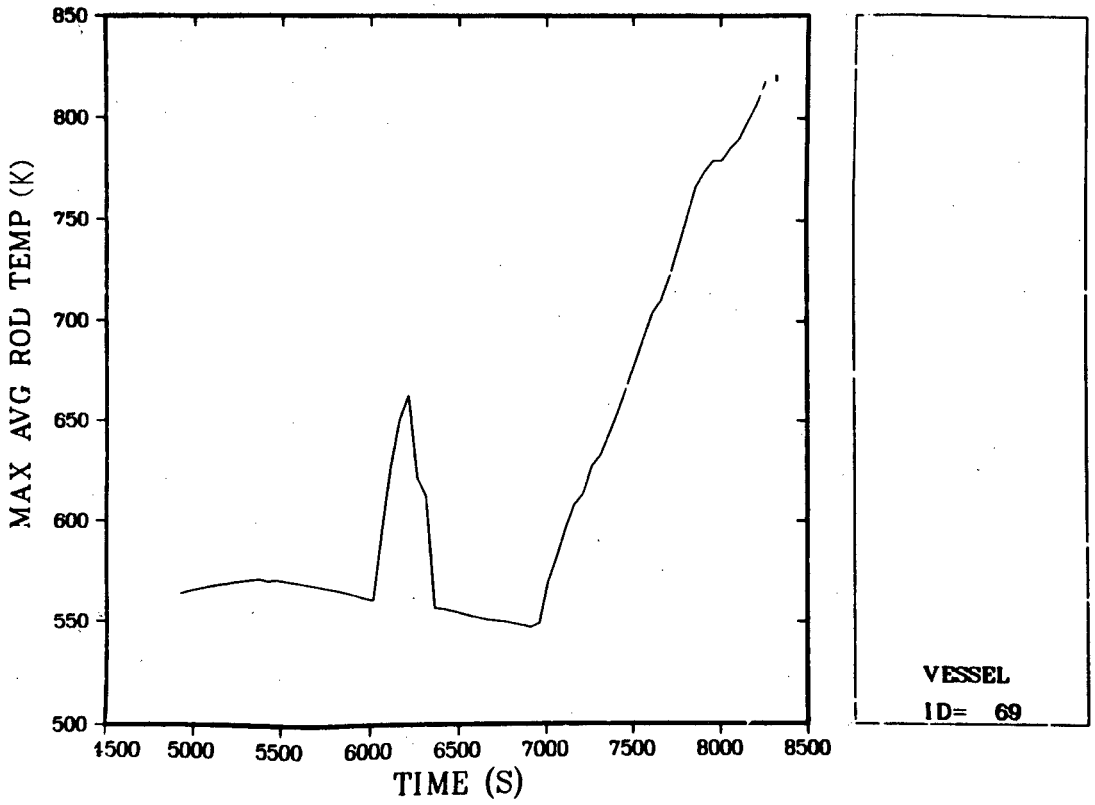

Maximum average rod temperature.

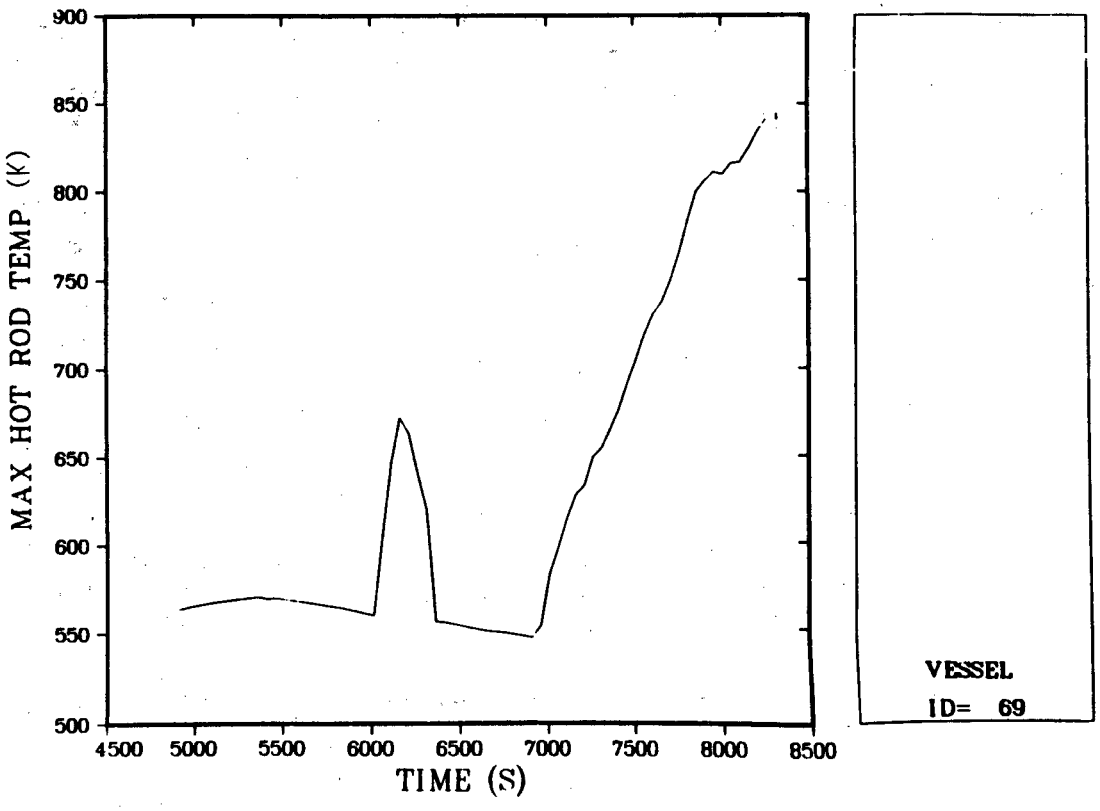

Maximum hot-rod temperature.

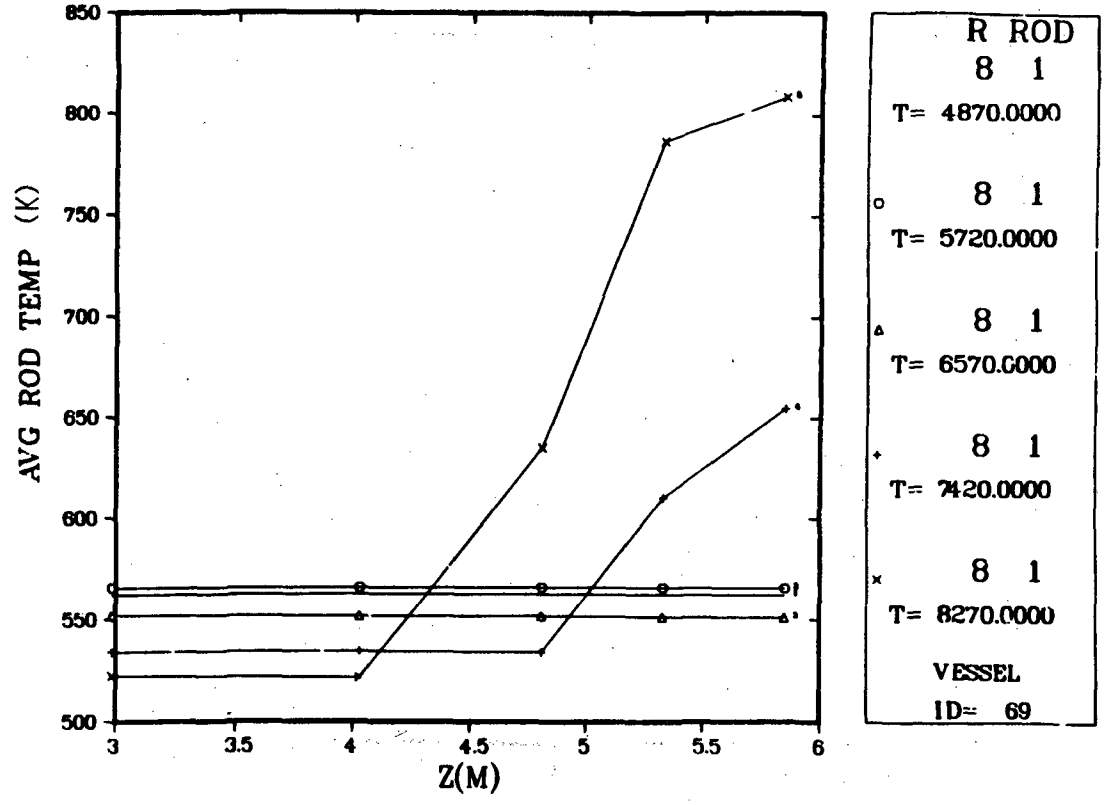

Average rod temperature profile vs time (Rod 1).

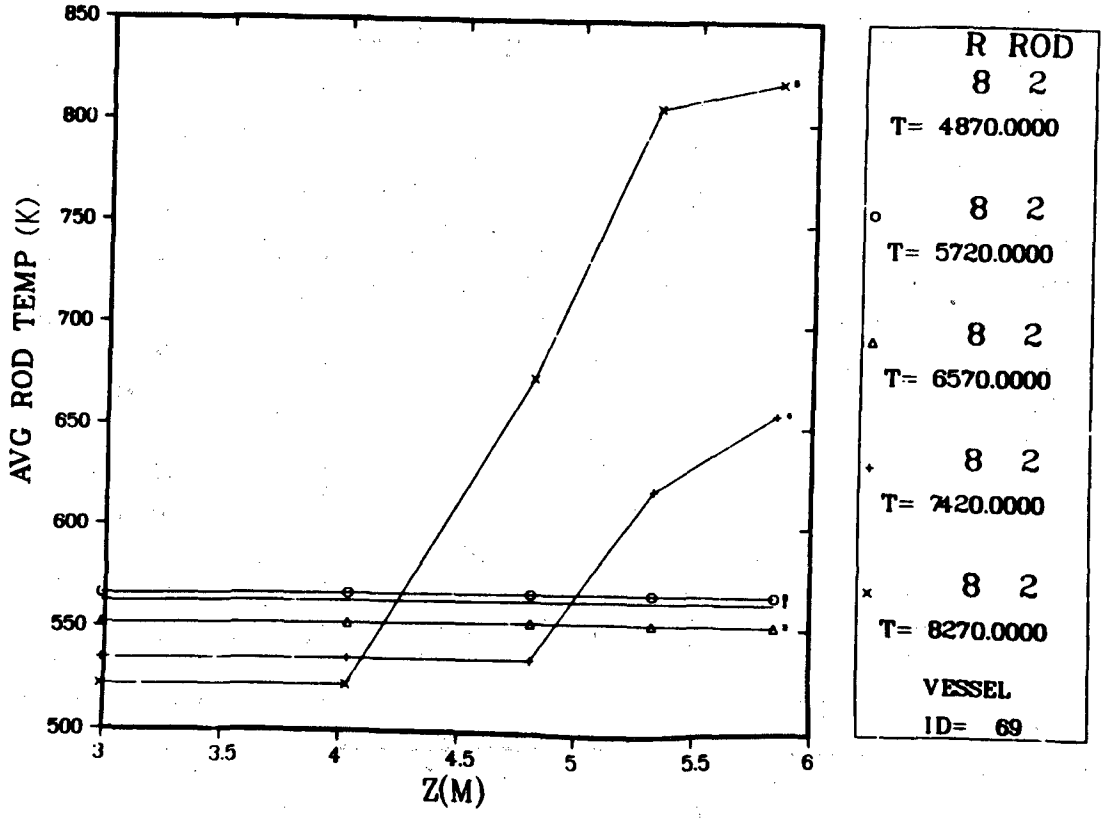

Average rod temperature profile vs time (Rod 2).

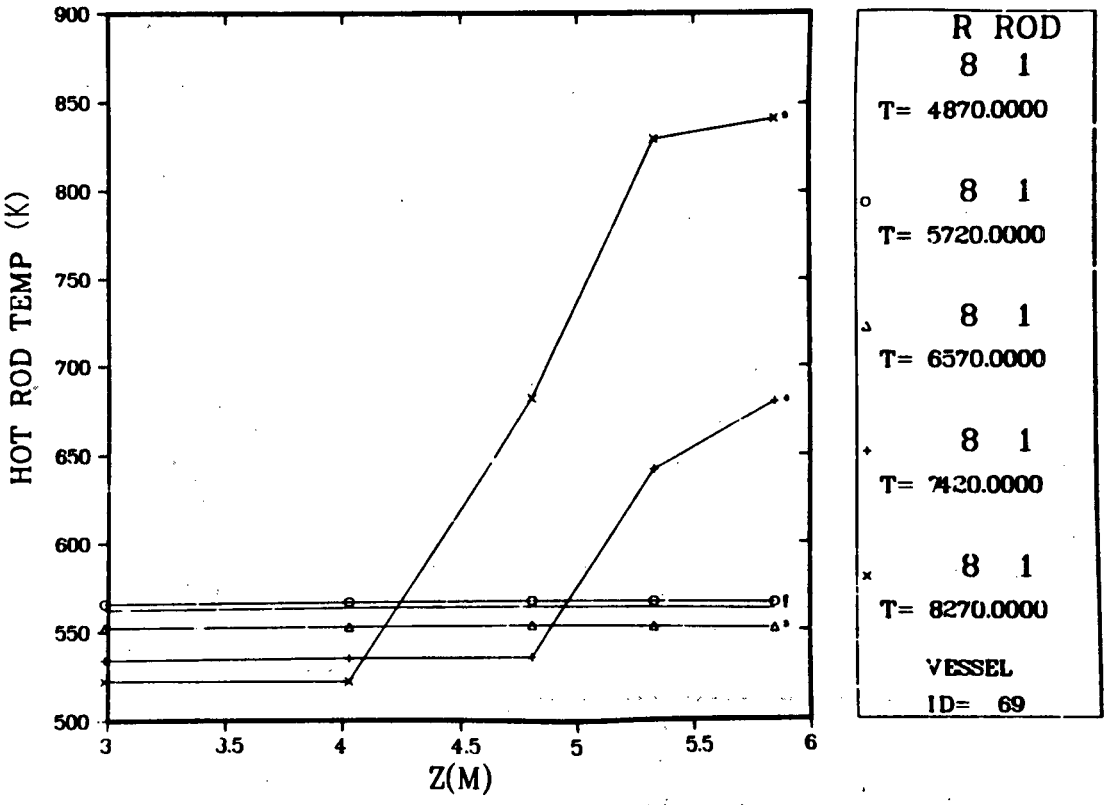

Hot-rod temperature profile vs time (Rod 1).

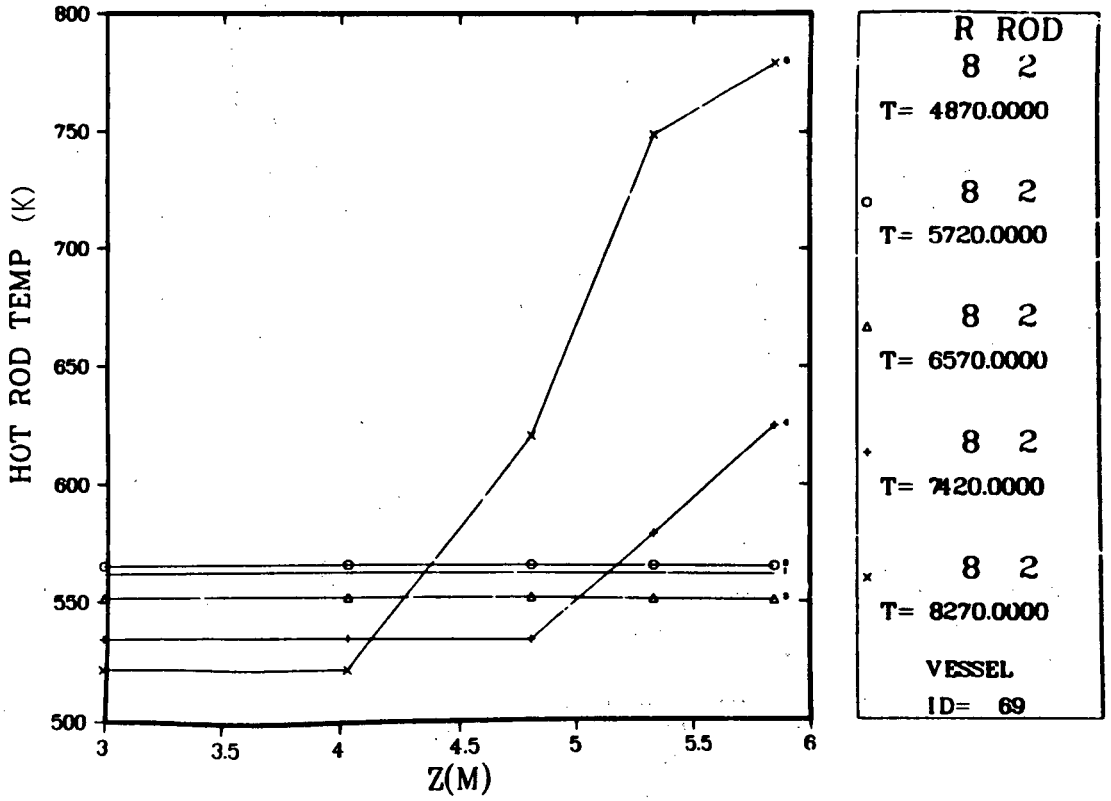

Hot-rod temperature profile vs time (Rod 2).

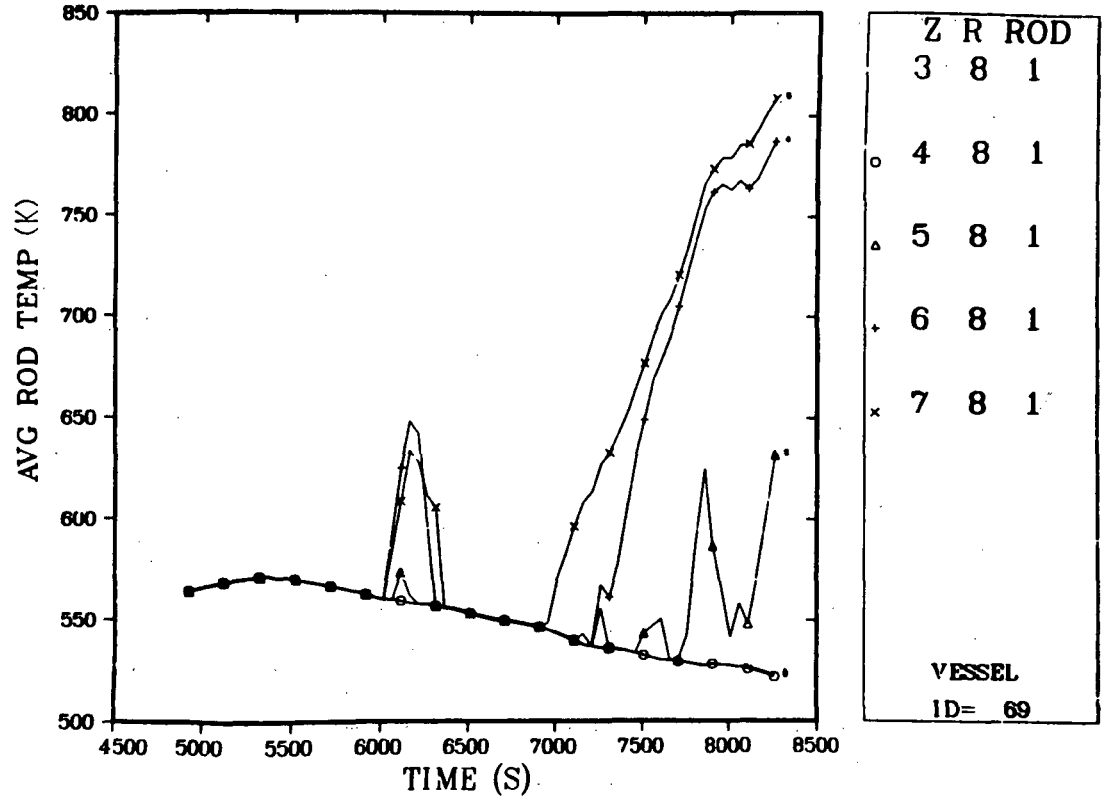

Average rod temperature axial profile (Rod 1).

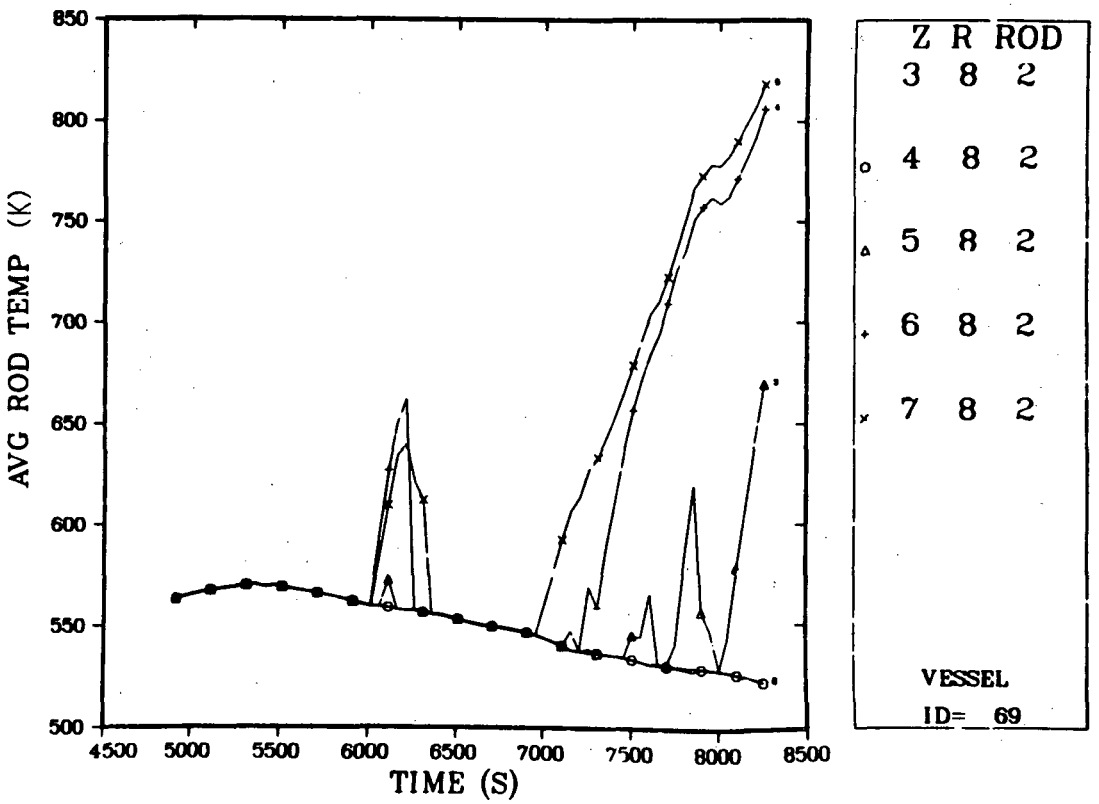

Average rod temperature axial profile (Rod 2).

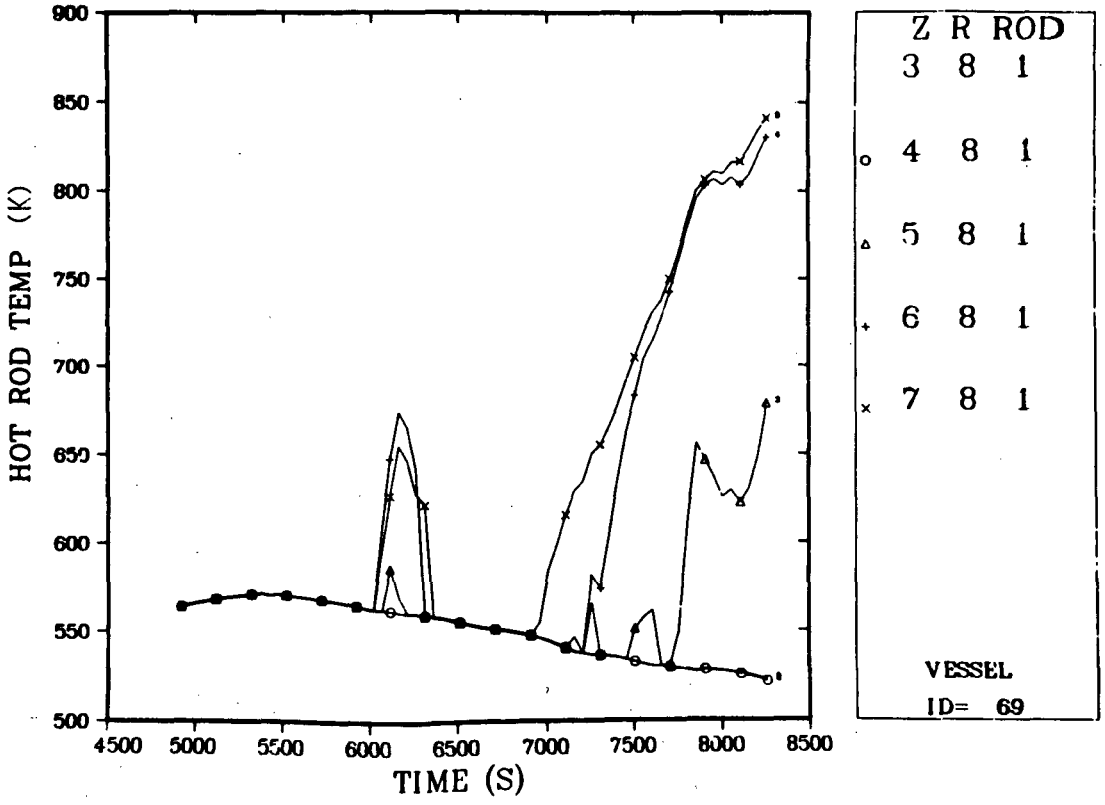

Hot-rod temperature axial profile (Rod 1).

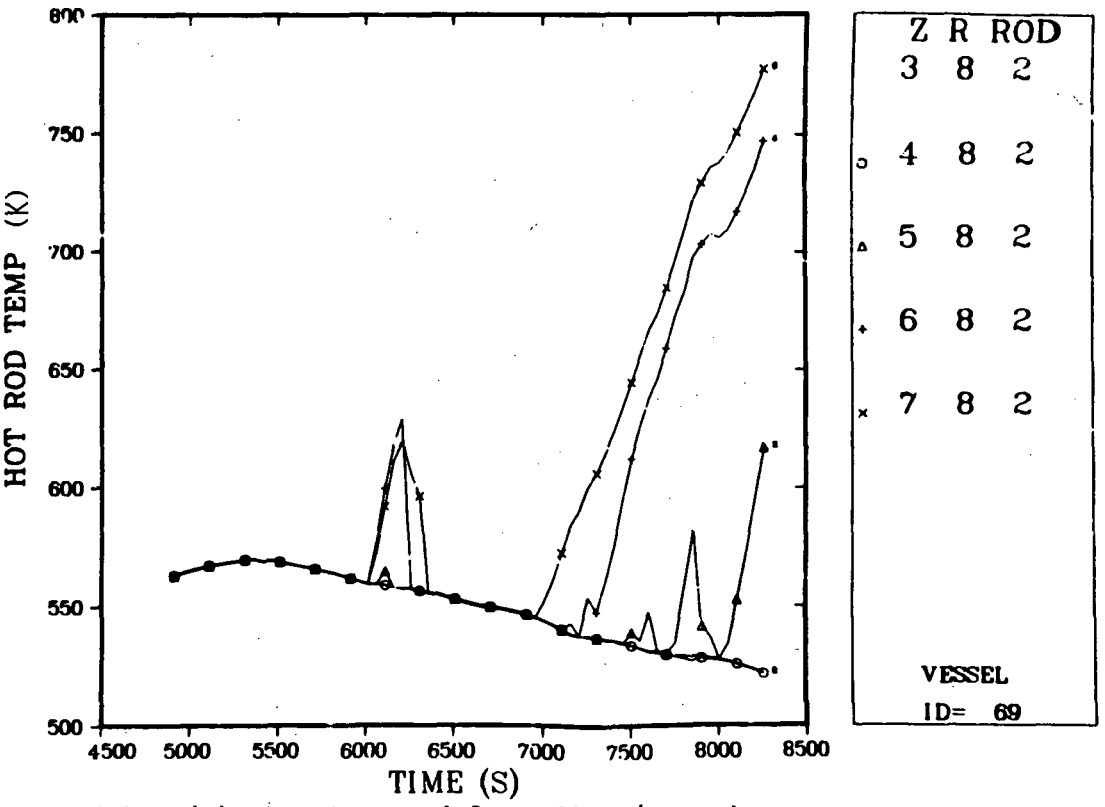

Hot-rod temperature axial profile (Rod 2).

138 min ≤ T ≤ 180 min

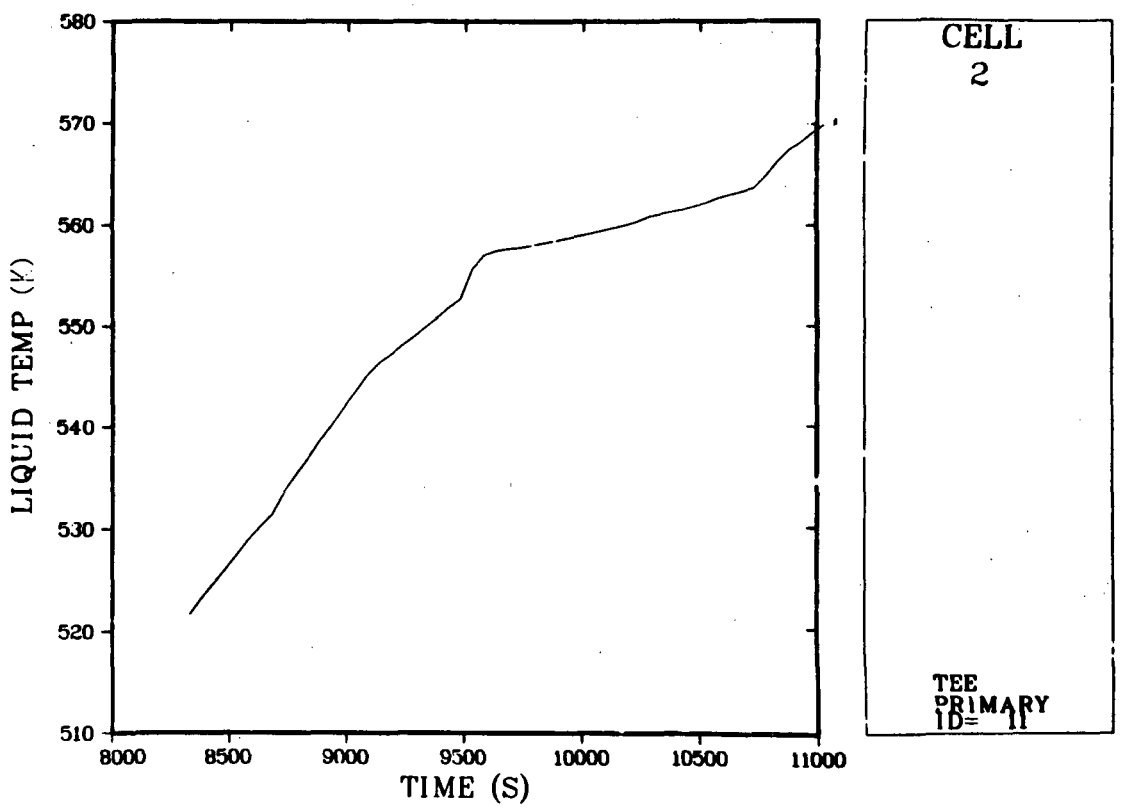

A Loop hot-leg liquid temperature.

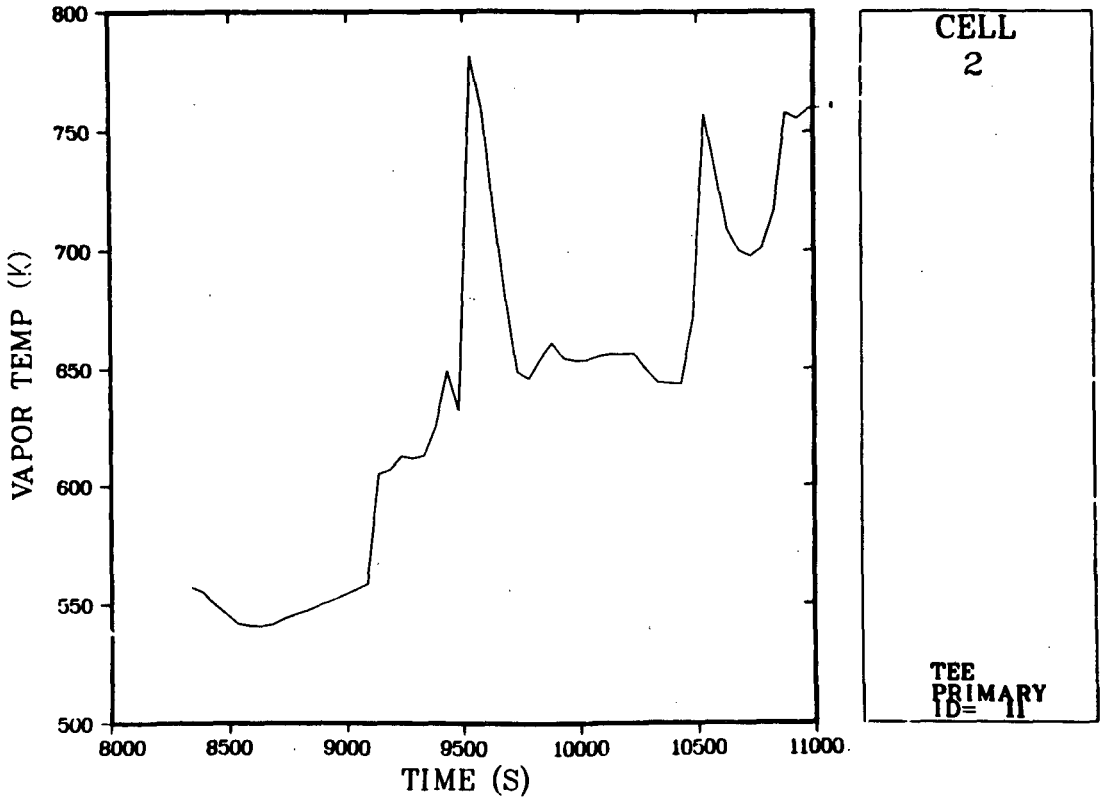

A Loop hot-leg vapor temperature.

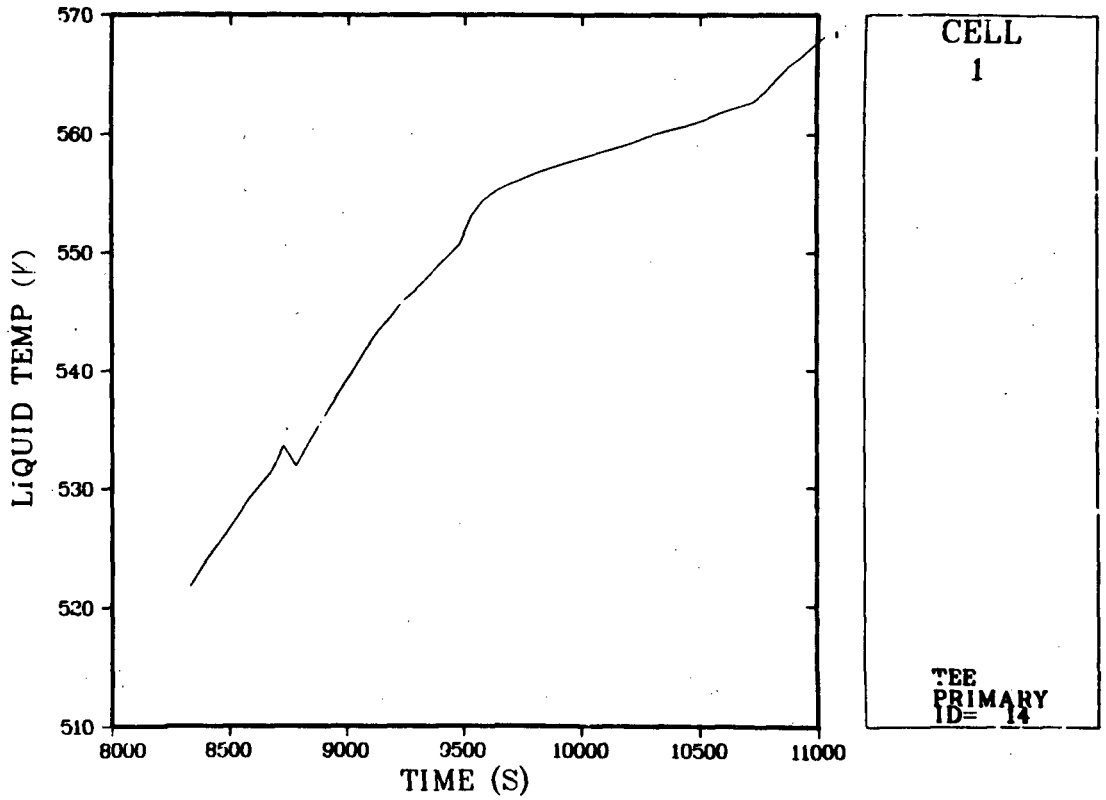

A Loop cold-leg liquid temperature.

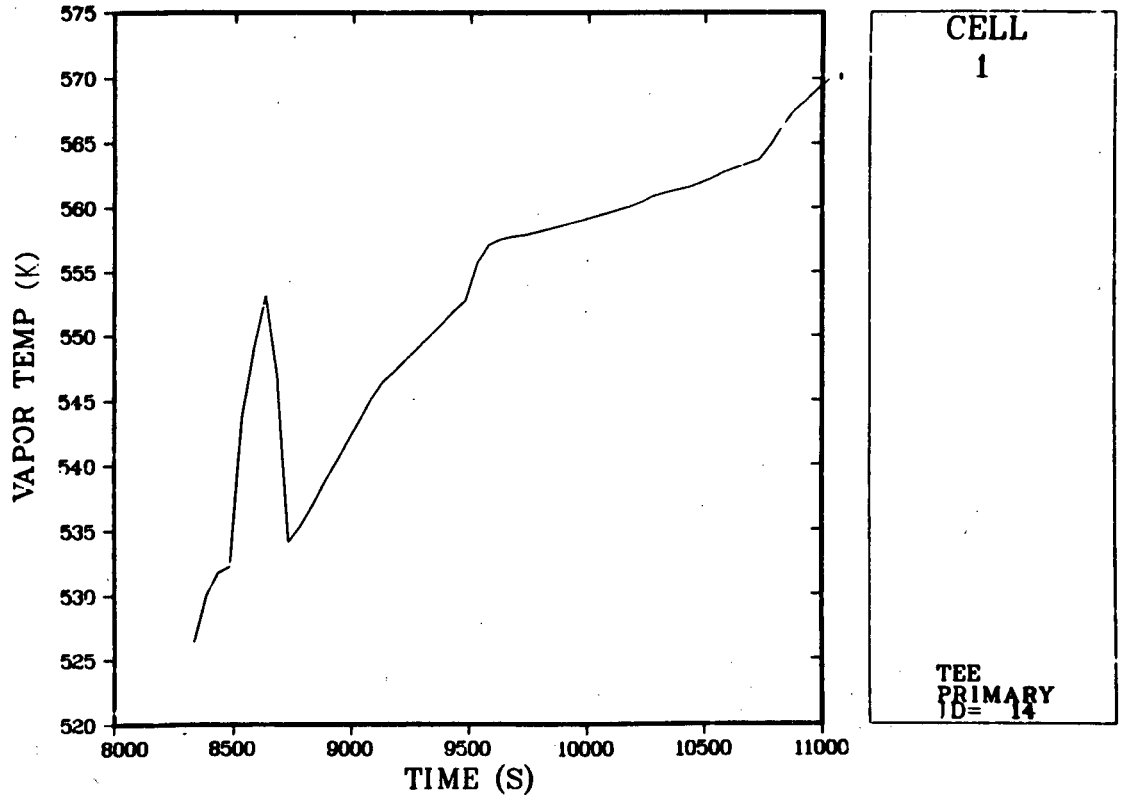

A Loop cold-leg vapor temperature.

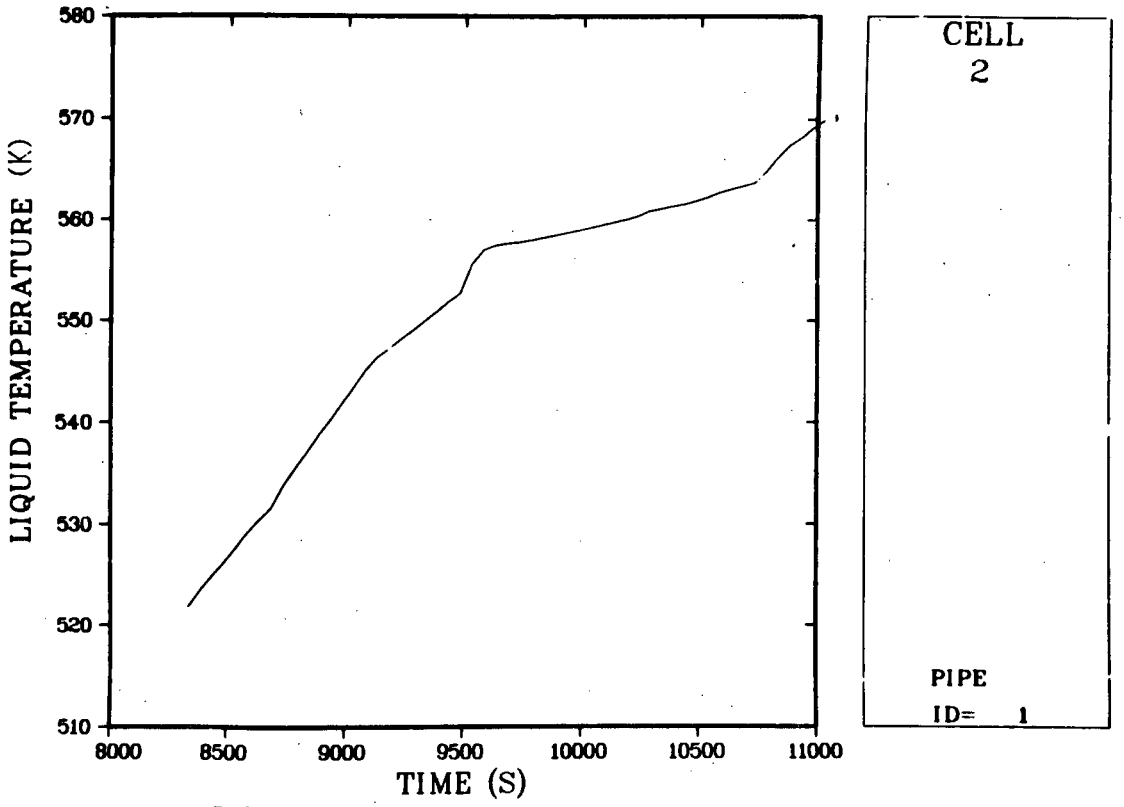

B Loop hot-leg liquid temperature.

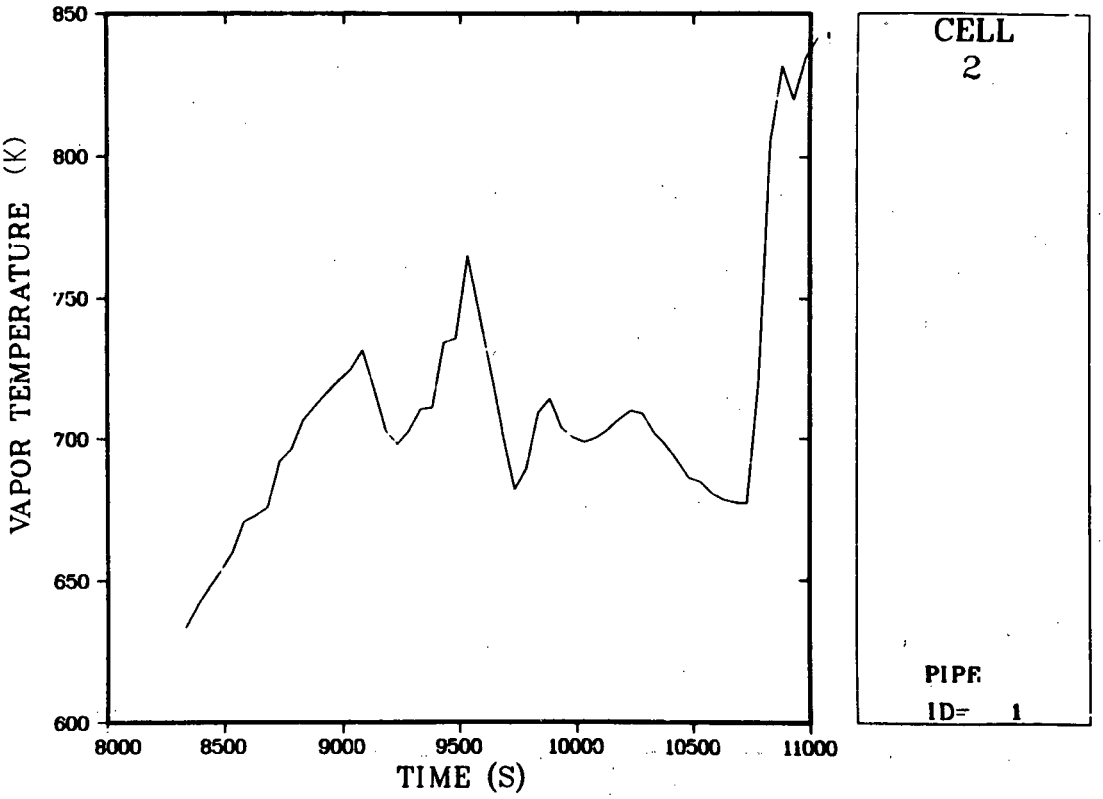

B Loop hot-leg vapor temperature.

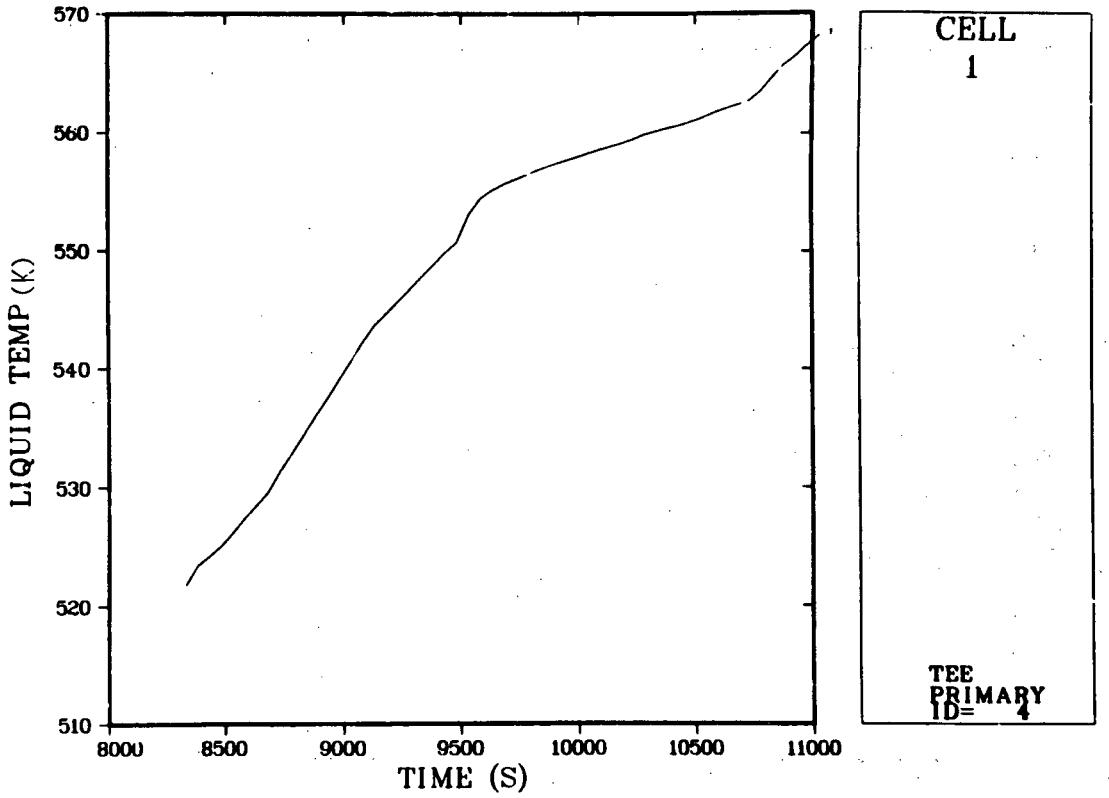

B Loop cold-leg liquid temperature.

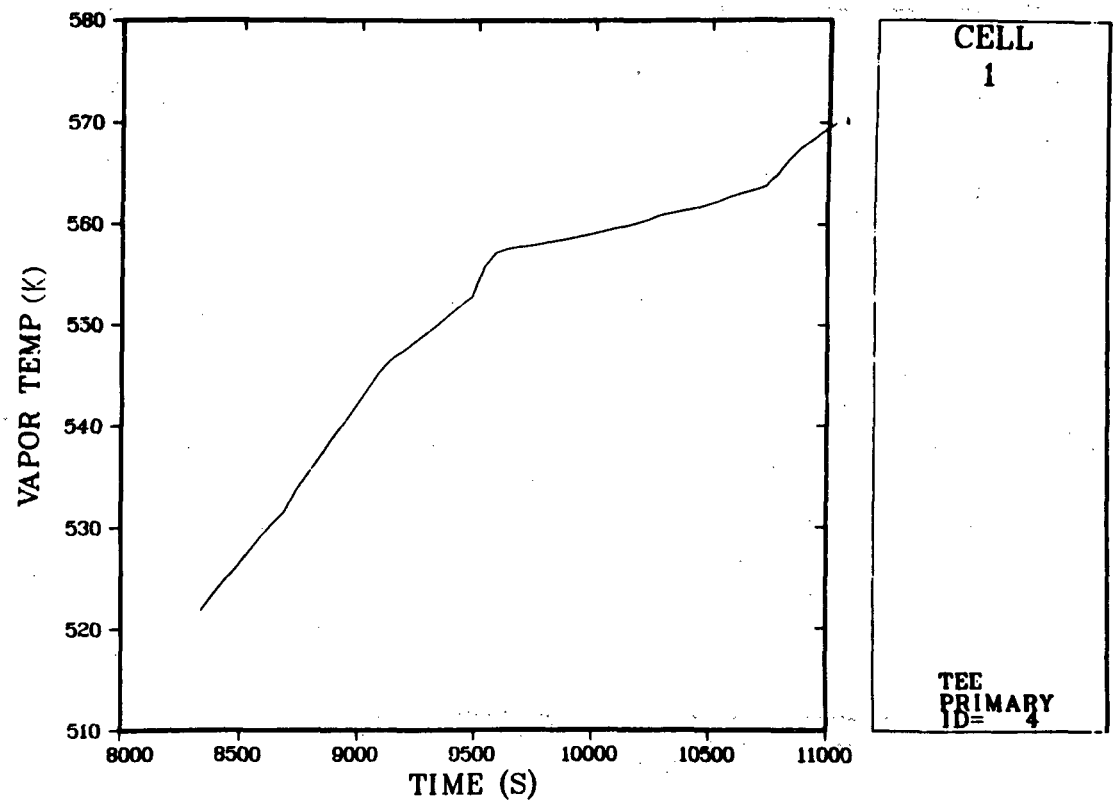

B Loop cold-leg vapor temperature.

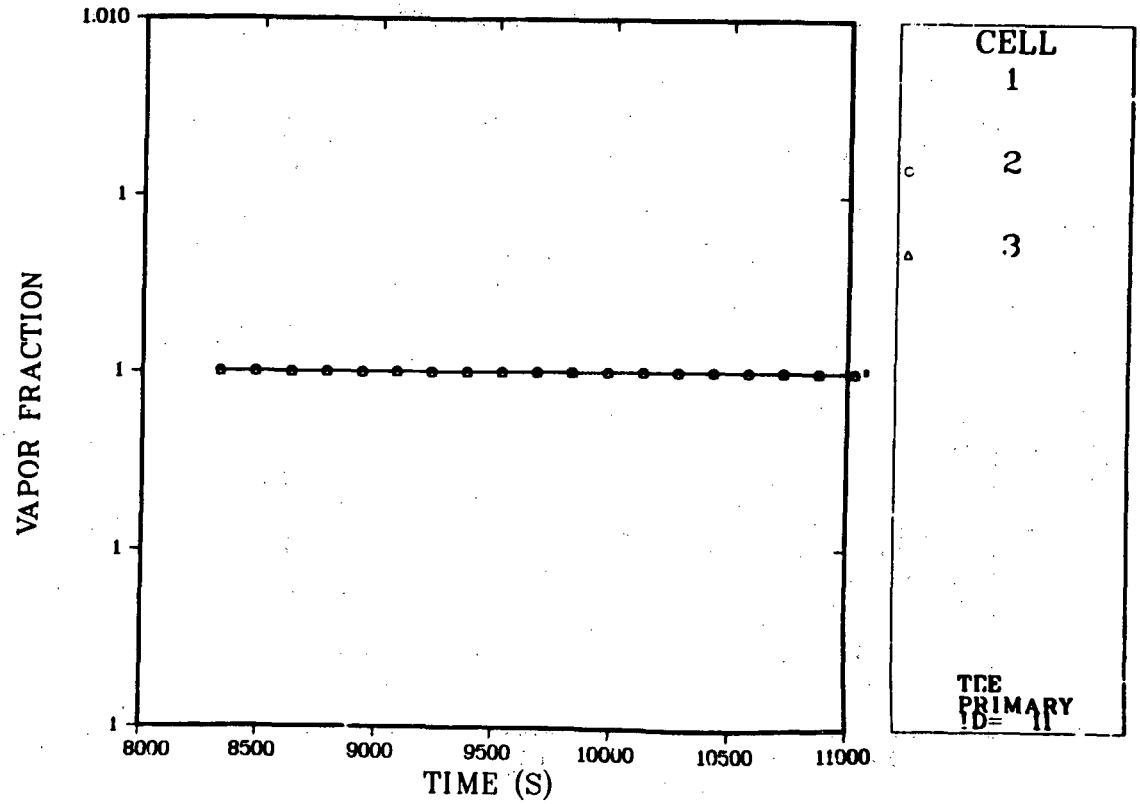

A Loop hot-leg void fraction distribution (Cells, 1, 2, 3).

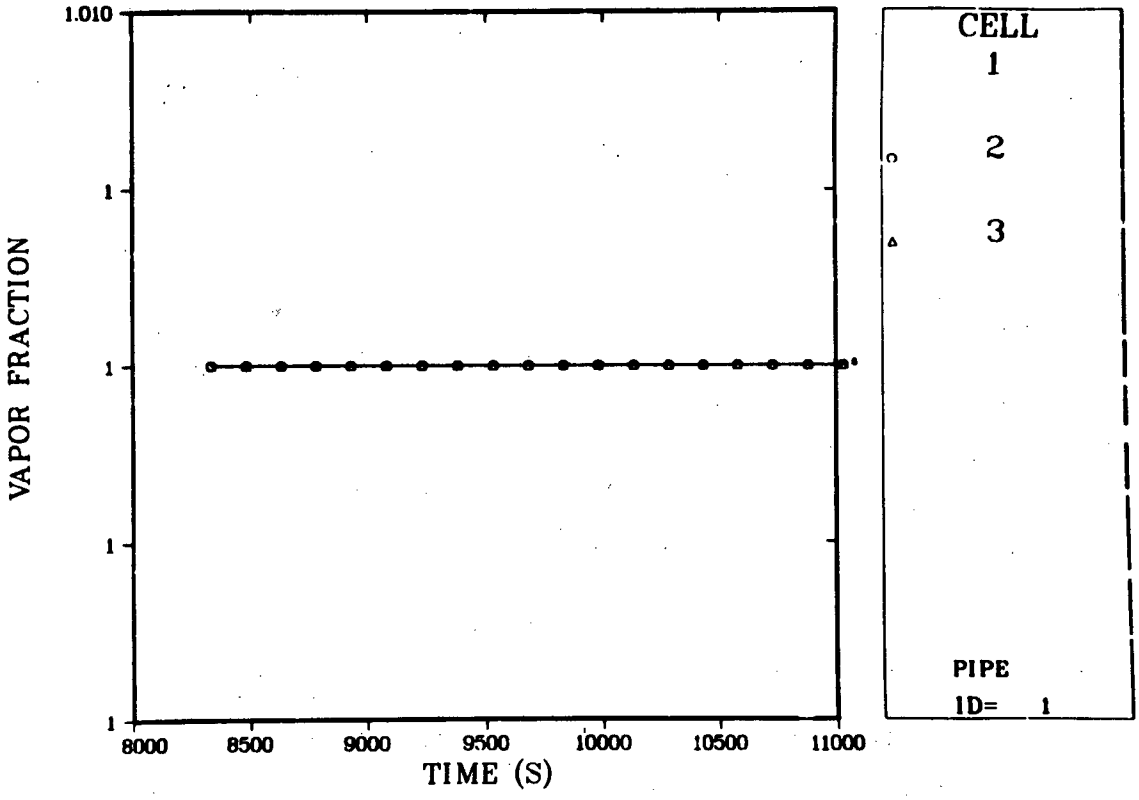

B Loop hot-leg void fraction distribution (Cells 1, 2, 3).

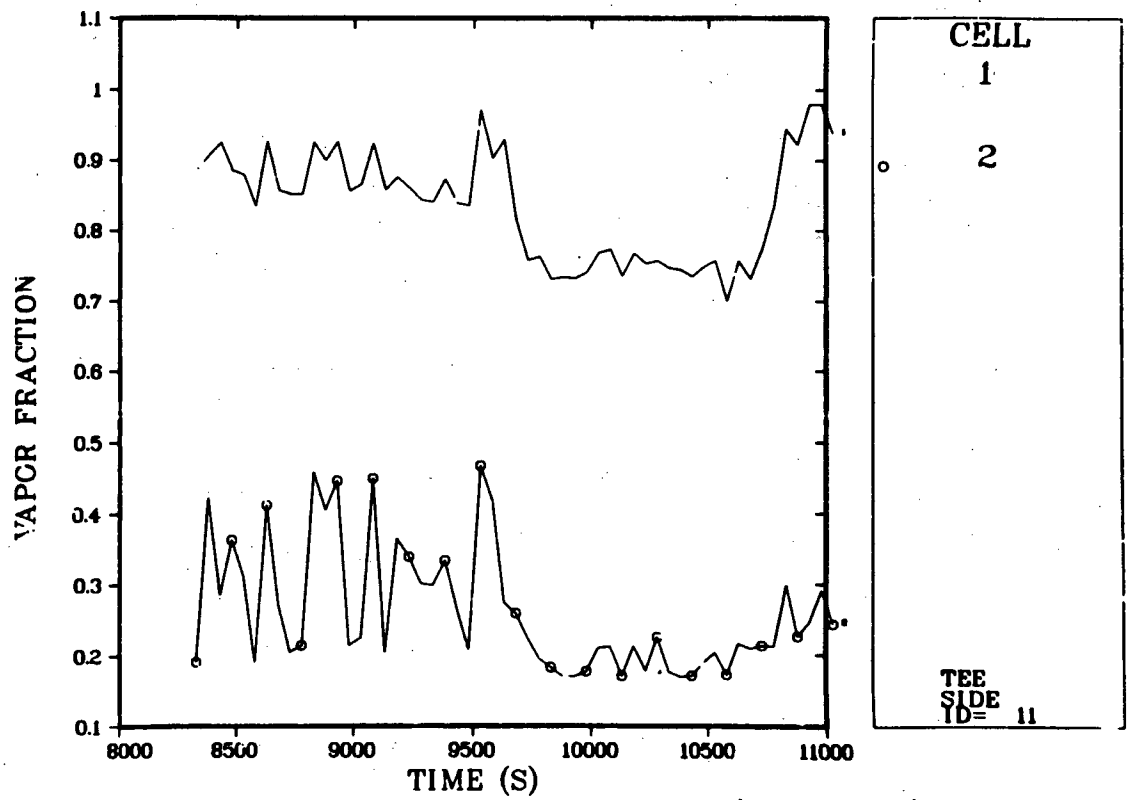

Pressurizer surge line void distribution (Cells 1, 2).

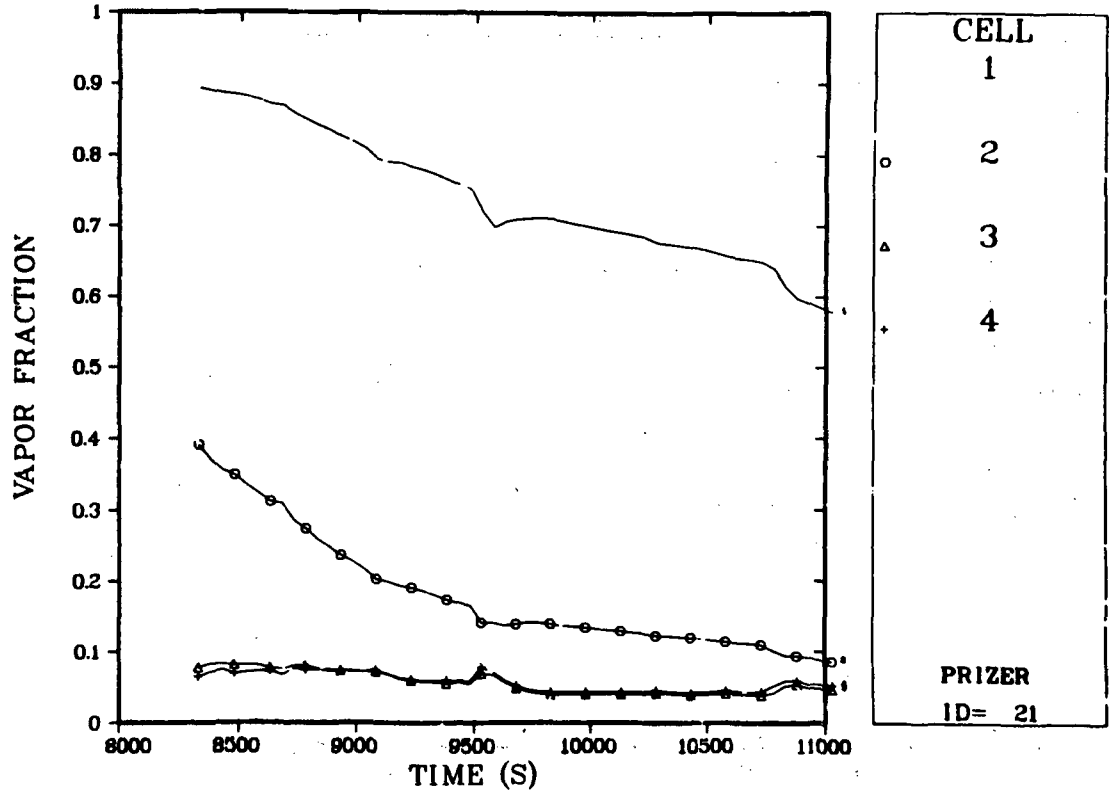

Pressurizer void fraction distribution.

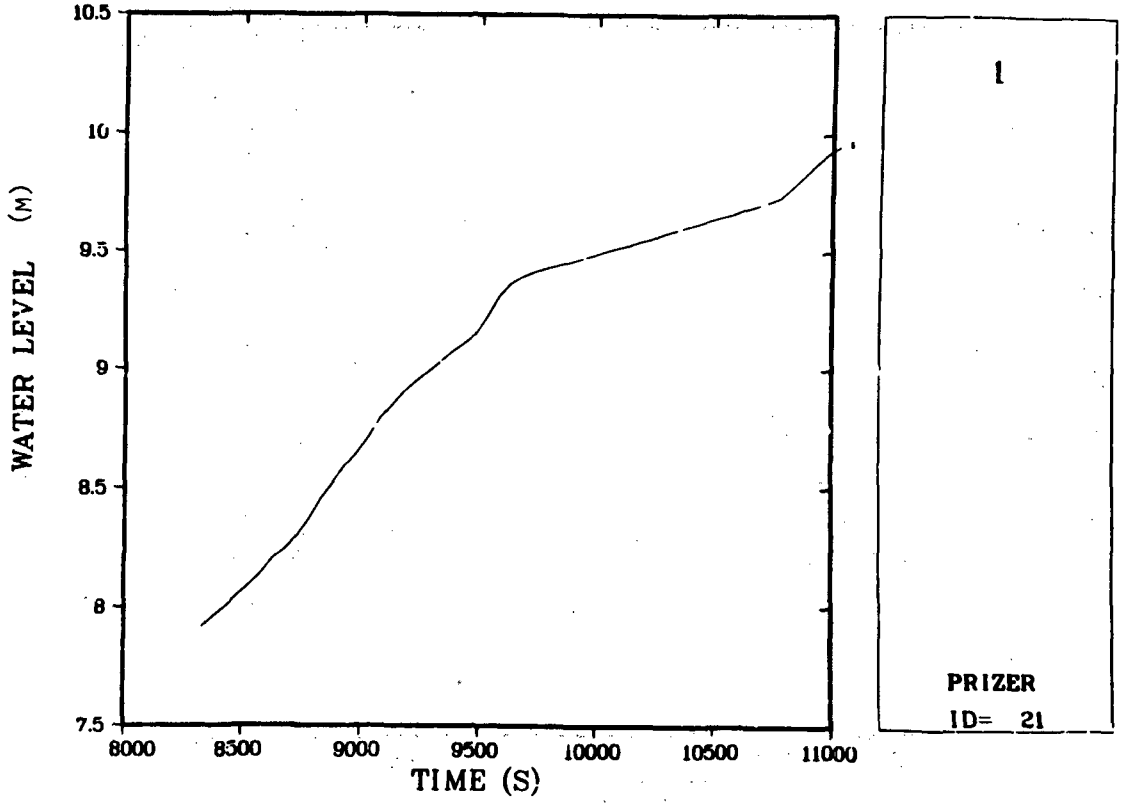

Pressurizer water level.

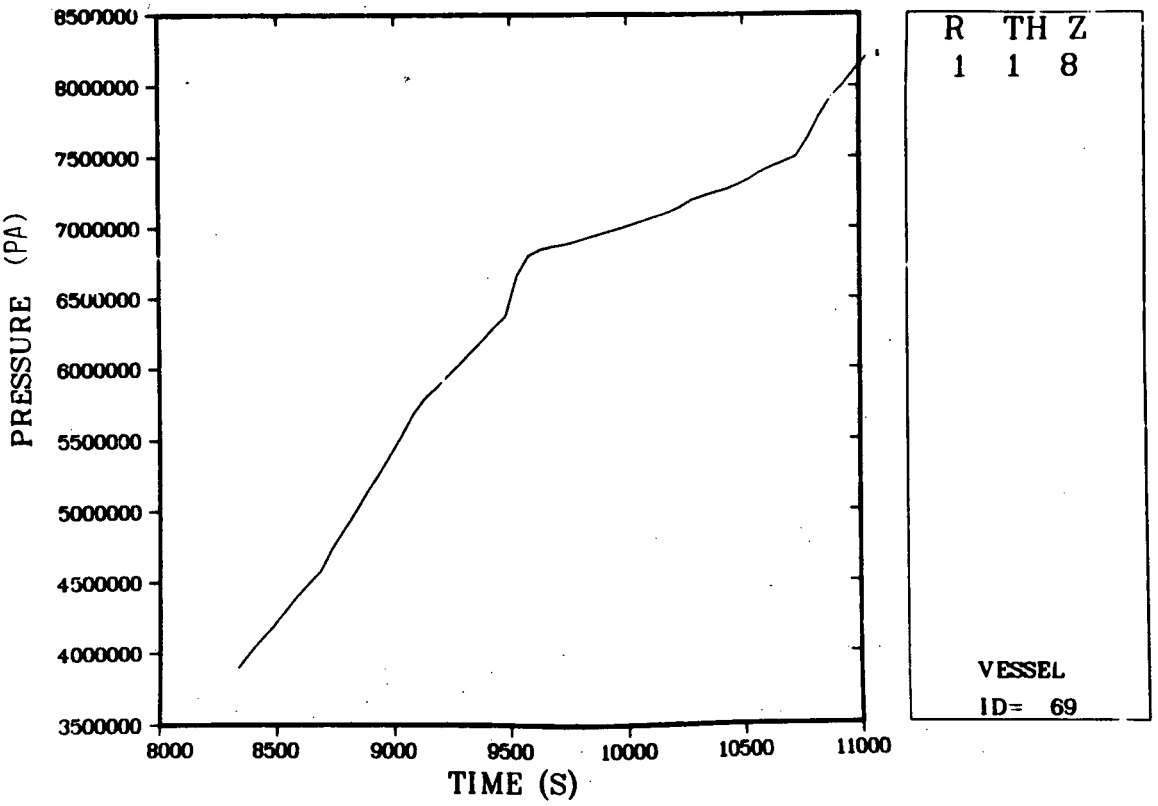

Upper plenum pressure.

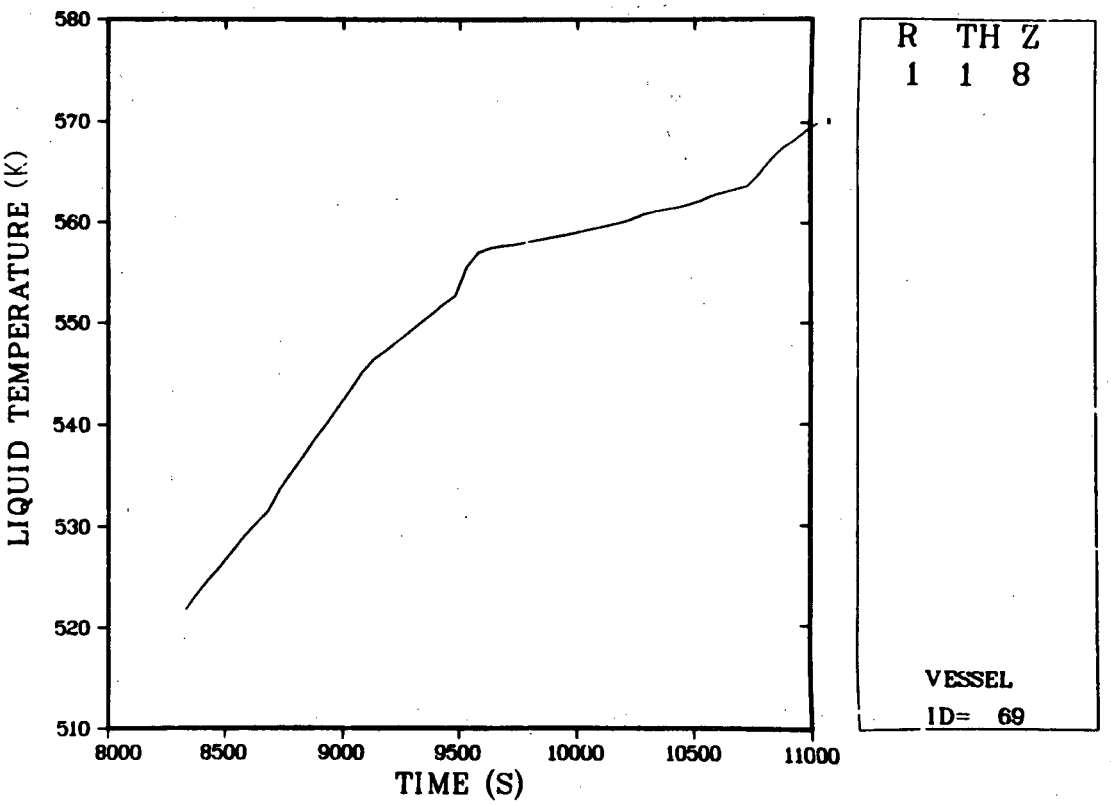

Upper plenum liquid temperature.

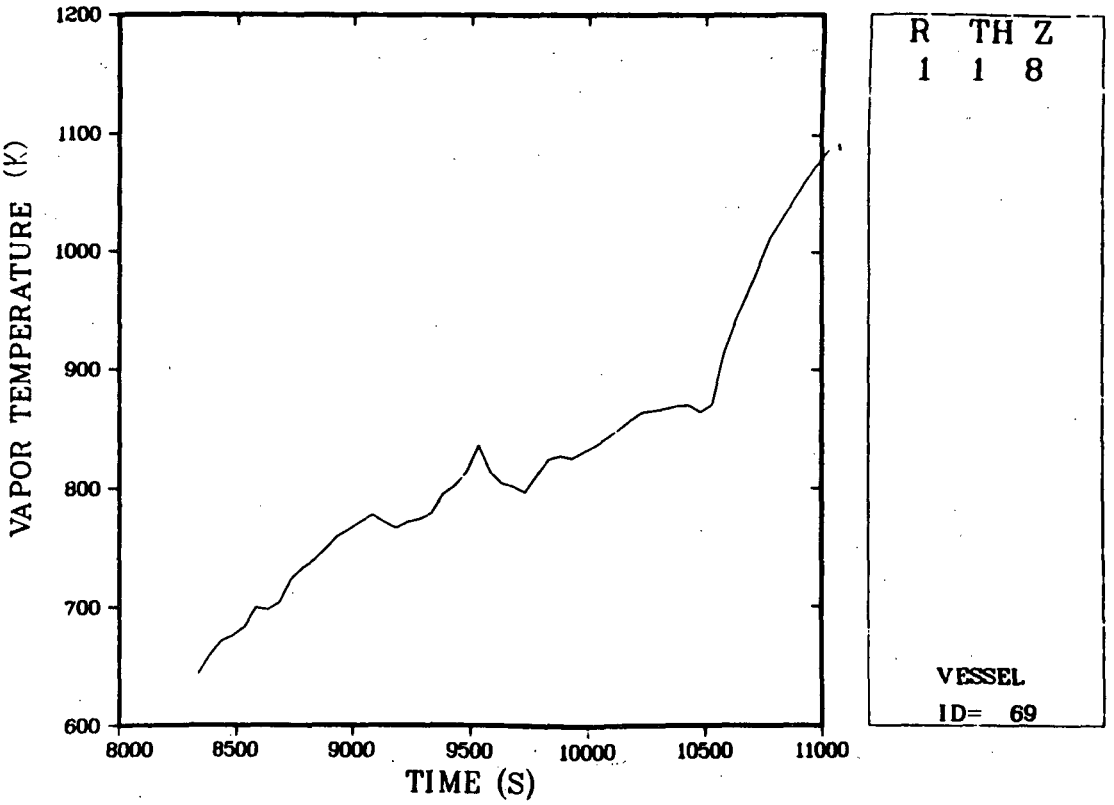

Upper plenum vapor temperature.

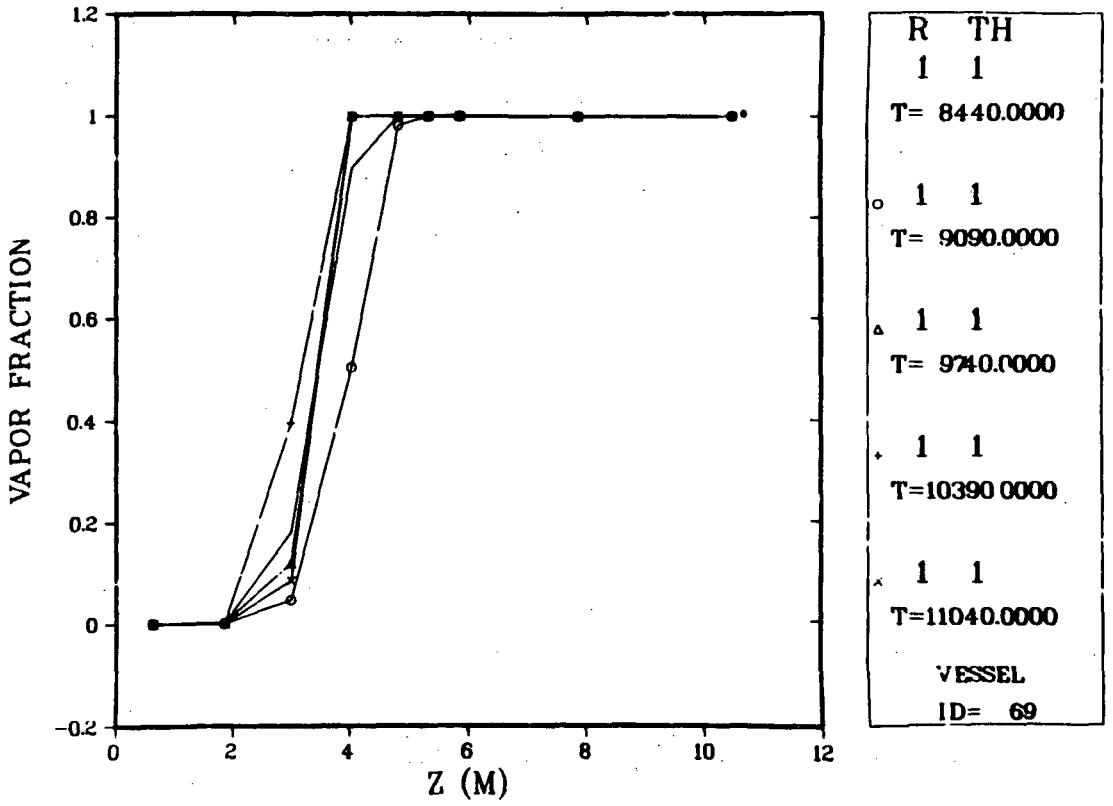

Vessel void fraction axial profile vs time (Cell 1).

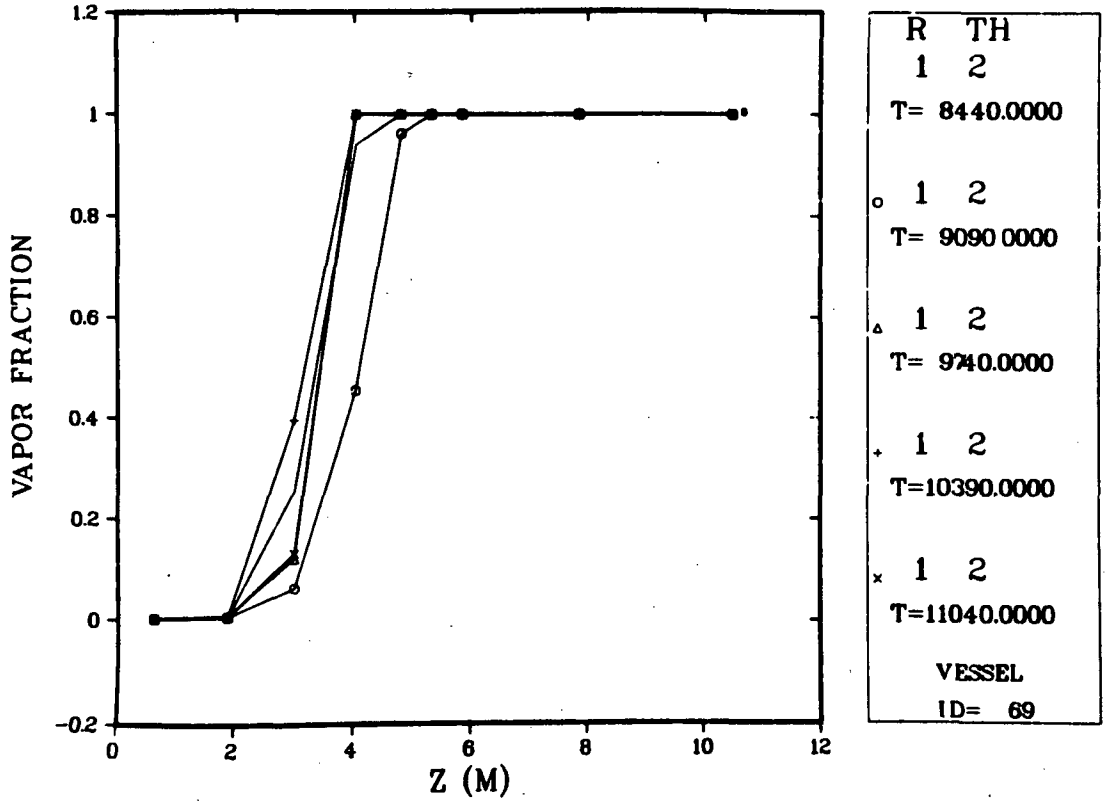

Vessel void fraction axial profile vs time (Cell 2).

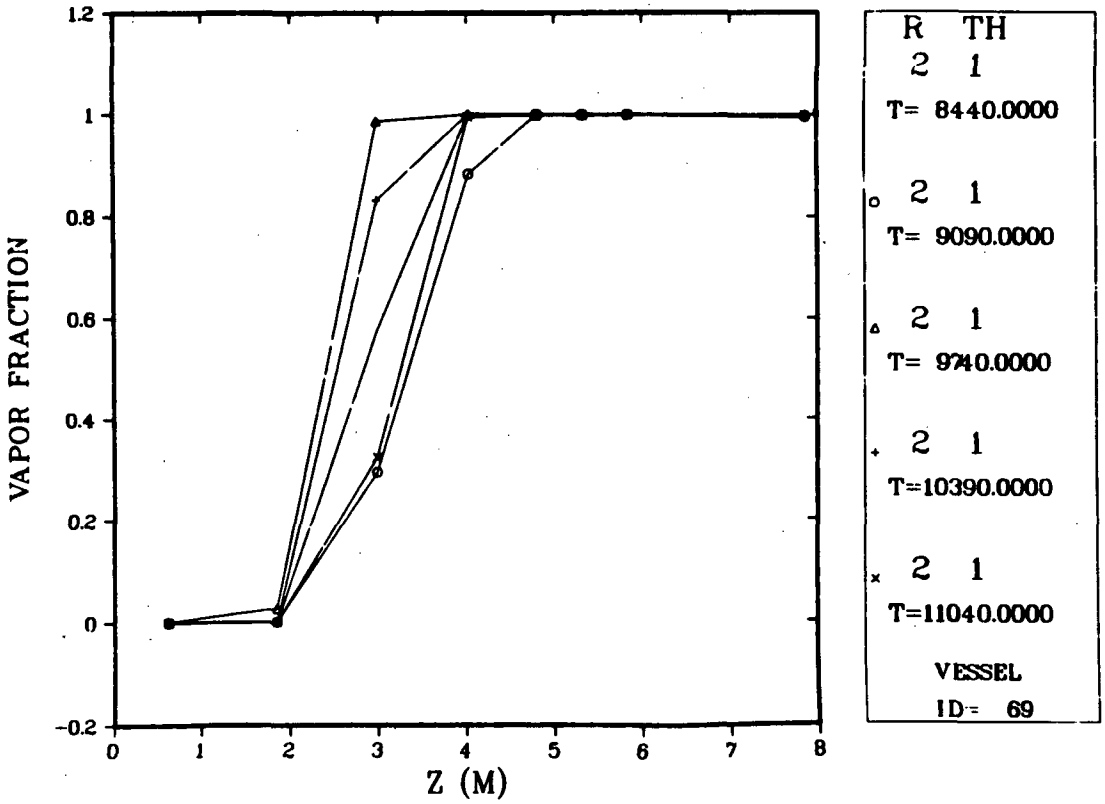

Downcomer void fraction axial profile vs time.

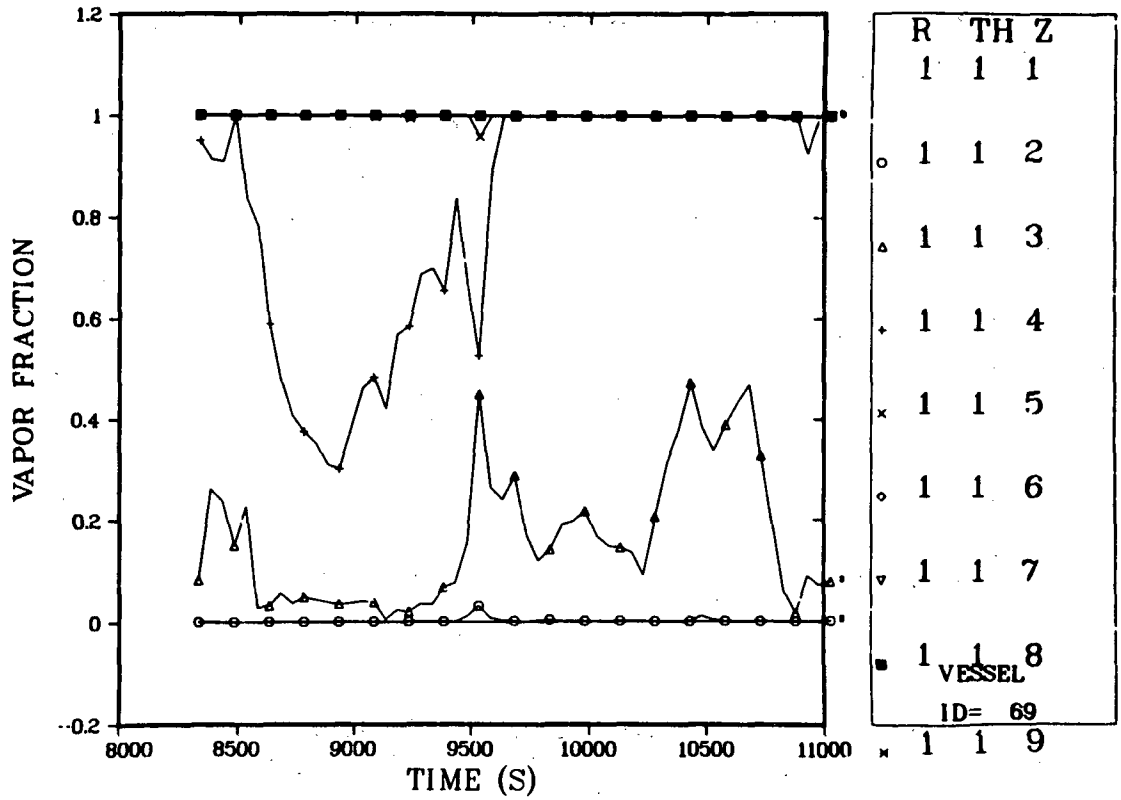

Vessel void fraction axial profile (Cell 1).

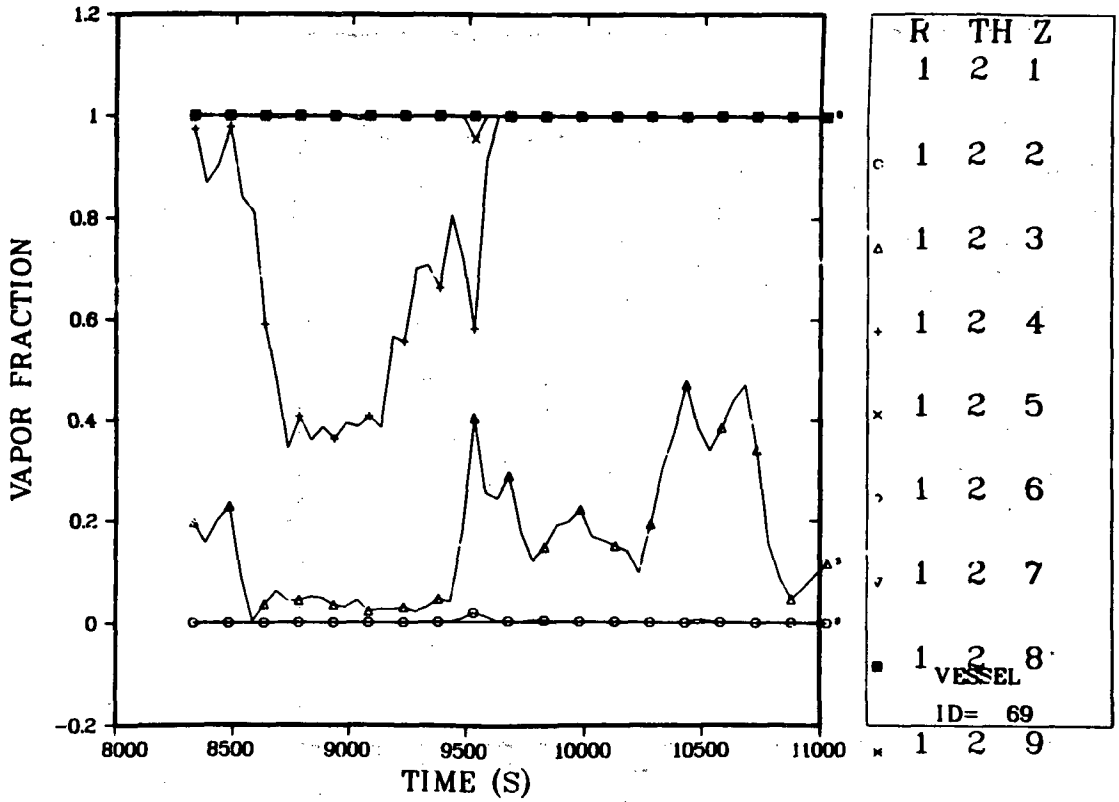

Vessel void fraction axial profile (Cell 2).

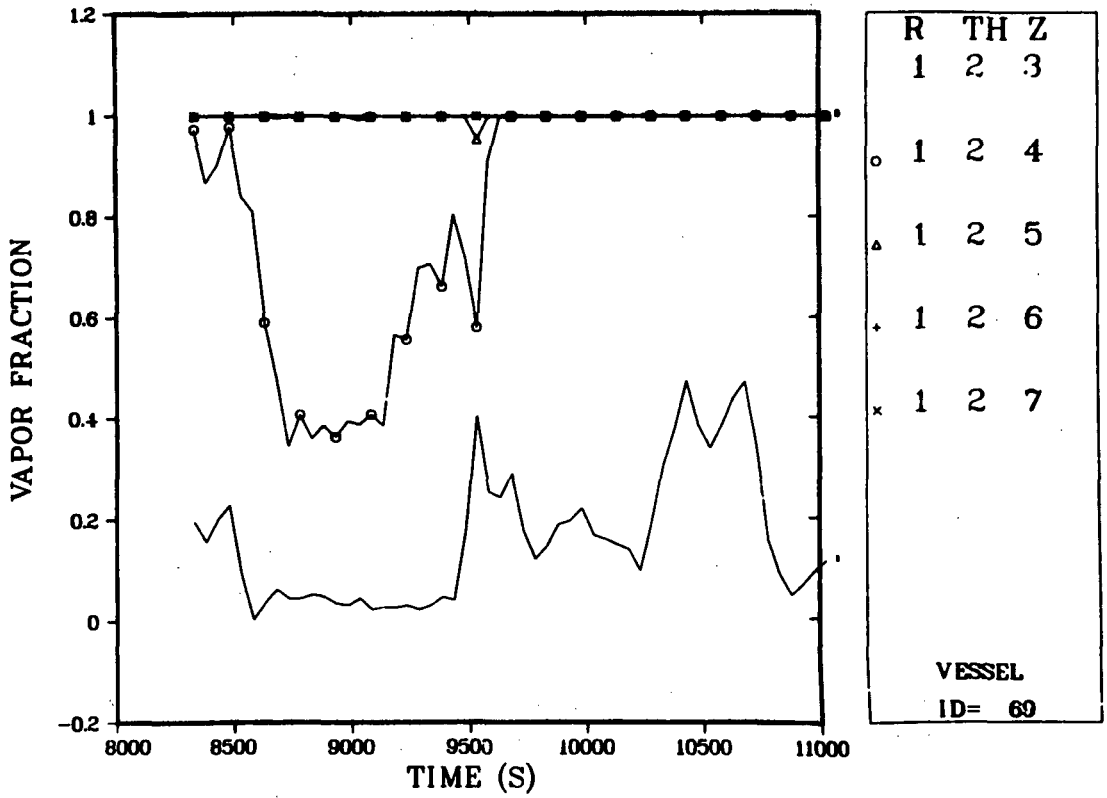

Core void fraction axial profile (Cell 2).

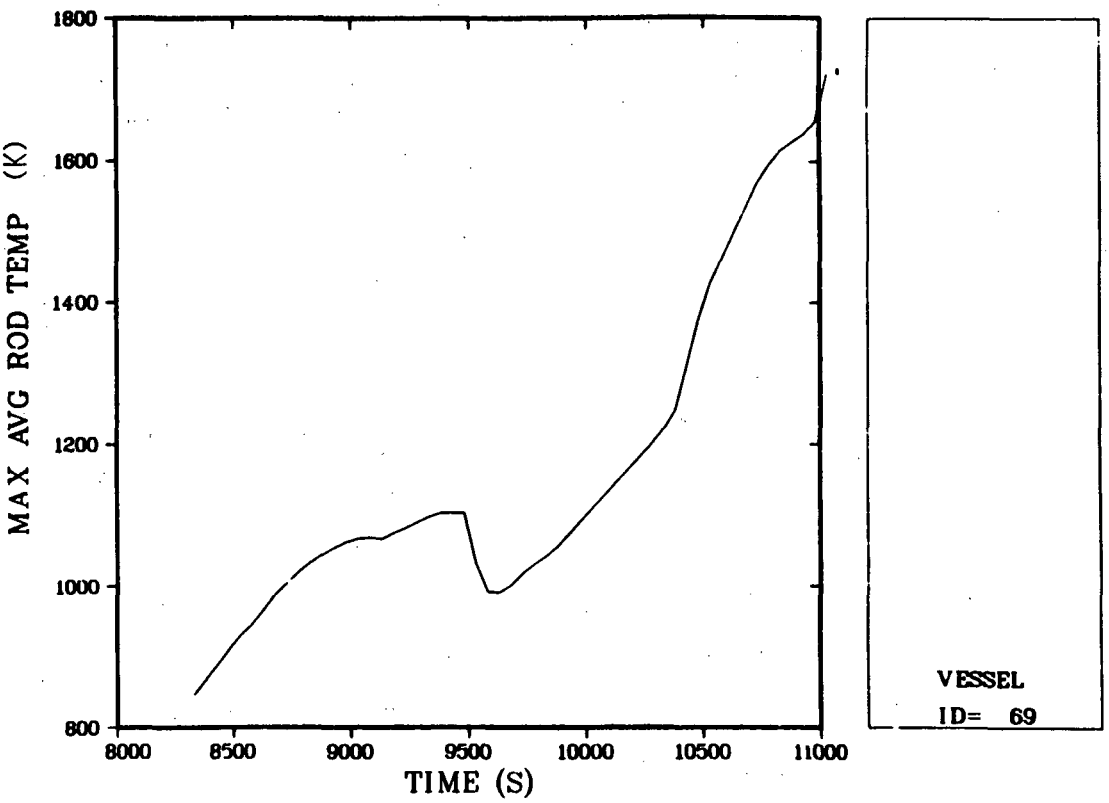

Maximum average rod temperature.

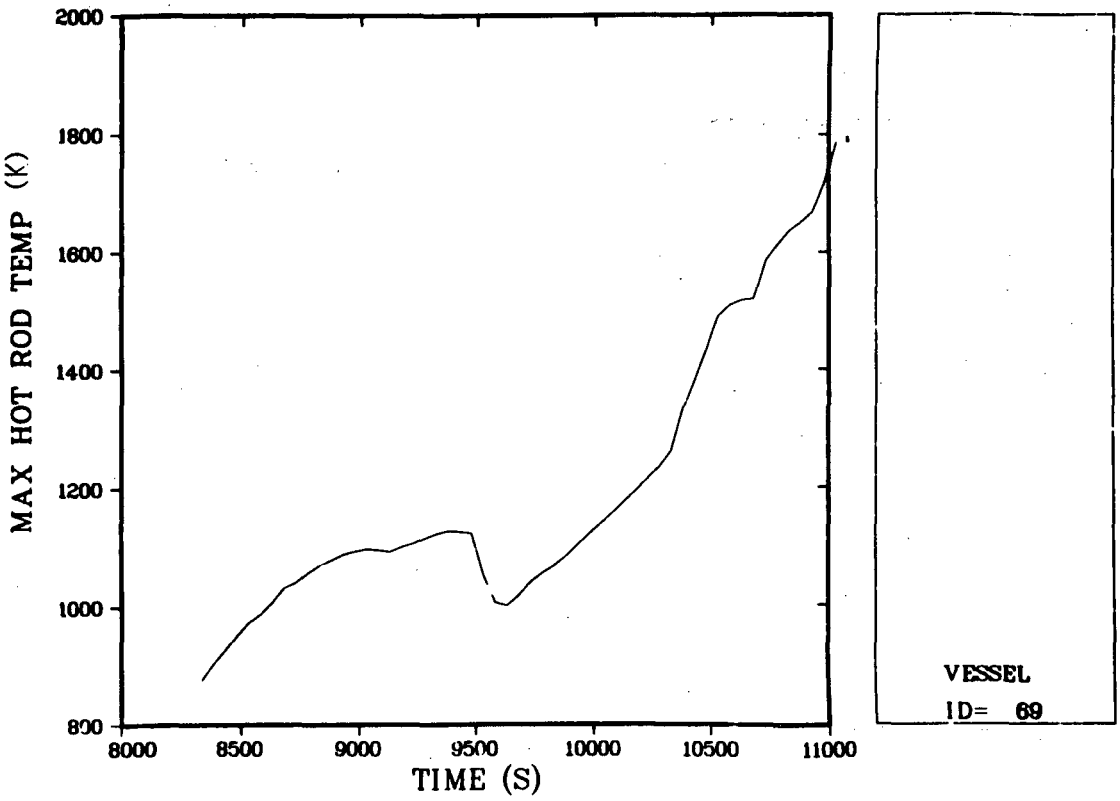

Maximum hot-rod temperature.

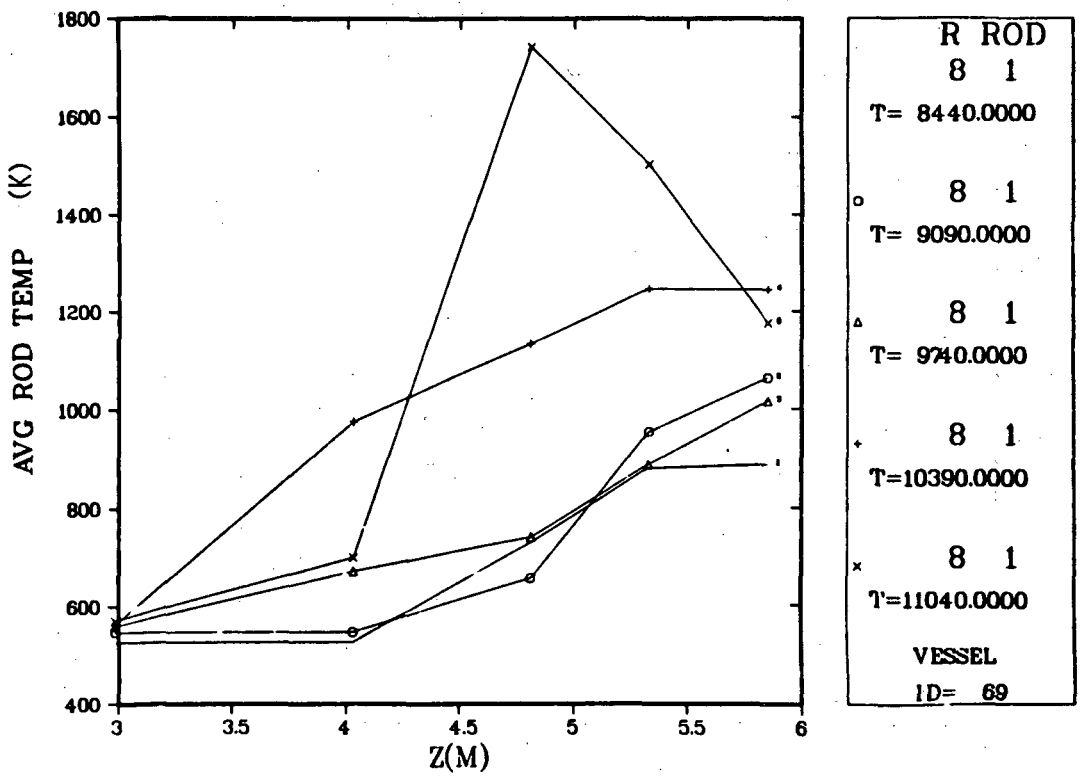

Average rod temperature axial profile vs time (Rod 1).

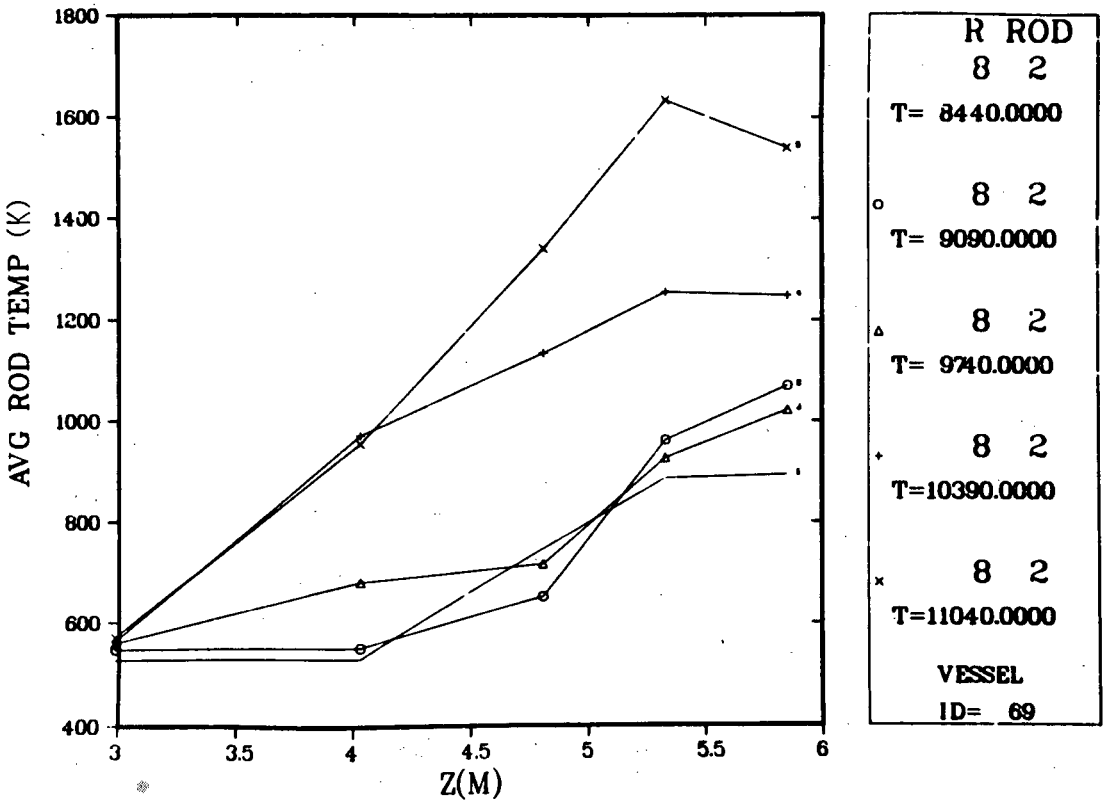

Average rod temperature axial profile vs time (Rod 2).

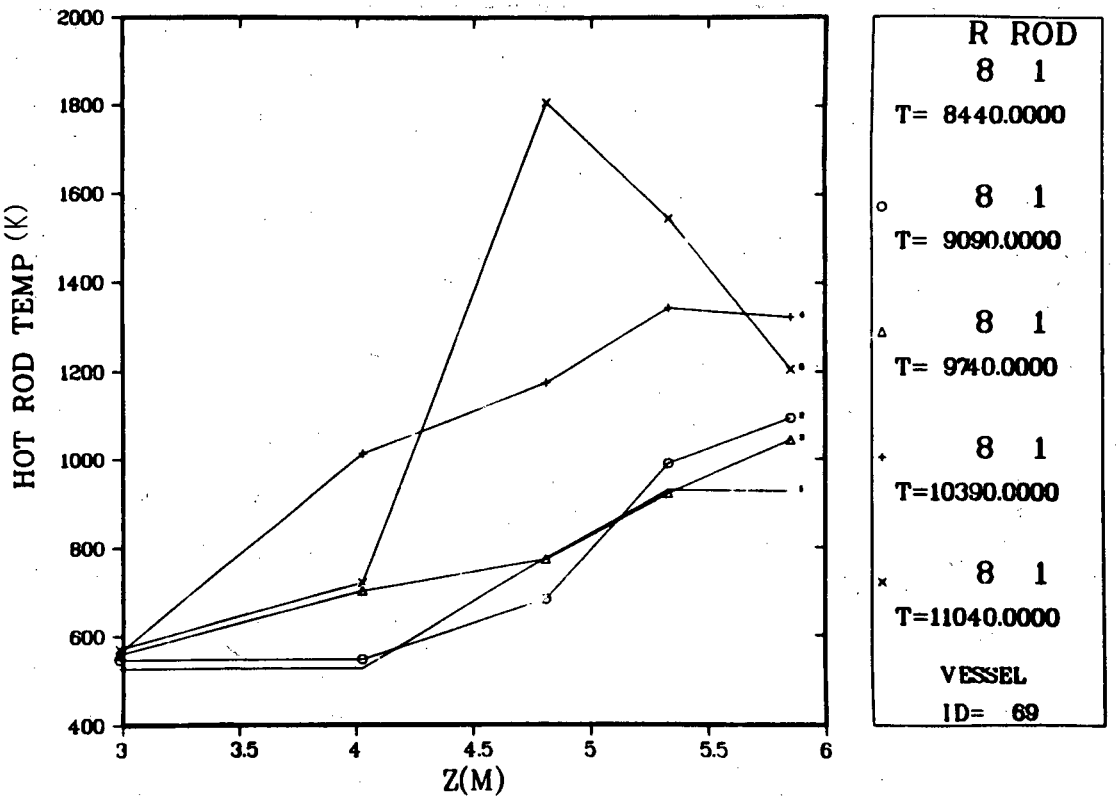

Hot-rod temperature axial profile vs time (Rod 1).

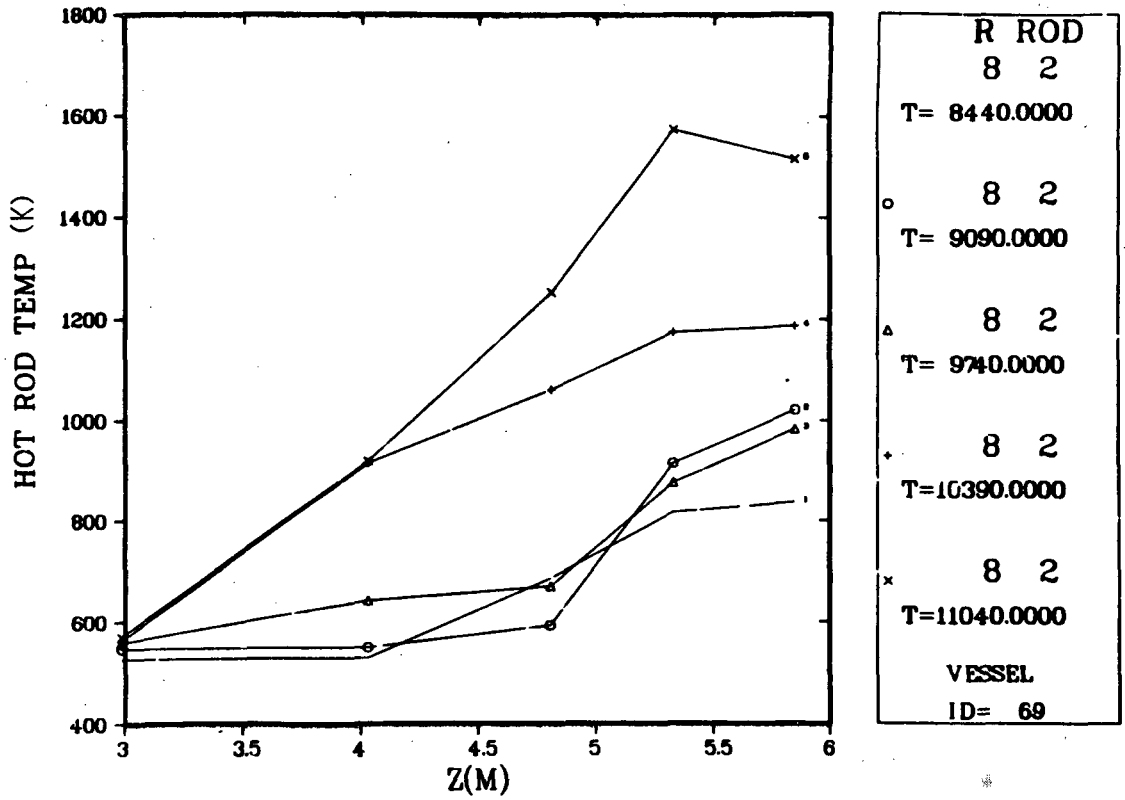

Hot-rod temperature axial profile vs time (Rod 2).

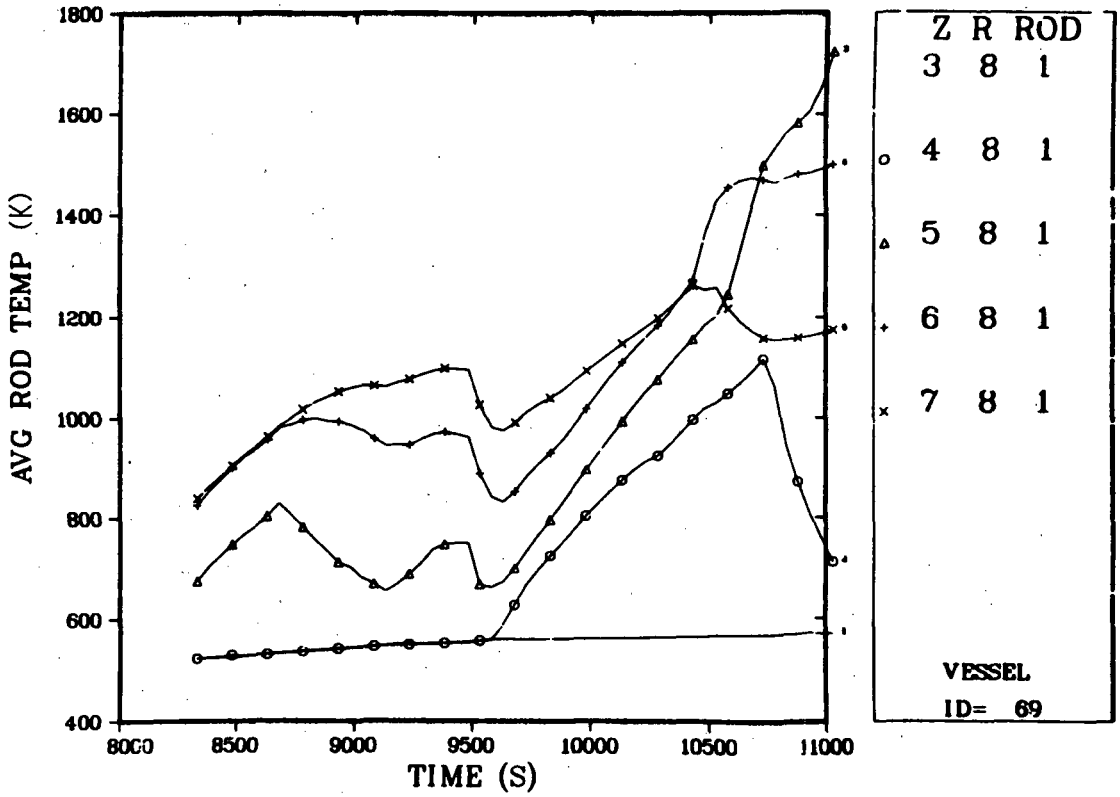

Average rod temperature axial profile (Rod 1).

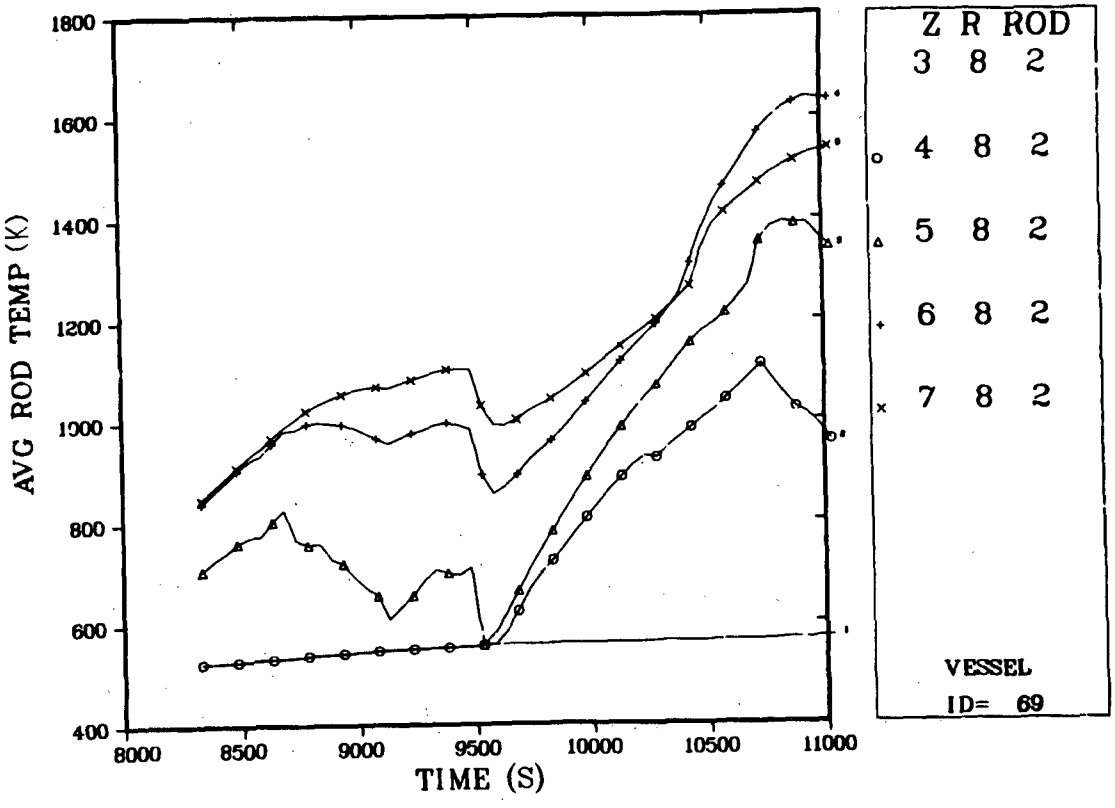

Average rod temperature axial profile (Rod 2).

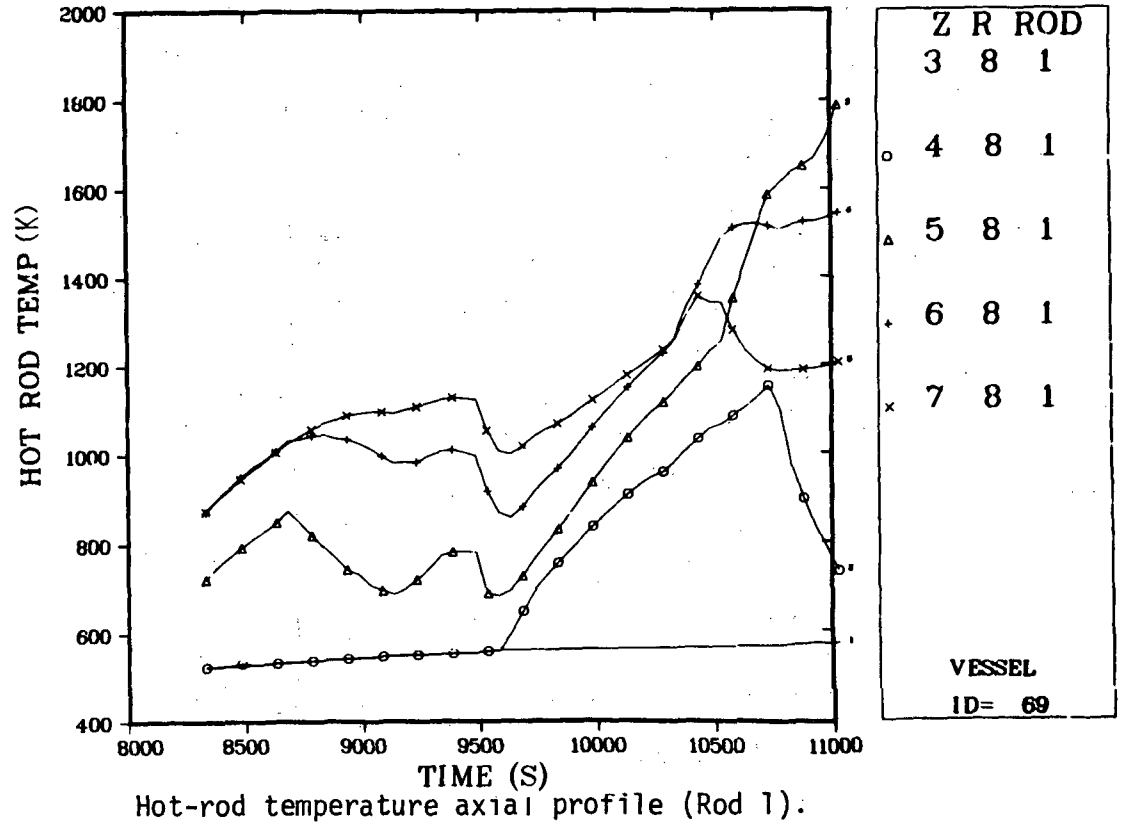

Hot-rod temperature axial profile (Rod 1).

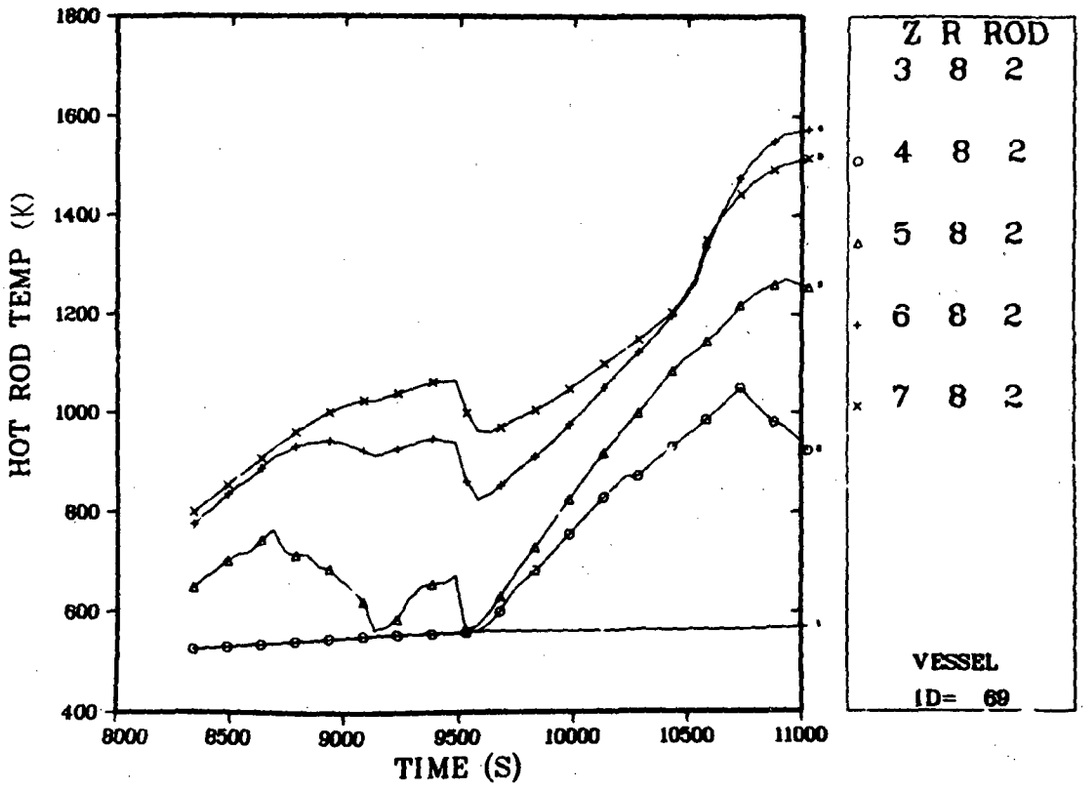

Hot-rod temperature axial profile (Rod 2).

DISTRIBUTION

	Copies
Nuclear Regulatory Commission, R4, Bethesda, Maryland	363
Technical Information Center, Oak Ridge, Tennessee	2
Los Alamos Scientific Laboratory, Los Alamos, New Mexico	___

NRC FORM 335 (7-77) U.S. NUCLEAR REGULATORY COMMISSION

BIBLIOGRAPHIC DATA SHEET

1. REPORT NUMBER *(Assigned by DDC)*
NUREG/CR-1353
LA-8273-MS

4. TITLE AND SUBTITLE *(Add Volume No., if appropriate)*

Preliminary Calculations Related to the Accident at Three Mile Island

2. *(Leave blank)*

3. RECIPIENT'S ACCESSION NO.

7. AUTHOR(S)

J. R. Ireland and others

5. DATE REPORT COMPLETED
MONTH March YEAR 1980

9. PERFORMING ORGANIZATION NAME AND MAILING ADDRESS *(Include Zip Code)*

Los Alamos Scientific Lab.
P.O. Box 1663
Los Alamos, New Mexico 87545

DATE REPORT ISSUED
MONTH April YEAR 1980

6. *(Leave blank)*

8. *(Leave blank)*

12. SPONSORING ORGANIZATION NAME AND MAILING ADDRESS *(Include Zip Code)*

Division of Reactor Safety Research
Office of Nuclear Regulatory Research
U. S. Nuclear Regulatory Commission
Washington, D. C. 20555

10. PROJECT/TASK/WORK UNIT NO.

11. CONTRACT NO.

13. TYPE OF REPORT

PERIOD COVERED *(Inclusive dates)*

15. SUPPLEMENTARY NOTES

14. *(Leave blank)*

16. ABSTRACT *(200 words or less)*

The Three Mile Island nuclear plant (TMI-2) was modeled using the Transient Reactor Analysis Code (TRAC-PIA) and a preliminary calculation, which simulated the initial part of the accident that occurred on March 28, 1979, was performed. The purpose of this calculation was to provide a better understanding of the system thermal-hydraulic and core thermal-mechanical response during the first 3 h and to evaluate how well TRAC compared to the overall accident scenario and measured system parameters. As a result of this base-case calculation, several parametric calculations were performed to investigate hypothetical variations to the TMI-2 accident sequence to determine the significance of system/operator actions on the course of the accident. Finally, based upon the results of the base-case calculation, estimates were made regarding the extent of core damage and the amount of hydrogen produced as a result of the zirconium-steam reaction.

17. KEY WORDS AND DOCUMENT ANALYSIS

17a. DESCRIPTORS

17b. IDENTIFIERS/OPEN-ENDED TERMS

18. AVAILABILITY STATEMENT

Unlimited

19. SECURITY CLASS *(This report)*
Unclassified

20. SECURITY CLASS *(This page)*

21. NO. OF PAGES

22. PRICE
S

NRC FORM 335 (7-77)

*U.S. GOVERNMENT PRINTING OFFICE : 1980 0-620-369/119

UNITED STATES
NUCLEAR REGULATORY COMMISSION
WASHINGTON, D. C. 20555

OFFICIAL BUSINESS
PENALTY FOR PRIVATE USE, $300

POSTAGE AND FEES PAID
U.S. NUCLEAR REGULATORY
COMMISSION